

Phenomenological modelling of the combustion processes in a dual-fuelled diesel engine using combustion bomb experiments

Author:

Hu, Bian

Publication Date:

1992

DOI:

<https://doi.org/10.26190/unsworks/8736>

License:

<https://creativecommons.org/licenses/by-nc-nd/3.0/au/>

Link to license to see what you are allowed to do with this resource.

Downloaded from <http://hdl.handle.net/1959.4/63620> in <https://unsworks.unsw.edu.au> on 2024-04-18



THE UNIVERSITY OF NEW SOUTH WALES
SCHOOL OF MECHANICAL AND MANUFACTURING ENGINEERING

**Phenomenological Modelling of the
Combustion Processes in a Dual-Fuelled Diesel Engine
Using Combustion Bomb Experiments**

by

Bian Hu *B. Sci.*

(The University of Science and Technology of China)

Supervisor: Professor B. E. Milton

**A Thesis Submitted in Partial Fulfillment of
the Requirements for the Degree of
Doctor of Philosophy**

March 1992

CERTIFICATE OF ORIGINALITY

I hereby declare that this submission is my own work and that, to the best of my knowledge and belief, it contains no material previously published or written by another person nor material which to a substantial extent has been accepted for the award of any other degree or diploma of a university or other institute of higher learning, except where due acknowledgement is made in the text.

(Signed)

ACKNOWLEDGEMENTS

My sincere thanks are extended to Professor B. E. Milton for his invaluable guidance and assistance throughout the course of this thesis; also to Dr. V. Krepl for his assistance in the experiments. I am grateful to Professor Y. Tanaka for several discussions which helped develop the thermodynamic model in the early stages of the project.

I would like to thank the staff of the Internal Combustion Engine Laboratory, particularly Mr. E. A. Carter, for their help in various aspects of the thesis. I would also like to thank my friend Mr. H. B. Ni for his help in overcoming obstacles in word processing and graph drawing of the thesis.

I am also grateful to NERDDC for funding the development of the combustion bomb for this project.

Finally, I would like to thank all member of my family, particularly my wife. This thesis would not be possible without their encouragement and support.

ABSTRACT

The dual fuel engine is a compression ignition engine in which some of the energy release during combustion comes about from the combustion of a gaseous fuel mixed with air prior to introduction to the cylinder. Within the cylinder, it is then ignited by a pilot distillate injection. Some aspects of both the fundamentals of dual fuel combustion and its application in engines need further clarification. These are particularly the problem of engine knock, the optimum use of diesel fuel, the reduction of unwanted emissions at light load, the reaction between the liquid and the gaseous fuel and its affect on the combustion, and the flame propagation in a dual fuel environment. Very few reports are available on modelling of the dual fuel combustion process in comparison with the substantial development which has occurred in modelling both SI engine and CI engine combustion.

A new quasi-dimensional phenomenological model for the combustion in a dual fuel engine has been developed here based partially on knowledge of flame propagation in SI engines and of spray burning in diesel engines. However, it is particularly based on an investigation of dual fuel combustion carried out using experiments in a constant volume combustion bomb developed for this purpose. The model's coefficients have been evaluated and a physical meaning given to some of the processes. A formula to calculate the dual fuel ignition delay has been proposed based on regression of the pressure rise delay data obtained from the combustion bomb. The effect of heat transfer is considered. Computational results have been compared with experimental for various initial conditions with good agreement. Preliminary work to incorporating the model into an engine simulation package has been carried out.

Combustion phenomena have been studied in the combustion bomb for both sole diesel and diesel-gas fuels. The ignition delay for diesel combustion was found to be very close to that obtained from actual diesel engines. In the dual fuel combustion experiment, normal combustion can still be achieved at gas substitution levels as high as 95% of the total energy. Suggestions for further analytical and experimental investigation are given.

Contents

Acknowledgements	i
Abstract	ii
Table of Contents	iii
List of Figures	xi
1 Introduction	1
1.1 Origin of the Question –the Use of Gas in Large IC Engines . . .	2
1.2 Basic Operating Problems of Dual Fuel Engines	4
1.3 General Research Background on Dual Fuel Engines	5
1.4 Brief Review of the Modelling of In-cylinder Processes	8
1.4.1 Multi-dimensional Models	8
1.4.2 Brief Review of the Phenomenological Model (PM) . . .	12
1.4.3 MDM vs PM	15
1.5 Some Typical Experimental Research on Dual Fuel Engine Com- bustion	15

1.6	Objectives and Structure of This Research	17
2	The Thermodynamic-thermochemical Sub-model of In-cylinder Combustion	21
2.1	Introduction	22
2.2	Tanaka's Thermodynamic Calculation	23
2.3	Thermodynamic Model, Fully-mixed Assumption	24
2.3.1	Main Assumptions	24
2.3.2	Model Equations	25
2.4	Chemical Equilibrium and Dissociation in Engine Combustion .	28
2.4.1	Brief review	28
2.4.2	Strehlow's calculation program and Weinberg's Rapid Convergent method	29
2.5	Samples of the model's predicted result	32
3	Modelling the Spark Ignition Combustion Processes	45
3.1	Introduction	47
3.2	Essential Features of the Combustion in Spark-Ignition Engines .	48
3.3	Literature Review on Modelling the Combustion in SI engines . .	48
3.3.1	Zero-Dimensional Models	48
3.3.2	Blizard-Keck's Turbulent Entrainment Model (The B-K Model)	50
3.3.3	Blizard-Keck-Tabaczynski (B-K-T) Model	50

3.3.4	Hires-Tabaczynski H-T Quasi-dimensional Model	56
3.3.5	B-R-K's Eddy Burning Model and Its Modification	58
3.4	The Laminar Burning Speed	62
3.4.1	The Definition of S_L	62
3.4.2	Dependence of S_L^0 on fuel/air equivalence ratio	63
3.4.3	Dependence of S_L on pressure, temperature and residual gas fraction	64
3.5	Turbulent Flame Propagation in Homogeneous Mixtures	68
3.5.1	Some developments of the B-K-T turbulent flame model	68
3.6	The Current Model	70
3.6.1	The model's assumptions	70
3.6.2	The burning law	71
3.7	Application of the Turbulent Flame propagation Model to a Constant Volume Combustion Bomb	72
4	Experiment Setup and Procedures of A Constant-Volume Dual- Fuel Combustion Bomb	83
4.1	Introduction	83
4.2	Research Using Combustion Bombs - A Brief Review	84
4.2.1	Spark ignition bomb with normal pressure and temperature	84
4.2.2	Spark ignition bomb with turbulence or swirl	87
4.2.3	Diesel bomb without combustion	88

4.2.4	Diesel bomb with combustion	89
4.3	Dual Fuel Combustion Bomb Used in the Current Research . . .	90
4.3.1	Difficulties in developing a dual fuel combustion bomb . .	90
4.3.2	Design of the Combustion Chamber	91
4.3.3	Design of the Single-Shot Diesel Injection System	94
4.3.4	The Air and Gas Supply	95
4.3.5	Instrumentation and Measurement	95
4.4	Injection Characteristics of the Injector	99
4.4.1	Shape of the spray	100
4.4.2	Injection Quantity, Measurement Error and Fuel Line Pressure	101
4.5	Cylinder Pressure Trace, Acquisition and Methods Analysis . . .	102
4.5.1	Data acquisition	102
4.5.2	Determination of the Ignition Delay	104
4.6	Discussion	106
5	Modelling the Spray combustion in Diesel Engines	113
5.1	Introduction	116
5.2	Essential Features of the Combustion Process in Compression Ignition Engines	117
5.3	Literature Review of Phenomenological Modelling of CI Engine Combustion	120

5.3.1	Zero-Dimensional Models	120
5.3.2	Kumar's Two Zone Model (1984)	122
5.3.3	Whitehouse-Balusway's four-zone model (1977)	124
5.3.4	Dent-Metha Spray Mixing Model (1981)	124
5.3.5	Hiroyasu et al's multi-zone spray combustion model [112] (1983)	127
5.3.6	The Cummins Engine Model	133
5.4	Spray Structure and Spray Motion for the Current Research . . .	137
5.4.1	Spray break-up length, tip penetration and angle	137
5.4.2	Spray evaporation	140
5.5	Ignition Delay	140
5.6	Air Entrainment	144
5.6.1	Various estimation methods	144
5.6.2	Entrainment of air into a spray for small injection quantities	145
5.7	A Model for Diesel Spray Combustion in A Constant Volume Vessel	146
5.7.1	Model assumptions	146
5.7.2	Model equations	148
5.8	Computational Results Compared with Experimental Records . .	150
5.8.1	About the entrainment function Ψ	150
5.8.2	About the heat loss rate \dot{q}	152

6 Features of Dual Fuel Combustion Observed From Combustion

Bomb Experiments	161
6.1 Introduction	161
6.2 Literature Review	162
6.2.1 General Combustion Features Observed in a Dual-Fuel Engine	162
6.2.2 Ignition Delay Observed in a Dual-fuelled Engine	163
6.2.3 Chemical Kinetic Model of Dual Fuel Ignition Delay	166
6.3 Ignition Conditions Observed from the Current Experiments	166
6.3.1 Minimum Temperature for Ignition	166
6.3.2 Effects of P_0 and ϕ_{gas} on ignition	168
6.3.3 Effects of P_0 and m_{inj} on ignition	171
6.3.4 Effects of T_0 and ϕ_{gas} on ignition	172
6.3.5 Minimum pilot fuel quantity	175
6.4 Dual Fuel Ignition Delay	175
6.5 General Dual Fuel Combustion Features	178
 7 Phenomenological Modelling of Diesel-Gas Dual Fuel Combustion	 191
7.1 Introduction	194
7.2 Literature Review	194
7.2.1 Sumbally heat release model [156]	194
7.2.2 Thyagarajan model [11]	195

7.2.3	RafiquillIslam combustion model for dual fuel IDI diesel engine	196
7.2.4	A Comparison of the Existing Models	197
7.3	Thermodynamic Sub-model for the Current Dual Fuel Combustion Model	198
7.3.1	Model Assumptions	198
7.3.2	Conservation of mass	199
7.3.3	Conservation of energy	200
7.3.4	Adiabatic compression of the unburned zone mixture . . .	201
7.3.5	Heat transfer	201
7.4	The Combustion Model	202
7.4.1	Model assumptions	202
7.4.2	Model equations	204
7.4.3	Empirical coefficients and correlations for the combustion model	206
7.5	Computational Results of the Model	209
7.6	Total Engine Simulation	210
8	Conclusions, Discussion and Recommendation for Further Research	221
8.1	Conclusions	221
8.2	Discussion and Recommendations for Further Research	224

Reference	227
------------------	------------

Appendix:

A Coefficients of linear enthalpy function	247
---	------------

B Properties of fuels used in the current model	251
--	------------

C Experimental results of dynamic pressure trace of diesel combustion in constant volume bomb	253
--	------------

D Experimental results of dynamic pressure trace of diesel-natural gas dual-fueled combustion in a constant volume bomb	291
--	------------

List of Figures

1.1	Typical variations of the ignition point of a dual fuel engine operating at constant speed and constant pilot quantity with methane. Reproduced from reference [154].	6
1.2	Schema of the Structure of a Typical Phenomenological Model .	19
2.1	Predicted Combustion Results for fuel $CH_4(G)$	32
2.2	Predicted Combustion Results of $CH_4(G)$	34
2.3	Predicted Combustion Results of $C_3H_8(G)$	35
2.4	Predicted Combustion Results of Diesel Fuel (diesel fuel is assumed to be $C_{10.8}H_{18.7}(L)$ in DFODES, and $C_{12}H_{26}(L)$ in Tanaka' model	36
2.5	Predicted Combustion Results of $CH_4(G)$	37
2.6	Predicted Combustion Results of $C_3H_8(G)$	38
2.7	Maximum adiabatic combustion pressure of methane and propane gas at $T_0=500$ K, $\phi = 0.6$. Predicted by DFODES.	39
2.8	Maximum adiabatic combustion temperature of methane and propane gas at $T_0=500$ K, $P_0 = 18$ bar. Predicted by DFODES. .	40
2.9	Maximum adiabatic combustion pressure of methane and propane gas at $P_0 = 18$ bar, $\phi = 0.6$. Predicted by DFODES.	41

2.10	Maximum adiabatic combustion temperature of methane and propane gas at $T_0 = 500$ K, $\phi = 0.6$. Predicted by DFODES. . .	42
2.11	Maximum adiabatic combustion temperature of methane and propane gas at $P_0 = 18$ bar, $T_0 = 500$ K; Predicted by DFODES. . .	43
2.12	Maximum adiabatic combustion temperature of methane and propane gas at $P_0 = 18$ bar, $\phi = 0.6$. Predicted by DFODES. . .	44
3.1	A Pressure-volume diagram for an SI engine cycle	49
3.2	Turbulence Structure in the B-K-T Model	52
3.3	Structure of the “Vortex Tube” in the B-K-T Model	53
3.4	BKT’s Small-Scale Turbulence Flame Model	56
3.5	“Thick” Turbulent Flame Implied by Keck et al’s Model	61
3.6	Various Reports of Laminar Burning Speed $S_L^0(\phi)$; CH_4 -Air Mixture at $P = 1$ atm.	65
3.7	The development of the laminar flame speed in the combustion of a propane-air mixture at $P_0 = 2$ MPa, $T_0 = 500$ K, and $\phi = 1.0$. .	68
3.8	The development of the laminar flame speed in the combustion of a propane-air mixture at $P_0 = 2$ MPa, $T_0 = 500$ K, and $\phi = 0.5$. .	69
3.9	Schema of spherical turbulent flame propagation in a combustion bomb with central ignition at point O.	73
3.10	Turbulent Flame Propagation in the Bomb of Fig. 3.9.; CH_4 -Air mixture at $P_0 = 9$ Bar, $T_0 = 500$ K, $\phi = 1.0$, and $u' = 0.7$	76
3.11	Turbulent Flame Propagation in the Bomb of Fig. 3.9. C_3H_8 -Air mixture at $P_0 = 9$ Bar, $T_0 = 500$ K, $\phi = 1.0$, $u' = 0.7$	77

3.12	Affect of P_0 on the flame propagation in the combustion bomb. CH_4 -air mixture at various P_0 . $T_0 = 500$ K, $\phi = 1.0$, $u' = 0.7$.	78
3.13	Affect of T_0 no the flame propagation in the combustion bomb. CH_4 -Air mixture at various T_0 . $P_0=9.0$ bar, $\phi = 1.0$, $u' = 0.7$.	79
3.14	Affect of ϕ no the flame propagation in the combustion bomb. CH_4 -air mixture at various ϕ . $T_0 = 500$ K , $P_0 = 9$ bar, $u' = 0.7$.	80
3.15	Affect of u' no the flame propagation in the combustion bomb. CH_4 -Air mixture with various turbulent intensities. $P_0=9.0$ bar, $\phi = 1.0$, $T_0 = 500$ K.	81
3.16	Affect of diameter:height ratio r^* no the flame propagation in the combustion bomb. CH_4 -Air mixture of $P_0=9.0$ bar, $\phi = 1.0$, and $T_0 = 500$ K. Volume of combustion chamber remains unchanged as $V_0=0.1923\text{ m}^3$	82
4.1	Views of the dual fuel combustion rig	85
4.2	Scheme of the dual fuel combustion experimental rig	86
4.3	Outside view of the combustion chamber.	92
4.4	Inside view of the combustion chamber.	93
4.5	Principal elements of the injection system.	95
4.6	Scheme of the water-cooled injector	96
4.7	Principal elements of the control system.	97
4.8	Data acquisition system.	98
4.9	A view of the developing non-combustion diesel spray in the present rig.	100
4.10	A close view of an approximate conical diesel spray	101

4.11	Fuel line pressure of injector at rack setting 0	103
4.12	fuel line pressure of injector at rack set 1	104
4.13	Fuel line pressure of injector at rack setting 2	105
4.14	Fuel line pressure of injector at rack setting 3	106
4.15	Fuel line pressure of injector at rack setting 4	107
4.16	Fuel line pressure of injector at rack setting 5	108
4.17	Typical cylinder pressure trace for dual fuel combustion in a constant volume combustion bomb. Data are recorded at two points per milli-second. (A) shows the entire combustion process, (B) shows the ignition delay period.	109
4.18	Typical cylinder pressure trace for diesel combustion in a con- stant volume combustion bomb. Data are recorded at five points per milli-second. (A) shows the entire combustion process, (B) shows the ignition delay period.	110
4.19	Spacial variation in temperature (T_h is the temperature of the heating element inside the combustion chamber).	111
5.1	Fuel injection, heat release and cylinder pressure of a typical DI diesel engine (reproduced from Ref. [134].) . . .	119
5.2	Circular Jet in Kumar's Two-Zone Model	123
5.3	Schema of the spray combustion in the Hiroyasu multi-zone model	128
5.4	Schema of multi-zone spray of the Hiroyasu model	129
5.5	Schema of Spray Package Combustion in the Hiroyasu Model . .	132
5.6	Multi-Zone Spray in the Cummins Engine Model	134

5.7	Schematic representation of spray cross-section in the Cummins model	135
5.8	Schematic of diesel fuel spray defining its parameters	139
5.9	Contour Map of Ignition Delay Calculated by Equations 5.40 and 5.41.	143
5.10	Values of the entrainment function	151
5.11	Dynamic combustion bomb pressure, computed result (dashed lines) and measured results.	154
5.12	Dynamic combustion bomb pressure, computed result (dashed lines) and measured results	155
5.13	Dynamic combustion bomb pressure, computed result (dashed lines) and measured results	156
5.14	Dynamic combustion bomb pressure, computed result (dashed lines) and measured result	157
5.15	Dynamic combustion bomb pressure, computed result (dashed lines) and measured result	158
5.16	Dynamic combustion bomb pressure, computed result (dashed lines) and measured result	159
5.17	Dynamic combustion bomb pressure, computed result (dashed lines) and measured result	160
6.1	Typical variations of the ignition point of a dual fuel engine operating at constant speed and constant pilot quantity with methane. Reproduced from reference [154].	164

6.2	Typical variation in the ignition point with the total equivalence ratio of a dual fuel engine fuelled with different fuels at different intake temperatures and constant pilot quantity. Reproduced from reference [154].	165
6.3	Minimum ignition temperature at “optimum” condition of pilot injection and gas-air ratio. For dual fuel combustion, $P_0 = pp_{air} + pp_{gas}$	167
6.4	Minimum ignition temperature of dual fuel combustion as a function of gas-air equivalence ratio at initial pressure ($pp_{air} + pp_{gas}$) $P_0 = 20.5$ bar.	169
6.5	Minimum ignition temperature of dual fuel combustion as a function of total fuel-air equivalence ratio at initial pressure ($pp_{air} + pp_{gas}$) $P_0 = 20.5$ bar.	170
6.6	Effects of pressure P_0 and gas-air equivalence ratio ϕ_{gas} on dual fuel ignition.	171
6.7	Effects of pressure P_0 and gas-air equivalence ratio ϕ_{gas} on dual fuel ignition.	172
6.8	Effects of pressure P_0 and pilot quantity m_{inj} on ignition.	173
6.9	Effects of temperature T_0 and equivalence gas-air ratio ϕ_{gas} on ignition	174
6.10	Affects of $T_0 - \phi_{gas}$ on dual fuel ignition delay	178
6.11	Affects of $P_0 - \phi_{gas}$ on dual fuel ignition delay	179
6.12	Affects of $P_0 - m_{inj}$ on dual fuel ignition delay	180
6.13	Affects of $T_0 - m_{inj}$ no dual fuel ignition delay	181
6.14	Dual fuel ignition delay as a function of the initial conditions . .	182

6.15	Dual fuel ignition delay as a function of the initial conditions . .	183
6.16	Dual fuel ignition delay as a function of the initial conditions . . .	184
6.17	Dual fuel ignition delay as a function of the initial conditions . .	185
6.18	Typical pressure trace of dual fuel combustion with short ignition delay.	186
6.19	Typical pressure trace of dual fuel combustion with short ignition delay.	187
6.20	Typical pressure trace of dual fuel combustion with short ignition delay.	188
6.21	Typical pressure trace of dual fuel combustion with long ignition delay.	189
6.22	Typical pressure trace of dual fuel combustion with long ignition delay.	190
7.1	Effects of radiant heat transfer coefficients	207
7.2	Effects of convective heat transfer coefficients	208
7.3	NG+Diesel dual fuel combustion dynamic pressure trace.	211
7.4	NG+Diesel dual fuel combustion dynamic pressure trace.	211
7.5	NG+Diesel dual fuel combustion dynamic pressure trace.	212
7.6	NG+Diesel dual fuel combustion dynamic pressure trace.	212
7.7	NG+Diesel dual fuel combustion dynamic pressure trace.	213
7.8	NG+Diesel dual fuel combustion dynamic pressure trace.	213
7.9	NG+Diesel dual fuel combustion dynamic pressure trace.	214

7.10 NG+Diesel dual fuel combustion dynamic pressure trace.	214
7.11 NG+Diesel dual fuel combustion dynamic pressure trace.	215
7.12 NG+Diesel dual fuel combustion dynamic pressure trace.	215
7.13 NG+Diesel dual fuel combustion dynamic pressure trace.	216
7.14 NG+Diesel dual fuel combustion dynamic pressure trace.	216
7.15 NG+Diesel dual fuel combustion dynamic pressure trace.	217
7.16 NG+Diesel dual fuel combustion dynamic pressure trace.	217
7.17 NG+Diesel dual fuel combustion dynamic pressure trace.	218
7.18 NG+Diesel dual fuel combustion dynamic pressure trace.	218
7.19 NG+Diesel dual fuel combustion dynamic pressure trace.	219
7.20 NG+Diesel dual fuel combustion dynamic pressure trace.	219

Chapter 1

Introduction

NOMENCLATURE

a	empirical constant in combustion rate function,-.
c	empirical constant in combustion rate function,-.
d	empirical constant in combustion rate function,-.
\dot{E}	rate of internal energy,W,kW.
e	empirical constant in combustion rate function,-.
h_j	enthalpy of species j, J,kJ.
h	heat transfer coefficient, $W/m^2 K$.
LPG	liquified petroleum gas.
m	empirical constant in combustion rate function,-.
\dot{m}_j	mass flow rate of species j, kg.
MDM	multi-dimensional model.
NG	natural gas.
Nu	Nusselt number,-.
P	pressure, Pa,kPa.
Pr	Prandtl number,-.
PM	phenomenological model.
\dot{Q}	heat flow rate ,W,kW.
R	gas constant.
Re	Reynold number,-.
T	temperature, K, $^{\circ}C$.
TDC	top dead centre.
\dot{W}	work transfer rate in energy conservation equation,W,kW.
X_b	burned mass fraction, -.
ρ	density, kg/m^3 .
θ	crank angle,degree.

1.1 Origin of the Question –the Use of Gas in Large IC Engines

Energy crises and the increasing level of pollution of the environment have focused attention and financial resources towards a better understanding of the combustion process in engines as a means of improving fuel consumption and reducing exhaust emissions. In addition, considerable resources have been devoted to obtain suitable alternative fuels for IC engines. One of the most active fields is the substitution of gas for diesel oil. Use of a gaseous fuel in a diesel engine has many advantages, three important aspects being (1) Gas, particularly natural gas is a relatively abundant and low cost fuel; (2) The combustion of gas releases much less carbon dioxide than any other fuel; (3) The existing diesel engine can be adapted to operate with gas with relative ease. Several countries, including Australia, Canada, Holland, Italy and New Zealand, have large research programs on gas substitution for diesel oil. In Australia, at least \$5 million has been invested and 12 organizations have been involved [16].

Two methods of using gas in diesel engines are possible, these being total substitution by conversion to large spark ignition engines or partial substitution with the retention of distillate injection at a reduced level, basically for ignition purposes. The former is often referred to as an SI gas engine and the latter as a dual fuel diesel engine. The combustion process of dual fuel diesel engines is the subject of this thesis.

The dual fuel engine is a conventional diesel engine in which some of the energy release during combustion comes about from the combustion of a gaseous fuel such as natural gas (predominately methane) or liquified petroleum gas (predominately propane or butane) which the liquid diesel fuel ignites. During combustion, the gas provides most of the energy release but the distillate, through timed cylinder injection, provides the remaining part [1]. It has been shown that the dual fuel engine has, in principle, superior power producing characteristics to those of the conventional diesel engine, superior

emission characteristics, quieter and smoother operation, improved low ambient operation and reduced thermal loading. It also has superior operational characteristics to those of the corresponding SI gas engine because it offers superior control when accepting a much wider spectrum of fuels. It does not require the various changes in spark ignition timing needed in SI gas engines with changes in load and fuel and it has the ability to operate over a wide range of charge mixture strength thereby permitting quality control without resorting to throttling and its attendant deficiencies [158].

The SI gas engine is the preferred option for some countries for several reasons which are as follows: (1) compared to the dual fuel engine, it is easier to fuel with gas and (2) it does not need to carry two fuels simultaneously. However, the SI gas engine has some disadvantages in comparison with the corresponding dual fuel engine. These are: (1) The cost is high when conversion from diesel operation to SI gas is undertaken and reversion to diesel use if necessary is also difficult. Conversion of the diesel engine to dual fuel operation is of relatively low cost and the reversion, when needed, is easier; (2) The SI gas engine requires a low compression ratio (10.5 to 12.0 for liquified petroleum gas and about 15 maximum for natural gas) with low gas concentration to avoid auto ignition. Under these conditions, the flame ignited by the electronic spark takes a long time to propagate through the entire gaseous fuel. This may cause low efficiency and a high level of unburned fuel, particularly in a large engine. The dual fuel engine is able to operate on a much wider range of charge mixture strengths, the distillate pilot spray in the dual fuel engine providing larger ignition energy and a larger number of ignition nuclei than that of a spark thus enabling a better combustion of the gaseous fuel.

However, the dual fuel engine has its own disadvantages and some basic operating problems. These will be discussed in the next section.

1.2 Basic Operating Problems of Dual Fuel Engines

Dual fuelling a diesel engine is not a new concept, it having been used on a number of occasions over many decades when diesel oil is in short supply. A dual-fuelled diesel engine is operated on the following principles. Gaseous fuel is introduced to mix with the incoming air either by use of suitable carburettion equipment or by direct in-cylinder injection. The gas-air mixture is then compressed to just below its auto-ignition condition. Because the compression ratio is fixed, this dictates the maximum gas/air ratio which can be used. This compressed mixture is then ignited by the injection of pilot liquid fuel (usually as a conventional diesel oil spray) near the top dead centre position. The primary fuel is generally gaseous at atmospheric conditions and controls the power output. The pilot liquid fuel, which is injected through the conventional diesel injection equipment, may contribute substantially to the power but, to conserve petroleum stocks, it is desirable that it provides less than 10% of the maximum power output.

Although it has been shown that the dual fuelled engine has generally better operational characteristics than the corresponding conventional diesel engine and the spark ignition gas engine [158], the dual fuel diesel engine has its own basic operating problems. In particular, the dual fuel engine has relatively poor performance, low output efficiency and inferior emission characteristics at light load operation when compared to the corresponding diesel engine. The reason for this is that the flame is unable to propagate throughout and consume the fuel mixture due to it being either too lean and/or well below the effective flammability limit under the prevailing conditions. In addition, the maximum load and maximum substitution level of gas in a dual fuel engine are restricted by the engine knock limit because engine knock, which is mainly the end-gas auto-ignition knock similar to that in an SI engine but also the ignition delay type knock characteristic of diesel engines, occurs at high gas concentration and high compression ratio [10]. Furthermore, the combustion processes in a typical dual fuel engine tend to be complex as they are combinations of the problems

encountered in diesel and spark ignition engines.

1.3 General Research Background on Dual Fuel Engines

Dual fuel diesel engines have been investigated for a long time. The origin of the dual-fuel engine can be traced back to Dr Diesel himself who patented an engine running on essentially the dual-fuel principle [3], [4]. Work in the early stages of development was directly orientated towards the operational mode of the dual fuel engine. In 1951, Elliot and Davis [5] suggested that the poor efficiency at part load was probably due to the fact that at loads below a certain limit, part of the charge passed through the combustion process without apparently taking part in the combustion reaction. Moore and Lewis [6] confirmed that, at very weak mixtures it was most probable that only the portion of the charge directly in contact with the pilot spray was fully reacted. Part-load efficiency could be improved by increasing the pilot quantity thereby providing more ignition energy and ignition nuclei, by preheating the intake charge so that the temperature of the gas-air mixture is higher, and/or by throttling of the main air charge to obtain an effectively richer gas mixture for the same amount of gaseous fuel addition. Felt and Steel [7] suggested that the addition of lead alkyls to the main fuel was effective in retarding the onset of knock and that the loss of combustion control in the dual-fuel engine is similar to that of knock in spark ignition engines. Karim et al [4] investigated the phenomenon of uncontrolled combustion in a dual fuel engine and observed that, when running at weak mixtures the ignition delay was very large. They found that increasing the gaseous concentration led initially to a reduction of the ignition delay to a minimum after which a rapid increase in the delay occurred until the point of ignition failure was reached, as shown on Figure 1.1. They also found that increasing the temperature reduced the ignition delay. More recently, in an investigation of dual fuel engine operation under cold intake temperature conditions, Karim and Burn [8] suggested that the increase in dual-fuel ignition delay is due primarily to the kinetic role played by the gaseous fuel in the

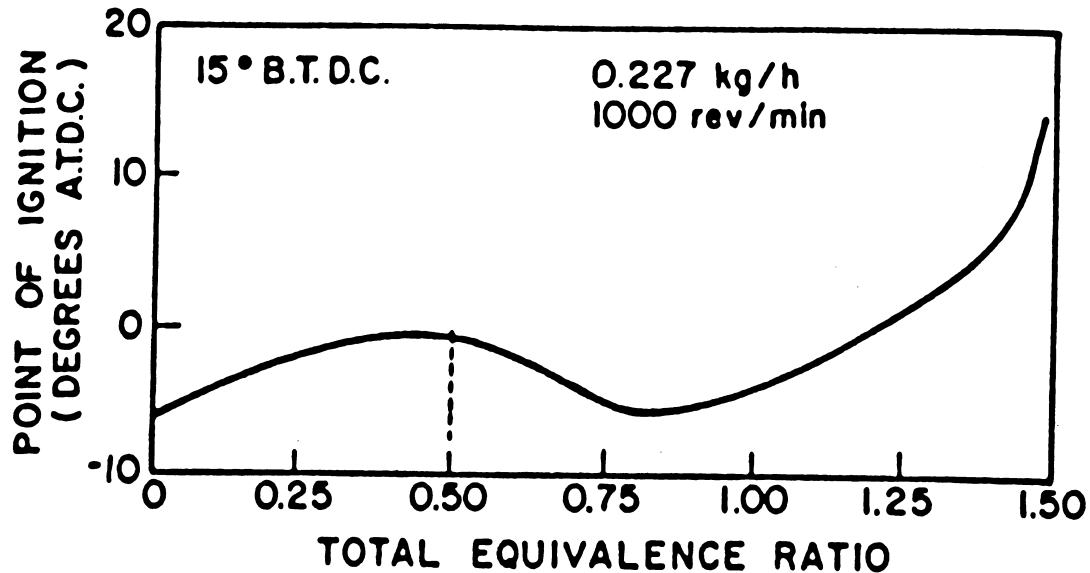


Figure 1.1: Typical variations of the ignition point of a dual fuel engine operating at constant speed and constant pilot quantity with methane. Reproduced from reference [154].

pre-ignition reactions of the pilot fuel. They also predicted that a substantial increase in the maximum power output could be obtained from the dual fuel engine when it is operating under cold intake temperature conditions. In a study of diesel oil, n-heptane, or cetane as the pilot fuels and hydrogen, carbon monoxide and methane as the gaseous fuels for a dual fuel engine test, Nielsen, Qvale and Sorenson [9] noted that several engine parameters affected dual-fuel ignition delay. In an investigation of small dual-fuel engine performance, Milton [10] investigated the maximum gas substitution of both NG and LPG. He observed that at the knock limit, the ignition delay with NG is greater than that with LPG. The addition of gas always resulted in an increase in the ignition delay, differing from Karim's observation [4]. That is, while there is general consensus that the ignition delay of the pilot fuel is altered by the addition of gas and that it usually increases, some difference exists regarding the details.

In relation to the modelling of the dual fuel combustion processes, few works have been reported. Thyagarajan and Gajendra Babu [11] applied a single zone (or zero-dimensional) model combined with an empirical spray model in order to build up a heat release model for dual fuel combustion. They then used this model to predict the operating parameters of a diesel-biogas dual-fuel DI engine.

Similarly, RafiqulIslam et al [12] calculated the heat release of a diesel-biogas IDI dual fuel engine by applying a single-zone heat release model which was originally developed for diesel engines. At a more detailed level, by evaluating and combining several single fuel reaction models, Nielsen and Sorenson [13] suggested a kinetic model to predict the increase of dual-fuel ignition delay until the point of ignition failure.

In spite of all these efforts, there are at least five areas where further clarification is needed [8],[14], both for application to an engine and for clarification of the fundamentals of the combustion process.

Those that are essentially related to application are:

- (1) The problem of knock in dual fuel engines;
- (2) The optimum use of diesel fuel in relation to the gaseous fuel;
- (3) The reduction of the emission of unburnt hydrocarbon and carbon monoxide under light load operation and oxides of nitrogen under high loads;

and to the fundamentals of combustion are:

- (4) The reaction between liquid and gaseous fuel and its affect on both the pre-ignition and post-ignition process;
- (5) The flame propagation in the gaseous fuel under different conditions of swirl, turbulence and distillate burning.

Moreover, very few reports are available on modelling of the combustion in dual fuel engines and no completely satisfactory model is yet available, This should be compared with the substantial development that has occurred in modelling the combustion in both spark ignition engines and compression ignition engines in recent years.

Hence, a further fundamental study of combustion in the dual fuel engine is required as a base for establishing a proper analytical model, having both application and academic value. This is the purpose of this thesis. Some background on modelling and on dual fuel combustion is presented in the next two sections.

1.4 Brief Review of the Modelling of In-cylinder Processes

Before attempting a model of the dual-fuelled combustion process, it is important to examine the models already available of IC engine combustion, both for spark ignition and compression ignition engines. To date, two distinct modelling approaches to in-cylinder processes are available, these being the Multi-dimensional model (MDM) and the Phenomenological Model (PM) [19]. The MDM attempts to solve conservation equations for mass, momentum, energy and species in several spatial dimensions and time for the evolution of in-cylinder flows, heat and mass transfer, and combustion. On the other hand, the PM describes complex engine processes in terms of separated, physically-based submodels. MDM and PM are briefly described in the following two subsections.

1.4.1 Multi-dimensional Models

Multi-dimensional models are also known as dimensional-based models. They are complete fluid-dynamic based models which include combustion phenomena. They can exist as one dimensional, two-dimensional and three-dimensional models.

As summarized by Heywood [19], the principal components of MDM are:

- Mathematical models or equations which are used to describe the flow processes. Of especial importance are the turbulence sub-models which

describe small-scale features.

- Discretization procedures which are used to transform the differential equations of the mathematical model into algebraic relations.
- Solution algorithms which are necessary to solve the algebraic equations.
- Computer codes which must be developed to actually perform the numerical algorithm and calculation. These must provide an easy interface for the input/output of information.

Some of these are dealt with in greater detail below.

Mathematical model: Besides the well known conservation equations of mass, energy, momentum and species, turbulence models are important because they provide a means of calculating the small-scale motion whose direct numerical solution from governing equations is still impractical because of the significant spatial and temporal variations that turbulent flows exhibit over a large range of scales.

There are two main approaches to turbulence modeling, these being full-field modelling (FFM), also known as statistical flux modeling (SFM), and Large-eddy simulation (LES).

FFM define the turbulence as the deviation of the flow at any instant from the average over many cycles of the flow at the same point in space and oscillation phase. These have been used by many researchers such as Gosman et al [29] who use phase averaging (or ensemble averaging) turbulent variables, Rubesin et al, [30], [31] who use mass-weighted (or Favre averaging) turbulent variables, Reynolds [30], who combined the ensemble and Favre averaging, and El Tahry [36], who applied the Reynolds stress model to engines. Much research has also carried out on investigating the turbulent stresses (also called Reynolds stress, as contained in Reynolds' momentum equations [30], [19]) . The most widely used model is the $k-\epsilon$ model [32], [33], [34], [35]. The $k-\epsilon$ model assumes a Newtonian relationship between the turbulent stresses and the mean strain rates, allowing

the turbulent viscosity appearing in this relationship to be computed from the local turbulent kinetic energy k and its dissipation rate ϵ .

Large-eddy simulation is a three-dimensional, time-dependent calculation of the large-scale turbulence [30], [19]. Differing from FFM, LES defines the turbulence in terms of variations about a local average. Thus turbulence in LES is always related to events in the current cycle. In LES, only the small eddies might be modelled, the large eddies being computed explicitly [37]. Clark et al [38] have performed some subgrid scale model evaluations. Kwak et al [39], Shaanan et al [40] and Mansour et al [41] studied LES in homogeneous isotropic turbulence. Mansour et al have studied LES applications in free-shear flows [42]. Amsden et al [43] and Bulter, et al [44] have applied LES in engine simulation. A number of fluid mechanics codes are now available which include the above features. The basic conservation equations may be incompressible or compressible from a range of available turbulence models. Typical examples are PHOENIX [160] and KIVA [161].

Discretization of Model Equations and Solution Algorithms: In order to apply the equations to an engine, appropriate configuration and solution mechanisms need to be determined. Cylindrical grid arrangements were employed in references [45], [46], [47], [67] for the restriction created by a cylindrical combustion chamber, while the more flexible “body-fitted” coordinate frame/grid also has been used by Butler et al [49] and Amsden et al [43].

It is common to use first-order upwind differencing for the convective transport terms and second-order central differencing for the diffusive terms. Blending the first-order upwind and use of a higher-order approximation to delineate the “higher-order” overshoots also has been applied [36], [50]. However, it has been found that true mesh-independent solutions could not be achieved even with densities of up to 50 nodes in each coordinate direction [71].

First-order temporal discretization of the transport equations differ in

forward differencing (leading to implicit discrete equations) and backward differencing (leading to explicit discrete equations). When these numerical methods are applied to compressible flows in internal combustion engines, it is usually inefficient at low Mach number because of the wide disparity between the time scales associated with the convection and with the propagation of sound waves. One procedure used is semi-implicit. That is, all terms in the governing equation that are not associated with sound waves are explicitly advanced with a larger time step Δt similar to that used with implicit methods, while terms associated with acoustic waves (the compression terms in the continuity and energy equations and the pressure gradient in the momentum equation) are explicitly advanced using a small time step δt that satisfies the sound-speed stability criterion, and of which the main time step is an integral multiple. This is also called the acoustic subcycling method. It works well at Mach numbers which are not too low, but is not suitable when Mach numbers tend towards zero because the number of subcycles ($\Delta t/\delta t$) then tends to infinity. In applications, this is when $\Delta t/\delta t$ is greater than 50 [19]. Under this situation, the Mach number has to be increased artificially by multiplying the pressure gradient in the momentum equation by a time-dependent scaling factor $1/\alpha(t)^2$, where $\alpha(t) > 1$ [43].

Application of the One-dimensional Model : The most frequently used MDM in engine design processes is the one-dimensional model of flow in the intake and exhaust system. In combustion research, Sirignano [51] proposed the first one-dimensional model of spark-ignition engines with a planar flame propagation. This assumed that the bore-to-stroke ratio is much smaller than unity and the primary direction of flame propagation is axial. Westbrook [52] used a one-dimensional planar model to study flame propagation in homogeneous and stratified-charge engines. Singh and Surakomol [53] developed a one-dimensional cylindrical flame propagation model to analyze the heat release rate in spark ignition engines. One-dimensional models including the $k-\epsilon$ turbulence model have also been applied to calculate the heat transfer losses through cylinder walls [54], nitric oxide formation in homogeneous and stratified charge spark ignition engines [55], and to study flame quenching processes in

spark ignition engines [58]. One-dimensional models have also been used to analyze two-phase flows in diesel engines [56], and to study the dynamics of flow processes in the induction and exhaust systems [57]. They have also been applied in rotary engine modelling [59], [60].

Application of the Two (or more) Dimensional Model : For SI engines, two or three dimensional MDM have been applied to analyze turbulent flame structure and propagation [61], [62], [63], [70], [72], to predict heat release and pressure as a function of the engine load and rpm [64], [65], and to predict the flow field [66], [67], [68], [69]. For diesel engines, MDM is mostly applied to the analysis of the flow field [79], [80], [73], [81], spray modeling [82], [74], [75] and vaporization of liquid fuel [76], [77], [78]. Models for combustion and heat transfer have also been reported [80], [83].

1.4.2 Brief Review of the Phenomenological Model (PM)

Only a brief general description of phenomenological models for internal combustion engines is presented here. More detailed and comprehensive literature reviews about the modeling of engine combustion are presented in Chapters 3, 5 and 7. Phenomenological models (PM), also known as thermodynamic-based models, have been used extensively in the analysis of engine design and operating philosophies. The structure of a typical PM has been described as shown on Figure 1.2 by Blumberg et al [84].

Common Assumptions, As reviewed by Blumberg et al [84], most of the PM have used the following common assumptions:

- *Combustion rate* is specified by some functional relationship for the zero-dimensional model where the start of combustion θ_s , the combustion duration $\Delta\theta_c$ and the current crank angle are related. Two examples of such function are the cosine burning law

$$\frac{dX_b}{d\theta} = \frac{\pi}{2\Delta\theta_c} \cdot \sin\left[\pi\left(\frac{\theta - \theta_s}{\Delta\theta_c}\right)\right]$$

and the Wiebe function

$$\frac{dX_b}{d\theta} = a(m+1)\left(\frac{\theta - \theta_s}{\Delta\theta_c}\right)^m \exp\left[-a\left(\frac{\theta - \theta_s}{\Delta\theta_c}\right)^{m+1}\right]$$

Combustion rate can also be obtained by solving the equations of the quasi-dimensional model.

- *Gas properties* can be specified by use of curve-fitted data on fuel vapour, air and burned products or by a combination of curve-fitting and approximations to thermodynamic equilibrium calculations. In calculating the properties of a mixture, the individual gases are modeled as ideal gases.
- *Heat transfer* Heat transfer in reciprocating IC engines is generally modeled using the Nusselt-Reynolds number correlation

$$N_u = cR_e^d Pr^e$$

which is derived for heat transfer in steady turbulent non-reacting flows over pipes and plates. Here c, d, e are empirical constants. Typically, $d = 0.8$, $Pr^e = 1$ and $c = 0.023$. Heat transfer is assumed not to occur across the flame front during combustion.

- *Mass flow past valves and orifices* are modeled by the equation for adiabatic isentropic flow through a nozzle. A discharge coefficient is used to yield the effective area for the particular constriction.
- *Nitric oxide calculations* are performed using the extended Zeldovich kinetic scheme.
- *Pipe dynamics* are calculated in some multicylinder spark- ignition and diesel engine simulation by solving the one-dimensional, unsteady gas dynamic equations.
- *Governing equations:* The primary equations governing the system are

[1] the first law of thermodynamics for an open system

$$\dot{E} = \sum_j h_j \dot{m}_j - \dot{Q} - \dot{W}$$

[2] the equation of state

$$P = \rho RT$$

[3] the momentum equation which is satisfied by assuming the pressure is uniform within each open system.

PM Application in SI Engine Simulation: Phenomenological models have been applied in predicting NO_x formation [20], [86], [87], [88], [89], [90]; fuel economy and engine performance [85], [95], [94]; CO formation [91], [92], [93]; burning rate modeling [96], [97], [98], [125], and [126] ; heat transfer [99], [100]; hydrocarbon emission [101], [100]; and engine knock [102], [103].

PM Application in Stratified Charge Engines: Here only a brief review will be given for the open chamber stratified charge engines since the divided chamber engine is less related to this research.

Because of the complex nature of stratified charge operation, most of the PM models heavily rely on simple formulations of fairly complex phenomena. Two typical examples are: (1) the Texaco Controlled Combustion System (TCCS) [104], in which the entire combustion process is described as consisting of a rapid combustion coinciding with the injection rate, plus a diffusive combustion controlled by air entrainment into the burned gas plume. A submodel for fuel spray and a submodel for plume entrainment have been applied. (2) the Ford Programmed Combustion Engine (PROCO), for which, PM have been applied to study the NO_x , and CO formation.

PM Application in Diesel Engine Simulation: The early practice of phenomenological modelling were usually zero-dimensional. Engine performance was studied by utilizing empirical heat release rates obtained from experimental pressure traces [105], [106], [107], [108], [109], [110]. More recently, many quasi- dimensional models have been developed where some dimensional factors are introduced into sub-models. Those quasi-dimensional models, which relieve some unrealistic assumptions such as those of homogeneous dispersion during fuel injection, have been applied for both combustion modelling [108]

,[111], [112], [113], [114], [115] and emission modelling [116], [117], [118], [119], [120].

1.4.3 MDM vs PM

Compared to phenomenological models, dimensional-based models have the advantage of being capable of providing detailed information of the spatial and temporal variation of the velocity, temperature and pressure field in one, two or three dimensions. However, MDM require much more computing effort than do PM. This disadvantage limits their application in entire engine simulation. On the other hand, phenomenological modelling requires less computing effort because it describes complex engine processes in term of separated physically-based sub-models, which very often are empirical correlations. Thus, PM have been commonly used for calculation of engine performance particularly in entire engine simulation. Because of the complexity of dual fuel combustion, the author of this thesis chose the PM approach rather than the MDM for this research because the time and effort required for developing a MDM of dual fuel engine combustion is unwarranted at this stage of development.

1.5 Some Typical Experimental Research on Dual Fuel Engine Combustion

As has been described previously, most of the dual fuel combustion research has been orientated directly towards the operational mode of engines.

In 1967, Karim et al investigated experimentally the knock-free limit of dual fuel engine operating parameters experimentally [4]. Their experimental apparatus was a four stroke, single-cylinder direct-injection Gardner engine of $4\frac{1}{4}$ in. bore and 6 in. stroke. Experiments were conducted at compression ratios of 14.2:1 and 11.6:1, respectively. Common gaseous fuels including methane, propane, ethylene, acetylene, hydrogen and some of their mixtures were used. They studied the effects of gas concentration, pilot injection quantity, injection

timing, swirl, the cetane number of the fuel and intake temperature on the onset of engine knock and ignition delay. They found that the ignition properties of the pilot fuel have relatively little effect in determining the onset of knock, compared with that of the main primary gas fuel. They also observed that the behaviour of all the hydrocarbon fuels used and their mixtures follow a similar consistent pattern. They believed that the knock in dual fuel engines is predominantly of an auto-ignition nature in the gaseous charges.

The same Gardiner diesel engine was also used by Karim et al [8] for the investigation of dual fuel engine performance and exhaust emissions under cold intake temperature condition. They observed that the extent of the increase in ignition delay is extremely sensitive to the intake temperature of the mixture. A very low intake temperature with small pilot quantities produced erratic running and led to ignition failure, particularly at very low loads. One of their important observations was that dual fuel operation tended to increase the maximum brake power available from normal diesel operation for the same overall fuel-air ratio. This indicates that potentially more power can be produced from the dual fuel system with the same cylinder size. They also observed that the concentration of carbon monoxide and unburned gaseous fuel in the exhaust showed a slight increase over the diesel for low load dual fuel operation, but were much lower at high loads. NO_x emissions also decreased substantially at cold intake temperatures. They also observed that cold intake temperatures suppressed the tendency of the engine to knock. It is therefore believed that the maximum power output can be increased with cold intake temperatures.

Milton investigated the dual fueling performance of a four stroke, 4-cylinder IDI Perkins diesel engine of 92.0 mm bore, 101.6 mm stroke [10]. NG and LPG were used as primary gaseous fuels, maximum gas proportion being measured under the limit of either engine knock, excessive unburned HC levels in exhaust, or engine stumble or misfire. He observed that injection advance was able to increase the engine efficiency over most of the speed range (600 - 3600 rpm) with up to about 6° of advance providing continuing improvement with natural gas. He also found that gas substitution levels can be improved by reducing the compression ratio. However, this was offset by a reduction in efficiency.

Some researchers have used a dual fuel engine to investigate the dual fuel ignition delay [9], [154]. However, no satisfactory formula has been achieved for its calculation because of the complex nature of dual fuel ignition. These papers are reviewed in detail in Chapter 6.

As can be seen from the aforementioned research activities, information obtained from engine experiments has usually been directly related to the operating parameters of an engine. In many cases, the information is also strictly restricted to a particular engine configuration. Because it is extremely difficult to fully control each parameter separately and to measure them precisely during engine operation, it is important to resort to devices other than the actual engine for combustion research. As has happened in SI and CI engine research, the high-pressure constant-volume combustion bomb is a useful tool, particularly for the research of in-cylinder processes. Much knowledge of flame propagation in SI engine cylinders and of spray motion and ignition delay in diesel engines, has been obtained from extensive combustion bomb experiments. Later chapters in this thesis will show how the experiments carried out in a constant volume combustion bomb are used in developing an analytical model for diesel combustion and dual fuel combustion, respectively.

1.6 Objectives and Structure of This Research

The main purpose of this research is establishing a phenomenological model for dual-fuel combustion, in order to study the optimization/minimization of diesel fuel usage in the dual-fuel diesel engine. In order to achieve this purpose, the project is divided into several sub-tasks and this thesis is arranged and structured according to those sub-tasks as follows:

(1) A thermodynamic-thermochemical sub-model for in-cylinder dual-fuel combustion will be developed. This is the cornerstone of a combustion model and is described in detail in chapter 2.

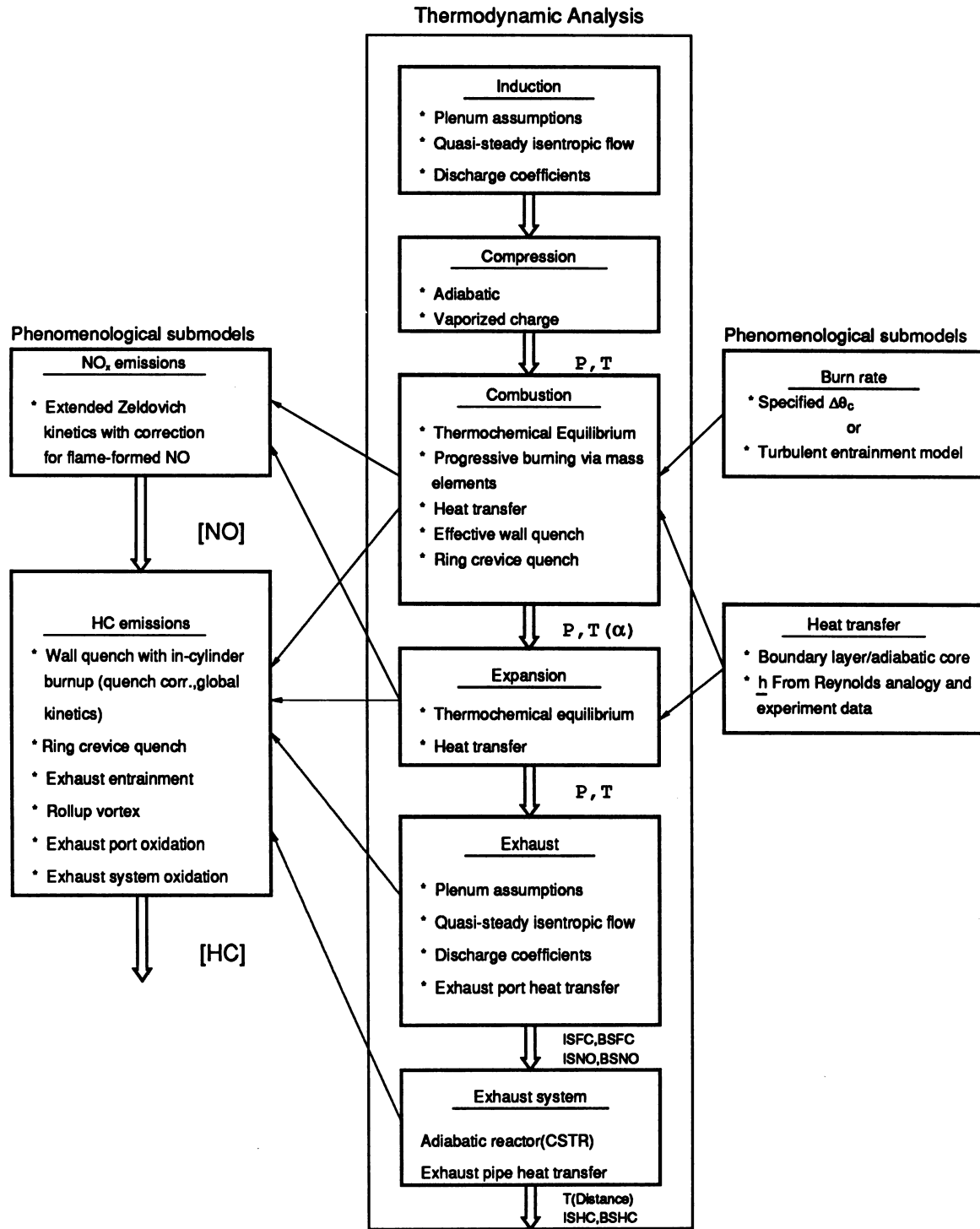
(2) This research features dual fuel combustion which is essentially that of a

homogeneous gas-air mixture ignited by a injected pilot liquid fuel. Therefore, the gas-liquid dual fuel combustion would be expected to exhibit features both from the SI type combustion, which is essentially homogeneous, and CI type combustion, which is essentially heterogeneous. Modelling the flame propagation of SI engine combustion is therefore investigated in chapter 3, and modelling of diesel engine combustion in chapter 5.

(3) In order to obtain experimental validation of the model, a constant volume dual-fuel combustion bomb has been developed and experiments have been carried out. The experimental setup and procedure are described in Chapter 4. Experiments have been carried out for both sole diesel fuel and diesel-gas dual fuel respectively. The experimental results of diesel combustion are analyzed in Chapter 5 and the results of dual fuel combustion in Chapter 6. Special effort has been made in studying the dual fuel ignition condition, ignition delay and its affect on later combustion. The analytical model of diesel-gas dual fuel combustion is developed in Chapter 7. Computational results are also presented in comparison with measured data from the combustion bomb.

(4) The conclusions and discussion of the research are summarized in chapter 8. Problems for further study are also discussed.

Figure 1.2: Schema of the Structure of a Typical Phenomenological Model



Structure of Ford Research Homogeneous Charge Conventional Engine Simulation

Chapter 2

The Thermodynamic-thermochemical Sub-model of In-cylinder Combustion

NOMENCLATURE

Symbols:

a empirical constant in the polynomial function for the enthalpy of non-fuel species,-.

A_f empirical constant in the polynomial function for enthalpy of fuel,-.

c_m linear regression coefficient for enthalpy, J/K/kg, kJ/K/kg.

e specific internal energy, J/kg, kJ/kg.

E total internal energy, J, kJ.

\tilde{h} dimensionless enthalpy for non-fuel species in the polynomial approximation,-.

\tilde{h}_f enthalpy of fuel species in the polynomial approximation, J, kJ.

h_j specific enthalpy of a species j , J/kg, kJ/kg.

h_m linear regression coefficient for enthalpy, J/kg, kJ/kg.

h_f^0 enthalpy of formation at the standard state of 1 atm.

m mass, kg.

n molar number of ideal gas, -.

p partial pressure, bar, Pa, kPa.

P pressure, bar, Pa, kPa.
 P fictitious pressure.
 Q heat flow, J, kJ.
 R_j gas constant for species j .
 \tilde{R} universal gas constant.
 T temperature, K, °C.
 V Volume, m^3 .
 v specific volume, m^3/kg .
 \bar{v} average specific volume, m^3/kg .
 W work, J, kJ.
 X_j mass fraction of species j in an ideal gas mixture, kg/kg.
 x_b burned mass fraction, kg/kg.

Subscripts:

0 initial state
 b burned zone
 m modelling coefficient, -
 u unburned zone state

Superscripts:

0 standard state of 1 atmosphere.

2.1 Introduction

The in-cylinder combustion in an internal combustion engine is a complex process and includes phenomena such as subsonic fluid flow, turbulent transport of mass, momentum, and energy, wall heat transfer, turbulent flame propagation and quenching, pollutant formation, and some times, fuel spray dynamics. Phenomenological models (PM) describe this complex engine behaviour in terms

of separated, physically-based submodels. The thermodynamic-thermochemical sub-model is the cornerstone of it. For this, many thermodynamic analytical models have been proposed as summarized by Blumberg et al [84] and Heywood [18]. Two successful approaches have been described by Heywood [19], these being a fully mixed model and an unmixed model. The fully mixed model assumes that the burned gas is uniform. The unmixed model, which is sometimes more accurate but which requires more calculations, assumes that no mixing occurs between gas elements that burn at different times and that each burned gas element is therefore separately, adiabatically compressed. These are the two extremes. The reality is somewhere in between. The fully-mixed model has been commonly used by many researchers in various applications [20], [97], [122], [159], and it has been shown that the fully-mixed model can provide sufficient accuracy for engine combustion calculations. The fully-mixed model is therefore used in this thesis.

2.2 Tanaka's Thermodynamic Calculation

Tanaka has developed a computing code for combustion calculations which can perform the thermodynamic calculation for some 26 gaseous and liquid fuels. The assumptions on which the program is based are described in reference [159]. Briefly, these are: (1) The gas in the vessel under consideration is divided into a burned zone and an unburned zone by an infinitesimally thin flame front. (2) The vessel volume and the mass of gas in the vessel remain unchanged during combustion. The pressure is uniform at any instant. (3) The First Law of Thermodynamics and the Equation of State for a perfect gas are used to estimate variations in the regionally averaged quantities of the gas states in the burned and unburned zone gases, respectively. (4) The composition of unburned gas is frozen while the burned gas is assumed to be always in chemical equilibrium. It includes 12 species, these being O_2 , N_2 , H_2O , CO_2 , CO , H_2 , OH , NO , O , H , C , and N . (5) There is no heat transfer and mass exchange between the unburned zone and the burned zone. The unburned zone gas undergoes an isentropic compression.

Most of these assumptions are used in the thermodynamic-thermochemical sub-model of this thesis, with minor modifications as described in the next section. Computing results of the present thermodynamic-thermochemical model are compared with those calculated by Tanaka's program in a later section.

2.3 Thermodynamic Model, Fully-mixed Assumption

2.3.1 Main Assumptions

The fully-mixed model used in this study is established using the following main assumptions:

- (1) At the temperature and densities in an internal combustion engine, it is a reasonable first approximation to assume that the volume of the reaction zone is negligible and that the mixture within a combustion vessel (that is, a cylinder or combustion bomb) consists of a burned fraction in thermodynamic equilibrium plus an unburned zone frozen at its original composition [20].
- (2) The total combustion duration occurs in such a short time that the volume of the combustion vessel is considered to remain constant during the combustion. It is also assumed that there is no heat loss, and that the pressure is uniform throughout the vessel during the entire combustion period.
- (3) The total mass of the fuel/air mixture in the vessel remains unchanged while burning.
- (4) Gases in the burned and unburned zones are both considered to be mixtures of different ideal gases with constant specific heats [20], [19]
- (5) It is also assumed that there is no heat transfer between the burned zone and the unburned zone. Therefore, while combustion is in progress, gases

in the unburned zone are compressed adiabatically.

This is similar to Tanaka's model but differs in the calculations of the enthalpies of the species and the equilibrium system of the burned zone gases. Tanaka used discrete data in computing the enthalpies for the energy balance while the current model uses linear and polynomial approximations as described later. Tanaka's model considered the burned zone gases as a 12 species equilibrium system while the current model uses Strehlow's model [24] which considers the products of combustion to be a 14 species system. This calculation is also described in a later section.

2.3.2 Model Equations

The equations are based on the principles of conservation of mass and energy and the ideal gas law. Also, internal energy is evaluated by a simple function of temperature. Compression of burned and unburned gases is assumed to occur adiabatically. The equations are as follows:

(1) Ideal Gas Law

$$Pv_i = R_i T_i; \quad i = 0, u, b \quad (2.1)$$

where subscripts 0, u, b stand for the initial state, the unburned zone and burned zone state, respectively.

(2) Internal Energy of Ideal Gases

For an ideal gaseous mixture,

$$e(T) = h(T) - RT \quad (2.2)$$

where e is the internal energy and h is the enthalpy. Internal energy and enthalpy are pressure independent, that is

$$h(T) = [h^0(T) - h^0(298)] + h_f^0$$

where superscript ⁰ stands the standard state pressure of 1 atmosphere. Values of standard enthalpies $h^0(T)$, $h^0(298)$, and h_f^0 can be obtained from thermodynamic property tables such as those given in [21].

Use is made here of a linear temperature function to approximate the value of $h^0(T) - h^0(298)$ for the burned zone, that is

$$h^0(T_b) - h^0(298) = c_m T + h_m,$$

then

$$h(T_b) = c_m T_b + [h_m + h_f^0] \quad (2.3)$$

Here, c_m and h_m are linear regression coefficients. Physically, c_m is an equivalent specific heat over a particular temperature change interval (1000° C -3000° C for the present study) while h_m is the enthalpy at the lower temperature. Details of the linear regression used and values of c_m , h_m , are given in Appendix A.

Polynomial functions [26], [27] are used to approximate the value of $h^0(T) - h^0(298)$ for the initial state and the unburned zone. For non-fuel species, the polynomial function being commonly used [26], [27], [19] is as followed,

$$\frac{\tilde{h}}{\tilde{R}T} = a_1 + \frac{a_2}{2}T + \frac{a_3}{3}T^2 + \frac{a_4}{4}T^3 + \frac{a_5}{5}T^4 + \frac{a_6}{T} \quad (2.4)$$

For fuel species, the polynomial function chosen has the format

$$\tilde{h}_f = A_{f1}t + A_{f2}\frac{t^2}{2} + A_{f3}\frac{t^3}{3} + A_{f4}\frac{t^4}{4} - \frac{A_{f5}}{t} + A_{f6} + A_{f8} \quad (2.5)$$

In both equation 2.4 and 2.5, $t=T(K)/1000$. Values of a_i and A_{fi} are listed in Appendix A.

Once $h(T) - h(298)$ for all species in the initial state, burned zone and unburned zone are calculated, the internal energy of the ideal gas can be calculated by applying equation 2.2,

$$e_0 = \sum_O X_i [h_{fi}^0 + h_i(T_0) - h_i(298) - R_i T_0] \quad (2.6)$$

$$e_u = \sum_U X_i [h_{fi}^0 + h_i(T_0) - h_i(298) - R_i T_0] \quad (2.7)$$

and

$$e_b = \sum_b X_i [h_{fi}^0 + c_{mi} T_b + h_{mi} - R_i T_b] \quad (2.8)$$

(3) Conservation of mass:

$$\frac{V_0}{m_0} = \int_0^{x_b} v_b dx + \int_{x_b}^1 v_u dx \quad (2.9)$$

where x_b is the burned mass fraction at a given instant. The above equation also can be written as

$$\bar{v}_0 = x_b \bar{v}_b + (1 - x_b) \bar{v}_u \quad (2.10)$$

where

$$\bar{v}_b = \int_0^{x_b} v_b dx / x_b$$

and

$$\bar{v}_u = \int_{x_b}^1 v_u dx / (1 - x_b)$$

(4) Conservation of energy (First Law of Thermodynamics):

$$\frac{E_0 - W - Q}{m_0} = \int_0^{x_b} e_b dx + \int_{x_b}^1 e_u dx$$

or

$$e_0(T_0) - \frac{W}{m_0} - \frac{Q}{m_0} = x_b e_b(T_b) + (1 - x_b) e_u(T_u) \quad (2.11)$$

(5) Adiabatic compression of unburned gases:

$$T_u = T_0 \left(\frac{P}{P_0} \right)^{(\gamma_u - 1)/\gamma_u} \quad (2.12)$$

where $\gamma_u = c_{pu}/c_{vu}$

Therefore, by substituting \bar{v}_0 , \bar{v}_b , \bar{v}_u from eq 2.1 into eq 2.10, eq 2.10 becomes

$$\frac{R_0 T_0}{P_0} = (1 - x_b) \frac{R_u T_u}{P} + x_b \frac{R_b T_b}{P} \quad (2.13)$$

Substituting e_b into eq 2.11 by use of eq 2.8 and rearranging gives:

$$x_b (h_{mb} + h_{fb}^0 - e_u) + x_b T_b (c_{mb} - R_b) = e_0 - e_u - \frac{Q + W}{m_0} \quad (2.14)$$

where

$$h_{mb} = \sum_b X_b h_{mb}$$

$$c_{mb} = \sum_b X_b c_{mb}$$

The above equations use kmol as the base.

Once the expression for the work W and the heat transfer Q are given, x_b , T_b , and T_u can be solved from eq 2.12, eq 2.13, and eq 2.14 as functions of pressure P . A simple case is when $W = 0$ and $Q = 0$. This can be considered as the condition for an adiabatic combustion bomb. Some sample calculation results are presented in the last section of this chapter for this case.

2.4 Chemical Equilibrium and Dissociation in Engine Combustion

2.4.1 Brief review

The equilibrium composition of a mixture varies with temperature even if no reaction occurs. There are at least two reasons for making equilibrium mixture calculations. (1) Under the conditions prevailing in the combustion chamber, dissociation of the products affects the flame temperature and other thermodynamic functions substantially. (2) The chemical nature of the products of combustion is affected and needs examination.

The assumption that the mixture is always in equilibrium is not valid in the expansion and exhaust process, nor is it in the pollutant formation processes, because the time available may not be sufficient for all substances to reach equilibrium. However, a good approximation for performance estimations can still be provided by regarding the combustion product mixture as being in chemical equilibrium throughout [19] [22]. The working fluid of an internal combustion engine can usually be regarded as being made up of a hydrogen

+ carbon + oxygen + nitrogen (HCON) system without carbon deposition. Also the equilibrium mixture can be considered as being composed of either six species, ten species, 12 or more species, depending on the desired accuracy [22]. Standardized computer methods for this calculation have been developed, typical examples being the NASA program [27] and Strehlow's program [24]. This research applies Strehlow's program for calculation of the chemical equilibrium composition.

2.4.2 Strehlow's calculation program and Weinberg's Rapid Convergent method

Chemical equilibrium calculations for a large number of species is normally very time consuming. However, there are techniques which can minimize that calculation problem, the best known being that of Strehlow [24]. Strehlow's calculation, based on a technique described by Weinberg [25], regards the equilibrium mixture as consisting of 14 species: H_2 , O_2 , H_2O , CO , CO_2 , OH , H , O , N_2 , N , NO , NO_2 , CH_4 , and I . Here I is an inert species such as argon.

A 'fictitious pressure', P , of the elements is defined. This is the partial pressures that the elementary constituents would attain if they were present as monatomic gases. For example, for methane (CH_4) as a fuel, this can be expressed as:

Carbon:

$$\mathcal{P}_C \equiv p_{CO_2} + p_{CO} + p_{CH_4}$$

Oxygen:

$$\mathcal{P}_O \equiv 2p_{O_2} + 2p_{CO_2} + p_{CO} + p_{H_2O} + p_{OH} + p_{NO} + 2p_{NO_2} + p_O$$

Hydrogen:

$$\mathcal{P}_H \equiv 2p_{H_2} + 2p_{OH} + p_H + 4p_{CH_4}$$

Nitrogen:

$$\mathcal{P}_N \equiv 2p_{N_2} + p_{NO} + p_{NO_2} + p_N$$

Inert species:

$$\mathcal{P}_I \equiv p_I$$

The following four equations can then be obtained as ratios.

$$RCO \equiv \frac{n_c}{n_o} = \frac{\mathcal{P}_c}{\mathcal{P}_o} \quad (2.15)$$

$$RHO \equiv \frac{n_H}{n_o} = \frac{\mathcal{P}_H}{\mathcal{P}_o} \quad (2.16)$$

$$RNO \equiv \frac{n_N}{n_o} = \frac{\mathcal{P}_N}{\mathcal{P}_o} \quad (2.17)$$

$$RIO \equiv \frac{n_I}{n_o} = \frac{\mathcal{P}_I}{\mathcal{P}_o} \quad (2.18)$$

Additional independent equilibrium equations are then added (9 having been arbitrarily chosen here):

(1) Carbon dioxide dissociation: $CO_2 \rightleftharpoons CO + \frac{1}{2}O_2$

$$K_{p1} = \frac{p_{CO} \cdot p_{O_2}^{1/2}}{p_{CO_2}} \quad (2.19)$$

(2) The dissociation of water: $H_2O \rightleftharpoons H_2 + \frac{1}{2}O_2$

$$K_{p2} = \frac{p_{H_2} \cdot p_{O_2}^{1/2}}{p_{H_2O}} \quad (2.20)$$

(3) The formation of the hydroxyl radical: $H_2O \rightleftharpoons \frac{1}{2}H_2 + OH$

$$K_{p3} = \frac{p_{H_2}^{1/2} \cdot p_{OH}}{p_{H_2O}} \quad (2.21)$$

(4) The dissociation of hydrogen: $\frac{1}{2}H_2 \rightleftharpoons H$

$$K_{p4} = \frac{p_H}{p_{H_2}^{1/2}} \quad (2.22)$$

(5) The dissociation of oxygen: $\frac{1}{2}O_2 \rightleftharpoons O$

$$K_{p5} = \frac{p_O}{p_{O_2}^{1/2}} \quad (2.23)$$

(6) The formation of methane : $4H_2 + CO_2 \rightleftharpoons CH_4 + 2H_2O$

$$K_{p6} = \frac{p_{CH_4} \cdot p_{H_2O}^2}{p_{H_2}^4 \cdot p_{CO_2}} \quad (2.24)$$

(7) The formation of nitrogen atoms: $\frac{1}{2}N_2 \rightleftharpoons N$

$$K_{p7} = \frac{p_N}{p_{N_2}^{1/2}} \quad (2.25)$$

(8) The formation of nitric oxide: $\frac{1}{2}N_2 + \frac{1}{2}O_2 \rightleftharpoons NO$

$$K_{p8} = \frac{p_{NO}}{p_{N_2}^{1/2} \cdot p_{O_2}^{1/2}} \quad (2.26)$$

(9) The formation of nitrogen dioxide: $\frac{1}{2}N_2 + O_2 \rightleftharpoons NO_2$

$$K_{p9} = \frac{p_{NO_2}}{p_{N_2}^{1/2} p_{O_2}} \quad (2.27)$$

A final equation is then obtained from the partial pressure, this being

$$P = \sum_{i=1}^s p_i \quad (2.28)$$

where P is the specified pressure of the system and p_i the partial pressures.

The 14 unknown partial pressures can be solved from the set of equations eq 2.15 to eq 2.28.

A FORTRAN program developed by Strehlow[24] has been tested and has been found to converge over the range

$$700 \leq T \leq 4700K, \quad 25KPa \leq P \leq 1MPa$$

$$3.76 \leq RNO \leq 0.00001; \quad 0.3 \leq \phi \leq 2.0$$

$$10^{-2} \leq RHC \leq 10^{+2};$$

2.5 Samples of the model's predicted result

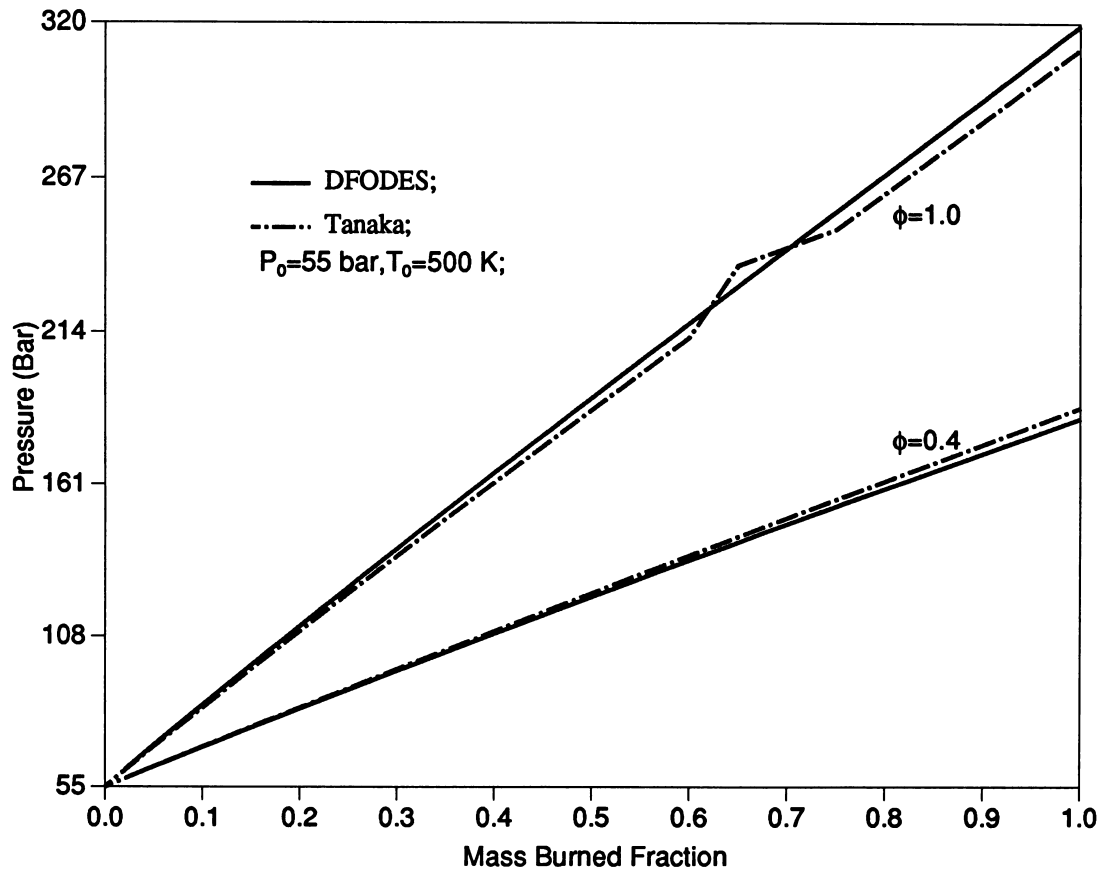


Figure 2.1: Predicted Combustion Results for fuel $CH_4(G)$

The computational model described above is here called DFODES. Figures Fig 2.1 to Fig 2.6 present some sample computational results of DFODES which are compared with the results predicted by Tanaka's model in which all

assumptions are the same as in this research except that Tanaka used (1) tabular enthalpy data, and, (2) a 12 species HCON chemical equilibrium system. In all these numerical tests, the computations were found to converge even beyond the original WEIN's pressure and equivalence ratio convergent ranges, that is: $25\text{KPa} \leq P \leq 1\text{MPa}$ and $0.3 \leq \phi \leq 2.0$. In Fig 2.4, the results of DFODES were based on a fuel $C_{10.8}H_{18.7}(L)$ while those of Tanaka were based on $C_{12}H_{26}(L)$. In Fig 2.5, pressure profiles calculated by DFODES and Tanaka are almost identical in the range of $\phi = 0.4$ to $\phi = 1.0$.

During the numerical testing, it was found that Tanaka's program can only run well when the equivalent fuel-air ratio is not less than a limit at about 0.4. That is, $\phi > 0.4$, for those fuels of interest to this research such as $CH_4(G)$, and $C_3H_8(G)$. DFODES does not have this limit and provides very close results within the Tanaka program's working range despite the fact that DFODES is mathematically simpler and requires less CPU time. Also, DFODES has a structure which allows it to be easily incorporated into engine calculations. DFODES was therefore chosen for further work in this research.

It is noted that there are some discrepancies between the two burned zone temperatures obtained from Tanaka's program and DFODES, particularly at high fuel-air equivalence ratios. This is believed to be mainly caused by the different methods of Tanaka and DFODES in calculating the enthalpies of fuels. A higher value of ϕ means that more fuel is being used. This leads to a bigger difference between the enthalpy value of the two calculations, and therefore also to the temperatures. In addition, the two different equilibrium assumptions (12 species in Tanaka's calculation and 14 species in DFODES) contribute somewhat to further differences in the predicted burned zone temperatures.

Fig. 2.7, 2.8, and 2.9 present the maximum combustion pressure calculated by DFODES at various initial conditions of P_0 , ϕ , and T_0 for gaseous fuels CH_4 and C_3H_8 . It is noted that an increase in P_0 and ϕ leads to a linear increase in the maximum combustion pressure. However, increase in T_0 leads to a decrease in the maximum combustion pressure. This is because the increase in

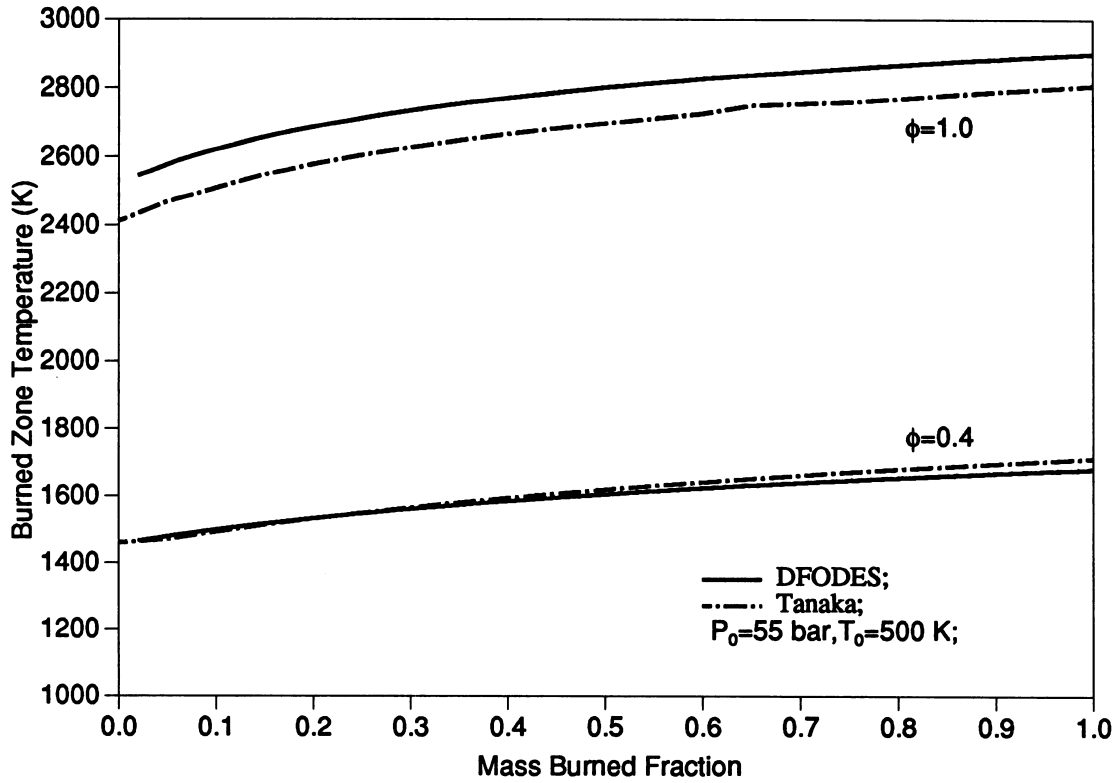


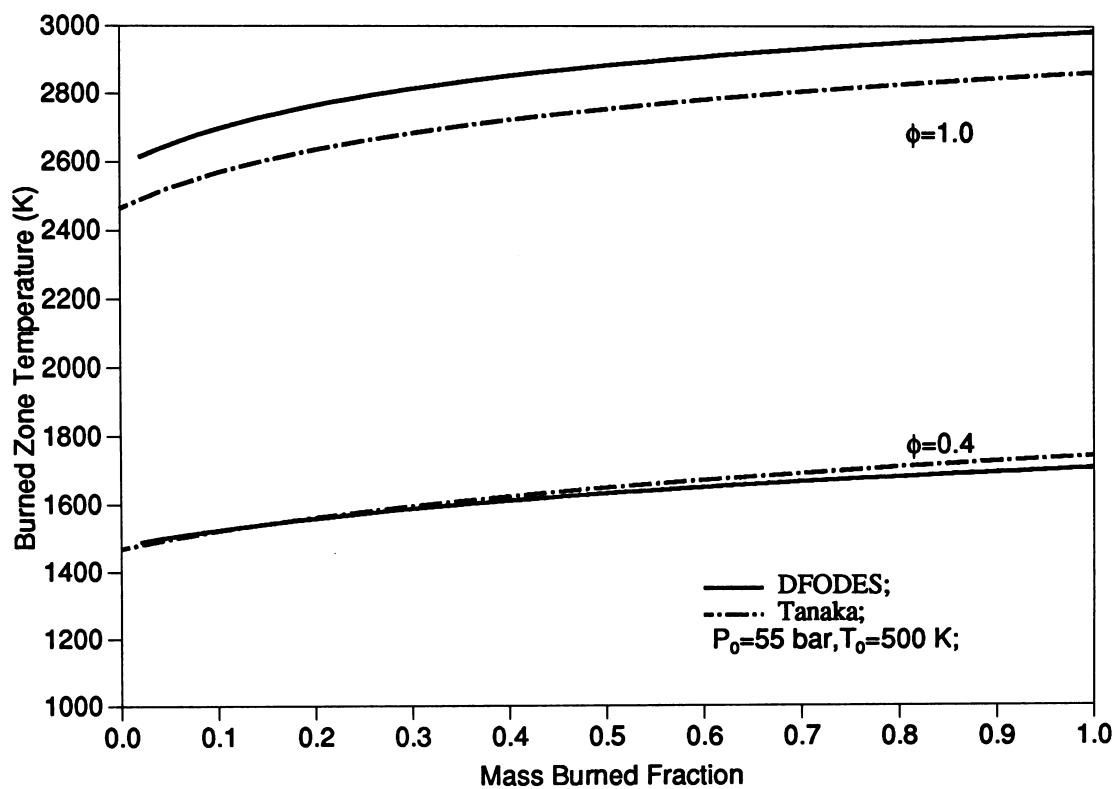
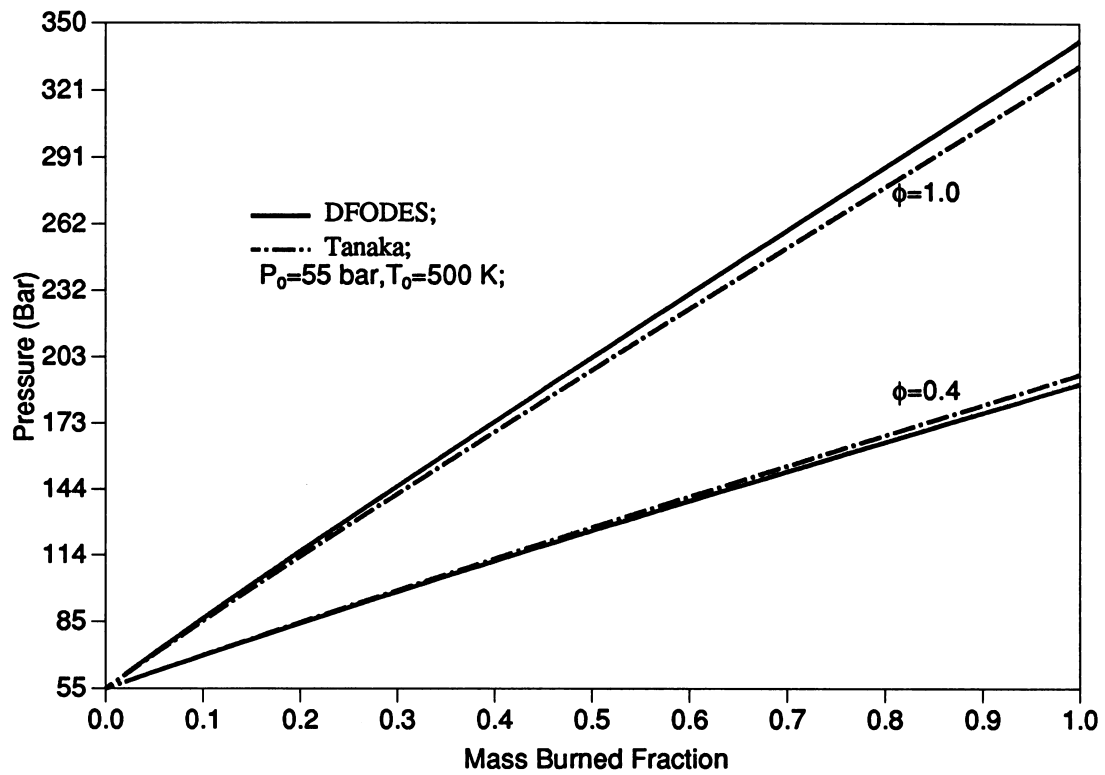
Figure 2.2: Predicted Combustion Results of $CH_4(G)$

the maximum combustion temperature cannot match the increase in the initial temperature, as shown on Fig. 2.12. This causes the ratio $\frac{R_b T_b}{R_0 T_0}$ to reduce and hence the maximum combustion pressure P to reduce.

Fig. 2.10, 2.11, and 2.12 present the maximum combustion temperature calculated by DFODES at various initial conditions of P_0 , ϕ , and T_0 for gas fuels CH_4 and C_3H_8 . It can be seen that the maximum adiabatic combustion temperature is linearly related to initial temperature T_0 and fuel-air equivalence ratio ϕ , while it is almost independent of the initial cylinder pressure P_0 for the range of initial conditions being tested.

Comparing the temperature and pressure profiles of CH_4 and C_3H_8 , it can be seen that the combustion characteristics of methane and propane are very similar except that the combustion pressure and temperature of propane are usually slightly higher than those of methane.

Figure 2.3: Predicted Combustion Results of $C_3H_8(G)$



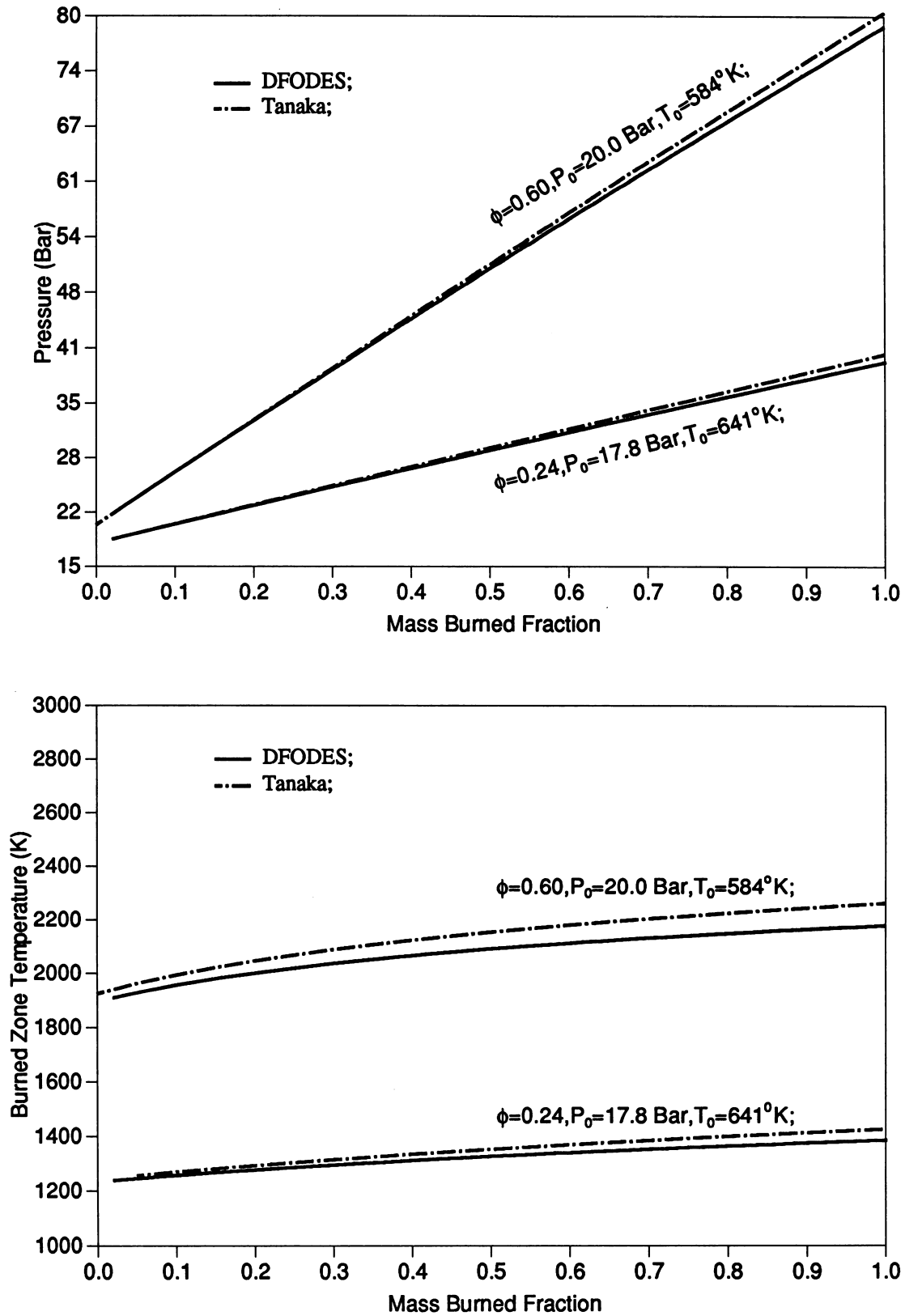


Figure 2.4: Predicted Combustion Results of Diesel Fuel (diesel fuel is assumed to be $C_{10.8}H_{18.7}(L)$ in DFODES, and $C_{12}H_{26}(L)$ in Tanaka' model

Figure 2.5: Predicted Combustion Results of $CH_4(G)$

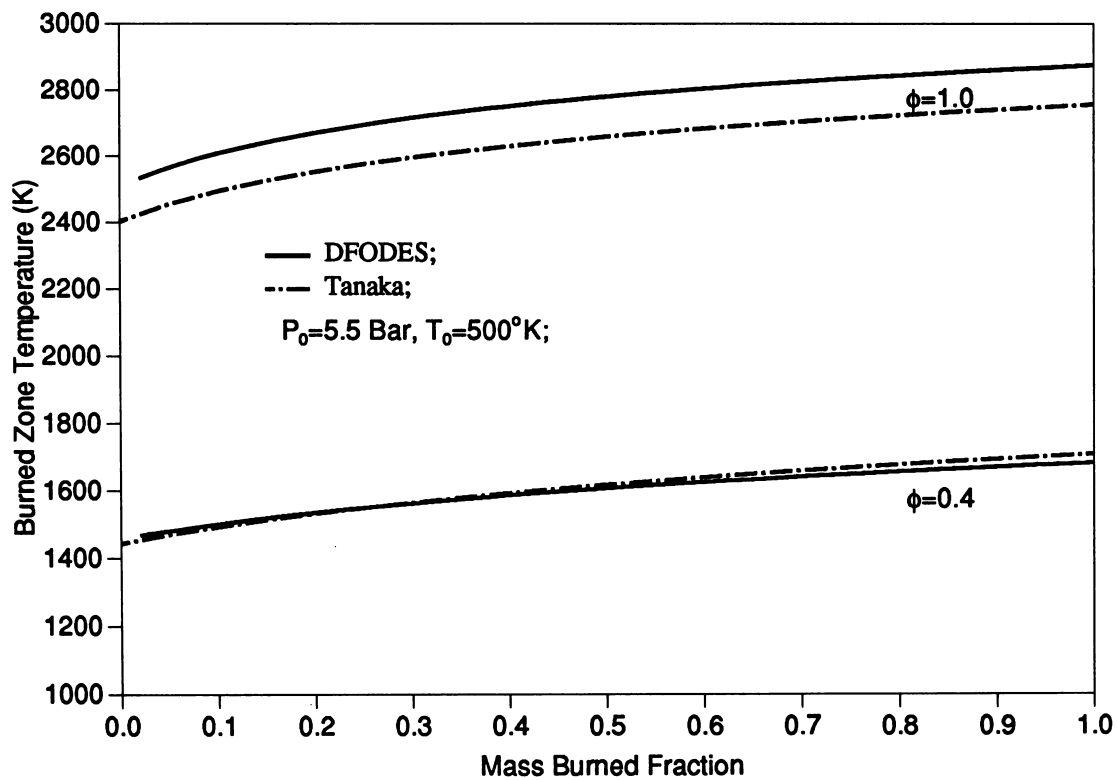
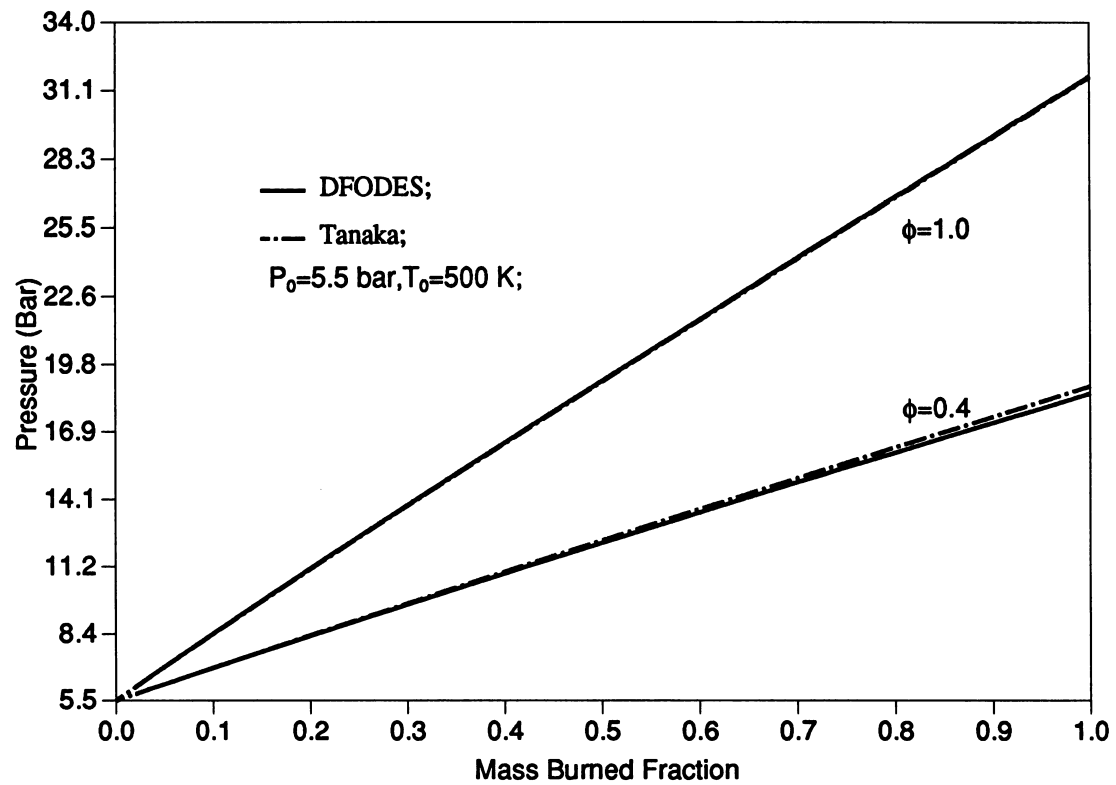
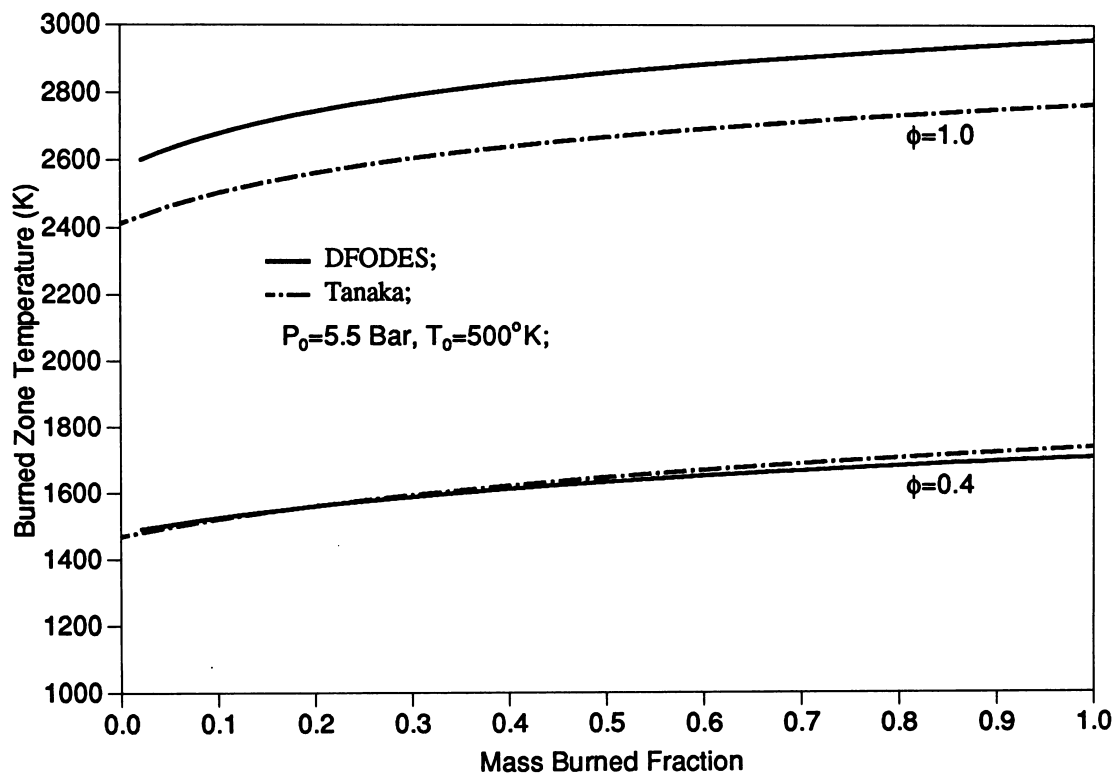
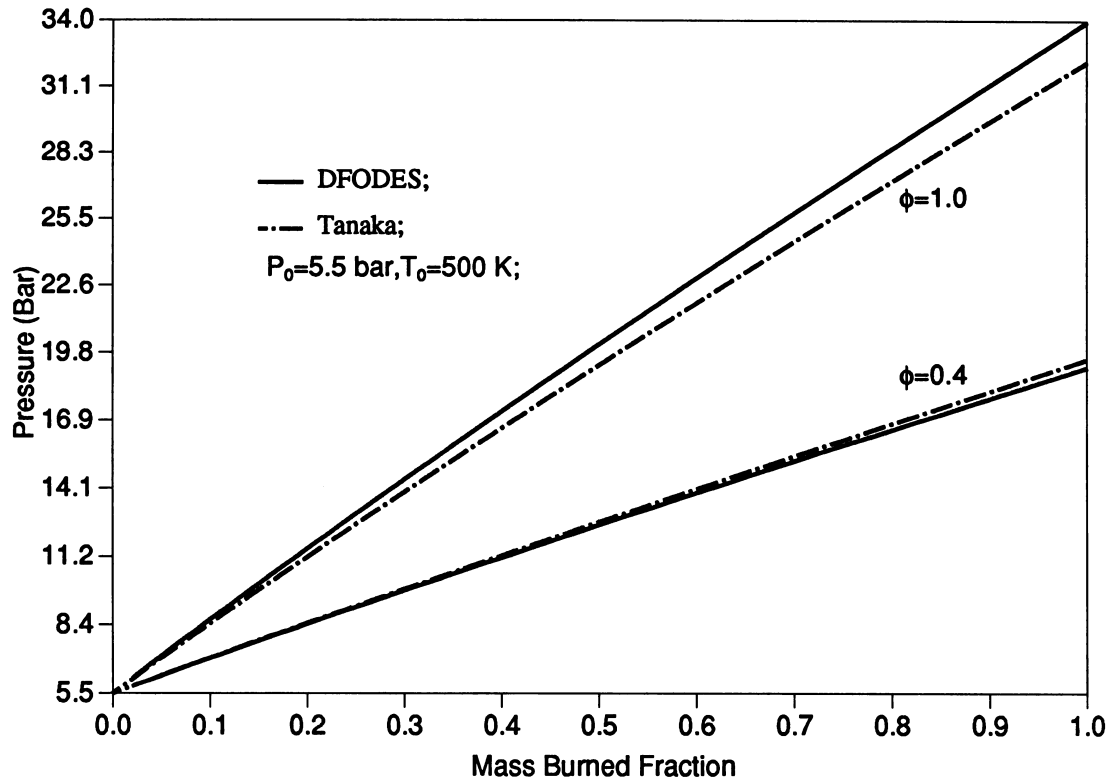


Figure 2.6: Predicted Combustion Results of $C_3H_8(G)$



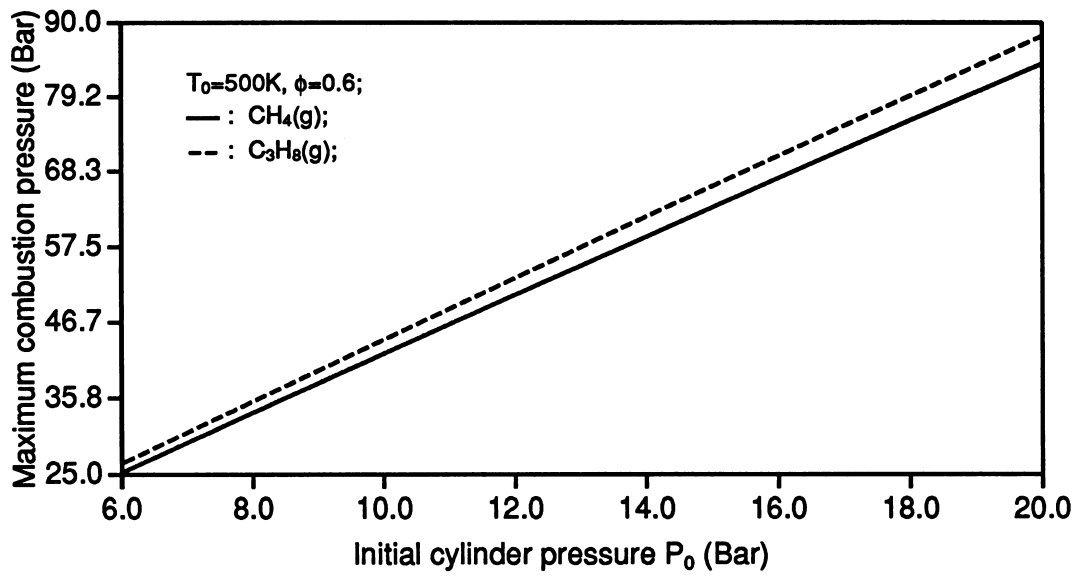


Figure 2.7: Maximum adiabatic combustion pressure of methane and propane gas at $T_0=500\text{ K}$, $\phi = 0.6$. Predicted by DFODES.

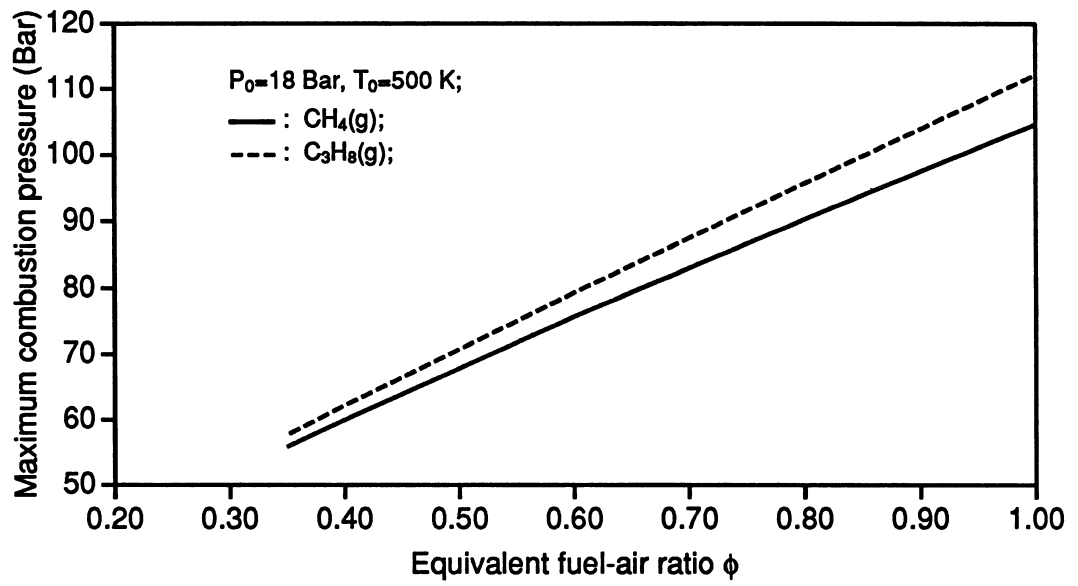


Figure 2.8: Maximum adiabatic combustion temperature of methane and propane gas at $T_0=500 \text{ K}$, $P_0 = 18 \text{ bar}$. Predicted by DFODES.

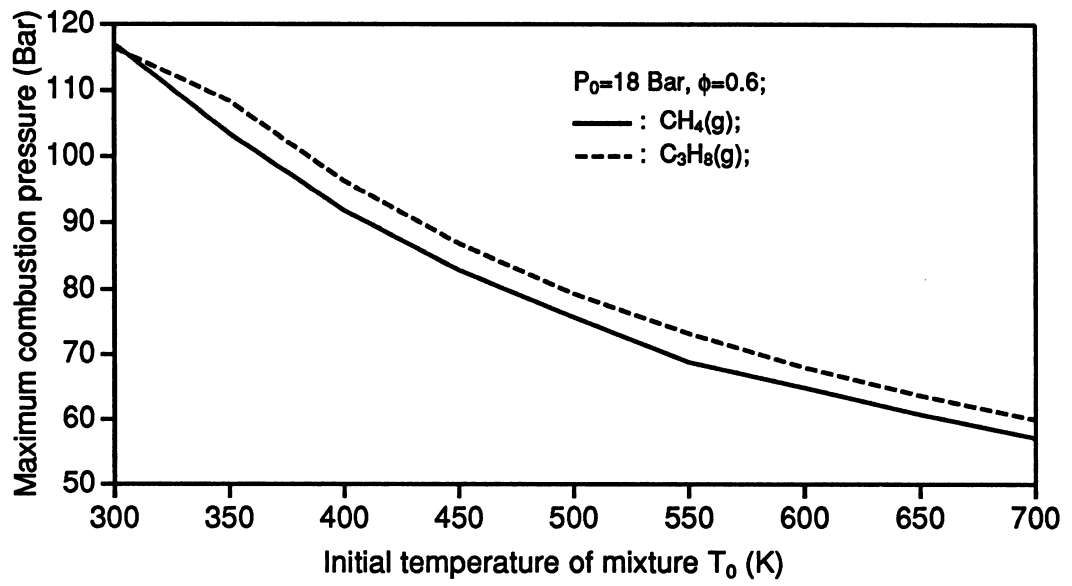


Figure 2.9: Maximum adiabatic combustion pressure of methane and propane gas at $P_0 = 18 \text{ bar}$, $\phi = 0.6$. Predicted by DFODES.

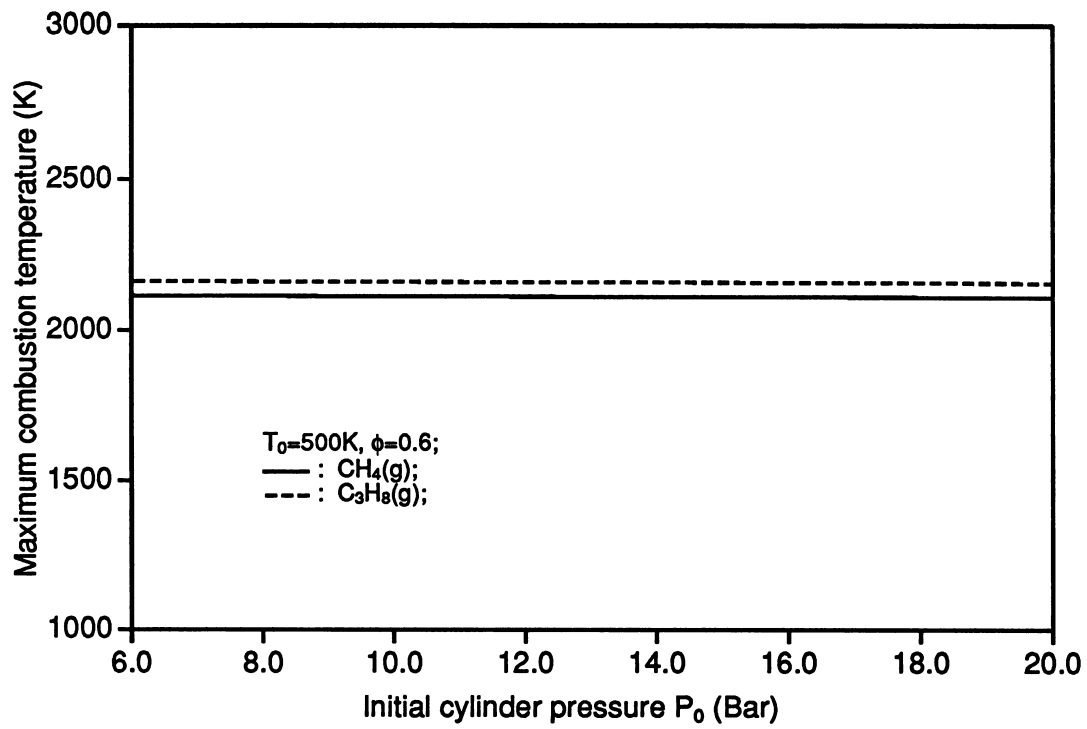


Figure 2.10: Maximum adiabatic combustion temperature of methane and propane gas at $T_0 = 500$ K, $\phi = 0.6$. Predicted by DFODES.

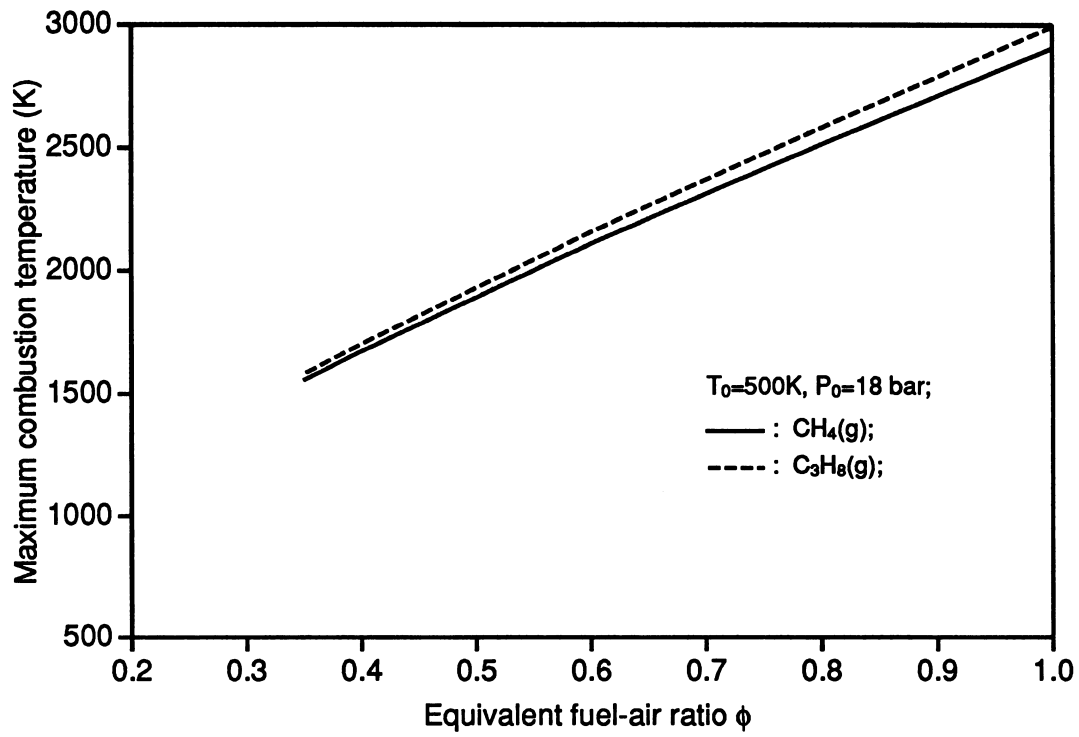


Figure 2.11: Maximum adiabatic combustion temperature of methane and propane gas at $P_0 = 18\text{ bar}$, $T_0 = 500\text{K}$; Predicted by DFODES.

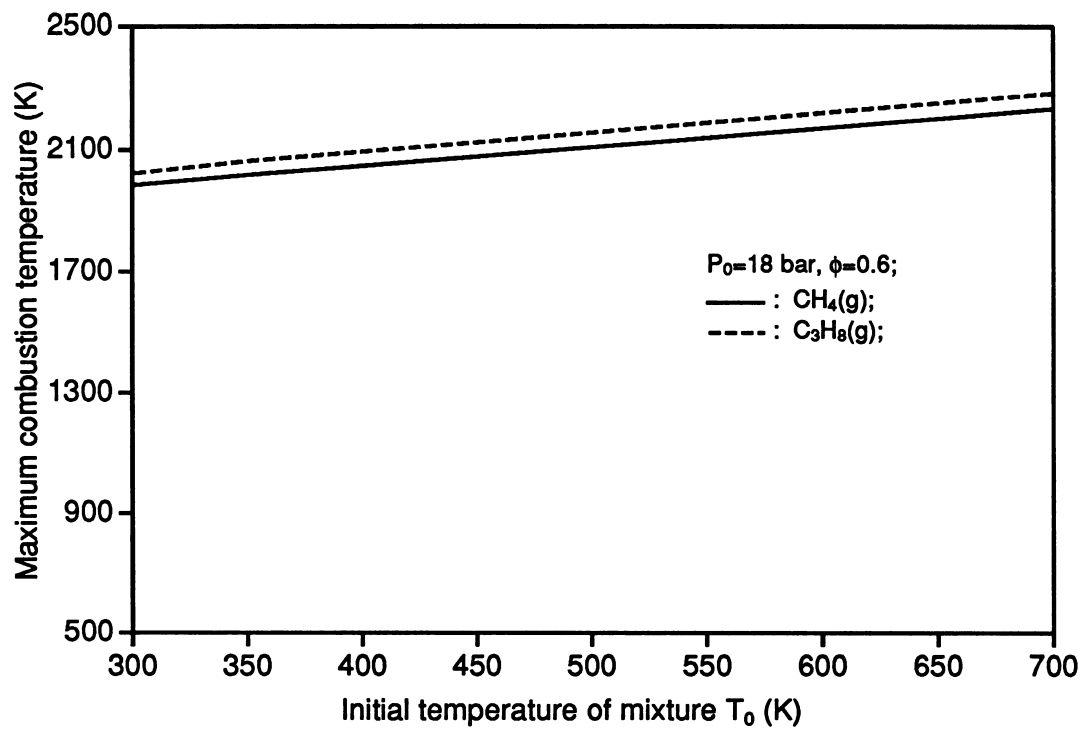


Figure 2.12: Maximum adiabatic combustion temperature of methane and propane gas at $P_0 = 18 \text{ bar}$, $\phi = 0.6$. Predicted by DFODES.

Chapter 3

Modelling the Spark Ignition Combustion Processes

NOMENCLATURE

<i>a</i>	empirical constant, -
<i>A</i>	area, area of flame front, m^2
<i>b</i>	empirical constant, -
<i>B</i>	constant
BMF	Burned mass fraction,-
<i>C</i>	constant,-
<i>e</i>	internal energy of unit mass, J/kg, kJ/kg
<i>E</i>	internal energy, activation energy, J, kJ
<i>H</i>	height of combustion bomb, m
<i>K</i>	coefficient constant, -
<i>l</i>	length, m
<i>L</i>	integral length of large scale turbulence, m
<i>m</i>	mass, kg
<i>M_R</i>	molecular weight, kg/mol
<i>P</i>	pressure, Pa,kPa
<i>Q</i>	heat flow, J,kJ
<i>r</i>	radius, m

R ideal gas constant, radius of combustion bomb
 R_L Reynold number, -
 S speed, m/sec
 T temperature, K, $^{\circ}C$
 t, t' time. second, mili-second
 u speed, m/sec.
 u' turbulent intensity, m/sec
 V Volume, m^3
 v specific volume, m^3/kg
 \bar{v} average specific volume, m^3/kg
 W work, J, kJ
 x, X mass fraction, kg/kg
 x_b, X_b burned mass fraction, kg/kg
 Y mole fraction, -
 α coefficient
 β coefficient
 ϵ coefficient, rate of turbulence dissipation
 η Kolmogorov scale, m
 ϕ fuel-air equivalence ratio, -
 λ Taylor microscale, m
 μ parameter mass, -
 ρ density, kg/m^3
 θ crank angle, degree
 τ characteristic reaction time, sec
 ν kinematic viscosity, m^2/sec

Subscripts:

0 initial state
 b burned zone state, burning

e entrainment
f, F flame, fuel
i ignition, ignition delay
L laminar
m modelling coefficient, mean average value
 O_2 oxygen
T turbulence
u unburned zone state
w wall, wall impingement

Superscripts:

0 standard state of 1 atmosphere

3.1 Introduction

Since this research concentrates on dual-fuel combustion, which is essentially a homogeneous gas-air mixture ignited by pilot fuel, it is necessary and helpful to investigate available phenomenological models of the nearest equivalent cases. These are the models of the conventional, homogeneous spark-ignition engine. Those to be discussed include thermodynamic-based zero-dimensional models and quasi-dimensional models.

In this chapter, Section 3.2 briefly describes some essential features of combustion in an SI engine; Section 3.3 reviews those phenomenological models that have played important roles to date in the modelling of SI engine combustion. Section 3.4 discusses the laminar burning speed while Section 3.5 further discusses modelling of turbulent combustion in homogeneous mixtures. Emphasis is placed on the model's application to combustion in a constant volume combustion bomb.

3.2 Essential Features of the Combustion in Spark-Ignition Engines

Figure 3.1 shows a typical SI engine cycle pressure-volume diagram. The diagram can be subdivided into several sections. The section from point a to point b represents the intake stroke following which the premixed charge begins to be compressed from point b, until a certain point c is reached before TDC when the spark is discharged. The homogeneous charge is then ignited and burns rapidly, almost at constant volume, to point d. Point d to point e represents the expansion stroke and e to a is the exhaust stroke. Therefore, the combustion in an SI engine is essentially a premixed homogeneous one and as a first approximation may be assumed to be taking place at constant volume. After ignition by the spark, laser shadowgraph photographs [19],[121] show that the flame propagates in a roughly spherical manner, except where intersected by the chamber wall. Schlieren photographs of the flame also show that the volume of the flame front (that is, the reaction zone where the fuel-air oxidation process actually occurs) is small compared with the clearance volume [19],[122].

3.3 Literature Review on Modelling the Combustion in SI engines

3.3.1 Zero-Dimensional Models

Zero-Dimensional models are also known as single-zone models or thermodynamic models. In zero-dimensional models, pressure, temperature and composition of the cylinder charge are assumed to be uniform, the thermodynamic state of the cylinder charge is defined in terms of average properties and burned and unburned gases are not distinguished. Zero-dimensional models consider the combustion as a heat addition process and the mass fraction burned usually is specified as a function of crank angle by means of Wiebe's function:

$$X_b = \{1 - \cos[\frac{(\theta - \theta_0)\pi}{\Delta\theta_b}]\}/2 \quad (3.1)$$

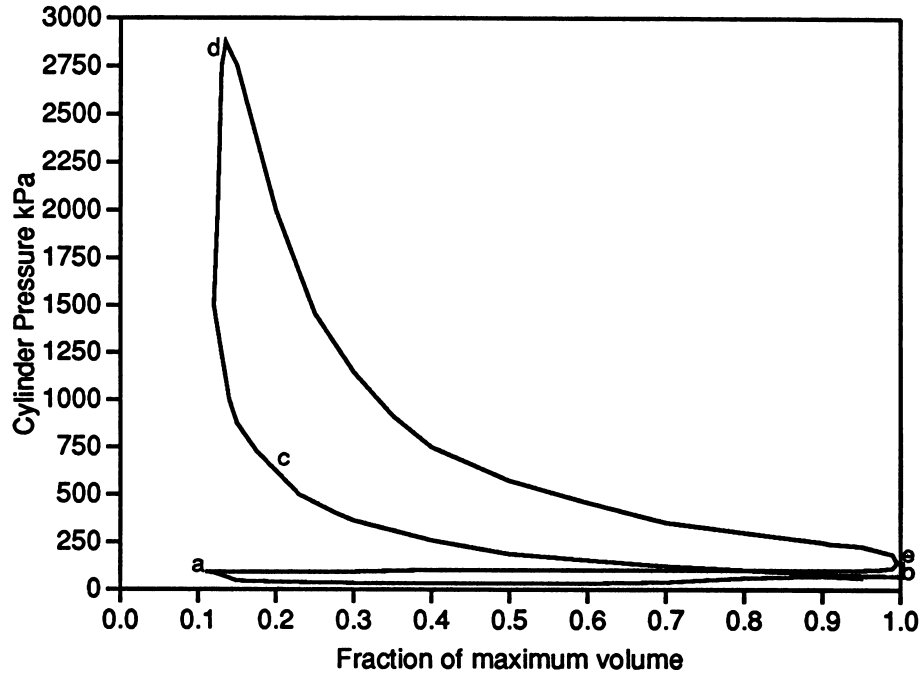


Figure 3.1: A Pressure-volume diagram for an SI engine cycle

or

$$X_b = 1 - \exp\left[-a\left(\frac{\theta - \theta_0}{\Delta\theta_b}\right)^{m+1}\right] \quad (3.2)$$

where $a=5$, $m=2$ [123], [19].

Zero-dimensional models have provided a simple approach to simulate the engine combustion. However, they are not able to account for the chamber geometry and flame propagation directly, and there is always a need to specify several parameters in the heat release rate functions such as θ_0 , $\Delta\theta_b$, a , and m in equations 3.1 and 3.2. Furthermore, the assumption of uniform temperature and composition in the combustion chamber is obviously unrealistic. These drawbacks have led to the development of quasi-dimensional models.

3.3.2 Blizard-Keck's Turbulent Entrainment Model (The B-K Model)

Blizard and Keck [96] proposed this model in 1974. It considers the flame propagation process as first, a turbulent entrainment of unburned mixture into the front which is then followed by a laminar burn-up process with a characteristic length scale. That is, the large scale turbulent eddy entrains the mixture at a slowly varying entrainment speed, u_e , while the small eddies (with dimension λ) burn in a laminar manner with a characteristic time $\tau = \lambda/S_L$. This consideration allows the rate at which mass is entrained by the flame front to be expressed as

$$\dot{m}_e = \rho_u A_f u_e$$

If it is assumed that the distribution of burning times for the entrained eddies is exponential, the mass burning rate is

$$\dot{m}_b = \dot{m}_e \int_0^t e^{-(t-t')/\tau} \frac{dt'}{\tau}$$

where t is the time after ignition and t' is a temporal coordinate. The flame front surface area, A_f , is considered to be a section of a sphere.

This model provided a compromise between the thermodynamic-based phenomenological model and the fluid-dynamic based multi-dimensional model by making use of the fundamental physical quantities of eddy size and turbulence intensity. It also raised the concept of a turbulent entrainment model for the first time. However, the model failed to predict the affect of equivalence ratio on the combustion duration, and it did not account for any changes in the turbulent field ahead of the expanding flame front.

3.3.3 Blizard-Keck-Tabaczynski (B-K-T) Model

The quasi-dimensional model often referred to as the Blizard-Keck-Tabaczynski model is a modification of the B-K model. The B-K-T model was developed first by Tabaczynski et al in 1977 [97] and was further refined in 1980 [124]. This model heavily depends on the structure of the turbulent flow field and has been

extensively used for homogeneous spark-ignition combustion and more recently for direct injection combustion.

The turbulent eddy structure

In order to construct a turbulent combustion model for a spark ignition engine, Tabaczynski et al [97] first assumed that the turbulence in a spark ignition engine has the same structure as that observed in plane shear flows [97] as shown on Figure 3.2. There are several important length scales in this structure, these being

L , the integral length, which defines the size of the large scale turbulence structure;

η , the Kolmogorov scale, which defines the dissipation length scale. It is also the scale of the vortex tubes (Figure 3.3)

λ , the Taylor microscale, which defines the spacing of the vortex tube (Figure 3.3)

Turbulent quantities as functions of engine geometry and operating condition

From the time of combustion initiation by the spark until the point at which 1% of the fuel mass has been burned, the turbulence intensity, u' , is assumed to be a linear function of engine speed and independent of the spark timing. The integral length scale, L , is assumed to be proportional to the instantaneous chamber height. After that point, the turbulence structure in the unburned gas ahead of the flame front is governed by conservation of angular momentum of the individual eddies.

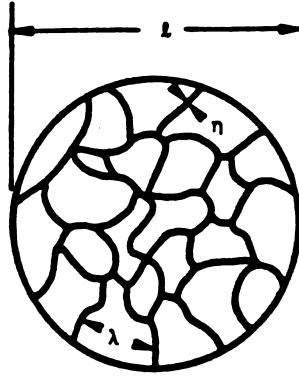


Figure 3.2: Turbulence Structure in the B-K-T Model

Governing equations

By making use of the entrainment model conceptualized by Blizard and Keck [96], the rate at which mass is entrained by the flame front is given by

$$\frac{dm_e}{dt} = \rho_u A_e u_e \quad (3.3)$$

For variable density flows, Ricou and Spalding [138] suggested that the entrainment velocity u_e should be modified by multiplying by a factor $(\rho_b/\rho_u)^{1/2}$.

Equation 3.3 therefore becomes

$$\frac{dm_e}{dt} = \sqrt{\rho_b \rho_u} A_e u_e \quad (3.4)$$

The rate at which mass is burned can be regarded as the mass in the burning zone consumed during the characteristic burning time. This mass is itself the mass entrained minus that burned. Hence,

$$\frac{dm_b}{dt} = \frac{m_e - m_b}{\tau} \quad (3.5)$$

By applying the assumption of angular momentum conservation for each individual eddy, the turbulence intensity, u' , and the integral scale, L , can be

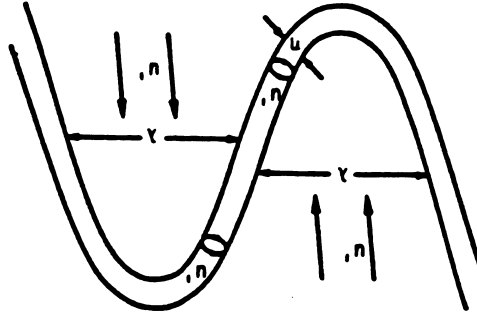


Figure 3.3: Structure of the "Vortex Tube" in the B-K-T Model

given by

$$u' = u'_r(\rho_u/\rho_{u,r})^{1/3} \quad (3.6)$$

$$L = L_r(\rho_{u,r}/\rho_u)^{1/3} \quad (3.7)$$

Here u'_r and L_r are the turbulence intensity and the integral scale, respectively and are arbitrarily defined as at the instant when 1% of the mass fraction has been burned. The assumption of conservation of angular momentum for rapidly compressed gases being used here is known as the rapid distortion theory and has been used for modelling turbulence in contractions such as the converging sections in wind tunnels. In effect this assumption implies that leaner mixtures or dilute mixtures will burn slower than mixtures near to stoichiometric. This is because the initially slower flame speed in the former will result in less compression of the turbulence in the unburned gases further reducing the relative burning rate.

The characteristic reaction time, τ , in equation 3.5 was first defined as the time taken to burn the mass of an eddy of size equal to the integral scale, L . However, this definition was amended later in the refined model.

The entrainment surface, A_e , is, as with Blizard and Keck in [96], assumed to be a spherical section in a right circular cylindrical combustion chamber. When calculating the laminar burning speed, S_L , a correlation proposed by Van Tiggelen was employed, this being

$$S_L = K C_m [Y_F^a Y_{O_2}^b \exp(-\frac{E}{RT_m})]^{0.5} \quad (3.8)$$

where

$C_m = \sqrt{8RT_m/\pi M_R}$ is the mean molecular speed of chain carriers whose mean molecular weight is M_R ;

Y_F mole fraction of fuel molecules in the unburned mixture;

Y_{O_2} mole fraction of oxygen molecules in the unburned mixture;

a = reaction order with respect to the fuel;

b = reaction order with respect to the oxygen;

E = activation energy;

$T_M = T_u + 0.74(T_b^0 - T_u)$ which is the mean temperature of the reaction zone

For all hydrocarbons, it is found that $a+b=1$.

However, there are many empirical equations for S_L and Eq.3.8 may be replaced by any appropriate correlation.

Thermodynamic model

This model assumes that the mass of burning gas is small compared to the mass in the cylinder, thus

$$V/m = x_b \bar{v}_b + (1 - x_b) \bar{v}_u$$

$$E/m = x_b \bar{e}_b + (1 - x_b) \bar{e}_u$$

The average internal energy and specific volume of the unburned or burned gas is computed based on the average unburned or burned gas temperature and pressure.

Refinement of the B-K-T model [124]

This refinement clarifies the model in that it assumes an instantaneous burning occurs within the dissipative region which is of the order of the Kolmogorov scale, η , as shown on Figure 3.3. Ignition sites propagate at the speed of $u' + S_L$ while the charge behind the propagating front burns up with a laminar burning speed, S_L . This burning process is depicted in Figure 3.4 and the equations governing the burning process are modified accordingly.

$$\frac{dm_e}{dt} = \rho_u A_e (u' + S_L) \quad (3.9)$$

$$\frac{dm_b}{dt} = \frac{m_e - m_b}{\tau} \quad (3.10)$$

Here the characteristic reaction time, τ , has been redefined in term of the Taylor microscale λ as

$$\tau = \lambda / S_L \quad (3.11)$$

This permits a flame to continuously develop after ignition. It should be pointed out that this is one of the most important advances of this more refined model over its predecessor. That is, the original model used two separate sub-models to calculate the burned mass fraction, these being a “fully developed flame” model for the “fully developed flame” period and an “ignition delay” model for the “ignition delay” period. In the “fully developed flame” period, the characteristic reaction time, τ , was defined to be the time required to burn the mass of an L size eddy. The “ignition delay” period was defined as the period of time in which the first 1% of the fuel mass is burned. This ignition delay is assumed equal to a characteristic time τ_b , which is correlated by Tabaczynski et al as

$$\tau_b = C(L/u')^{1/3}(\lambda/S_L)^{2/3} \quad (3.12)$$

In the refined model, τ as defined in Eq. 3.11 applies over the whole burning period. The refined model also employed the correlation proposed by Hires et al [98] to obtain the turbulent flame speed. This is

$$\frac{S_T}{S_L} = C(u'/S_L)^{1/3}(\rho_u/\rho_{ui})^{1/9}(u'L/\nu)^{1/3} \quad (3.13)$$

It assumes that the turbulence field is isotropic and homogeneous at the time of ignition. Thus

$$\lambda/L = C_1 \left(\frac{u'L}{\nu} \right)^{-0.5} \quad (3.14)$$

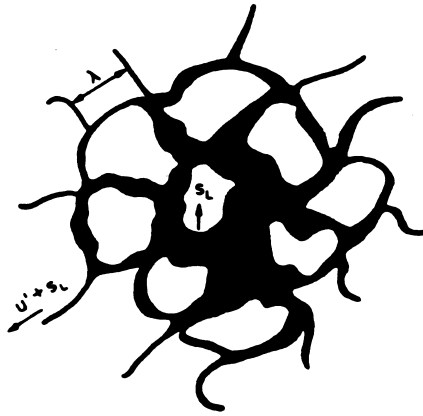


Figure 3.4: BKT's Small-Scale Turbulence Flame Model

Several empirical constants in this model have also been determined by comparing the model's prediction with engine experimental data. It is found that this model gives good agreement with the experimental data for variation in EGR, engine load and speed, and air/fuel ratio. However, it is highly dependent on correlations for S_L , λ , and u' .

3.3.4 Hires-Tabaczynski H-T Quasi-dimensional Model

The burning process may be considered as a flame front area propagating through the unburned mixture at a turbulent flame speed. Hires et al [98] proposed an approach to link the rate of burning with the fundamental

physical quantities, these being turbulence integral scale, turbulence micro-scale, turbulence intensity, and laminar burning speed.

Hires' model [98] is an extension of the B-K-T model and is based on the following assumptions:

- 1 Turbulent eddies are essentially spherical and the ignition of gas within an eddy occurs at its centre;
- 2 After ignition, the flame propagates along vortex tubes at a rate determined by the sum of the turbulence intensity u' and the laminar burning speed S_L ;
- 3 Each micro-cell of dimension λ burns at the laminar burning speed S_L . Thus it burns up with a characteristic time:

$$\tau = \lambda/S_L$$

- 4 The size of the micro-cell which is the Taylor microscale, λ , is a function of the turbulence Reynold Number, $u'L/\nu$, based on isotropic turbulent theory. L is the turbulence integral length scale and ν is the kinematic viscosity.

The “effective flame front” is defined as that which divides the fully burnt charge from the unburned. This effective flame front moves at a rate relative to the unburned charge as specified by L/τ . The rate at which mass is burned is then given as:

$$\frac{dm_b}{dt} = \rho_u A_f (L/\tau)$$

in which m_b , ρ_u , and A_f represent the instantaneous value of the burned mass, unburned density, and effective flame surface area, respectively. The characteristic reaction time, τ , is evaluated by the same method as for the ignition delay time in the B-K-T model, this being as given by equation 3.12,

$$\tau \propto (L/u')^{1/3} (\lambda/S_L)^{2/3} \quad (3.15)$$

As in the BKT model, turbulence intensity and integral scale are calculated by assuming that the turbulence intensity and integral scale of the unburned gas are governed by the conservation of angular momentum of the individual eddies. That is

$$u' = u'_i(\rho_u/\rho_i)^{1/3} \quad (3.16)$$

$$L = L_i(\rho_i/\rho_u)^{1/3} \quad (3.17)$$

Subscript “ i ” refers to quantities evaluated at the end of the ignition delay.

The turbulent flame speed, defined by $S_T = L/\tau$, can then be linked to the four fundamental turbulent flow field quantities: S_L , u' , L , and λ , by using the relationship for λ , τ , and L implied by equations 3.15, 3.16 and 3.17. This gives

$$\frac{S_T}{S_L} = C(u'/S_L)^{1/3}(\rho_u/\rho_{ui})^{1/9}(u'L/\nu)^{1/3}$$

in which C is a constant determined by experimental data for a given engine configuration.

Application of this model to a given engine configuration requires two empirical constants that are invariant when the operating conditions are changed. While the model provides good agreement for the ignition delay and the combustion duration when compared with experimental results obtained over a variety of operating and design conditions (e.g. engine speed and load, spark timing, EGR, air-fuel ratio, and compression ratio) given by the authors and the shape of the burned mass fraction curves obtained from other work, this model's definition of the “ignition delay” period as one percent of the total cylinder mass being burned is arbitrary.

3.3.5 B-R-K's Eddy Burning Model and Its Modification

Using measured data and optical observations of engine tests, e.g., the mass fraction burned, flame propagation and geometry, and cylinder pressure trace, Beretta et al modified the B-K-T model to account for the initial expansion of the flame front which is close to that of a laminar flame [125], [122]. This model contains three parameters in the burning equations: the laminar burning

speed S_L , a characteristic speed u_T , and a characteristic length l_T . The burning equations were expressed as:

$$\frac{dm_b}{dt} = \rho_u A_f S_L + \frac{\mu}{\tau_b} \quad (3.18)$$

$$\frac{d\mu}{dt} = \rho_u A_f u_T - \frac{\mu}{\tau_b} \quad (3.19)$$

where μ is a “parametric mass” defined by $\mu = m_e - m_b$. and A_f is defined as a spherical flame front area with a radius r_f containing the enflamed volume V_f . The term μ represents the unburned mass entrained behind the flame front, that is, $\mu = \rho_u(V_f - V_b)$. Beretta et al concluded from their experimental

observations that $\frac{(V_f - V_b)}{(A_L - A_f)}$ is equal to a characteristic length l_T which is defined as $l_T = \tau_b S_L$. That is

$$\frac{V_f - V_b}{A_L - A_f} = l_T$$

Here A_L is a laminar burning area. Thus

$$\mu = m_e - m_b = \rho_u(V_f - V_b) = \rho_u l_T (A_L - A_f)$$

The characteristic length l_T can be computed by an empirical correlation

$$l_T = 0.8 L_{iv} \left(\frac{\rho_i}{\rho_u} \right)^{3/4}$$

where L_{iv} is the valve lift and ρ_i is the inlet density. The characteristic speed, u_T , is defined by

$$L_T = u_T \tau_b \quad (3.20)$$

which again can be computed by an empirical correlation

$$u_T = 0.08 \bar{u}_i \left(\frac{\rho_u}{\rho_i} \right)^{0.5} \quad (3.21)$$

Here L_T in equation 3.20 is the characteristic turbulent flame thickness; and \bar{u}_i in equation 3.21 is the mean inlet gas speed.

Equations 3.18 and 3.19 are similar to those previously proposed by Blizard and Keck[96] but contain the important additional term $\rho_u A_f S_L$ in Eq. 3.18

to describe correctly the dependence of the initial burning rate on the laminar speed S_L .

In order to provide a clear physical meaning, this empirically-based model was further modified by Keck, Heywood, and Noske in 1987 [126]. In the modification, a term of the type $(1 - e^{-t/\tau_b})$ was introduced to equation 3.19 in order to explain the initial flame growth before time τ_b . Although this equation is arbitrary, it provides for a more rapid growth in entrainment as the combustion proceeds. This fits the observed data. Thus the burning equations become

$$\frac{dm_b}{dt} = \rho_u A_b S_L + \frac{\mu}{\tau_b} \quad (3.22)$$

$$\frac{d\mu}{dt} = \rho_u A_b u_T (1 - e^{-\frac{t}{\tau_1}}) - \frac{\mu}{\tau_b} \quad (3.23)$$

where $\tau_1 = l_1/S_L$ is the burning time of the first eddy burned. A_b is a spherical burning area determined from the burned gas volume V_b .

Heywood offered the interpretation that the term $\mu = m_e - m_b$ is the unburned mass within the entrained region, that the first term in the right hand side of Eq. 3.18 represents the laminar (diffusive) propagation forward of the approximately spherical front of the “thick” turbulent flame and that the second term represents the burning of mixture entrained within this flame front. In Eq. 3.19, the first term in the right hand side represents turbulent convection of the unburned mixture across the spherical flame front and the second term represents the mass burning rate of entrained but unburned mixture contained within the “wrinkles” and “islands” (Figure 3.5) while the exponential term within the brackets indicates that a time of about τ_b is required before the initial spherical and approximately laminar flame sheet develops into a turbulent flame. This physical process is depicted more clearly on Figure 3.5. The approximately spherical front of the “thick” turbulent flame (dashed line) diffuses outwards at the laminar burning speed S_L . Fresh mixture also crosses this front at a characteristic velocity u_T due to turbulent convection. δ_L in Figure 3.5 is a reaction-sheet thickness, and l_T is the characteristic scale of wrinkles in the sheet.

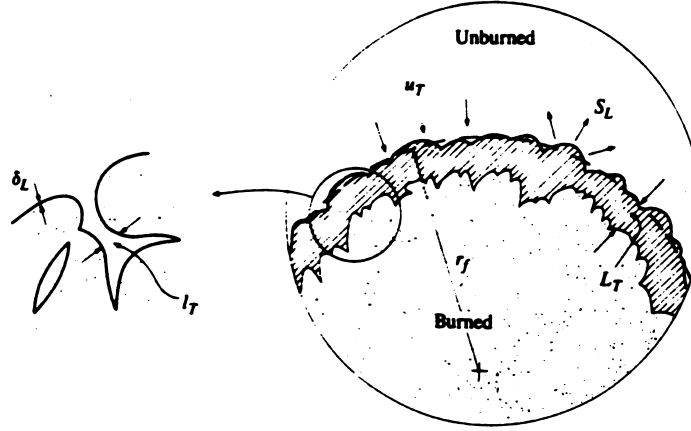


Figure 3.5: "Thick" Turbulent Flame Implied by Keck et al's Model

This model's burning law equations also imply four important limit situations as follows

1. For a quiescent mixture, $u_T \rightarrow 0$ or $l_T \rightarrow \infty$. The flame should then propagate at the laminar flame speed. Thus the burning speed

$$S_b \rightarrow S_L$$

2. Initially, as $t \rightarrow 0$ and $\mu = m_e - m_b \rightarrow 0$, from Eq. 3.22, it can be seen that

$$\frac{dm_b}{dt} \rightarrow \rho_u A_b S_L$$

Comparing this with the definition of burning speed that $S_b = \frac{dm_b}{dt}$, one can then obtain

$$S_b \rightarrow S_L$$

This also can be understood as the initiation of a flame propagating at an approximatively laminar flame speed.

3. For a quasi-steady state, $d\mu/dt \simeq 0$,

$$S_b \simeq u_T + S_L$$

4. The final burning stage after the flame front reaches the wall is,

$$\frac{\dot{m}_b}{\dot{m}_b(t_w)} = e^{-(t-t_w)/\tau_b}$$

Here, $t \geq t_w$ (when $A_f \rightarrow 0$),

These limiting expressions were suggested by the experimental data and were used in determining the form of the empirical equations 3.22 and 3.23.

3.4 The Laminar Burning Speed

3.4.1 The Definition of S_L

As indicated by the equations in Section 3.3, the laminar burning speed, S_L , is an important characteristic for studying in-cylinder premixed combustion. S_L is defined as the velocity relative to and normal to the flame front and is that with which unburned gas moves into the front and is transformed to products, under laminar flow conditions. Under engine conditions, the laminar flame thickness is negligible, and thus the laminar burning speed is given by

$$S_L = \frac{dm_b/dt}{A_f \rho_u}$$

For a given fuel, S_L is a function of the fuel/oxidant ratio, the fraction of inert material in the unburned gas, the unburned gas temperature T_u and the pressure P . In spark-ignition engines, equivalence (fuel/air) ratio ϕ and the mass fraction of residual gases, F , are the appropriate measures of the fuel/oxidant ratio and inert gas fraction. Thus

$$S_L = S_L(P, T_u, \phi, F) \quad (3.24)$$

Various forms of the functional relationship have been proposed and wide variation of experimental data have been reported even for conventional fuels like methane and propane.

3.4.2 Dependence of S_L^0 on fuel/air equivalence ratio

S_L^0 represents the value of S_L at $T_u = 298$ K, $P = 1$ atm with no residual gas in the mixture. That is, $S_L^0(\phi) = S_L(1, 298, \phi, 0)$ if S_L is expressed as in Eq. 3.24.

Figure 3.6 is reproduced from Ref.[127] updated to including some recent data from [128] and [129]. Amongst these experimental and numerical results, Yu et al's result has moderate values and covers a relatively wide range of ϕ . Therefore it was chosen for use in the present modelling. For the purpose of programming convenience, the author has developed a nonlinear regression function for Yu et al's experimental data for a CH_4 and air mixture by using the Gauss-Newton least-squares method, this being given in Eq. 3.25 as

$$S_{L,CH_4}^0(\phi) = a_1 + a_2\phi^{b_1} + a_3\phi^{b_2} + a_4\phi^{b_3} \quad (3.25)$$

where, $0.55 \leq \phi \leq 1.55$; and $a_1 = -2.2677E+4$, $a_2 = 3.5219E+4$, $a_3 = -1.2518E+4$, $a_4 = 1.4162E+1$; and $b_1 = 9.0328E-2$, $b_2 = 2.4091E-1$, $b_3 = -3.3885E0$. Residual error of this equation is

$$\sigma \equiv \sum_i (S_{L,i}^0 - S_{L,CH_4}^0(\phi_i))^2 = 0.08382$$

For other fuels like propane, ethanol, isooctane, and gasoline, experimental data have been fitted [19] to

$$S_L^0(\phi) = B_m + B_\phi(\phi - \phi_m)^2 \quad (3.26)$$

Table 3.1, gives the values of regression constants B_m , B_ϕ , and ϕ_m for several fuels.

Fuel	ϕ_m	B_m	B_ϕ
		cm/s	cm/s
Methanol	1.11	36.9	-140.5
Propane	1.08	34.2	-138.7
Isooctane	1.13	26.3	-84.7
Gasoline	1.21	30.5	-54.9

Table 3.1: Parameters for S_L Equation

3.4.3 Dependence of S_L on pressure, temperature and residual gas fraction

The functional relationship given by Eq. 3.24 has been expressed in various formats. These are reviewed in Reference [130]. Many of these formulae were obtained from correlating measured data, others were based on simplified chain-branching theory. The computing code used in the present research has been designed so that a user can choose any one of the following calculation formulas: power law [19], Kuehl's formula [164], Ohyagi's correlation[131], and ODES¹ correlation.

¹ODES, the *Otto Diesel Engines Simulation*, is an engine simulation package developed by F.J. Wallance & Associates. Version 1.0 and 1.1 were written in FORTRAN programming language.

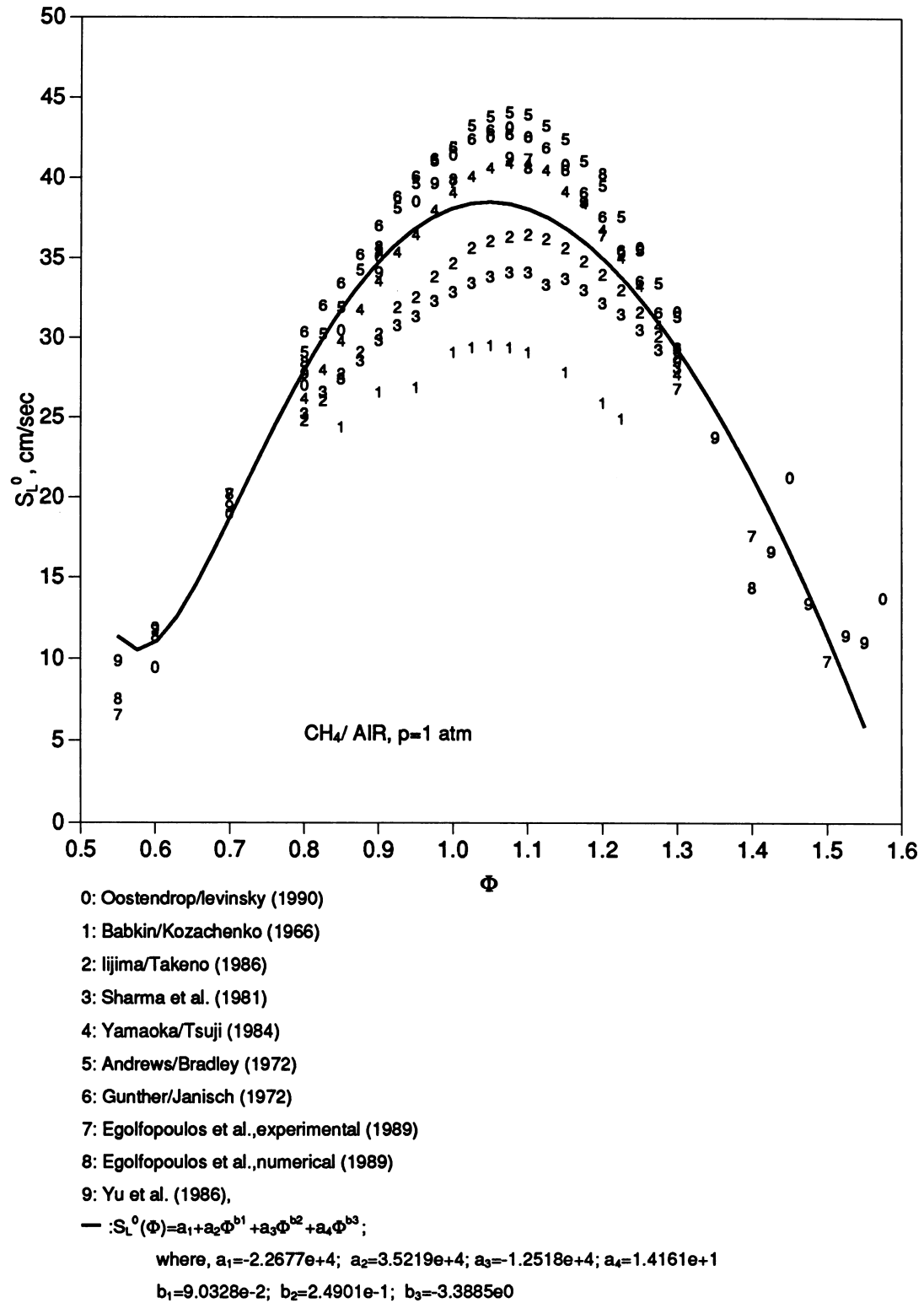


Figure 3.6: Various Reports of Laminar Burning Speed $S_L^0(\phi)$; CH_4 -Air Mixture at $P=1$ atm.

gaseous fuel	α	β
$C_3H_8, C_8H_{18}, CH_3OH$	$2.18 - 0.8(\phi - 1)$	$-0.16 + 0.22(\phi - 1)$
$C_{8.26}H_{15.5}$	$2.4 - 0.271\phi^{3.51}$	$-0.357 + 0.14\phi^{2.77}$

Table 3.2: Index of power law S_L

S_L in the form of a power law

For propane (C_3H_8), isooctane (C_8H_{18}), methanol (CH_3OH), and gasoline ($C_{8.26}H_{15.5}$), the laminar burning velocity S_L at any unburned gas temperature T_u and pressure P can be expressed in term of S_L^0 as:

$$S_L = S_L^0 \left(\frac{T_u}{T_0} \right)^\alpha \left(\frac{P}{P_0} \right)^\beta \quad (3.27)$$

where α and β are functions of ϕ as given on Table 3.2 [19]. For methane (CH_4),

$$S_L = S_L^0 \left(\frac{\rho_u}{\rho_{u0}} \right)_s^\epsilon \quad (3.28)$$

the subscript “s” indicating that the unburned gas is compressed isentropically. The value of ϵ is recommended as 0.17-0.19.

Kuehl's correlation

Kuehl's correlation[164] for propane is

$$S_L = \frac{7784(P_0/P)^{0.02}}{\left(\frac{10000}{T_b} + \frac{900}{T_u} \right)^{4.938}} \quad (3.29)$$

This was obtained from tests on propane/air mixtures for a 0.1 - 1.0 atm pressure range, and for $\phi = 1.1$.

Ohyagi et al's correlation

Ohyagi et al's correlation [131]

$$S_L = S_L^0 \left(\frac{\rho_u}{\rho_{u0}} \right)^\alpha \exp \left[\frac{E}{2R} \left(\frac{1}{T_{b0}} - \frac{1}{T_b} \right) \right] \quad (3.30)$$

was used in their own SI engine combustion simulation program. Here R is the universal gas constant. Empirical constants were taken as $E = 491 \text{ MJ/kmol}$; $\alpha = -0.4$, $S_L^0 = 0.316 \text{ m/s}$; $\rho_{u0} = 1.05 \text{ kg/m}^3$ and $T_{b0} = 2440 \text{ K}$.

ODES' correlation

The formula used in ODES is a modification of Kuehl's correlation. As the original Kuehl formula was obtained for the condition of 0.1 - 1.0 atm pressure and $\phi=1.1$, this formula should only be used for the similar conditions.

$$S_L = \frac{7800 \left(\frac{P}{P_0} \right)^{-0.09876}}{\left(\frac{10000}{T_b} + \frac{900}{T_u} \right)^{4.938}} \quad (3.31)$$

Fig. 3.7 and 3.8 shows a comparison of these four S_L calculation formulas for propane at $\phi = 1.0$ and $\phi = 0.5$ respectively. It should be noted that not all of these formulas are valid at the selected testing conditions. Generally, the formula proposed by Heywood in [19] (the power law format) includes more fuels and is valid for wider pressure and fuel-air equivalence ratio ranges than the others. It also gives better result in combustion calculations. Therefore, unless otherwise specified, computational results in this study are obtained by employing that formula to estimate the laminar burning speed.

Once the laminar burning speed S_L had been decided by one of these aforementioned formulas, the additional effect of burned gas appearing in the unburned mixture (i.e. the residual gases fraction) can be estimated by [19]

$$S_L(\tilde{x}_b) = S_L(\tilde{x}_b = 0)(1 - 2.06\tilde{x}_b^{0.77}) \quad (3.32)$$

where \tilde{x}_b is the mole fraction of residual gases in the unburned mixture.

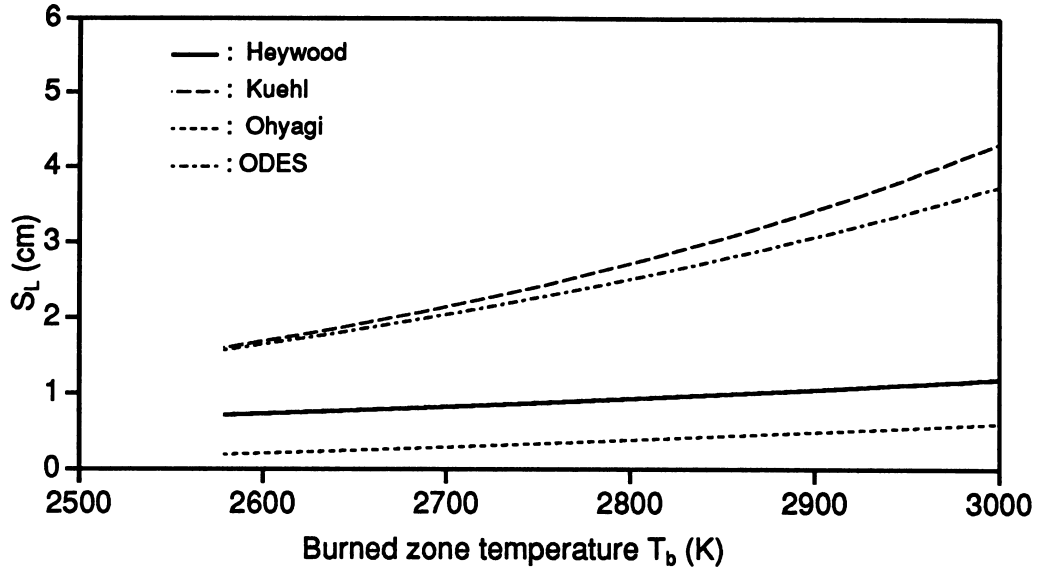


Figure 3.7: The development of the laminar flame speed in the combustion of a propane-air mixture at $P_0=2$ MPa, $T_0=500$ K, and $\phi=1.0$

3.5 Turbulent Flame Propagation in Homogeneous Mixtures

3.5.1 Some developments of the B-K-T turbulent flame model

Daneshyar et al [132] and Hill [133] demonstrated the validity of Tabaczynski et al's hypothesis of small-scale turbulence on the flame propagation in SI engines basing their analysis on both the isotropic turbulence theory and experimental results which included measurement data and shadowgraphs in engines as well as a combustion bomb. Important turbulent quantities, such as the integral scale, micro-scale, turbulence intensity and turbulent flame speed were further analyzed under typical engine and combustion bomb conditions. Some of their results are summarized as follows:

- The integral scale L during the combustion period is of the order of the combustion chamber height. (From two-point spatial correlations of LDV

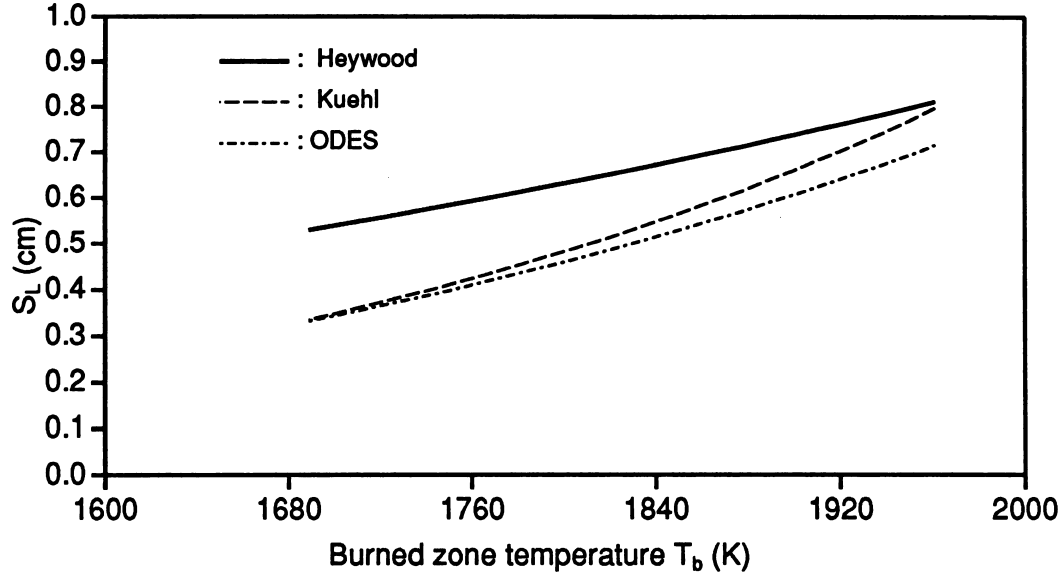


Figure 3.8: The development of the laminar flame speed in the combustion of a propane-air mixture at $P_0=2$ MPa, $T_0=500$ K, and $\phi=0.5$

measurements Fraser et al[165] estimated L as being about one-fifth of the minimum clearance height at tdc);

- The turbulence intensity, u' , is estimated as

$0.3 < u' < 0.7$ m/sec (fan motion generated turbulence in the combustion bomb used in their experiment);

$1.0 < u' < 2.0$ m/sec (engine with an unshrouded valve);

$4.0 < u' < 6.0$ m/sec (engine with a shrouded valve);

- The turbulent flame speed, S_T , under the conditions of $R_L \equiv u'L/\nu > 1000$ and $u'/S_L > 10$, is

$$S_T = S_L + Cu' \quad (3.33)$$

where, $C = 2.0 \pm 0.1$;

- The kinematic viscosity of the unburned mixture towards the end of compression was found to be $\nu \simeq 6 \times 10^{-6} \text{m}^2/\text{sec}$;

- The Taylor micro-scale, λ , can be estimated for homogeneous isotropic turbulence. For local isotropic turbulence [166], the rate of disappearance of turbulent kinetic energy due to viscosity is given as

$$\epsilon = \frac{u'^3}{L} = 15\nu\left(\frac{u'}{\lambda}\right)^2 = \nu\frac{v^2}{\eta^2}$$

where the velocity $v = (\nu\epsilon)^{1/4}$ is the Kolmogorov velocity. The above relationship implies that

$$\frac{L}{\lambda} = \frac{1}{\sqrt{15}}R_L^{0.5} = \frac{1}{15}R_\lambda$$

Therefore, the Taylor micro-scale can be given as

$$\lambda = \sqrt{15}L/R_L^{0.5}$$

3.6 The Current Model

3.6.1 The model's assumptions

The turbulent flame propagation model constructed here is principally that of Blizard-Keck-Tabaczynski, with modifications as given in the last section. One further modification is that, when calculating the laminar burning speed S_L , Eq. 3.27 is used instead of Eq. 3.8. The model's assumptions are listed as:

- (1) The turbulent field is isotropic and homogeneous at the time of ignition.
- (2) The turbulence intensity before ignition, u'_i , is determined as follows. In the case of an engine, u'_i is proportional to the mean piston speed. The conditions to be satisfied have been taken as $u'_i = c\bar{V}_P$ with u' falling in the range $1.0 < u'_i < 2.0$ m/s for an unshrouded valve and $4.0 < u'_i < 6.0$ m/sec for a shrouded valve. In the case of a combustion bomb, where turbulence is generated by fan motion, the condition is simply that $0.3 < u'_i < 0.7$ m/s.

- (3) The turbulent integral scale, L , before ignition is about the order of the instantaneous chamber height. This implies that the turbulence has relaxed to the shape of the vessel.
- (4) Ignition occurs across a highly dissipative region (of the order of the Kolmogorov scale, η) and burning within this region is instantaneous. However, ignition propagates along the vortex tubes at the rate of $S_L + Cu'$ and the unburned mixture entrained by the flame front burns up at the laminar burning speed S_L (see Fig. 3.4).
- (5) The flame propagates spherically with the spark point as its centre and the thickness of the flame front is negligible.
- (6) After ignition, the turbulence intensity and integral scale are governed by the conservation of angular momentum:

$$L = L_i(\rho_{ui}/\rho_u)^{1/3}$$

$$u' = u'_i(\rho_u/\rho_{ui})^{1/3}$$

- (7) The thermodynamic conditions of the mixture are the same as given in Sec.2.3 of Chapter 2.

3.6.2 The burning law

Equations of the burning law of turbulent flame propagation in a homogeneous mixture are as follows:

- (1) The rate of mass fraction entrained by the flame front is

$$\frac{dX_e}{dt} = \frac{\rho_u A_e}{m_0} (Cu' + S_L) \quad (3.34)$$

where, m_0 is the total mass of mixture, A_e is the area of a spherical flame front centred at the spark point, and C is an empirical constant.

- (2) The rate of mass fraction burned is

$$\frac{dX_b}{dt} = \frac{X_e - X_b}{\tau} \quad (3.35)$$

where,

$$\tau = \lambda/S_L \quad (3.36)$$

(3) The Taylor micro-scale λ , in isotropic homogeneous turbulent flow is

$$\lambda = \sqrt{15}L/R_L^{0.5} \quad (3.37)$$

where R_L is the integral Reynolds number of the mixture, defined as

$$R_L \equiv u'L/\nu$$

(4) Conservation of angular momentum gives:

$$L = L_i(\rho_{ui}/\rho_u)^{1/3} \quad (3.38)$$

$$u' = u'_i(\rho_u/\rho_{ui})^{1/3} \quad (3.39)$$

Burning law equations 3.34 to 3.39 in conjunction with the equations of the thermodynamic submodel in Sec. 2.3 of Chapter 2, construct the governing equation set for this turbulent flame propagation model.

In the next section, the computational results of this model are presented and discussed.

3.7 Application of the Turbulent Flame propagation Model to a Constant Volume Combustion Bomb

Figure 3.10 and 3.11 show the computational results of a turbulent flame propagation in an adiabatic, constant volume, cylindrical combustion bomb for a methane-air and a propane-air mixture respectively. Because this research is aimed at understanding of the dual fuel combustion process where the pre-mixed fuel is gaseous, only methane and propane have been considered as fuel. Ignition is assumed to occur at the top centre of the bomb (point O in Fig. 3.9) and the subsequent flame propagates spherically outwards. The entrainment

front, A_e , is the intersection of this sphere and the wall of the combustion chamber, given as:

$$A_e(r_f) = \begin{cases} 2\pi r_f^2 & r_f \leq H \\ 2\pi r_f H & H < r_f \leq R \\ 2\pi r_f (H - \sqrt{r_f^2 - R^2}) & R < r_f \leq \sqrt{R^2 + H^2} \end{cases} \quad (3.40)$$

The entrainment volume behind the entrainment front, V_e , is given as:

$$V_e(r_f) = \begin{cases} \frac{2}{3}\pi r_f^3 & r_f \leq H \\ \pi r_f^2 H - \frac{\pi}{3}H^3 & H < r_f \leq R \\ \pi R^2 r' + \pi r'^2 (H - r') - \frac{\pi}{3}(H^2 - r'^2) & R < r_f \leq \sqrt{R^2 + H^2} \end{cases} \quad (3.41)$$

where r_f is the flame front radius, $r' = \sqrt{r_f^2 - R^2}$ and it is assumed $R > H$.

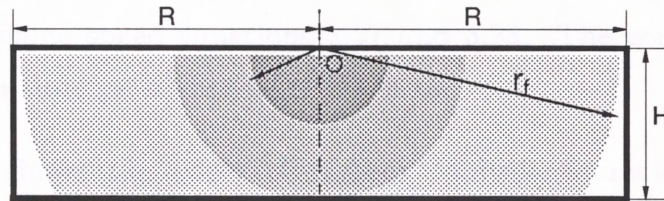


Figure 3.9: Schema of spherical turbulent flame propagation in a combustion bomb with central ignition at point O.

For the calculations presented here, the combustion bomb is assumed to have 108 mm diameter and 21 mm height. The incremental rate of pressure increase, dp/dt is proportional to the rate of burning. Therefore, a peak in dp/dt means that the burning rate reaches its maximum. At the start of ignition, dp/dt approaches zero. The results show that the mass entrained fraction x_e is always slightly ahead of the MBF until all charge has been burned. Comparing Fig. 3.10

with Fig. 3.11, it is found that burning of the propane-air mixture is faster than the burning of the methane-air mixture. This is because propane has a faster laminar flame speed than has methane.

Fig. 3.12 shows the affects of initial pressure on the flame propagation in the combustion bomb. The R^0 in the Figure is the normalized entrainment radius. $R^0 = 0$ indicates that the spherical flame front has reached the furthestmost point of the combustion chamber from the ignition position. It can be seen that the flame propagates faster at the higher initial pressure P_0 if other conditions remain unchanged. This is because the laminar flame speed increases with the pressure. The cylinder charge therefore burns more quickly.

Fig. 3.13 shows the affect of initial temperature on the flame propagation. As has been discussed in Chapter 2, if P_0 and ϕ remain unchanged, a higher initial temperature T_0 causes a reduction in the maximum combustion pressure because of the decrease in the ratio of $\frac{R_b T_b}{R_u T_0}$. This is because the increase in maximum combustion temperature is less than that of T_0 . The laminar flame speed therefore reduces because of the lower density. This can also be seen from the laminar flame speed equations 3.27 and 3.28. The combustion therefore takes a longer time, as is shown on Fig. 3.13.

Fig. 3.14 shows the affect of fuel-air equivalence ratio ϕ on the flame propagation. As S_L is sensitive to ϕ , reducing the value of ϕ prolongs the combustion duration substantially.

Fig. 3.15 shows the affect of the turbulence intensity on the flame propagation. Naturally, stronger turbulence intensity makes the flame front move faster even at the same S_L . Fig. 3.15 shows that flame propagation is strongly affected by the turbulence intensity in the cylinder as the combustion duration appears to be very sensitive to u' . It also shows that the entire cylinder charge is entrained into the flame front before it is burned out, as indicated by the fact that the normalized entrainment radius R^0 reaches 1 before the BMF does.

The current turbulent flame propagation model can also be used to study the affect of cylinder geometry on the combustion. Fig. 3.16 shows the calculated

results for three combustion bombs of which the diameter to height ratio r^* are 0.194 (108 mm diameter, 21 mm height), 0.350 (88.8 mm diameter, 31.0 height) and 0.500 (78.8 mm diameter, 39.4 mm height) respectively with identical volumes of 0.1923 m^3 . It can be seen that increasing the value of r^* prolongs the combustion substantially.

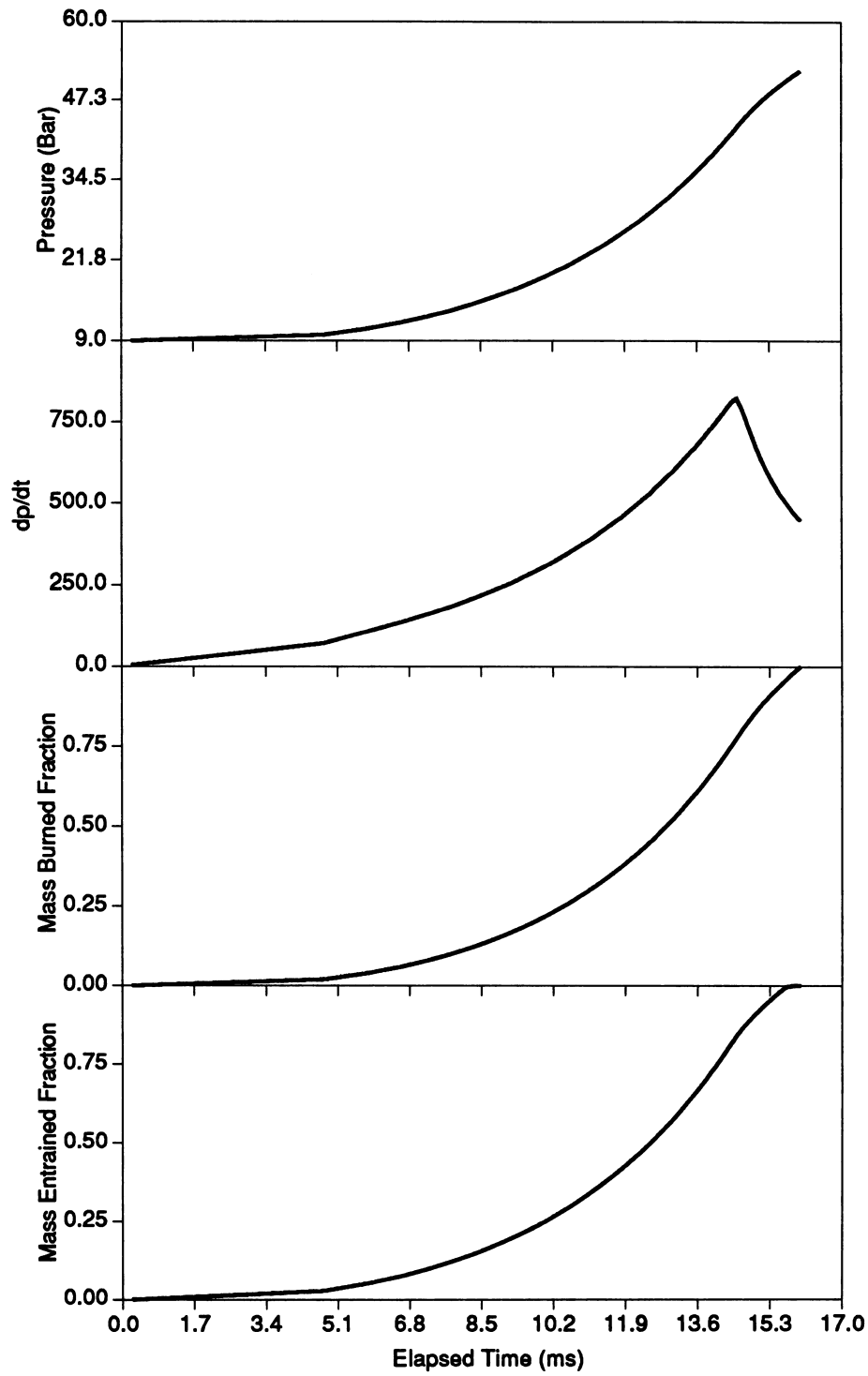


Figure 3.10: Turbulent Flame Propagation in the Bomb of Fig. 3.9.; CH_4 -Air mixture at $P_0 = 9$ Bar, $T_0 = 500$ K, $\phi = 1.0$, and $u' = 0.7$.

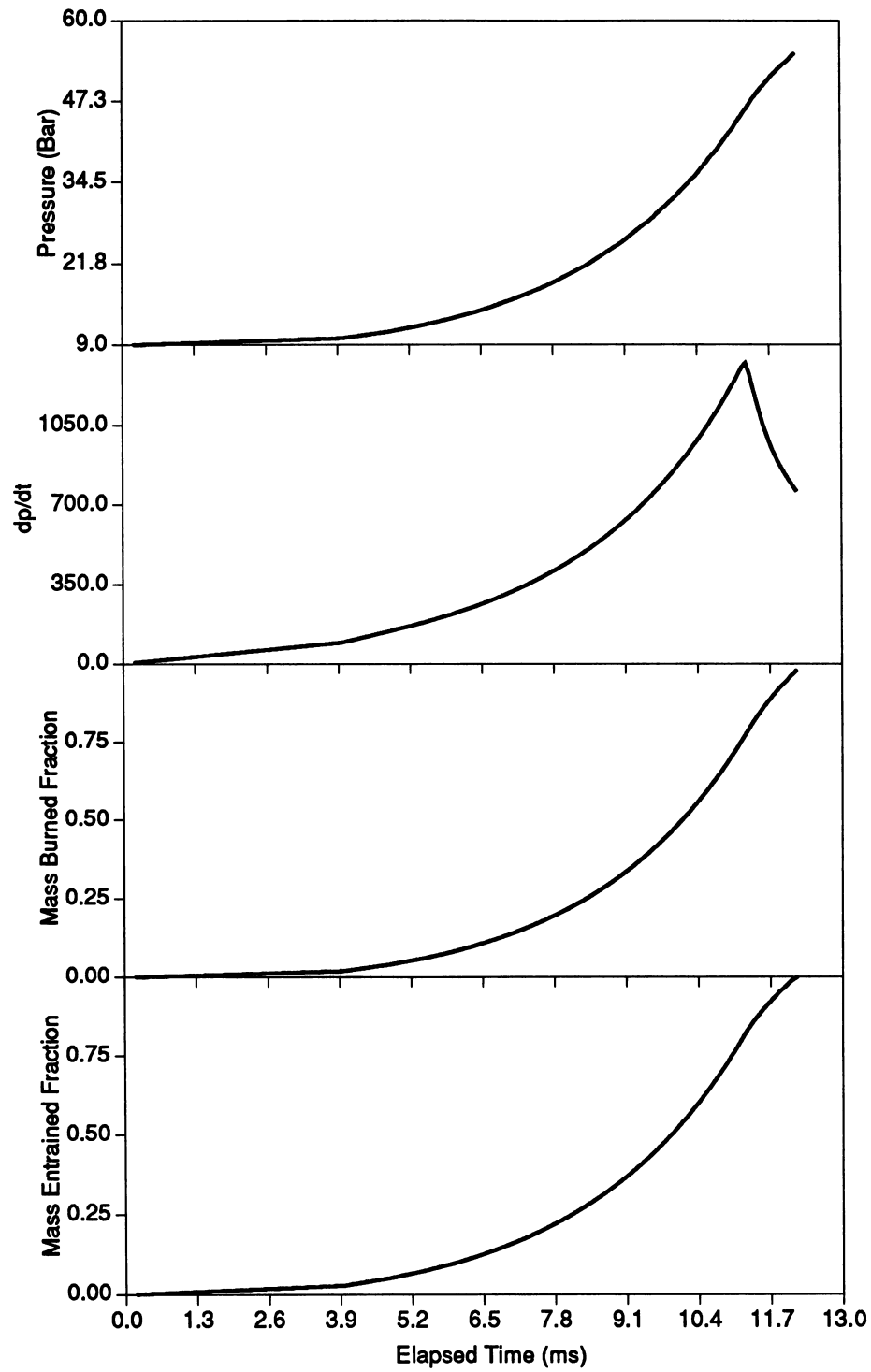


Figure 3.11: Turbulent Flame Propagation in the Bomb of Fig. 3.9. C_3H_8 -Air mixture at $P_0 = 9$ Bar, $T_0 = 500$ K, $\phi = 1.0, u' = 0.7$.

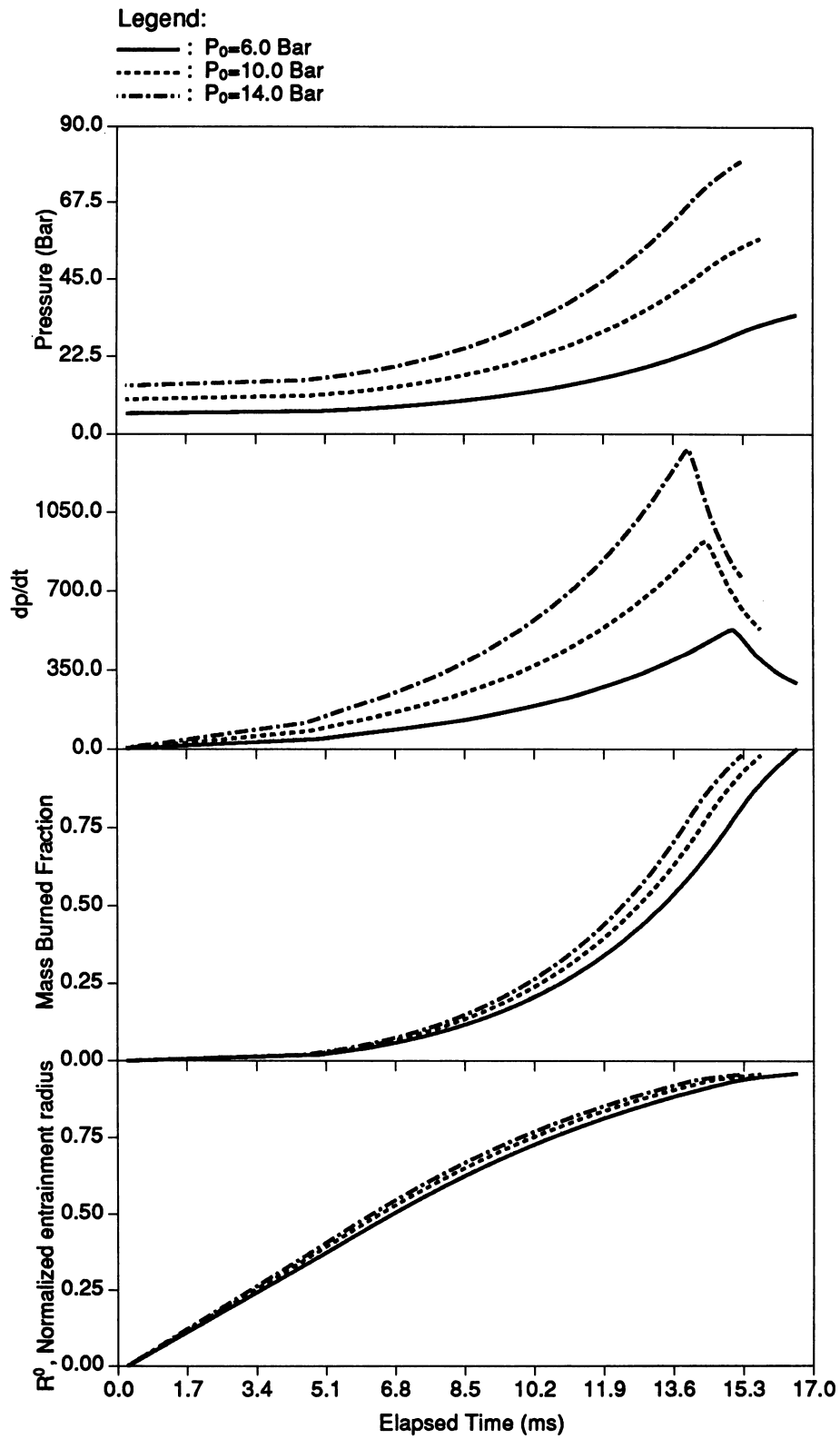


Figure 3.12: Affect of P_0 on the flame propagation in the combustion bomb. CH_4 -air mixture at various P_0 . $T_0 = 500$ K, $\phi = 1.0$, $u' = 0.7$.

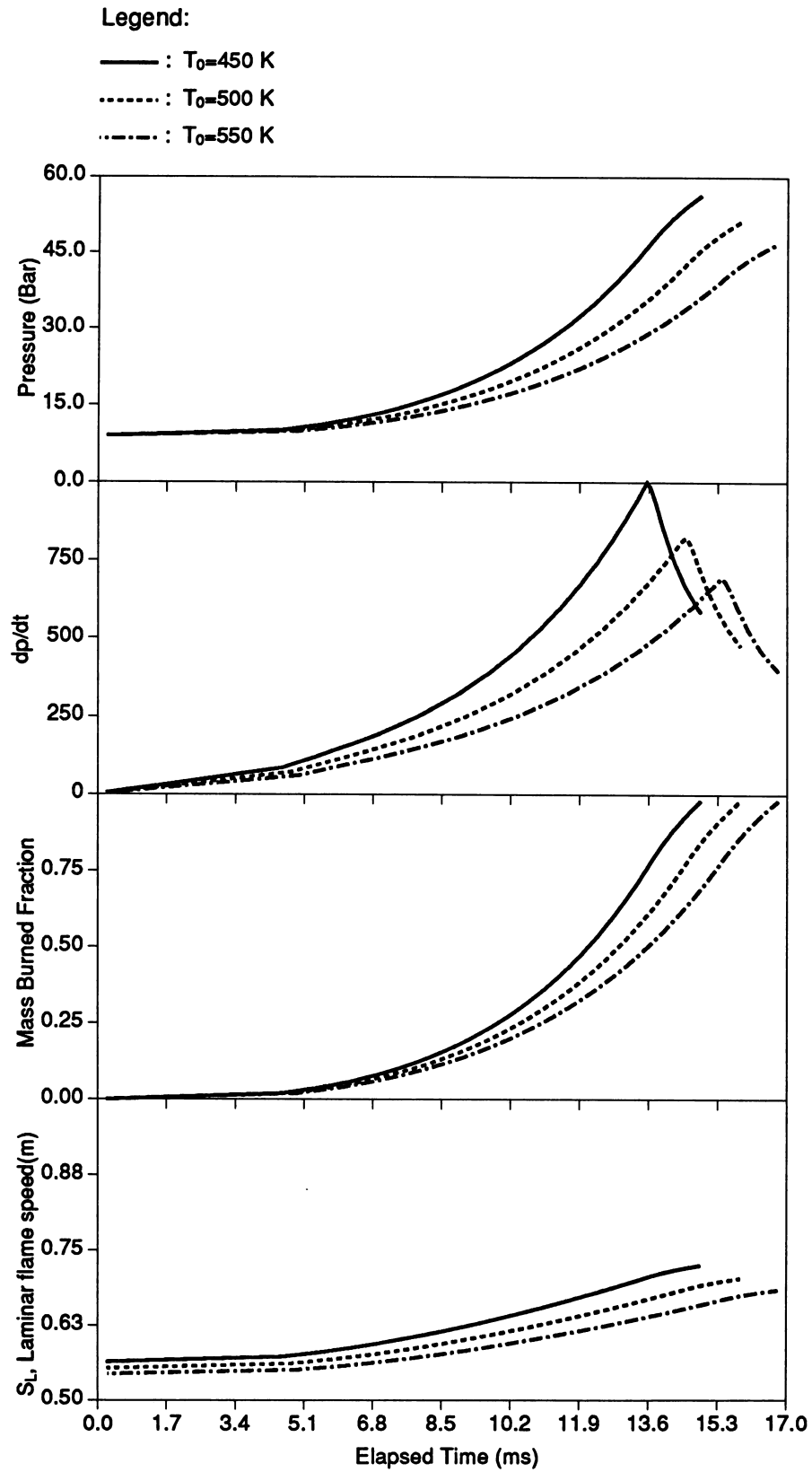


Figure 3.13: Affect of T_0 no the flame propagation in the combustion bomb. CH_4 -Air mixture at various T_0 . $P_0=9.0$ bar, $\phi = 1.0$, $u' = 0.7$.

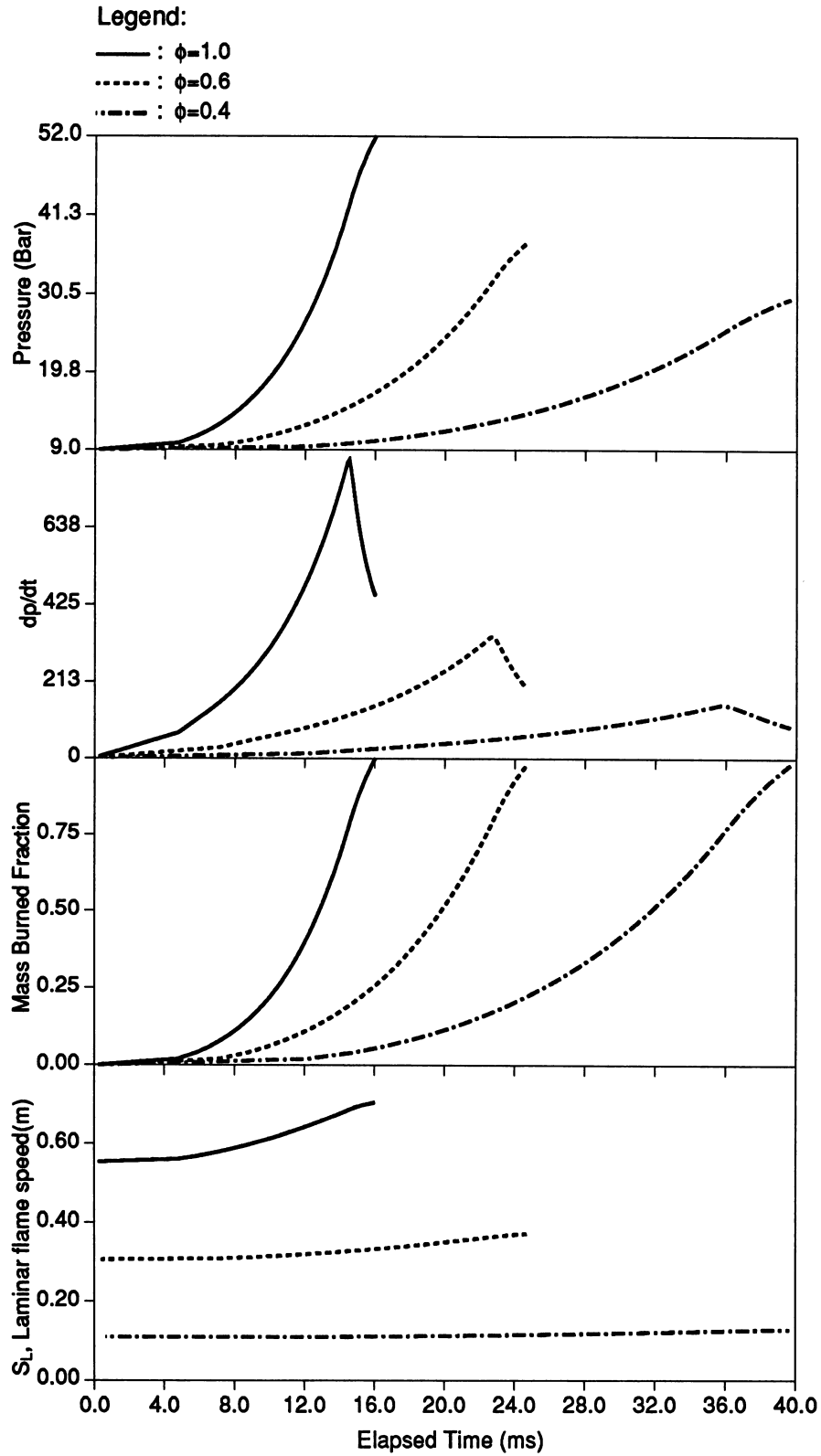


Figure 3.14: Affect of ϕ no the flame propagation in the combustion bomb. CH_4 -air mixture at various ϕ . $T_0 = 500$ K , $P_0 = 9$ bar, $u' = 0.7$.

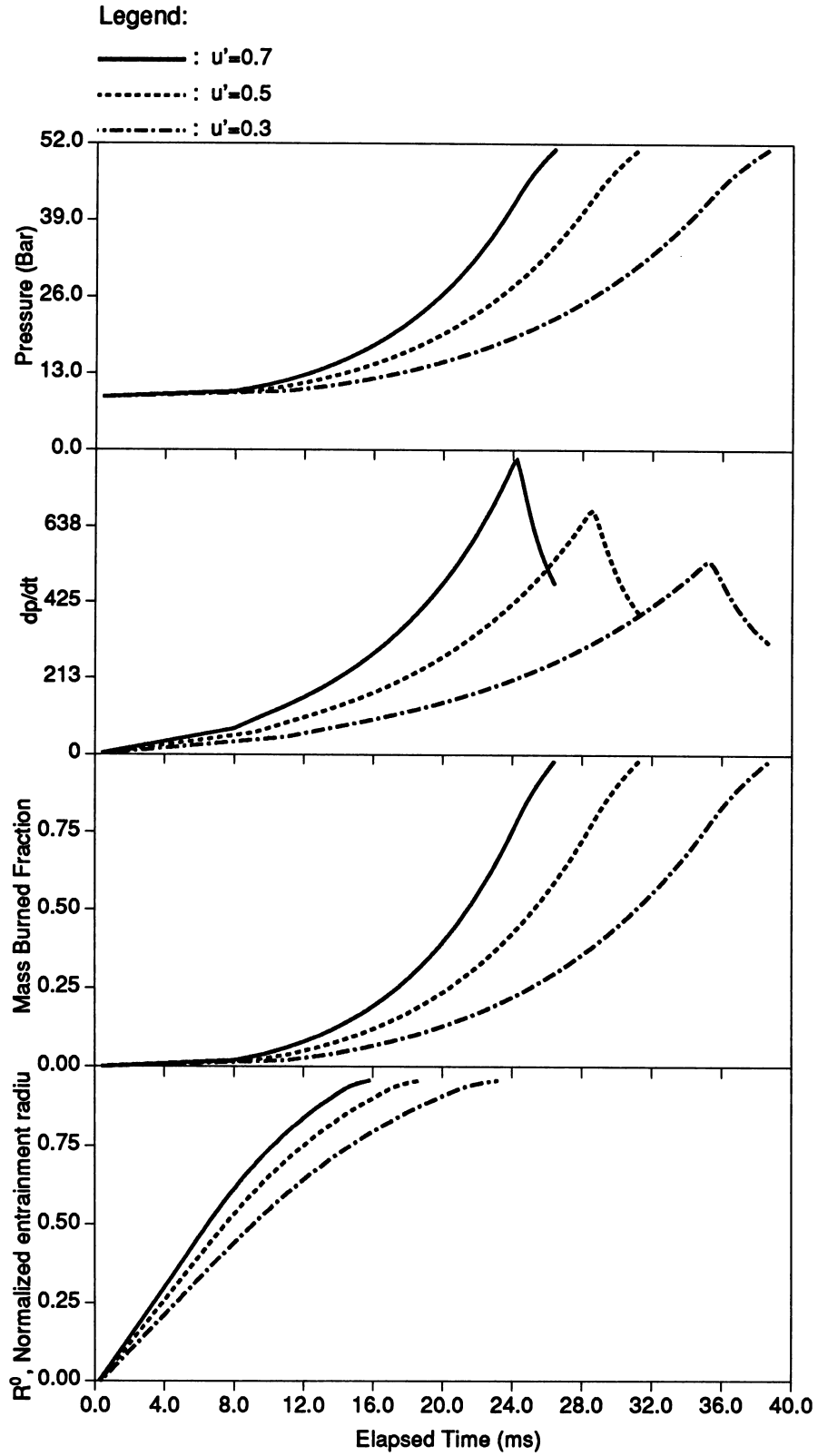


Figure 3.15: Affect of u' no the flame propagation in the combustion bomb. CH_4 -Air mixture with various turbulent intensities. $P_0=9.0$ bar, $\phi = 1.0$, $T_0 = 500$ K.

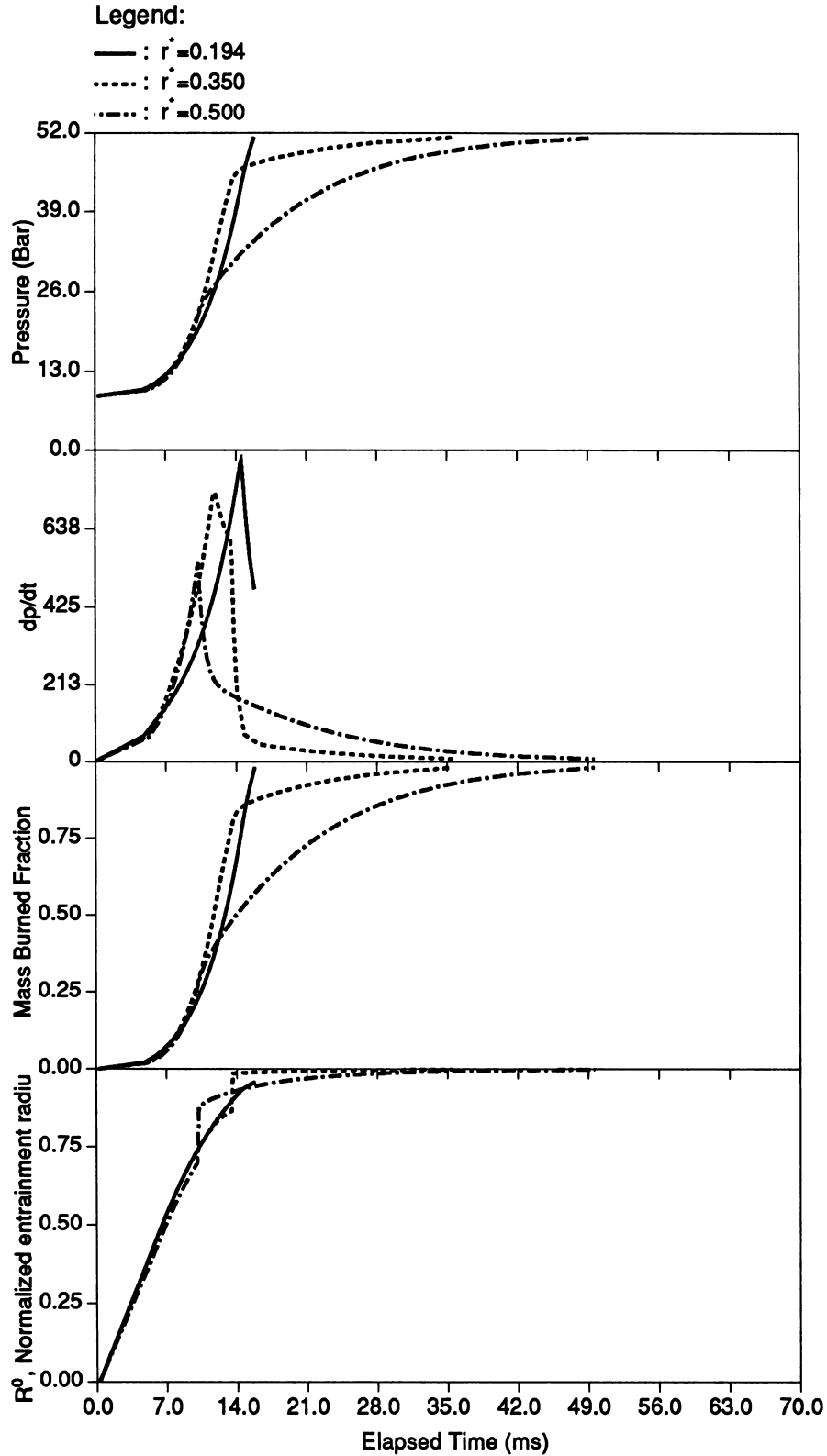


Figure 3.16: Affect of diameter:height ratio r^* no the flame propagation in the combustion bomb. CH_4 -Air mixture of $P_0=9.0$ bar, $\phi = 1.0$, and $T_0 = 500$ K. Volume of combustion chamber remains unchanged as $V_0=0.1923 \text{ m}^3$

Chapter 4

Experiment Setup and Procedures of A Constant-Volume Dual-Fuel Combustion Bomb

4.1 Introduction

As has been discussed previously, specially designed combustion devices are useful, sometimes inevitable in the study of engine combustion. This is particularly the case when full control and precise measurement and observation of in-cylinder processes and phenomena are required. Many researchers have used constant volume combustion bombs to assist their understanding of combustion in both the SI engine and, to a lesser extent, the conventional diesel engine. However, no reports using a combustion bomb in dual fuel combustion research have been found.

In this chapter, a dual fuel combustion bomb experimental apparatus and procedures for its use are presented in detail. It has been used for the present study of dual fuel combustion. This combustion bomb was designed, developed and constructed at the University of New South Wales [170]. It was designed particularly for the study of gas-diesel dual fuel combustion, but can also be run for sole diesel fuel combustion. Figure 4.1 is a view of the experimental

apparatus and Figure 4.2 is the schematic diagram of it. The experimental apparatus consists of four main components: the air-gas supply system, the diesel fuel injection system, the combustion chamber and the control and data acquisition system. These components are described in detail in this chapter. Since the current experiments includes both diesel combustion and dual fuel combustion which are distinct, experimental results for the diesel combustion are presented in chapter 5 while results for dual fuel combustion are discussed in chapter 6 and chapter 7. The principal experimental procedures and methods of acquiring and analyzing the data are described in this chapter.

Because of the complex nature of dual fuel combustion and also because no reference about the design and tests of a dual fuel combustion bomb are available, many difficulties were encountered in developing the current experimental rig as well as during the dual fuel combustion experiments. Some of these problems are discussed in this chapter.

4.2 Research Using Combustion Bombs - A Brief Review

4.2.1 Spark ignition bomb with normal pressure and temperature

Much research has been carried out in spark ignition combustion bombs with the cylinder charge being pre-set at normal atmospheric pressure and temperature condition before ignition. This type of combustion device is usually used for investigation of ignition and flame propagation.

Milton et al [169] measured the laminar burning velocity of gaseous fuels in a spherical combustion bomb (the MIT bomb, which was also used in several other projects such as [171]) which was 15.25 cm inside diameter with a central ignition system. The combustible mixture was prepared directly within the combustion bomb and manifold. The spherical flame front was checked by comparing its arrival times at individual ionization probes, while a laser

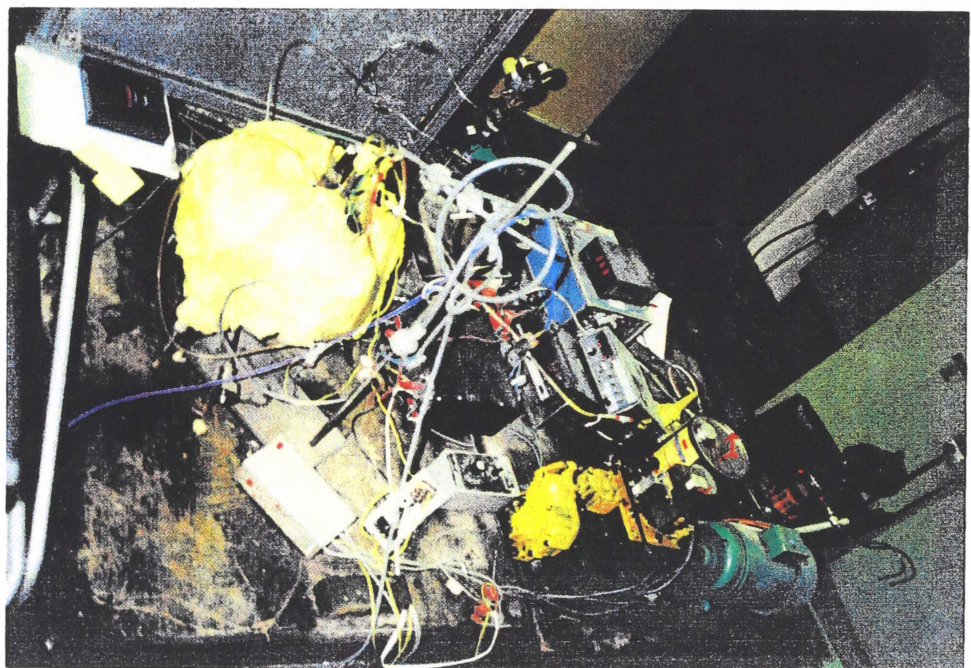
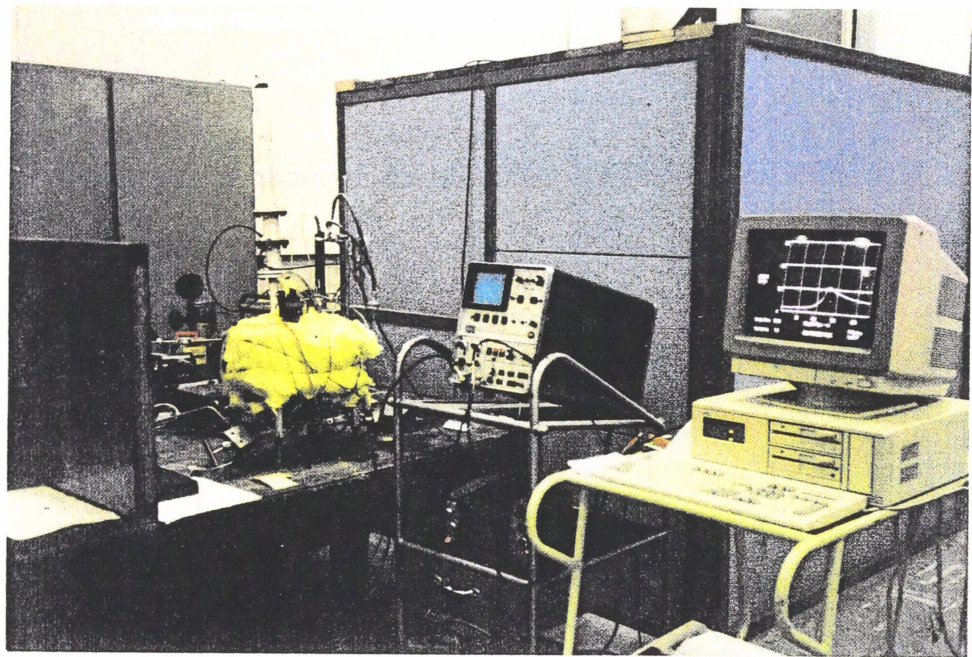
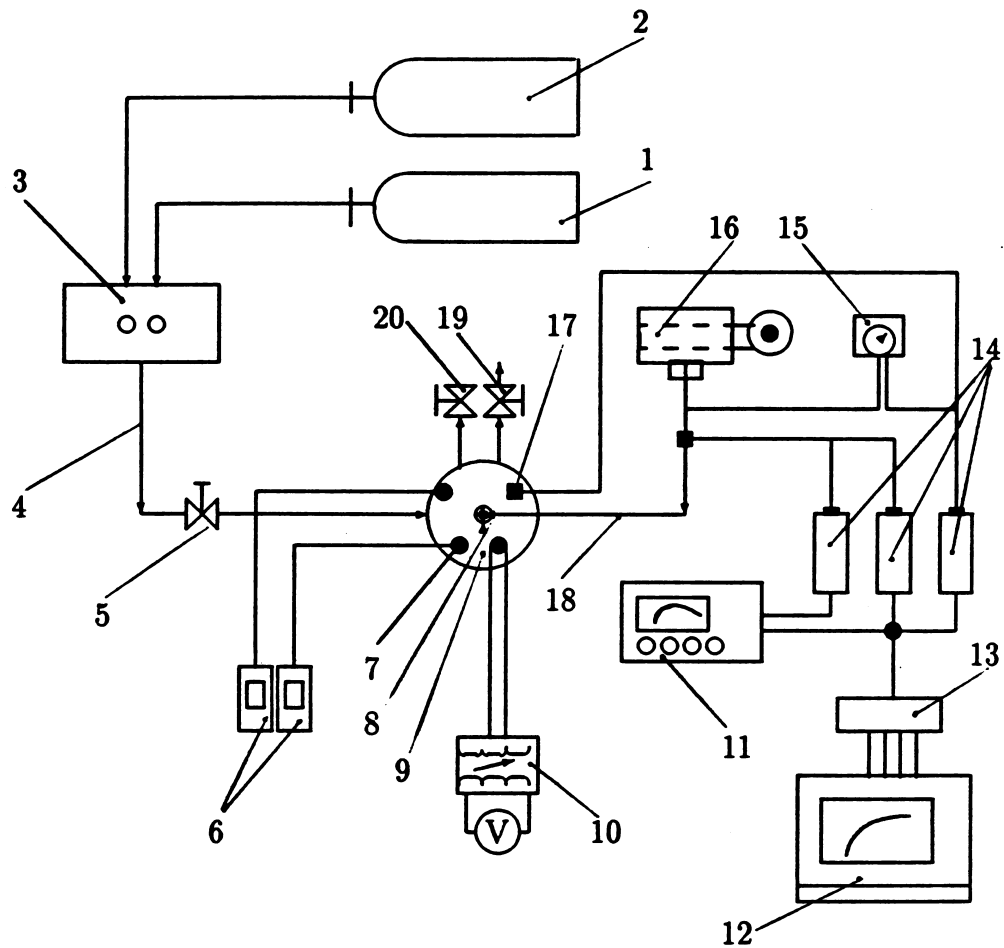


Figure 4.1: Views of the dual fuel combustion rig

Figure 4.2: Scheme of the dual fuel combustion experimental rig



- 1: compressed air; 2: compressed gaseous fuel; 3: air-gas supply-control panel;
 4: air-gas line; 5: inlet valve; 6: digital data taker; 7: thermocouple;
 8: water-cooled injector; 9: combustion bomb; 10: heater power
 supply-control; 11: oscilloscope; 12: PC; 13: data acquisition board;
 14: signal amplifier; 15: control unit; 16: fuel pump and rack;
 17: dynamic pressure transducer; 18: fuel line; 19: outlet valve;
 20: safety valve.

shadowgraph was used to obtain an internal consistency check on the flame radius computed from the pressure transducer readings. Flame speeds of various mixtures were investigated.

Ko et al [172] investigated the flame kernel development of a propane-air mixture in a cylindrical, constant volume steel bomb by means of high-speed laser schlieren photography. The bomb was 83 mm internal diameter and length with an inductive type power source which was able to provide variable spark power levels and discharge durations. Timing of the photographing laser beam was controlled by an acousto optic modulator. Atmospheric pressure propane-air mixtures were used in the experiments. An analytical model to simulate the kernel growth was developed based on the experiment [173].

4.2.2 Spark ignition bomb with turbulence or swirl

Tanaka and Milton [180] investigated the flame propagation generated from dual spark ignition. Experiments were conducted in a box-type vessel with dimensions of $12\text{cm} \times 12\text{cm} \times 6.7\text{cm}$. Stoichiometric propane-air mixtures were prepared at room temperature and pressure for the experiments. Experimental results for various dual spark locations and various time lags between the two sparks were obtained. A theoretical method to simulate the combustion pressure trace and the flame shape in this situation were developed and the calculation results were found to be in good agreement with the experiment. Means of reducing the combustion duration were also suggested.

Bradley et al [181] used a combustion bomb with fan generated turbulence to investigate the ignition of a gaseous mixture. Different spark power-time profiles were obtained by varying the spark discharge duration and energy level. Methane-air mixtures at $\phi = 0.6$ were used in the experiment. Ignition and flame propagation were observed with high speed schlieren cinephotography. A mathematical model for the ignition was presented. Calculated results of the model were compared with the experimental observation at various spark discharge profiles and turbulence intensities.

Hamamoto et al [168], [174] used a constant volume vessel to investigate the laminar burning velocity and the turbulent burning velocity of a propane-air homogeneous mixture. The combustion chamber was a cylindrical vessel 125 mm in diameter and 35 mm deep (about 430 cm^3 volume) with a central spark ignition. The homogeneous propane-air was prepared and stored in a large tank (1920 cm^3) before it was introduced tangentially to the cylindrical wall into the combustion chamber. Swirl was therefore produced by the tangential flow. As the swirling flow decays with the lapse of time, combustion for various flow fields can be obtained by igniting the mixture at various times after the mixture introduction. The pre-ignition temperature of the mixture remained at room temperature while the pressure was varied to different values below 347 kPa. The flame propagation speed was determined from the time of flame travel across the distance between two He-Ne laser beams and the flame front was detected by the refraction of a laser beam due to the rapid change in the refractive index at the flame front. The laminar burning velocity, the turbulent burning velocity, and the burning zone thickness were measured.

4.2.3 Diesel bomb without combustion

A diesel bomb without combustion has often been used to study diesel fuel droplet or spray behaviour.

Nishida et al [175], [176] investigated diesel spray evaporation in a high pressure bomb with holographic technology. The cylindrical diesel bomb used in the experiment was 150 mm in diameter and 150 mm in length with two 60 mm diameter quartz glass windows in both sides of the bomb for optical access. In order to avoid burning of the injected diesel, the bomb was filled with nitrogen to 3.1 MPa. This high pressure gas was also heated to 773 K in order to simulate the conditions in a diesel engine. A rotating plate was located inside the bomb to stir the gas in order to obtain a spacially uniform temperature. Shadowgraphs, schlieren photographs and micrographs were taken from the setup and spray width and equivalence ratio of fuel droplets were microscopically measured. Spray width was found to have a tendency to decrease as the temperature

increased.

Elkott et al [179] investigated droplet evaporation in a high pressure bomb with quartz windows. Nitrogen gas was used to charge the bomb to high pressure. The nitrogen was preheated in a 2-kW electrical furnace before it was slowly introduced into the bomb, where heating continued by use of another 2-kW heating element until it reached 673 K. Either a single droplet or a parcel of droplets was produced by a centrally mounted injection nozzle (single hole to produce a single droplet, multiple holes to produce a parcel of droplets which simulate a fuel spray). Droplet evaporation was photographed by a high-speed camera. Experiments were carried out for various commercial fuel and their blends. Generalized correlations were derived for the evaporation constant. An empirical correlation factor accounting for the droplet interaction effect on the evaporation constant was also proposed.

4.2.4 Diesel bomb with combustion

In early research, the experimental setup for a constant volume diesel combustion bomb was usually heating in a furnace. A typical example of this is that used by Hurn et al [177]. In Hurn et al's experiment, a cylindrical stainless steel bomb ($2\frac{1}{2}$ in. diameter, $3\frac{1}{2}$ in. length) equipped with a single-shot diesel injection device, was housed in a furnace so that a uniform high temperature was able to be obtained. The single-shot injection was effected by means of a latch mechanism which allowed the pump plunger to stroke for only a single cycle. Ignition delay was investigated at various pressures (up to 650 psi) and temperatures against different oxygen concentrations and fuel characteristics such as composition, volatility, crude-oil type, fuel additive and cetane number.

More recently, in Hiroyasu et al's experiments [178], a cylindrical combustion bomb (275 mm diameter, 660 mm length) contained a cubic (120 mm side length) electrical furnace to heat the charged gas in the bomb. The spontaneous ignition delay of fuel droplets was investigated at 0 to 40 atm gauge pressure and 220° C to 700° C gas temperature. Ignition of the droplet was identified

from photographs taken by a movie camera.

Fujimoto et al [162] used a constant volume combustion chamber (350 mm inner diameter, $3.3 \times 10^{-3} m^3$ volume) to simulate the combustion in a diesel engine. The diesel spray combustion process was studied by use of high speed photography through quartz windows mounted on the bottom of the combustion chamber. Correlations for pressure rise delay and illumination delay were obtained respectively from the experiment. Their combustion chamber was designed capable of being charged with air up to 8 MPa cylinder pressure. The charged gas was able to be heated up to 800 K by electrical heating elements set above the piston crown.

4.3 Dual Fuel Combustion Bomb Used in the Current Research

4.3.1 Difficulties in developing a dual fuel combustion bomb

The dual fuel combustion bomb being used in this research is essentially a combination of a diesel combustion bomb in that the appropriate high temperatures and pressures necessary for the ignition of the fuel spray must be obtained and a spark ignition bomb in that a pre-mixed fuel/air mixture must be retained prior to ignition. The unique difficulty of this kind of experiment is that a combustible mixture must be retained in the bomb at high pressure and temperature which is at the diesel spray spontaneous ignition conditions but below the gaseous mixture spontaneous ignition conditions. For this reason, the heating-temperature control and the gas filling-pressure control both need to be especially precise. Sealing of the bomb needs to be of a high order as the high pressure gas/air mixture must be held when the mixture is being heated. Also, the injector has to be protected from the hot gas in the bomb so that the fuel will not “bake” during the heating process. These difficulties do not occur or only occur to a much lesser degree in a spark ignition or a diesel bomb. This

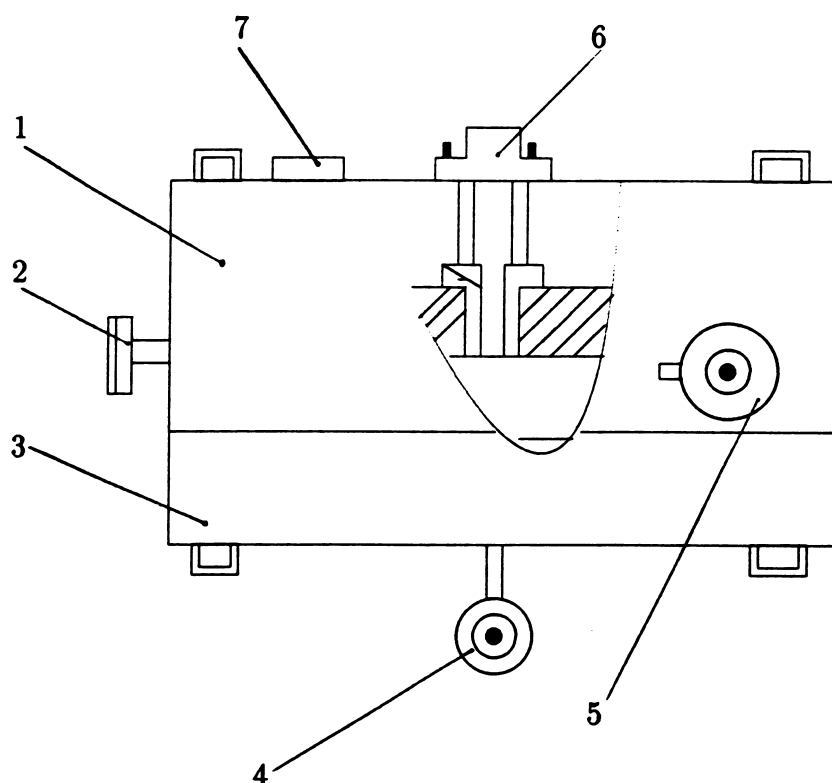
is because, as reviewed in the previous section, in the case of the spark ignition bomb, the mixture in the bomb does not need to be held at a high temperature and pressure as the pre-mixed charge is ignited by electrical spark, and in case of diesel bomb, only air (or nitrogen, for non-combustion experiment) is used in the bomb.

4.3.2 Design of the Combustion Chamber

The combustion chamber referred here consists of parts which are directly assembled with the combustion unit. It excludes parts which will be described under other systems such as the injector, thermocouple and pressure transducer. As shown on Fig. 4.3 and 4.4, it consists of a steel combustion cylinder where the combustion actually takes place, an upper and a lower mild steel disc, an outer ceramic ring for thermal insulation, upper and lower steel casings which provide the strength to withstand the high combustion pressure, two electrical heater elements which are attached on the side wall and bottom of the combustion cylinder respectively in order to provide heating of the cylinder charge, a small air circulation device, quartz windows to allow visualization tests if required, an inlet and an outlet valve, the nozzle seat to mount the diesel injector and a safety valve to release high pressure which may damage the experimental rig.

The combustion cylinder is designed to have the dimension of a typical large truck diesel engine near its top dead centre position, being 108 mm bore and 28 mm height originally. After placing an additional heating element at the bottom, it reduces to 21 mm height. Designed maximum working pressure of the bomb is 6MPa at 2250°C.

Partially stabilised zirconia (PSZ) was chosen as the material for the ceramic liner of the combustion chamber because of the high strength, high coherence and low thermal conductivity requirement. In the original design, ceramic liner discs were also used on the top and bottom of the cylinder in addition to the outer ring. However, one of these ceramic discs was damaged in another experiment [163] because, in the heating test the thermal expansion and growth



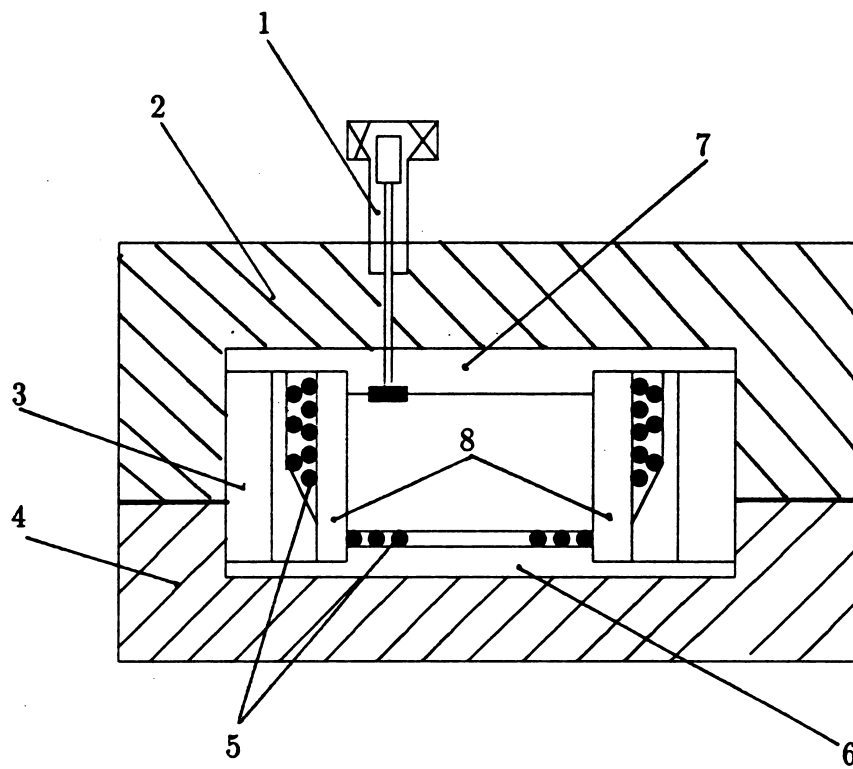
1: upper casing; 2: safety valve; 3: lower casing;

4: outlet valve; 5: inlet valve; 6: nozzle seat; 7: quartz window.

Figure 4.3: Outside view of the combustion chamber.

of the material proved to be different from the anticipated values. Two mild steel discs were then substituted, insulated by asbestos fibre.

Originally, only one 1000 watt heating element was used around the outside of the combustion cylinder. This heating element (coil) was wrapped in a sheet metal ring which was filled with ceramic, castable adhesive to attach it onto the side wall of the cylinder. That heating arrangement was found to be insufficient because it took a very long time to heat up the in-cylinder mixture [163] (it took about 1 hour to obtain 300° C in the cylinder). An additional 630 watt heating coil was therefore placed on the bottom of the combustion cylinder covered with a ceramic paper gasket-grooved steel disc. A small air circulation device, which



1: air circulation device; 2: upper casing; 3: ceramic ring; 4: lower casing;
5: heating coil; 6: lower mild steel disc; 7: upper mild steel disc; 8: cylinder.

Figure 4.4: Inside view of the combustion chamber.

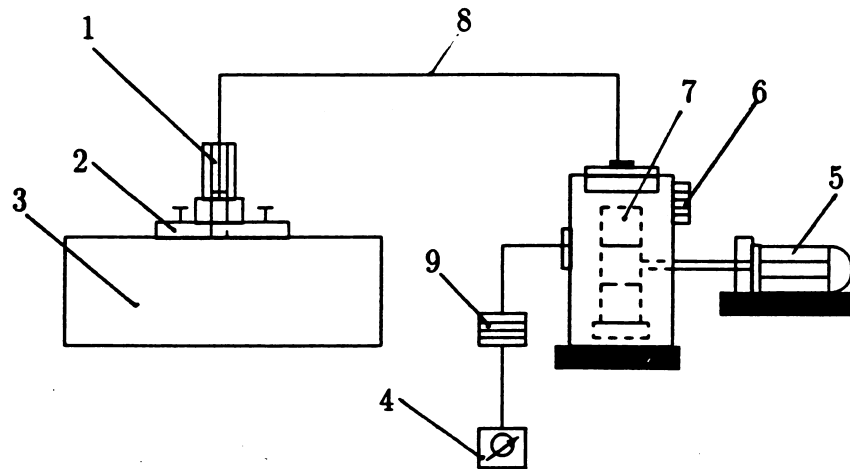
was driven by an oscillating solenoid valve, was used to generate circulation of the in-cylinder mixture. This provided a very low turbulence intensity. After this modification, heating of the mixture was very much improved.

Three small quartz tapered windows were mounted on top of the combustion chamber to allow flow and combustion visualization. The bomb is mounted with one inlet valve for introducing air and gas, one outlet valve for the exhaust of combustion products. A safety valve is incorporated which will burst and release the pressure when pressure exceeds 8.6 MPa. This device prevents the bomb being damaged from high explosive pressure which may occur during some combustion tests. A water-cooled fuel injector is mounted on the centre of the upper casing of the combustion chamber. Additional information on the combustion chamber can also be found in the BE thesis by Jackson [163].

4.3.3 Design of the Single-Shot Diesel Injection System

The injection system consists of a fuel pump and a motor that drives the pump, the fuel pipe, and a water-cooled injector as showed schematically on Fig. 4.5. The fuel pump is converted from a Caterpillar fuel pump from an eight cylinder diesel engine. The fuel pump is designed to deliver only one stroke per operation. The quantity of fuel injected is adjustable manually by a fuel rack which moves a cover to different positions over a spill port in the system. This controls the end of injection. As shown on Fig. 4.6, the injector is a conventional Caterpillar “pencil” type equipped with a water cooling device. The injector is linked to the fuel pump by a fuel pipe. It is mounted on the centre of the upper casing of the combustion chamber by a steel injector seat. This structure allows the injector to be changed when necessary. The injector nozzle is located near the top of the combustion cylinder perpendicularly and the nozzle holes are arranged just at the edge into the chamber. In general, a four hole caterpillar “pencil” injector was used in these experiments. Fuel is delivered as soon as the driving circuit activated the solenoid.

Figure 4.5: Principal elements of the injection system.



- 1: water-cooled injector; 2: injector seat; 3: combustion chamber;
4: injection control unit; 5: motor; 6: manual fuel rack; 7: fuel pump;
8; fuel line; 9: solenoid.

4.3.4 The Air and Gas Supply

Air and gaseous fuel are introduced from a compressed air tank and a compressed gas tank respectively via high pressure regulators in order to obtain the high charge pressure. A control panel ensures that air and gas are introduced into the combustion chamber separately. The appropriate gas/air equivalence ratio determines the partial pressures of the air so that the gas addition brings the bomb to the correct final pressure.

4.3.5 Instrumentation and Measurement

Fig. 4.7 shows the principal elements of the control system of the dual fuel combustion experimental rig. A set of valves in the air-gas supply control panel manually control the air and gas being introduced into the bomb separately. During experiments, air is introduced to the combustion chamber until the working partial pressure is reached. Gas is then introduced after the air route

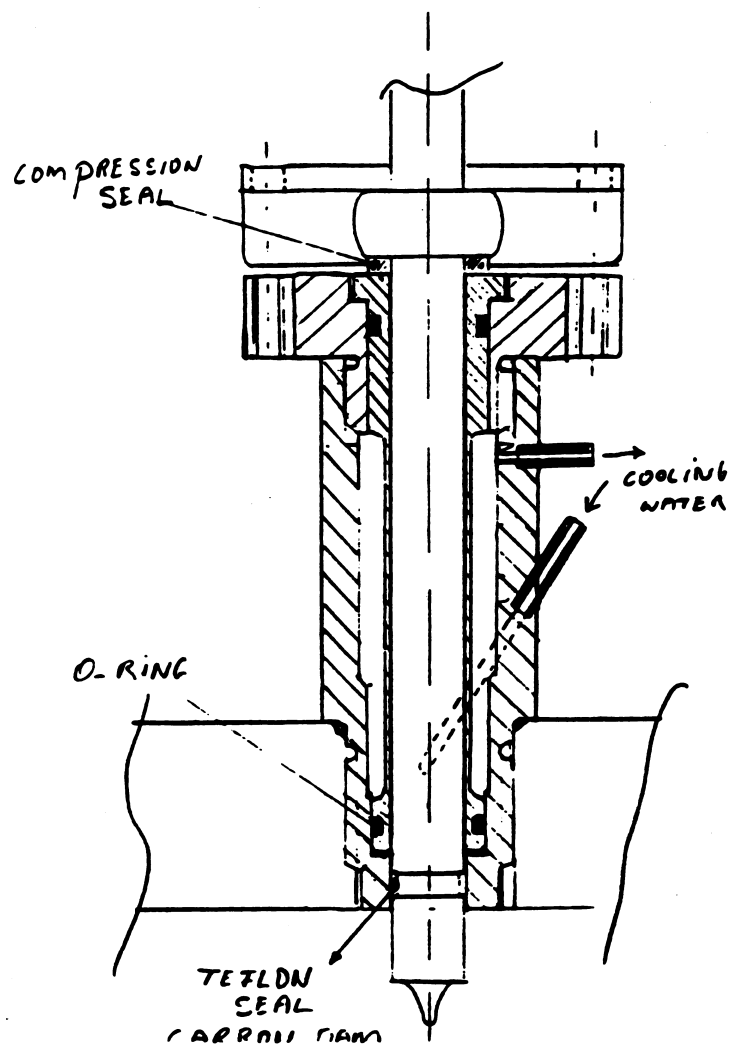
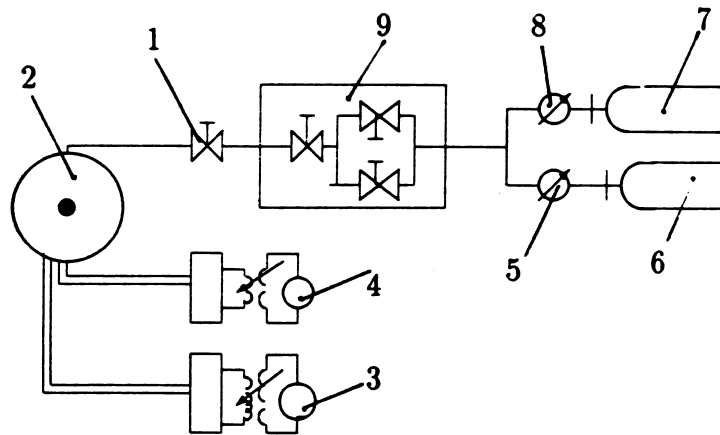


Figure 4.6: Scheme of the water-cooled injector



1: inlet valve; 2: combustion chamber; 3: bottom heater power supply;
 4: side-wall heater power supply; 5: high pressure air regulator; 6: compressed
 air tank; 7: compressed gas tank; 8: high pressure gas
 regulator; 9: air-gas supply and control panel.

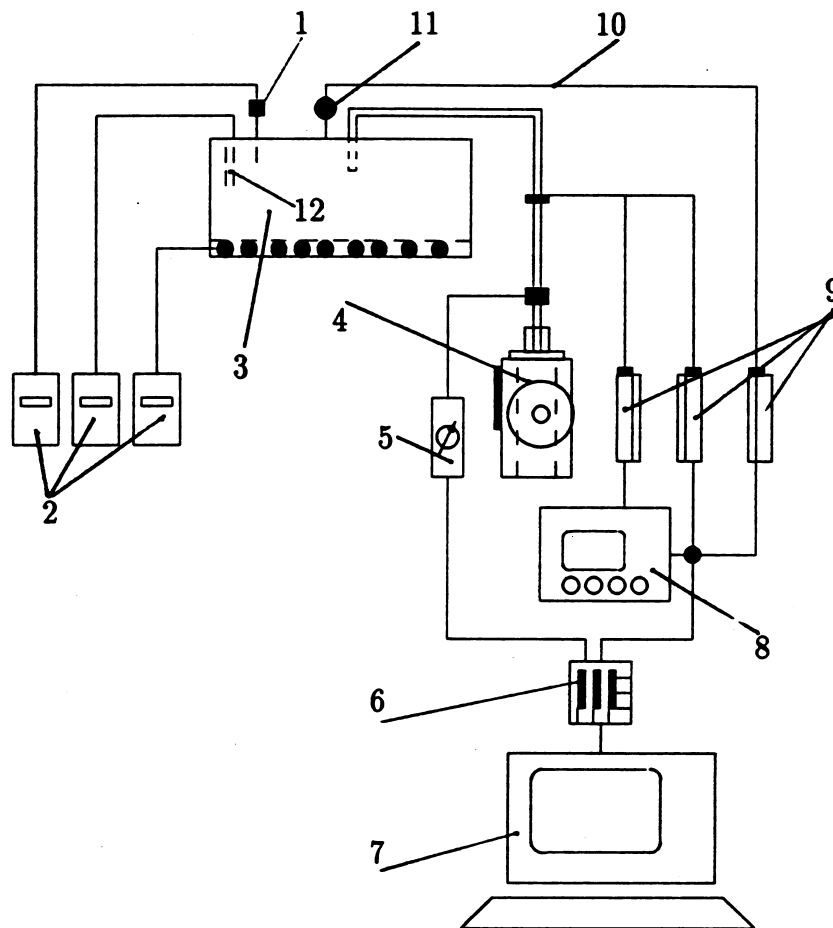
Figure 4.7: Principal elements of the control system.

is closed. By this method, any possible flash-back in the supply line can be avoided.

Heating elements are controlled manually by varying the power supply voltage to maintain the in-cylinder charge at a required pre-ignition temperature. The two heating elements are adjusted separately. Fig. 4.8 shows the principal elements of the data acquisition system. Two thermocouples are plugged into the combustion chamber. One is inside the combustion cylinder to monitor the temperature of the in-cylinder air or air-gas mixture, the other is inside the coil of the bottom heater to evaluate the temperature of the cylinder wall. A static pressure transducer (Kistler piezoresistive absolute pressure transducer Model 4201A-100 bar) is mounted in the combustion chamber to measure the cylinder pressure before injection. Temperature data are read from digital data takers connected with thermocouples. The static pressure data are read from a digital data taker connected to the static pressure transducer via an amplifier.

A dynamic pressure transducer (P.C.B. 112A04 high temperature piezoelectric 500 psi transducer) is mounted to the combustion chamber in a water-cooled adapter and is linked to an oscilloscope via an amplifier. Simultaneously, ampli-

Figure 4.8: Data acquisition system.



1: static pressure transducer; 2: digital data taker; 3: combustion cylinder;
 4: fuel pump; 5: injection control unit; 6: data acquisition board; 7: PC;
 8: oscilloscope; 9: signal amplifier; 10: fuel line; 11: dynamic pressure
 transducer; 12: thermocouple.

fied signals from the dynamic pressure transducer are also stored and displayed by an IBM PC compatible 386SX computer via a data acquisition board.

The data acquisition board used here with the PC is a RTI-860 high-speed simultaneous data acquisition board which can be plugged into one of the extension slots of the IBM PC AT compatible machine. It is high-level language programmable, providing 16 single-ended channels of analog input and A/D conversion resolution of either 8 or 12 bits, sample-and-hold capability for up to four analog inputs simultaneously and on-board RAM to allow up to 256K samples to be acquired. It can also be triggered by various methods including that used in the current experiment, which is an analog voltage originating from an input channel. The RTI-860 also supports a pre-trigger mode of operation that allows a predefined number of data samples to be stored in a circular buffer prior to receiving a trigger. All these features of the data acquisition board enable the entire history of the dynamic pressure of the combustion cylinder and the fuel line to be recorded at the required sampling frequency following an appropriate triggering signal level. Both frequency and triggering level are predefined programmably according to the requirements of each particular combustion experiment.

The start of injection is detected by a delay circuit in the control unit. As soon as injection is detected, the control unit triggers the oscilloscope and the data acquisition board.

4.4 Injection Characteristics of the Injector

The injector used in the current experiment is a caterpillar “pencil” type injector with four horizontal nozzle orifices. Nozzle orifices are 0.0203 mm in diameter, and 0.0605 mm in length. As the injector is located perpendicular to the top wall near the top of the cylinder, the fuel jets are delivered horizontally.

4.4.1 Shape of the spray

Fig. 4.9 are photographs taken from the injector under room temperature and 1 atm pressure showing the development of the spray without combustion. Fig. 4.10 shows a close view of the diesel spray jet of the current injector. It can be seen that it is reasonable to assume that a conical spray jet exists for the phenomenological modelling of diesel spray combustion.

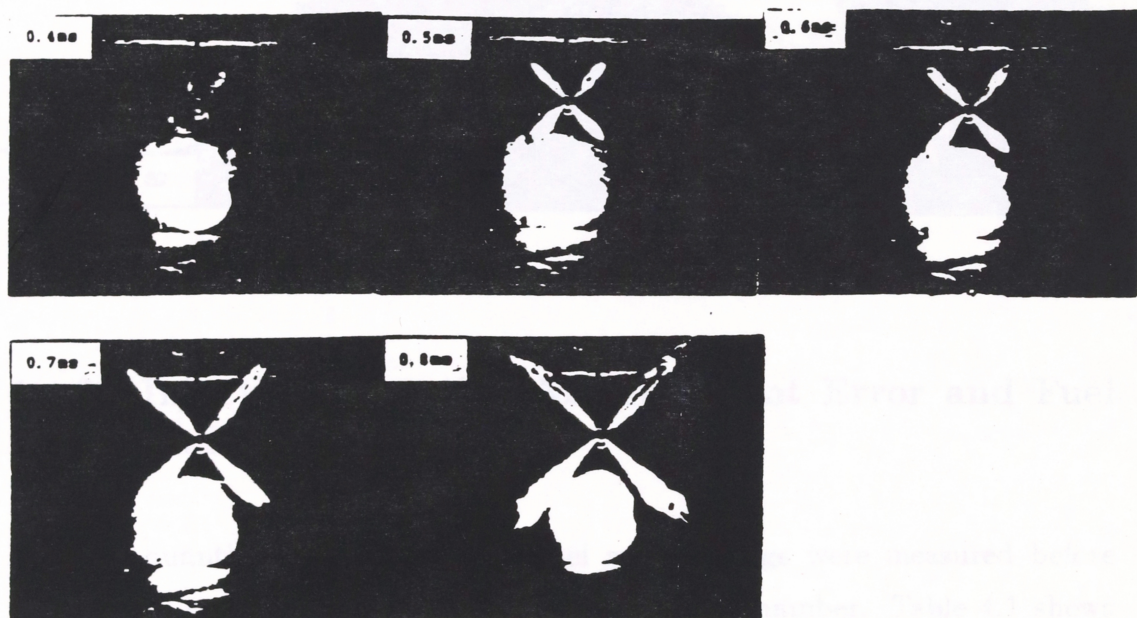


Figure 4.9: A view of the developing non-combustion diesel spray in the present rig.

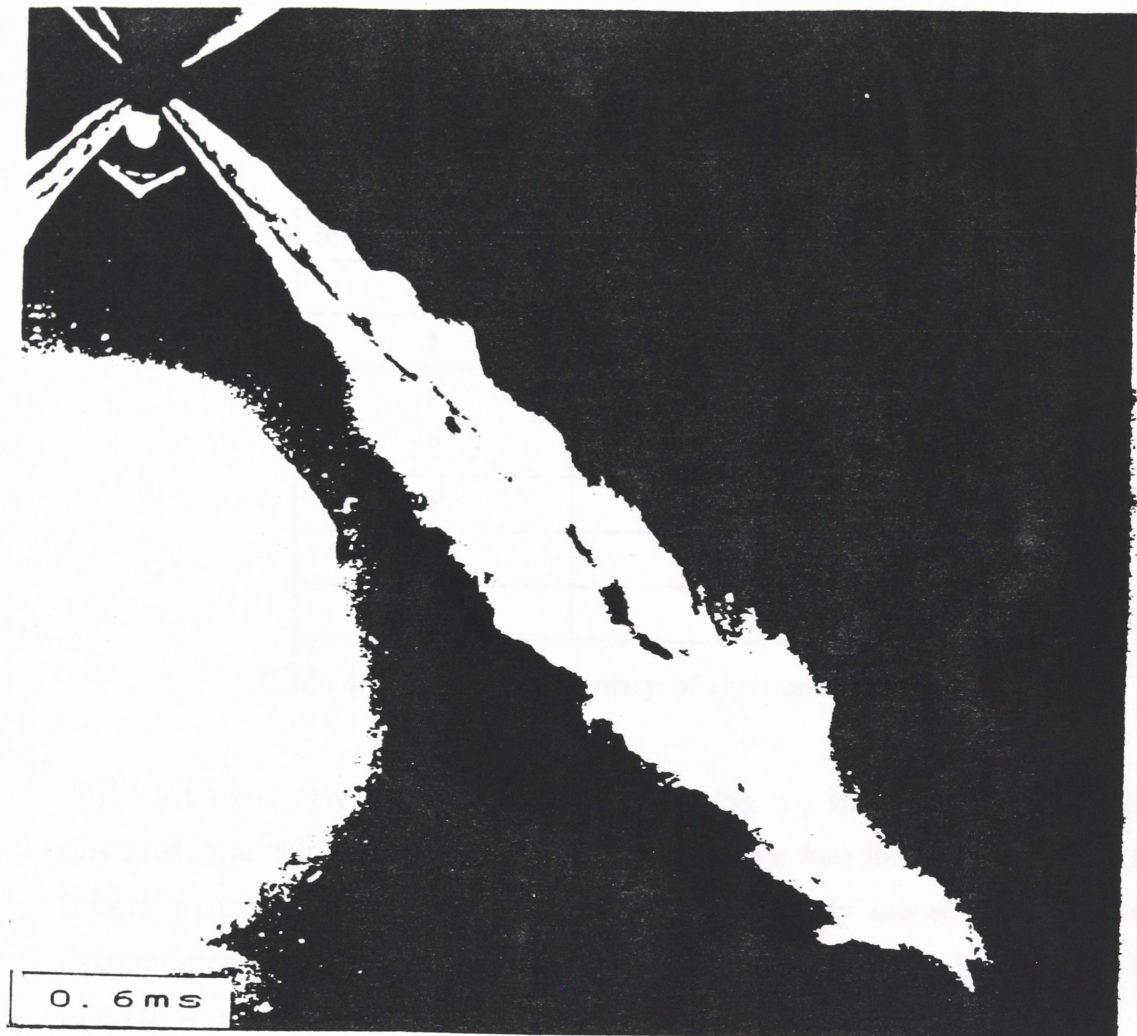


Figure 4.10: A close view of an approximate conical diesel spray

4.4.2 Injection Quantity, Measurement Error and Fuel Line Pressure

Injection quantities over a range of fuel rack settings were measured before the injector was assembled within the combustion chamber. Table 4.1 shows the injection quantity at various rack setting as average values taken from 20 shots. It should be pointed out that the current injector is not particularly designed for low fuel injection rates. That is, there appears to be some obvious unrepeatability in the injection. This can be best verified by the corresponding fuel line dynamic pressure diagram. Fig. 4.11 to 4.16 show the dynamic pressure diagrams which are recorded from the fuel line for various fuel rack setting. Each figure presents two pressure diagrams which were the maximum deviation recorded under the same working condition for a corresponding fuel rack setting. Generally, the deviation of the fuel line pressure (peak value) δ_{max} , was within

fuel rack position	injection quantity (mg)
0	21.4
1	17.9
2	14.5
3	11.0
4	7.6
5	4.1
6	0.04

Table 4.1: Injection quantity of the current injector

20%. At extremely low flow rate (rack setting 4), the maximum deviation observed, was 80%. The deviation of the average fuel line pressure over the injection duration, δ_p , is therefore estimated generally below 20%, with the extreme not more than 80%. According to the conventional formula for the mass flow in an incompressible fluid, the mass of pilot fuel is

$$m = \dot{m} \cdot t = A \cdot v \cdot \rho \cdot t = C_d A (\sqrt{2\rho\Delta P}) t$$

From the measurement error theory, the deviation of the injection quantity, δ_m , is therefore estimated to be about half of δ_p , making it generally less than 10% and in the extreme not more than 40%. The exact quantity of a particular injection needs to be further adjusted from the energy balance calculation, particularly in the phenomenological modelling.

4.5 Cylinder Pressure Trace, Acquisition and Methods Analysis

4.5.1 Data acquisition

Diagrams of the dynamic cylinder pressure measured for the combustion of a sole diesel fuel and diesel-NG dual fuel are collected in Appendixes C

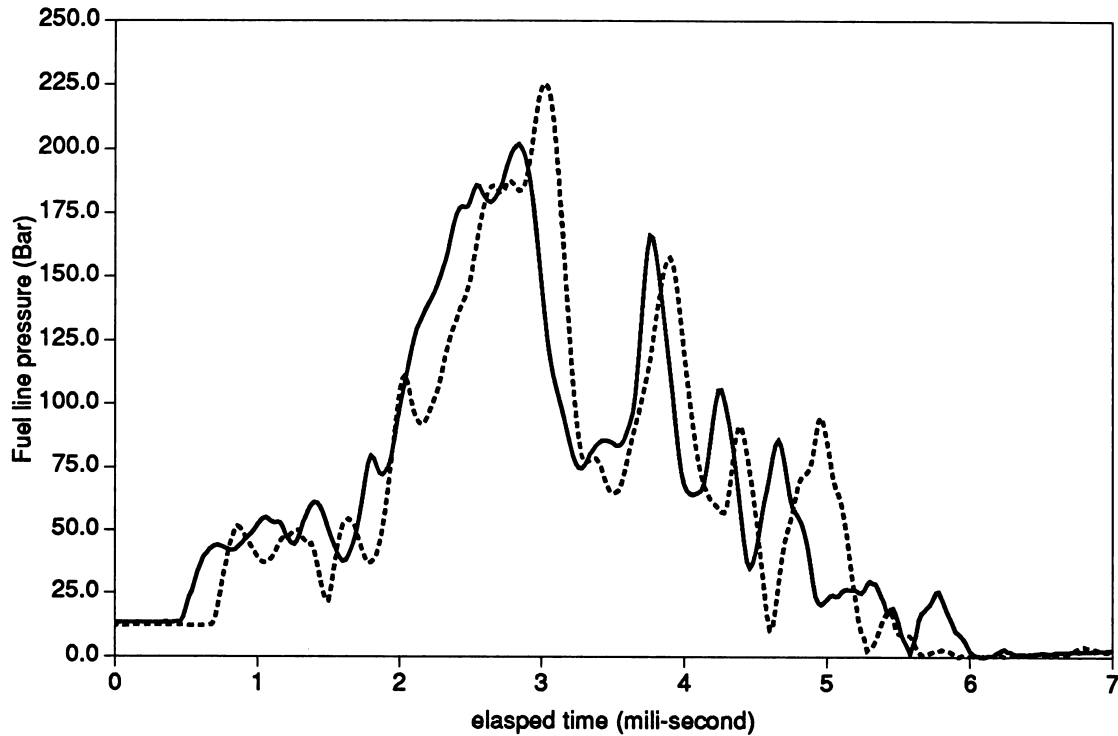


Figure 4.11: Fuel line pressure of injector at rack setting 0

and D respectively. Typical examples are shown on Fig. 4.17 of dual fuel combustion and Fig. 4.18 of sole diesel combustion. The entire combustion process is recorded over some 630 data points. The time interval for data recording is predefined, varying from 100 micro-seconds to 1000 micro-seconds programmably to suit the entire combustion duration (including the ignition delay period). Most of the combustion was complete within 300 milli-seconds with the exception of some dual fuel combustion for which the entire combustion process exceeded 400 or 500 milli-seconds. This is because the corresponding ignition delay period could be as long as 150 or 200 milli-seconds. In order to reduce random measurement error, experiments were usually repeated several times for each working condition if deviation in the pressure traces were significant. In correlating empirical formulae, all individual data samples were taken into account instead of considering only their mean values.

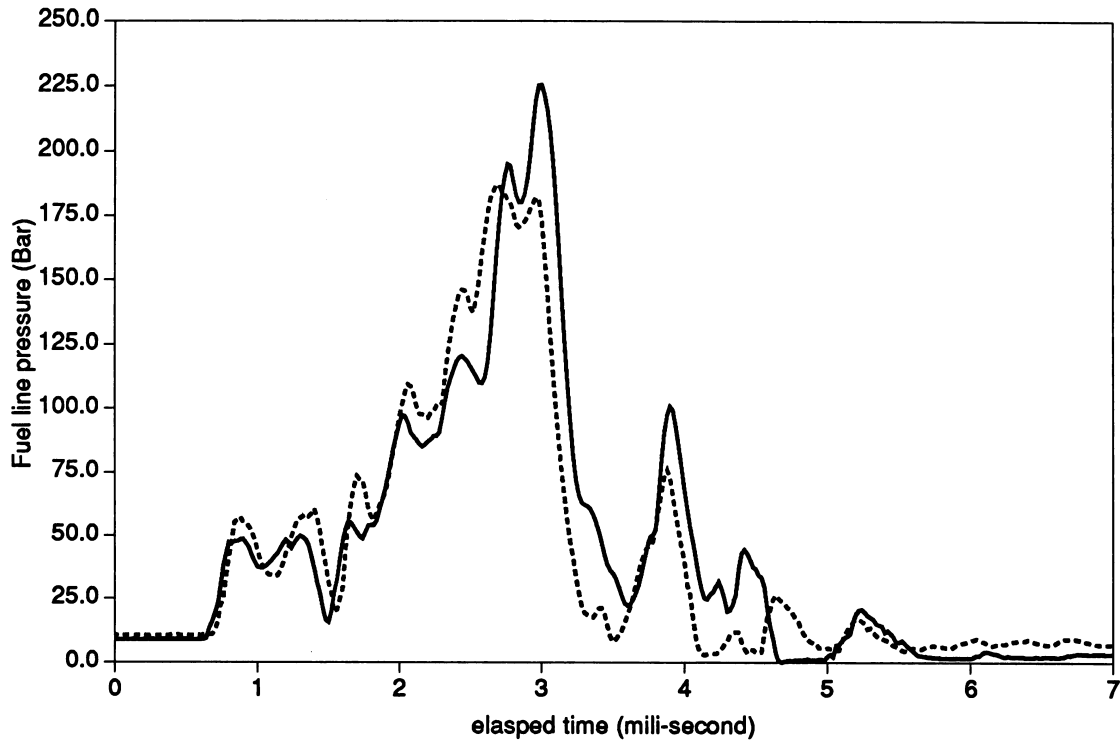


Figure 4.12: fuel line pressure of injector at rack set 1

4.5.2 Determination of the Ignition Delay

Pressure traces of both sole diesel and dual fuel combustion have been obtained. They will be discussed in detail later. However, some are used here to highlight methods of analysis. In the current investigation of combustion in a constant volume vessel, ignition delay is defined as the pressure rise delay. As described before, the entire combustion process including the ignition delay is recorded through the cylinder dynamic pressure trace. It is therefore possible to determine the ignition delay period from the pressure trace diagram. Pressure rise delay for both diesel and dual fuel combustion in the present constant volume combustion bomb is measured graphically based on the dynamic cylinder pressure diagram. The graphical methods used here can be explained by the following two examples:

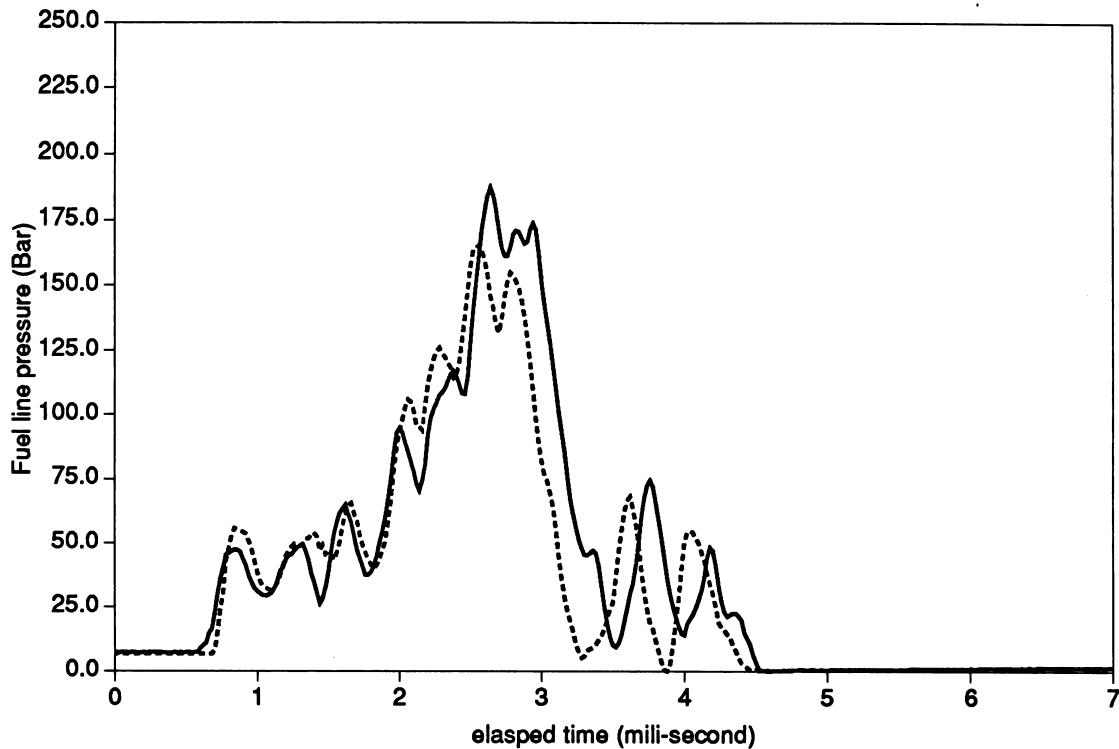


Figure 4.13: Fuel line pressure of injector at rack setting 2

Part A of Fig. 4.17 is a typical dynamic cylinder pressure trace diagram of dual fuel combustion. This pressure trace was plotted based on the recorded digital data. The diagram can be enlarged and replotted by a computer graphic package such as GNUPLOT so that the pressure rise delay period is distinct from the following rapid pressure rise caused by the ignition of the mixture. This is as shown on Part B of Fig. 4.17. The data recording is triggered by the injection and the disturbance near the original point indicates the point of the injection. The recording speed was predefined as two data points per milli-second. A substantial, rapid pressure rise begins at the point when the time equals 38 ms. This pressure rise is significantly different from the pressure disturbance caused by the injection of fuel. It is therefore considered to be caused by the ignition of the mixture. Hence, the ignition delay is evaluated to be 38 ms.

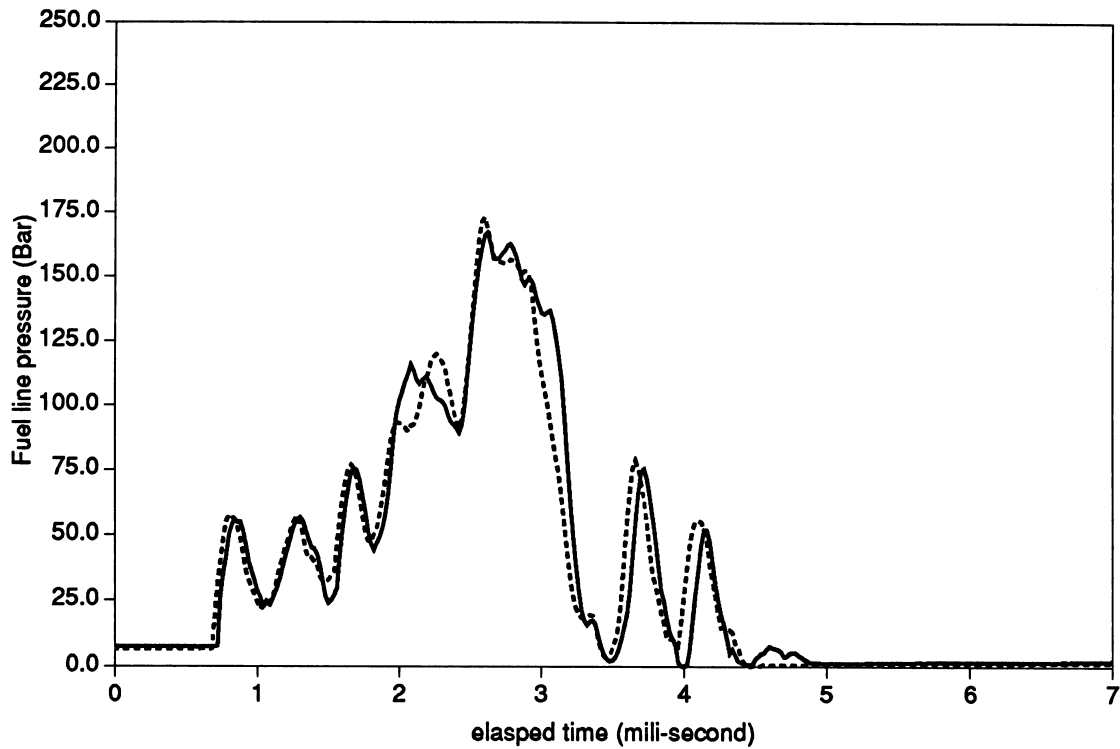


Figure 4.14: Fuel line pressure of injector at rack setting 3

Similarly, Fig. 4.18 is an example for diesel combustion in the bomb. Data reading speed is here set to five data points per milli-second. The ignition delay is evaluated to be 7.0 ms.

Correlations of empirical formulae for all these ignition delays recorded are discussed later in Chapters 5 and 7 respectively.

4.6 Discussion

Despite the fact that successful combustion experiments have been carried out for sole diesel fuel and diesel-gas dual fuel respectively, many difficulties were encountered during development the experimental setup as well as during the experiment.

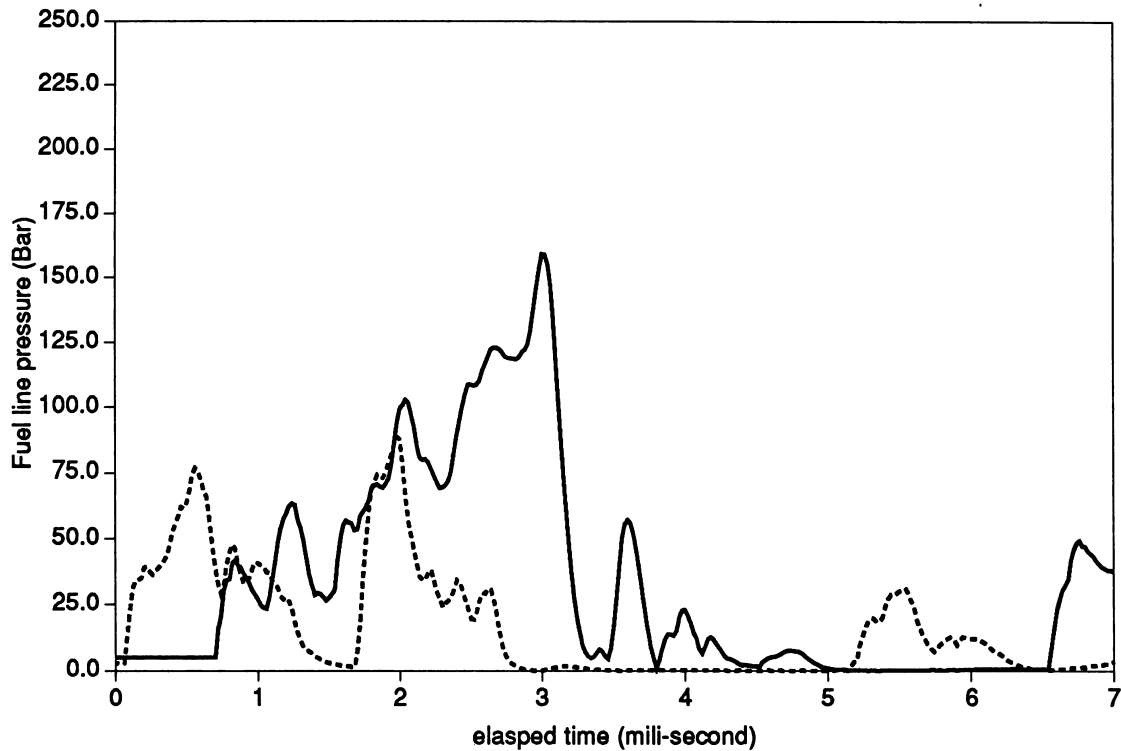


Figure 4.15: Fuel line pressure of injector at rack setting 4

Visual tests of the spray and combustion inside the combustion chamber have not as yet been successful because of insufficient window area to provide the necessary light and field of view for photography. It was also inhibited because the quartz windows are easily dirtied by the combustion. Appropriate lighting of the chamber will need to be considered in the future.

Leakage of air and gas from the combustion cylinder occurs during the experiments and the pressure cannot be held constant. In order to obtain a desired working pressure, the cylinder is usually first charged to a value higher than the required value and then allowed it to reduce gradually. Leakage rates vary slightly according to the cylinder pressure and temperature. Before ignition, the leakage rate is measured as 0.179 and 0.233 bar/s pressure drop at cylinder pressure being 20 and 24 bar respectively. This leakage adds to the difficulty in the accurate timing of the injection as well as in controlling the

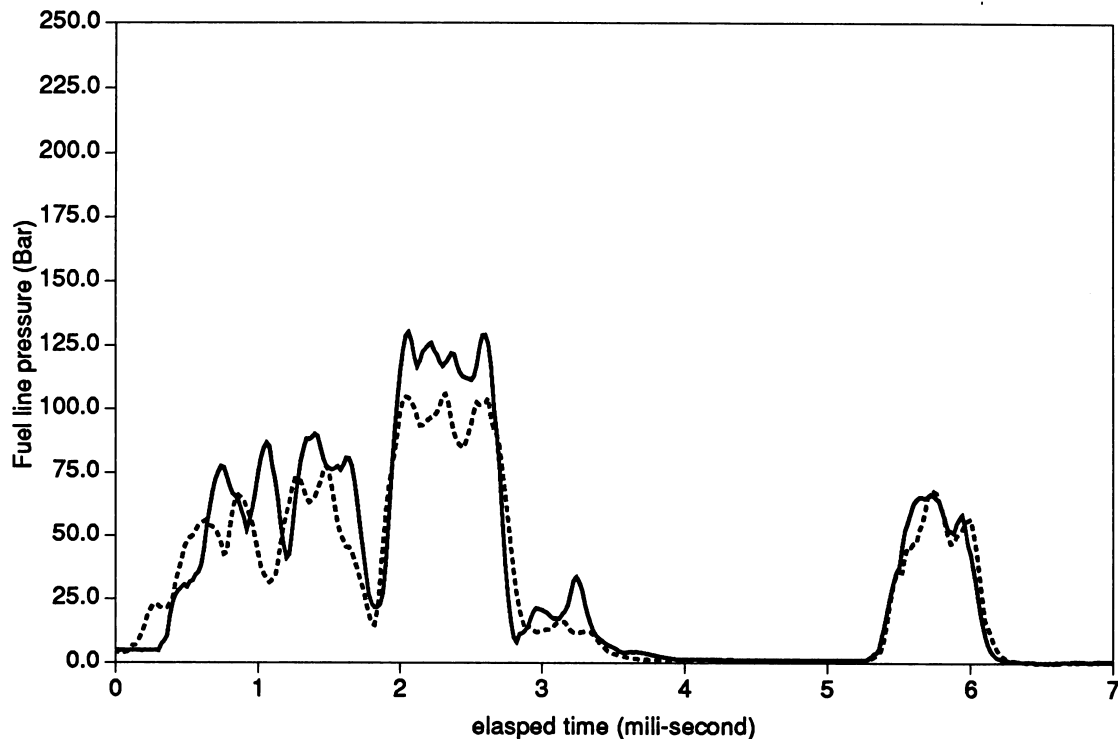
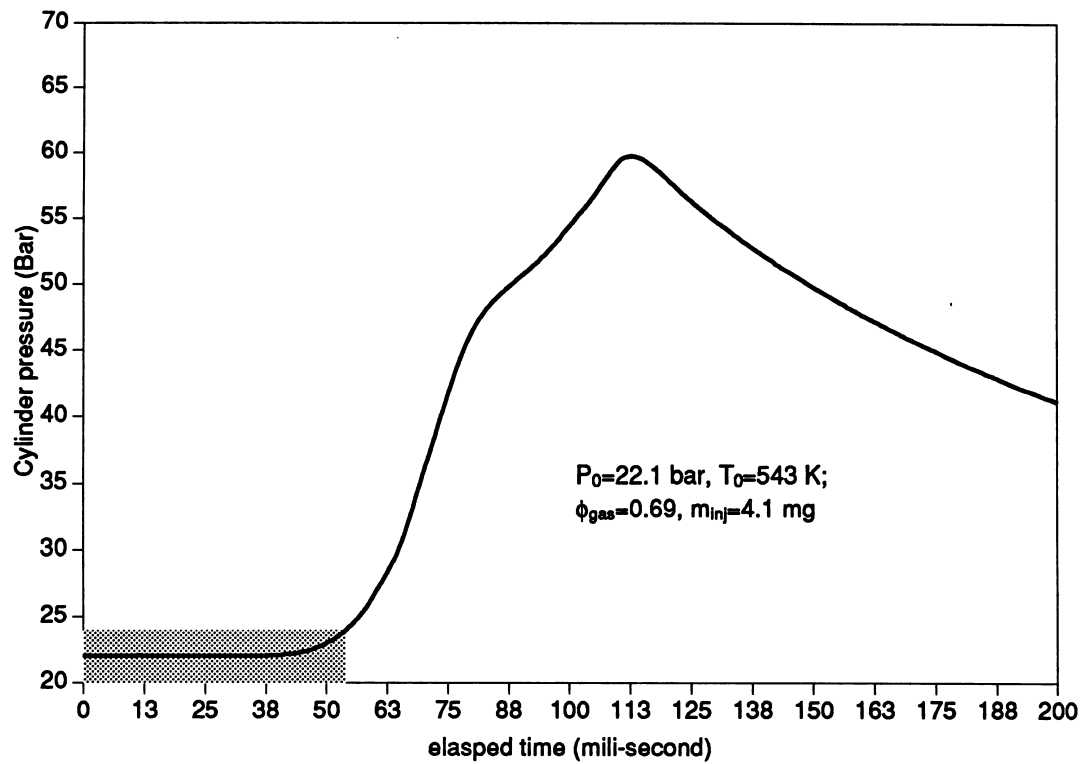


Figure 4.16: Fuel line pressure of injector at rack setting 5

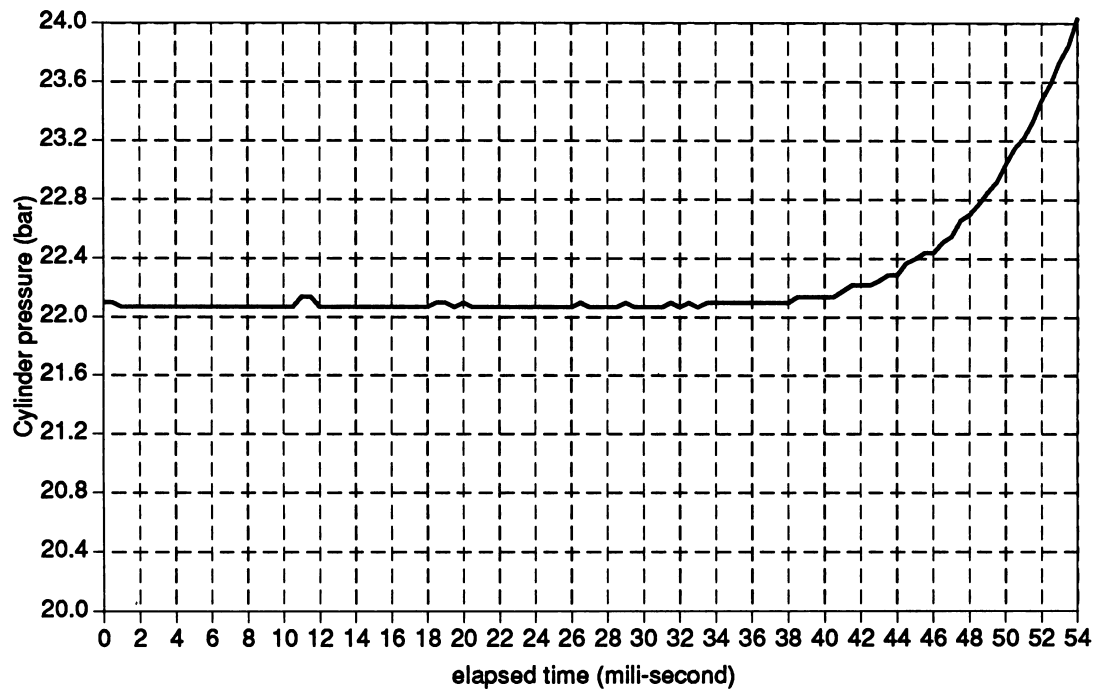
fuel-air ratio and diesel-gas ratio.

One of the two heating elements broke down during the experiments. This made it more difficult to maintain a uniform initial temperature distribution throughout the entire cylinder. Thus, the initial temperature reading may not be very accurate. Some efforts were made to attempt to reduce this measurement error. This included trying to reduce the power supply of the heater hoping to obtain a temperature of the heating element which is close to the initial temperature of the in-cylinder mixture. This attempt had only limited success because the power supply had to be held at a moderately high level in order to maintain a combustible cylinder temperature. The spacial variation in temperature at various initial temperatures are shown at Fig. 4.19.

Other difficulties and problems about developing the combustion bomb and

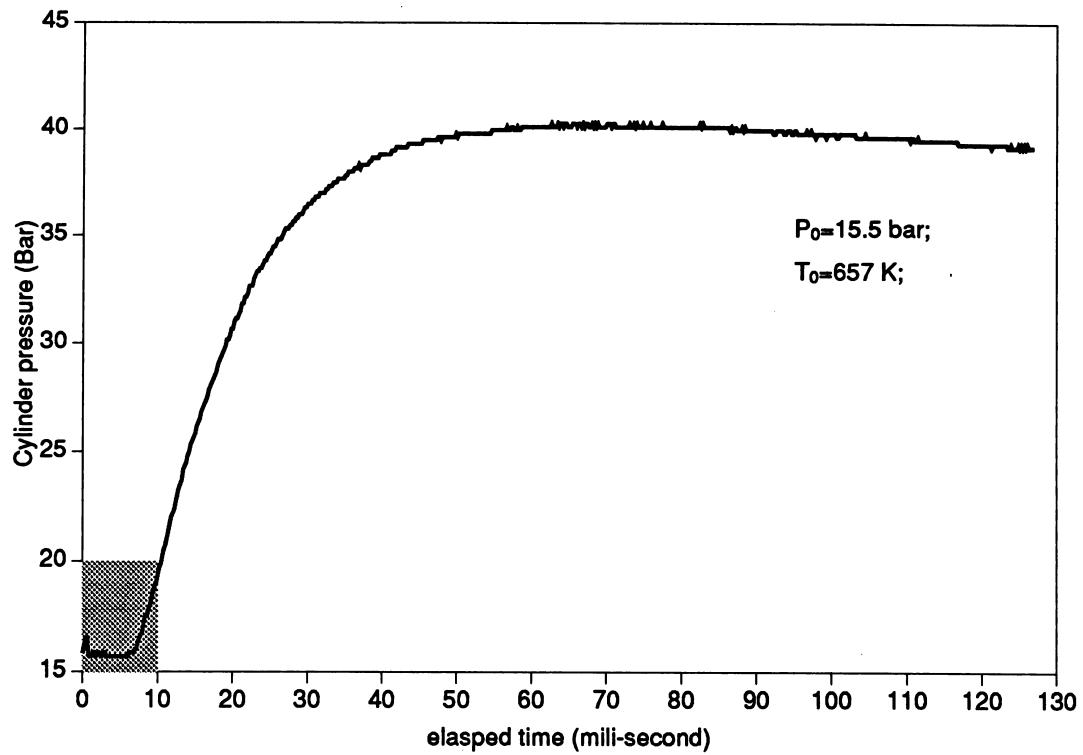


(A) Cylinder dynamic pressure trace of dual fuel combustion.

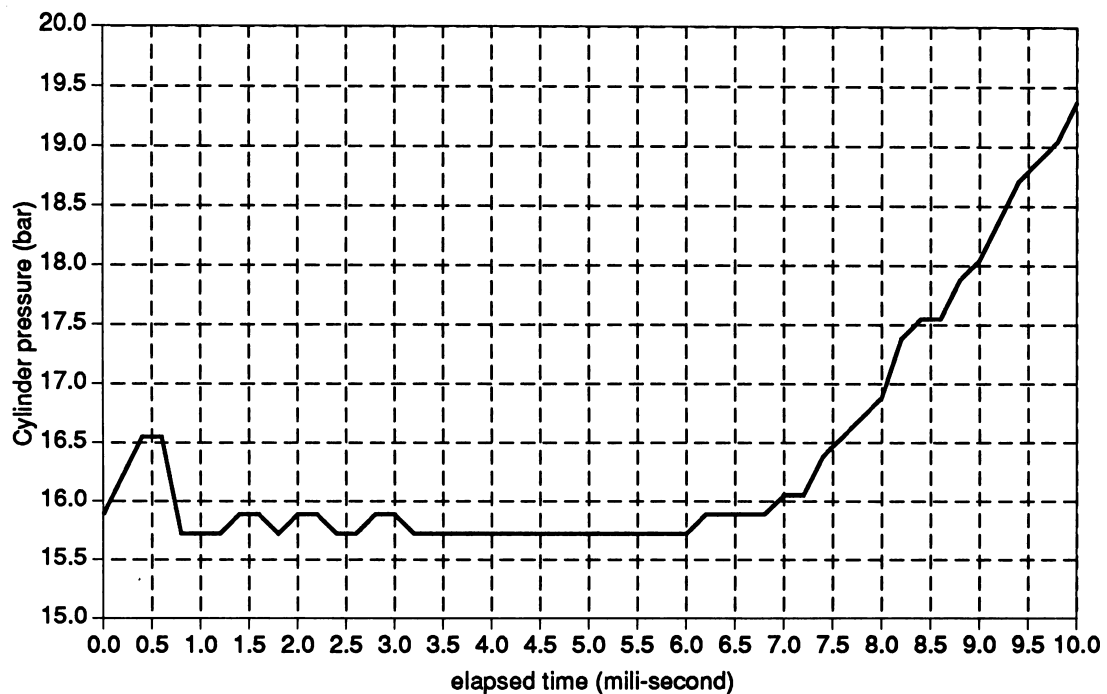


(B) Re-scale of the shadowed area in (A), shows the pressure rise delay.

Figure 4.17: Typical cylinder pressure trace for dual fuel combustion in a constant volume combustion bomb. Data are recorded at two points per milli-second. (A) shows the entire combustion process, (B) shows the ignition delay period.



(A) Cylinder dynamic pressure trace of dual fuel combustion.



(B) Enlargement of the shadow area in (A), showing the pressure rise delay.

Figure 4.18: Typical cylinder pressure trace for diesel combustion in a constant volume combustion bomb. Data are recorded at five points per milli-second. (A) shows the entire combustion process, (B) shows the ignition delay period.

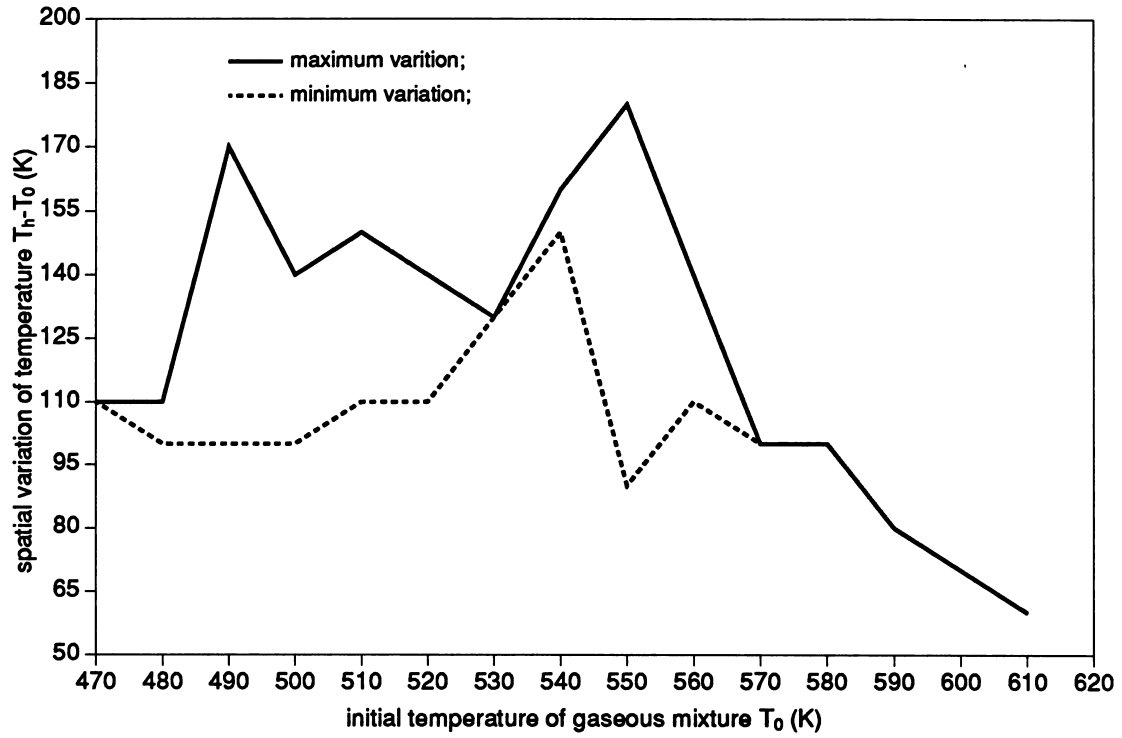


Figure 4.19: Spacial variation in temperature (T_h is the temperature of the heating element inside the combustion chamber).

dual fuel combustion experiments have been described previously [163].

The current experimental rig need to be improved for further experiments. Firstly, in order to obtain a precisely controlled pilot injection, a specially designed injector particularly for running at low fuel injection is necessary. Secondly, to reduce measurement errors, an improvement in the air-gas filling system is necessary so that the combustible mixture can be controlled precisely as required. For example, the method used by Hamamoto [168] in which the mixture is prepared in a large tank before it is introduced to the combustion cylinder is preferable. Furthermore, the broken heating element needs to be repaired and the problem of leakage needs to be overcome.

Chapter 5

Modelling the Spray combustion in Diesel Engines

NOMENCLATURE

- a coefficient constant in Watson heat release model, -
- act index constant in Whitehouse heat release model, -
- A area, area of spray, m^2
- b empirical constant, -
- B constant, -; cylinder bore, m
- BMF Burned mass fraction, -
- c, C constant, -
- c_p specific heat at constant pressure, $J/kg \cdot K$
- cr compression ratio, -
- d, d_0, d_n diameter of nozzle orifice, cm, m
- D diameter, m
- D_{32} Sauter mean diameter, m
- e internal energy of unit mass, J/kg, kJ/kg
- E internal energy, activation energy, J, kJ
- \mathcal{F}_1 premixed-burning function in Watson heat release model
- \mathcal{F}_2 mixing-controlled function in Watson heat release model
- h_c coefficient of convective heat transfer, $W/m^2 \cdot K$

H height of combustion bomb, m
 K, K' coefficient constant, -
 l length, m
 m, M mass, kg
 M_R molecular weight, kg/mol
 n number of nozzle hole, number of droplet, -
 N engine speed, rpm
 P pressure, Pa, kPa
 p_O partial pressure of oxygen, kPa, MPa, Bar
 \mathcal{P} rate of preparation of fuel, kg/deg crank
 ΔP pressure drop across nozzle orifice, Pa, MPa
 Q heat transfer, J, kJ
 \dot{q}, \dot{Q} heat transfer rate, W/sec
 \dot{Q} fuel injection rate, m^3/s
 r radius, m
 r_s swirl ratio, -
 R ideal gas constant, radius of combustion bomb
 R_L Reynold number, -
 \mathcal{R} rate of burning, kg/deg crank
 s spray tip penetration, cm
 S speed, m/sec
 T temperature, K, $^{\circ}C$
 t, t' time, second, mili-second
 u speed, m/sec
 u' turbulent intensity, m/sec
 V Volume, m^3
 v specific volume, m^3/kg ; velocity, m/sec
 \bar{v} average specific volume, m^3/kg
 W work, J, kJ

x, X mass fraction, kg/kg; spray penetration, cm
 x_b, X_b burned mass fraction, kg/kg
 X_j molar fraction of ideal gas species j, -
 Y_A mass fraction of vaporised fuel, -
 Y_{NO} NO concentration
 α coefficient; half of spray angle, degree
 β fraction coefficient in Watson heat release model
 ϵ rate of turbulence dissipation
 ϕ fuel-air equivalence ratio, -
 λ heat of evaporation, J/kg
 ρ density, kg/m^3
 θ crank angle, degree
 τ ignition delay time, turbulent mixing time, sec, ms
 τ_{id} ignition delay, degree crank, ms
 ν kinematic viscosity, m^2/sec
 ψ symbolic entrainment distribution function
 Ψ equivalent entrainment function

Subscripts:

0 initial state
 a air
 b burned zone state, burned, break-up length
 c convective heat transfer
 e entrainment
 f, F fuel
 g gas
 i ignition, ignition delay, injection
 j injection
 l liquid fuel

m mean average value

O, O_2 oxygen

T turbulence

u unburned zone state

v fuel vapour

w wall, wall impingement

Superscripts:

0 standard state of 1 atmosphere

5.1 Introduction

Since the dual-fuel combustion engine is essentially a modification of a conventional compression ignition diesel engine, it is essential that an investigation of the methods used to model diesel combustion is undertaken in order to assist in the understanding and modelling of the dual-fuel combustion process. However, the unsteady, heterogeneous and three dimensional nature of diesel engine combustion makes even that combustion process extremely complicated and an accurate, generally applicable mathematical model hard to achieve.

The phenomenological modelling approach used with CI engines, as with that of SI engines, has also developed from the relatively simple zero-dimensional type to the more developed, quasi-dimensional one. The objective of this chapter is first to review existing CI combustion models. With the addition of further experimental study on a constant volume diesel combustion bomb, it is then to construct an appropriate quasi-dimensional model for the compression ignited combustion of a liquid fuel spray in either a diesel engine or a combustion bomb. This modelling method should have the potential to be adapted further for use in studying dual-fuel combustion.

5.2 Essential Features of the Combustion Process in Compression Ignition Engines

Unlike the combustion in the SI engine cycle where a premixed fuel-air charge is compressed, only air is compressed in the compression stroke of a CI engine. Liquid fuel is then injected into the cylinder towards the end of the compression stroke. Atomized fuel droplets then mix with the high-temperature, high-pressure compressed air in the cylinder. At this time, due to the compression, the cylinder temperature and pressure are at or above the fuel ignition condition. Thus, after an ignition delay period, spontaneous ignition of the portion of fuel from the spray which has already mixed with air occurs. This is termed the 'pre-mixed' combustion phase. Injection continues after the initial combustion has started, the burning now being controlled by the rate at which fuel/air mixing can occur. This is termed the mixing controlled combustion phase. A further period of final burning of mixed fuel takes place at the end of this period. This provides a small contribution to the combustion process and is known as the late combustion phase.

While details of the process depend on many factors such as the fuel characteristics, the injection system, the engine design and the operational conditions, etc., the entire combustion process can be conveniently divided into a number of stages in the following order [134] (Fig 5.1):

- (1) Ignition Delay: The fuel is sprayed into the hot air in the cylinder. The fuel droplets are heated, vaporize and diffuse away from the core of the spray jet into the air to form an ignitable mixture. These initial physical processes are accompanied by pre-flame chemical reactions without appreciable heat release. Towards the end of the delay period, ignition occurs simultaneously at several places within the spray region where the mixture strength is favorable, i.e., near stoichiometric, and where the physical and chemical processes have progressed sufficiently. Once this stage is reached, the pressure begins to rise above the compression line.
- (2) Premixed combustion phase: Combustion spreads rapidly through the

mixture formed by the fuel which was already injected during the delay period. This part of the charge is essentially fully mixed and its burning causes a very rapid pressure rise until most of the accumulated air/fuel mixture has been consumed. The burning at this stage is predominantly non-luminous since the fuel and air were premixed.

- (3) Mixing-controlled (also known as diffusion controlled) combustion phase: Fuel is now continuously injected into the high temperature air but all the premixed air/fuel mixture has been consumed considerably increasing the pressure and local temperature. Consequently, ignition is now much more rapid. While several processes are involved – atomization, vaporization, mixing, and preflame chemical reactions – the burning rate is primarily controlled by the fuel vapor-air mixing process (i.e. the fuel's diffusion into the air). The heat release rate may reach a second peak (the first being during the premixed combustion phase) after which it decreases as the combustion continues. This mixing-controlled combustion governs a large proportion of the entire combustion duration. Also, much of the heat release occurs here. As the burning spreads to incompletely evaporated fuel, molecules high in carbon are generated by pyrolysis causing luminous flames to now appear.
- (4) Kinetic controlled late combustion: Heat release continues at a low rate well into the expansion stroke, mainly because the kinetics of the final burnout processes become slower as the temperature falls during expansion, but also because a small portion of fuel may remain unburned due to the formation of fuel-rich combustion products or soot.

The phenomenological modelling of CI engines attempts to simulate these processes as closely as possible by using separate submodels which will be described later in this chapter.

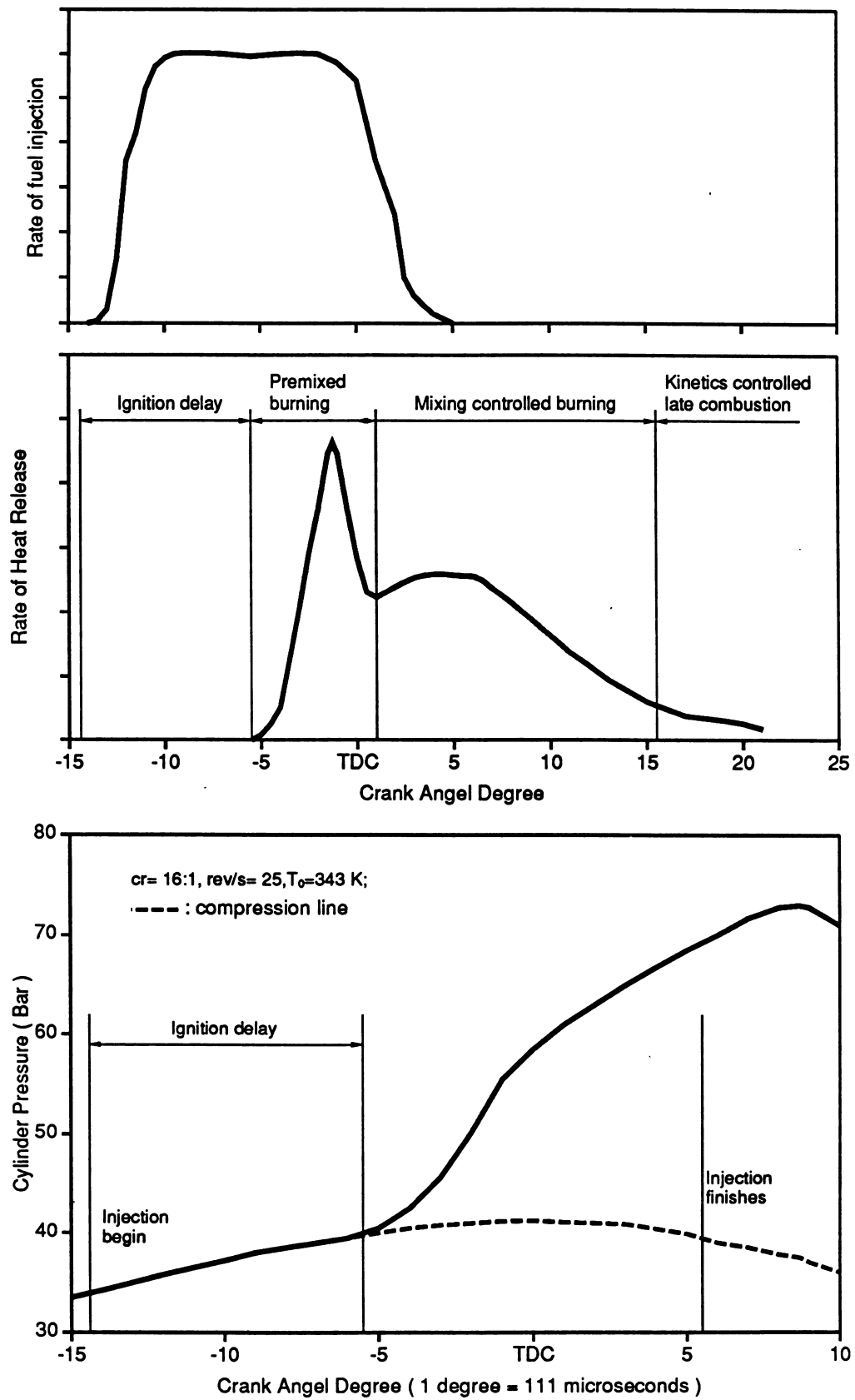


Figure 5.1: Fuel injection, heat release and cylinder pressure of a typical DI diesel engine (reproduced from Ref. [134].)

5.3 Literature Review of Phenomenological Modelling of CI Engine Combustion

5.3.1 Zero-Dimensional Models

Zero-dimensional models assume that a uniform cylinder charge mixture exists at any instant in time with instantaneous fuel-air mixing. The heat release rate is determined experimentally from the cylinder pressure diagram. Two zero-dimensional diesel engine models which are often cited are those of Whitehouse et al [107] and Watson et al [109].

The Whitehouse model is based on the assumption that the preparation rate of fuel which is ready to burn should be proportional to the total surface area of the droplet. This surface area is linked to the amount of fuel injected and to the unburned fuel mass by assuming that all fuel droplets are identical. Thus the mass of injection is:

$$M_i = n \rho \frac{1}{6} \pi D_0^3$$

or

$$n \pi = \frac{6 M_i}{\rho \cdot D_0^3}$$

The mass of unburned fuel is:

$$M_u = n \rho \frac{1}{6} \pi D^3$$

or

$$D = \left(\frac{6 M_u}{n \pi \rho} \right)^{1/3}$$

The total surface area of the droplets ready for burning is then:

$$Area = n \pi D^2 = n \pi \left(\frac{6 M_u}{n \pi \rho} \right)^{2/3} = (n \pi)^{1/3} \left(\frac{6 M_u}{\rho} \right)^{2/3} = \left(\frac{6 M_i}{\rho \cdot D_0^3} \right)^{1/3} \left(\frac{6 M_u}{\rho} \right)^{2/3}$$

Thus, $area \propto M_i^{1/3} \cdot M_u^{2/3}$. Whitehouse et al therefore assumed the rate of preparation to be of the form

$$\mathcal{P} = K M_i^{1-x} M_u^x p_O^m \quad (5.1)$$

if ρ and D_0 are constants. Here empirical constants K , x , m are determined by the engine conditions.

An Arrhenius type equation was also suggested to calculate the rate of reaction. This is based on the fact that the time taken by the burning of prepared fuel is initially negligible compared with the preparation time and the assumption that burning and preparation rates become equal as the combustion proceeds. That is, chemical kinetics becomes more important. The equation is:

$$\mathcal{R} = \frac{K' p_0 \exp(-act/T)}{N\sqrt{T}} \int (\mathcal{P} - \mathcal{R}) dx \quad (5.2)$$

where K' and act are characteristic coefficients of the fuel. Even though this model does not have an ignition delay submodel, the constants K' and act effectively control a delay period.

Eq. 5.1 and 5.2 had been used again by Whitehouse and Sareen [108] in their two-zone model in which spray motion and configuration were considered.

The Watson model also concentrates on simulating the engine heat release rate. The total burning rate at any instant is given by the sum of the rate of the pre-mixed burning and the sum of the diffusion burning weighted by a factor β which is assumed to be controlled by the ignition delay and the overall trapped equivalence ratio. That is,

$$\frac{m_{fb}(t')}{m_{f0}} = \beta \mathcal{F}_1 + (1 - \beta) \mathcal{F}_2 \quad (5.3)$$

where m_{bf} is mass of burned fuel, m_{f0} is the total injected fuel and t' is normalized time $t' = \frac{t-t_{ign}}{\Delta t_{comb}}$, \mathcal{F}_1 and \mathcal{F}_2 are phase functions. Watson et al found that experimental data were best represented by the following expressions for the phase functions. That is

$$\mathcal{F}_1 = 1 - (1 - t'^{K_1})^{K_2}$$

$$\mathcal{F}_2 = 1 - \exp(-K_3 t'^{K_4})$$

Empirical coefficients K_1, K_2, K_3, K_4 and a, b, c in the Watson model were determined experimentally with the proportional factor β being given by

$\beta = 1 - \frac{a\phi^b}{\tau_{id}^c}$. The ignition delay τ_{id} is calculated by a separated submodel and a value of 120 is recommended for the combustion duration Δt_{comb} .

These zero-dimensional models are easy to use for the entire engine simulation. However, their simple assumptions cannot relate engine design and operating variables to the details of the combustion process, neither can they fit the experimental data with sufficient accuracy.

5.3.2 Kumar's Two Zone Model (1984)

Kumar et al's two-zone model [111] divides a circular cylinder into a burning zone and a non-burning zone. Injection is assumed to be located at the centre of the cylinder with the fuel injected horizontally. The combustion process does not cause air entrainment, thus the only entrainment of air occurs because of the shearing action of the fuel spray. The model also assumes that the burning zone is homogeneous and there is no dissociation and so the products only consist of CO_2 , N_2 , H_2O and O_2 . For calculating the heat transfer, the model assumes that no heat transfer occurs between the burning and non-burning zones, that only convective heat transfer takes place between the non-burning zone and the wall, while both radiation and convective heat transfer may exist between the burning zone and the wall up until the time the jet tip reaches the wall. Spray tip penetration is given by Sareen's correlation [143].

$$x(cm) = 17.28 \left[\left(\frac{\Delta P(kgf/cm^2)}{\rho_b(kg/cm^3)} \right)^{0.5} d_n(cm) t(sec) \right]^{0.5} \quad (5.4)$$

and the spray cone angle 2α is taken as 20 degrees. The volumetric flow rate through the jet is

$$\frac{dV_j}{dt} = 2\pi \int_0^{r_0} r v(r) dr \quad (5.5)$$

where the velocity distribution $v(r)$ in the radial direction outwards from the injector nozzle of the fuel-vapour two-phase jet is given by

$$\frac{v(r)}{v_{max}} = (1 - y^{1.5})^2 \quad ; \quad y = r/r_0 \quad (5.6)$$

Here the velocity v_{max} is obtained from differentiating Eq. 5.4 with respect to t , that is $v_{max} \equiv \frac{dx}{dt}$.

Fig. 5.2 shows the spray jet configuration used by this model. From mass conservation, The entrainment of air is given by (Figure 5.2)

$$\frac{dm_e}{dt} = (\pi x^2 \tan^2 \alpha \frac{dx}{dt} - \frac{dV_b}{dt}) \rho_a \quad (5.7)$$

The rate of change of mass in the burning zone is equal to the rate of air entrainment plus the rate of burning of fuel in the burning zone, or

$$\frac{dm_b}{dt} = \frac{dm_e}{dt} + \frac{dm_{fb}}{dt} \quad (5.8)$$

Eq. 5.4 to 5.8, together with the application of energy and mass conservation to the burning and non-burning zones, forms a system of first-order differential equations for T_b , T_u , V_b , P and V_u . Further, the system assumes that the rate of air being burned is equal to the rate at which it is being entrained into the spray. That is, $\frac{dm_{ab}}{dt} = \frac{dm_{ae}}{dt}$. This differential equation system is solved numerically. Results were compared with that predicted by the single-zone model. It was found that some difference exists in the peak rate of pressure rise, whereas the effect of compression ratio, duration of injection and injection timing on the peak cylinder pressure are nearly the same as predicted by single-zone models. The authors also believe that the two-zone approach is a good compromise between single and multi-zone modelling.

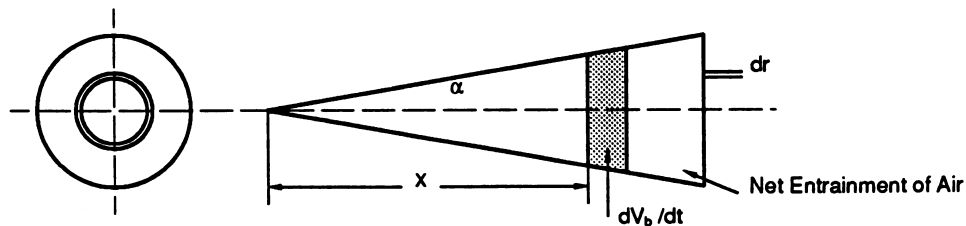


Figure 5.2: Circular Jet in Kumar's Two-Zone Model

5.3.3 Whitehouse-Balusway's four-zone model (1977)

This four-zone model [135] is a modification of Whitehouse-Sareen's two-zone model[108] and is fundamentally used for estimating the formation of nitric oxide in diesel engine combustion. In order to develop a four-zone model, the burning zone in a two-zone model is further divided into,

- (1) a fuel zone which contains only fuel, its mass increasing with decreasing fuel injection as the fuel reacts. Its temperature is taken as that of the burning zone in the two-zone model;
- (2) a stoichiometric burning zone, in which all chemical reactions take place stoichiometrically. The reaction rate is determined from the two-zone model. The required inflow of fuel and air are determined from those drawn from the inner fuel zone and the outer air-products zone respectively;
- (3) an air-products zone which contains combustion products transferred from the stoichiometric burning zone and air from the unburned zone.

While the transfer rate of combustion products from the stoichiometric burning zone to the air-products zone is unknown, the model assumes that it is proportional to the amount of products present in the stoichiometric burning zone, the empirical proportionality constant being obtained from experiment.

While this four-zone model has provided a useful concept for multi-zone modelling as well as an approach for the estimation of the nitric oxide formation in a diesel engine, its heavy dependency on many system-related empirical constants has been a severe weakness for its general application.

5.3.4 Dent-Metha Spray Mixing Model (1981)

The Dent-Metha's spray mixing model [114] is used for the purpose of predicting the combustion characteristics of a Quiescent Chamber Diesel engine.

Input data for the model's calculation are engine geometry and operating conditions including the injection pressure diagram and trapped air mass. The injection pressure diagram is discretised so that the following quantities can be determined over the discretised time step interval Δt . These are

- (1) Injection fuel quantity: Here, the volume flow rate of fuel \dot{Q} is

$$\dot{Q} = C_d (2\Delta P / \rho_f)^{0.5} A_0 \quad (5.9)$$

where C_d is the orifice discharge coefficient, A_0 is the orifice area and ΔP is the difference between the fuel line and engine cylinder pressure over the discretised time step.

- (2) Spray penetration: Two correlation are required. For a time period $t < 0.3$ ms, Hiroyasu's correlation [112] was used. That is:

$$s = 0.39(2\Delta P / \rho_f)^{0.5} t \quad ; \quad t < 0.3 \text{ ms}$$

for a time period $t > 0.3$ ms, Dent's formula [139] obtained from jet mixing theory was used. This is

$$s(\text{inch}) = 13.6 \left[\left(\frac{\Delta P}{\rho_a} \right)^{0.5} t d \right]^{0.5} \left(\frac{530}{T_g} \right)^{0.25} \quad (5.10)$$

- (3) Fuel droplet size and distribution: The injected fuel for a discretised time interval is assumed to be distributed in size around an instantaneous Sauter Mean Diameter (SMD),

$$SMD = 8.0 \Delta P^{-0.458} \dot{Q}^{0.209} \nu_f^{0.215} \quad (5.11)$$

where ν_f is the kinematic viscosity of the fuel.

The cumulative volume fraction (V_{cf}) of the injected fuel is expressed as a function of the normalized droplet diameter D_p where $D_p = d_p / SMD$. The value V_{cf} is given by Simmons correlation for gas turbine spray droplets:

$$V_{cf} = \exp(0.05328 D_p - 0.54174 D_p^2) \quad (5.12)$$

and this applies in the range $0.082 \leq D_p \leq 3$

A radial droplet distribution is assumed which is related to the concentration profile. For a two phase jet growth [137], this is

$$f/f_m = (1 - (r/r_j)^{3/2}) \quad (5.13)$$

where f is the mass concentration and f_m is that at the jet centerline. The penetration is equal to S and r_j is the jet's radius at S . The cumulative volume fraction is as given by Eq. 5.12 such that the normalized droplet distribution is

$$-dD_p/d\tilde{r} = (1/V_{fi})(dV_{fi}/d\tilde{r})/(dV_{cf}/dD_p) \quad (5.14)$$

where V_{fi} is the volume of fuel injected, \tilde{r} is the normalized jet radius $\tilde{r} \equiv r(S)/r_j(S)$;

During the injection, the model calculates the air entrainment into the spray in two parts, these being a free and a wall jet. The free jet is calculated by the Ricou and Spalding formula [138]

$$(\dot{m}_{ae} + \dot{m}_f)/\dot{m}_f = 0.32 S/d'_0 \quad ; \quad d'_0 = d_0(\rho_f/\rho_a)^{0.5} \quad (5.15)$$

where \dot{m}_f is fuel injected over the time the jet penetrates to a distance S and d_0 is the orifice diameter. After impingement, the wall jet entrainment is calculated by

$$(\dot{m}_{aw} + \dot{m}_f)/\dot{m}_f = 0.865 S_w/d'_0$$

where S_w is the wall jet penetration for a discretised time step. The total air entrainment rate is the sum of the free jet and the wall jet entrainment.

At the end of the injection, the mixing of spray with air is controlled by the turbulent kinetic energy dissipation in the fuel jets, this being expressed as

$$-dm_a/dt = C_l(m_a/\tau) \quad (5.16)$$

Here $\tau = (L^2/\epsilon)^{1/3}$ is the turbulent mixing time for the large scale eddies. Coefficient C_l is evaluated by equating the mean timewise entrainment rate over the whole injection period.

After comparing 160 experimental engine data points with the ignition delay empirical correlations recommended by different researchers, the Hardenberg et al formula [140] was chosen. This is (expressed in degrees crank angle)

$$\tau_{ig} = (0.36 + 0.22v_p) \exp[E_A((RT_m cr^{c-1})^{-1} - 5.817 \times 10^{-5}) + (\frac{21.2}{P_m cr^c - 12.4})^{0.63}]$$

Here v_p is the mean piston speed in m/s, R is the universal gas constant (8.31434 J/mole), T_m the absolute air temperature in the intake manifold, cr the compression ratio, c the polytropic exponent of compression and P_m the absolute air pressure in the intake manifold in bar.

The model assumes that combustion only occurs in the spray regions where the actual fuel vapor-air ratio (ϕ_v) falls within the inflammable limits: $0.028 \leq \phi_v \leq 0.2$ and in each of the burning regions where the burning is stoichiometric.

The model's prediction showed that the value of the coefficient 0.32 in Eq. 5.15 is too low. The authors believe that this may be due to the assumptions concerning the quasi-steady nature of the flow and the simple nature of the droplet distribution model. It was also found that the Hardenberg ignition delay used by the model was inadequate for highly retarded conditions (injection near TDC) and for idling and low load data. The wall jet entrainment model was also found to be inadequate.

5.3.5 Hiroyasu et al's multi-zone spray combustion model [112] (1983)

This spray combustion model for direct-injection diesel engines is a further improvement of a previous model proposed in 1976 which was based on the assumptions of a multi-zone spray structure and a droplet evaporation model. This analytical model actually contains two sub-models: a heat release model for the calculation of the evaporation and heat release during combustion; and an emission model for the calculation of NO and soot formation using the local temperature obtained from the heat release model. The review presented here concentrates on the heat release submodel only because the emission calculation is less relevant to the present research.

Description of the spray combustion processes

The model describes the spray combustion process in following way. Firstly, the fuel injected into the combustion chamber consists of liquid fuel, fuel vapour and air, since air entrainment into the spray and fuel evaporation occur immediately after injection, as shown schematically on Fig. 5.3. After the ignition delay period, ignition occurs in the gaseous mixture causing a sudden expansion of the spray. Thus more droplets evaporate and more fresh air is entrained. Vapourized fuel mixes with fresh air and the combustion products. The spray combustion continues, limited by either the rate of droplet vaporization (if vapour-air equivalence ratio $\phi_g \leq 1$) or the rate of air entrainment (if $\phi_g > 1$)

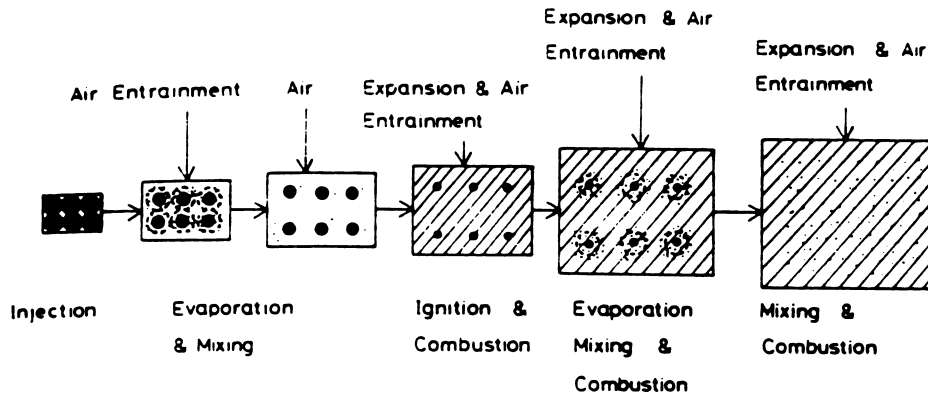


Figure 5.3: Schema of the spray combustion in the Hiroyasu multi-zone model

Spray motion and zone division

The conical fuel spray used in the model is shown schematically on Fig 5.4. The spray tip penetration is estimated from an experimentally based correlation:

$$S = \begin{cases} 0.39 \left(\frac{2\Delta P}{\rho_l} \right)^{0.5} \cdot t & \text{if } t < t_b \\ 2.95 \left(\frac{\Delta P d_0^2}{\rho_a} \right)^{0.25} \sqrt{t} & \text{if } t_b \leq t \end{cases} ; \text{ where } t_b = 28.65 \frac{\rho_l d_0}{\sqrt{\rho_a \Delta P}} \quad (5.17)$$

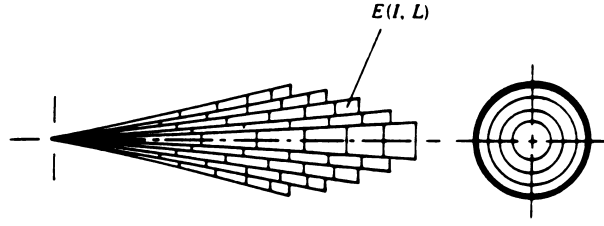


Figure 5.4: Schema of multi-zone spray of the Hiroyasu model

The whole spray is divided into many small equal mass packages along the penetration axis as well as radially. It is assumed that no mass transfer will occur between these small packages. Because the velocity at the edge of the spray is lower than that at the centre line, the penetration of an individual package is given by

$$S_L = S \cdot \exp(-8,557 \times 10^{-3}(L - 1)^2) \quad (5.18)$$

where L is an indication of the radial distance to the spray centerline with $L=1$ representing the case when the package is at the central portion of the spray and $L=10$ representing its position at the peripheral portion, respectively.

When there is swirl in the combustion chamber, the spray penetration is affected by a swirl factor C_s as follows:

$$S_s = C_s \cdot S \quad ; \text{ with } C_s = \left(1 + \frac{\pi r_s n S}{30 \left(\frac{dS}{dt}\right)_{t=0}}\right)^{-1} \quad (5.19)$$

where r_s is the swirl ratio and n is the engine speed.

Air entrainment to the spray

The rate of air entrainment is determined from the conservation equations applied to the spray motion. It is assumed that the momentum of each package will remain unchanged during penetration. That is, the momentum of the fuel

and air at time t will be equal to the initial momentum at time 0 for that package. Hence,

$$m_f \dot{S}(0) = (m_f + m_a) \dot{S}(t)$$

thus

$$m_a = m_f \left(\frac{\dot{S}(0)}{\dot{S}(t)} - 1 \right)$$

However, when the spray is ignited and the periphery of the spray is covered by the flame, the air entrainment into the spray is assumed to be decreased by a factor C_f , as follows:

$$\frac{dm_{af}}{dt} = C_f \frac{dm_a}{dt} \quad (C_f = 0.7)$$

In the case of impingement, the entrainment is enhanced by a wall jet factor C_w :

$$\frac{dm_{aw}}{dt} = C_w \frac{dm_a}{dt} \quad (C_w = 1.5)$$

When swirl is present, the deformation of the spray r_{def} which shows the tangential movement of each element is assumed as given by the following equation:

$$r_{ref} = S \cdot \frac{m_a}{m_a + m_f} \cdot \frac{\frac{n}{60} r_s 2\pi S}{0.5(u_0 + u)}$$

Here r_s is swirl ratio, u_0 and u are spray penetration speed at $S=0$ and $S=S$ respectively.

Ignition delay

In general, the ignition delay (τ_i) of a gaseous mixture is a function of mixture temperature, pressure equivalence ratio, and fuel properties. In a uniform air environment where the pressure and the temperature only change due to the cooling effect of the fuel-vaporization and fuel-heating process, correlation for τ_i usually has the form as

$$\tau_i = C \cdot P^n e^{\frac{A}{T}} \quad (5.20)$$

or

$$\tau_i = C \cdot P^n \Phi^{\gamma} e^{\frac{A}{T}} \quad (5.21)$$

where $P(\text{MPa})$ and $T(\text{K})$ are cylinder pressure and temperature respectively, Φ is equivalence ratio. The Hiroyasu model used the second form and found those empirical constants as $C = 40 \times 10^{-3}$, $n = -2.5$, $\gamma = -1.04$ and $A = 4000$.

In a field with varying temperature, pressure and equivalence ratio such as in an engine, ignition delay is usually used with the following empirical integral relation in order to account for the effect of changing condition:

$$\int_{t_{s,i}}^{t_{s,i} + \tau_{id}} \frac{1}{\tau} dt = 1$$

Here $t_{s,i}$ is the time of start of injection, τ_{id} is the ignition delay period, and τ is the ignition delay at the condition pertaining at time t .

Droplet evaporation

The model assumes that the range of size of the injected liquid fuel droplets may be dealt with by the use of a simple diameter, this being equal to the local Sauter mean diameter (D_{32}), which is found from a conventional, empirical spray model as

$$D_{32} = 23.9(\Delta P)^{-0.135} \rho_a^{0.12} B^{0.131} \quad (5.22)$$

Here B is the quantity of fuel injected per stroke(mg/st).

Evaporation starts immediately after injection and follows equations obtained from single droplet evaporation [167] which are:

$$\frac{dT_l}{dt} = \frac{1}{m_l C_{pl}} \pi D_l^2 h (T - T_l) + \lambda \frac{dm_l}{dt} \quad (5.23)$$

$$\frac{dD_l}{dt} = \frac{2}{\pi D_l^2 \rho_l} \left(\frac{dm_l}{dt} - \frac{\pi D_l^2}{6} \frac{d\rho_l}{dt} \right) \quad (5.24)$$

$$\frac{dm_l}{dt} = -\pi D_l^2 K \frac{Y_{AO} - Y_{A2}}{(1 + \xi) Y_{AO}} \quad (5.25)$$

These equations determine the diameter and temperature of a droplet in the vaporizing packages. Thus the amount of vapourized fuel m_{fg} may be found

$$m_{fg} = \frac{\pi}{6} (\rho_{l0} D_{l0}^3 - \rho_l D_l^3) N$$

where N is the number of droplets which is calculated from the original mass involved in each package and the droplet diameter D_{32} . The terms ρ_{l0} and ρ_l are densities of the liquid droplet, D_{l0} and D_l are diameters of the droplet, at $t=0$ and $t=t$ respectively.

The evaporation of a droplet also causes a fall in temperature. This is obtained from a simple energy balance,

$$\Delta T = \frac{Q - c_{pf} \frac{dm_l}{dt} (T - T_l)}{c_{pf} m_{fg} + m_a c_{pa}}$$

Combustion of the spray and its heat release

The combustion processes for spray packages in this spray model are shown schematically on Fig 5.5. When ignition takes place, combustion first occurs in the combustible, stoichiometric mixture prepared during the ignition delay

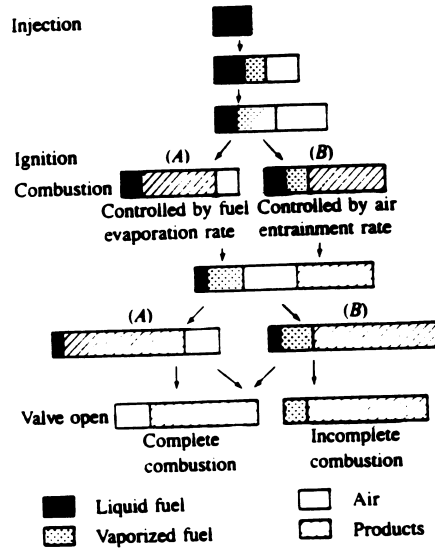


Figure 5.5: Schema of Spray Package Combustion in the Hiroyasu Model

period. When this stoichiometric combustion is completed, the combustion process for each package which follows immediately is determined by its

local fuel-air equivalence ratio ϕ_g . This is either evaporation or entrainment controlled. If $\phi_g \leq 1$, it is assumed that it is an evaporation controlled combustion shown as the (A) branch in Fig. 5.5 and the burning rate of fuel is equal to the evaporation rate

$$\Delta m_{fi} = \Delta m_{fui}$$

If $\phi_g > 1$, the combustion is assumed to be entrainment controlled and this is the (B) branch in Fig. 5.5. Thus the burning rate of fuel will be calculated according to the available amount of entrained fresh air and, with the fuel being allowed to burn stoichiometrically.

$$\Delta m_{fi} = \Delta m_{fci}$$

The heat release in an individual package during a computing time interval is given as

$$\Delta Q_{pi} = H_u \Delta m_{fi}$$

where Q is amount of heat release; H_u the calorific value of fuel; and m_{fi} mass of fuel burned. Finally, the total heat release of the entire spray can be found from the sum of the heat release by all individual packages.

5.3.6 The Cummins Engine Model

This model proposed by Shahed et al [113] [141] treats the fuel spray as a vapour jet. The vapour concentration is assumed to be continuous while the vapour jet is divided into a series of discrete combustion zones as shown on Fig. 5.6. Energy conservation, chemical equilibrium and nitric oxide rate chemistry are applied to each zone.

Spray motion

The spray tip penetration is calculated from an empirical formula [113] as

$$S = \frac{450 d_n^{0.5} (\rho_f / \rho_d)^{0.4}}{(1 + \rho_a / \rho_{atm})^{0.85}} \left(\frac{\rho_a}{\rho_{atm}} \right)^{0.5} (\Delta P)^{0.25} t^{0.6} \quad (5.26)$$

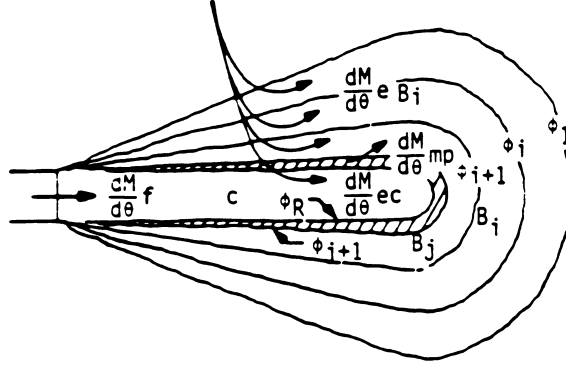


Figure 5.6: Multi-Zone Spray in the Cummins Engine Model

where $\rho_a, \rho_{atm}, \rho_d$ and ρ_f are the density of the air within the cylinder, the atmosphere, the diesel and reference fuel, respectively.

If there is swirl, the swirl affect S_s is calculated by

$$\frac{S - S_s}{S} = 0.35 \left(\frac{S_s Q_a}{d_n Q_f} \right)^{0.44} \quad (5.27)$$

where d_n is the injector nozzle diameter. The momenta of air and fuel, Q_a, Q_f are given as

$$Q_a = \rho_a S_s^2 \omega^2 \quad ; \quad Q_f = \rho_f V_0^2$$

where ω is the air angular velocity. The initial jet velocity is obtained from a conventional nozzle equation as

$$V_0 = C_d \sqrt{\left(\frac{2 \Delta P}{\rho_a} \right)}$$

After the spray detaches from the nozzle, the spray tail movement is estimated by assuming its velocity to be one-half of the spray tip penetration speed. A derivation of an empirical equation of the tail movement has not yet been found.

spray shape

The cross-sectional area of the spray is approximated by two ellipses or an equivalent circle of radius b , as shown on Figure 5.7

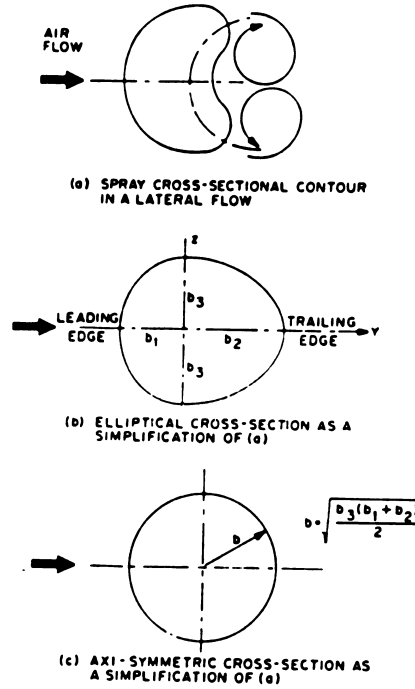


Figure 5.7: Schematic representation of spray cross-section in the Cummins model

$$b = \sqrt{\frac{b_3(b_1 + b_2)}{2}} \quad (5.28)$$

The growth rate of the spray width has been found to agree with Prandtl's mixing length theory[137]. The rate of growth of the spray width , b , can be expressed as

$$\frac{db}{dS} = 0.12\left(1 + \frac{\rho_a}{\rho_f}\right) \quad (5.29)$$

with

$$b_3 = b_1 + 0.11 \times (\rho_a/\rho_f) \quad \text{and}; \quad b_2 = b_1(1 + 0.0016 Re^{0.66})$$

where

$$Re = 2\pi\rho_a r\omega d_n/\mu_a$$

b_1 is found to be the same as that of a straight jet thus is given by Eq. 5.29.

Concentration distribution

The model assumes that the spray concentration is distributed hyperbolically along the spray axis (S- coordinate) and normally across the axis (r- coordinate). That is

$$C(S, r, t) = \frac{1 - (\frac{r}{b})^{1.5}}{\alpha(t) \cdot S + 1}$$

where $\alpha(t)$ must satisfy the overall mass balance of the spray plume. This can be obtained from

$$\int_0^t \frac{dM_f}{dt} = 2\pi \int_{S_t}^S \int_0^b C(S, r, t) \rho \cdot r dr dS$$

where dM_f/dt is the fuel injection rate and the local density ρ is

$$\rho = \frac{P_a}{[(1 - C(S, r, t))R_a + C(S, r, t)R_f]T_a}$$

Here R_a and R_f are the gas constants for air and fuel vapour, respectively.

Division into zones

The model divides the whole combustion chamber into three regions, these being: (A) the air region; (B) the combustible mixture region which is further divided into several subregions (zones) in order to carry out the numerical calculation; and (C) the fuel rich cone region (Fig. 5.6). The boundary between A and B is the lean flammable limit ϕ_L whilst the boundary between B and C is the rich flammable limit ϕ_R .

Mass transfer between zones

Once the concentration distribution and zones are determined, a mass transfer can then be calculated. Air entrainment rate into the fuel rich cone region C is

$$\frac{dm_{eC}}{dt} = 2\pi \frac{d}{dt} \int_{S_t}^S \int_{r=0}^{r(\phi_{j+1})} (1 - C(S, r, t)) \rho r dr dS \quad (5.30)$$

where S_t is the spray tail. ϕ_{j+1} is the boundary of the richest combustion zone. The fuel preparation rate which is defined as the rate at which the fuel mixture crosses the rich limit to the burning zone is

$$\frac{dm_{fP}}{dt} = 2\pi \int_{S_t}^S \int_{r(\phi_R)}^{r(\phi_{j+1})} C(S, r, t) \rho r dr dS \quad (5.31)$$

The associated preparation rate of air is

$$\frac{dm_{aP}}{dt} = 2\pi \int_{S_t}^S \int_{r(\phi_R)}^{r(\phi_{j+1})} (1 - C(S, r, t)) \rho r dr dS \quad (5.32)$$

Therefore, the rate at which the mixture is prepared is the sum of fuel and air preparation rate, as

$$\frac{dm_P}{dt} = \frac{dm_{aP}}{dt} + \frac{dm_{fP}}{dt}$$

Once the mixture preparation rate is determined, the burning rate can be obtained by solving the energy and mass conservation equations among all zones

5.4 Spray Structure and Spray Motion for the Current Research

As presented in the former literature review section, it is important that an accurate description model of the spray in the combustion chamber is constructed for a CI combustion model. As shown on Figure 5.8 , a spray should include the following parameters: the spray angle, break-up length, droplet size distribution, and spray tip penetration. An extensive review of the existing spray model including experimentally-based correlations and theoretically-based formulas was presented by Hiroyasu [142] in 1985.

5.4.1 Spray break-up length, tip penetration and angle

Break-up length and break-up time

In DI diesel engines, the injected liquid fuel column does not disintegrate into droplets until it passes a length, designated as the break-up length. Intensive

studies have been carried out to investigate the break-up length under engine conditions. A recent experimentally-based correlation proposed by Hiroyasu et al [142] is

$$L_b = 15.8 \sqrt{\frac{\rho_l}{\rho_a}} d_0 \quad ; \quad t_b = 28.6 \frac{\rho_l d_0}{\sqrt{\rho_a \Delta P}} \quad (5.33)$$

where L_b and t_b are break-up length (mm) and break-up time (second) respectively, ρ_l and ρ_a are the liquid and air densities(kg/m^3), respectively, D_0 is the nozzle diameter (m), and ΔP is the pressure drop across the nozzle(Pa)

Spray tip penetration and angle

Numerous formulas have been proposed for these calculation based on either theoretical analysis or experimental study. Those that have been often referred to in diesel engine combustion models are: (1) Sareen's correlation (1972) [143] as already given in Eq. 5.4; (2) Dent's formula (1971) [139] as given in Eq. 5.10; (3) Hiroyasu et al's correlation (1980) [136] as given in Eq. 5.17; and (4) Cummins correlation (1976) [113] as given in Eq. 5.26. In this research, the correlations of Sareen, Dent and Hiroyasu et al have all been incorporated into the numerical model in order to test them against the experimental results.

Some researchers have also taken account of swirl by relating it to some of the engine parameters. Eq. 5.19 in the Hiroyasu model and Eq. 5.27 in the Cummins engine model are typical of this approach. In estimating the spray angle , some researchers have used a fixed value such as the 20 degrees being used in the Kumar two-zone model [111] and the Whitehouse two-zone model [108]. Others such as in the Hiroyasu multi-zone model [112] use empirical correlations . Amongst those correlations reviewed by Hiroyasu in Reference [142], the two most recent are those by:

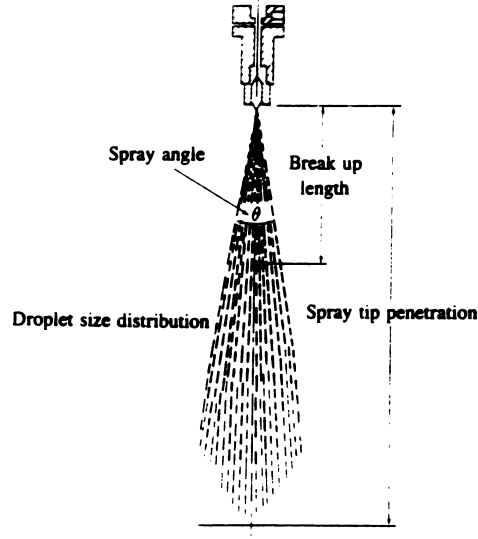


Figure 5.8: Schematic of diesel fuel spray defining its parameters

- (1) Reitz and Bracco's (1979) [144], which is

$$\tan\left(\frac{\theta}{2}\right) = \frac{1}{A} 4\pi \sqrt{\frac{\rho_g}{\rho_l}} \mathcal{F}\left(\frac{\rho_l Re_l}{\rho_g We}\right)^2 \quad (5.34)$$

Here $A = 3.0 + 0.28(L_n/d_n)$, ρ_l and ρ_g are densities of liquid and gas respectively, Re_l and We are jet Reynold number and Weber number

respectively given as $Re_j = \frac{\rho_l v_j d_n}{\mu_l}$ and $We_j = \frac{\rho_l v_j^2 d_n}{\sigma}$. $\mathcal{F}\left(\frac{\rho_l Re_l}{\rho_g We}\right)^2$ has

a maximum value of $\sqrt{3}/6$;

- (2) Hiroyasu et al's (1980) correlation [142], giving

$$\theta = 0.05 \left(\frac{\rho_a \Delta P d_n^2}{\mu_a^2} \right)^{0.25} \quad (5.35)$$

where μ_a and ρ_a are the viscosity and density of air, respectively, ΔP is pressure drop across the nozzle, and d_n is the diameter of the nozzle hole.

Both of these two correlations have been incorporated into a simulation program used in the work for this thesis to test against experimental results.

5.4.2 Spray evaporation

Spray evaporation may be caused by the sudden pressure drop after the liquid spray enters the combustion chamber, or heat transfer to the liquid fuel from the cylinder gases or the wall. A quantitatively accurate description of the evaporation within a diesel fuel spray requires the solution of coupled conservation equations for the liquid droplet and the air within the combustion chamber. Typical of this are Equations 5.23, 5.24 and 5.25 in the Hiroyasu model. At this stage of the study, however, a model of spray evaporation is not included in this research because of the fact that combustion in a typical, medium-speed DI diesel engine is largely a mixing-limited rather than evaporation-limited process. This is because 70 to 95 percent of the injected fuel has evaporated at the start of combustion and over 90 percent of evaporation is complete after 1 ms [19], [145]. In a dual fuel engine, droplet evaporation is believed to be complete in an even shorter time because the injected fuel is usually a small amount. Comprehensive investigation of spray evaporation and combustion can be found in articles by Elkotb (1982) [146], Sirignano (1983) [77], Faeth (1983) [147] and Bracco (1985) [148].

5.5 Ignition Delay

The two most common definitions of ignition delay are based on the pressure rise and the illumination. The pressure rise delay is defined by the point at which the pressure rise caused by the combustion is detached from the motoring curve. The illumination delay is marked by the emission of visible radiation. Experiment [152] has found that the onset of visible luminous combustion occurs after the start of detectable combustion-produced pressure rise by 0.1 to 0.3 ms.

The ignition delay is affected by many physical and chemical factors, these

being atomization of the liquid fuel jet, vaporation of the fuel droplets, mixing of vapor with air, precombustion reaction of the fuel, air and residual gas mixture. The air temperature plays a dominant role. Early research tried to describe ignition delay solely in term of an exponential rise of reaction rate with temperature T . Deduction from reaction kinetics shows that ignition delay is also inversely proportional to the pressure P . Based on these fundamental considerations, many calculation formulas have been proposed in the form

$$\tau_{ig} = A P^{-n} \exp\left(\frac{E_A}{RT}\right) \quad (5.36)$$

as reviewed by Hiroyasu [142]. Hiroyasu and Fujimoto took residual gas fraction into account by use of a factor $\phi = (P_{O_2}/0.21P)$. The formula then became

$$\tau_{ig} = A P^B \phi^C \exp(D/T) \quad (5.37)$$

More recently, Pischinger et al [149] proposed a different form which is

$$\tau_{ig} = \frac{C_1}{P^n} \exp\left(\frac{C_2}{T - T_{ref}}\right) \quad (5.38)$$

This was based on their visualization experiments in both a combustion bomb and engine. Here T_{ref} is an empirically constant reference temperature obtained from experiment.

In the case of an engine, because the pressure and temperature vary during the delay period, the following integral relation of the ignition delay is usually used

$$\int_{\tau_{si}}^{\tau_{is} + \tau_{id}} \left(\frac{1}{\tau}\right) dt = 1 \quad (5.39)$$

Here the quantity τ_{si} is the time at the start of injection, τ_{id} is the ignition delay period.

Experiments on the combustion bomb which has been described in Chapter 4 have been carried out by the author of this thesis to investigate pressure rise ignition delay of diesel spray combustion in a constant volume combustion bomb, particularly when injection of fuel is of small quantity. Experimental results are presented in Appendix C. For the ranges of pressure and temperature being used in the experiment, that is, pressure being $7.00 \text{ bar} \leq P \leq 38.3 \text{ bar}$,

temperature being $563 \text{ K} \leq T \leq 670 \text{ K}$, experimental results are fitted to equation

$$\tau_{ig}(ms) = A \times P^{-0.7837} \exp\left(\frac{880.8}{T}\right) \quad (5.40)$$

by using NAG Fortran library [157]. Here $A = 18.478$ if P is in atm, or $A = 18.668$ if pressure is in bar. The temperature T is in K.

It should be pointed out that the values of ignition delay given by different correlations such as listed in references [19] and [142], often vary substantially. This is mainly attributed to the following reasons:

- (1) Different methods in defining the ignition delay time. For example some researchers have defined the ignition delay as the time required for the internal energy change recovering to the value before vapourization [162] which is different to the normal definitions.
- (2) Different experiment setups do not give close results for the physical delay time. In particular, most of the correlations are based on engine data.
- (3) The properties of fuel used in different experiments may not be exactly the same.
- (4) Different numerical methods have been used in obtaining the empirical constants and these can also vary the values slightly.

However, the value given by the regression equation obtained by the current combustion bomb experiments is found to be quite close to that given by the ODES correlation which is

$$\tau_{ODES} = 3.454 \times P(atm)^{-1.0218} \exp\left(\frac{2100.8}{T}\right) \quad (5.41)$$

Fig 5.9 gives a comparison of the current regression (Eq. 5.40) with the ODES correlation.

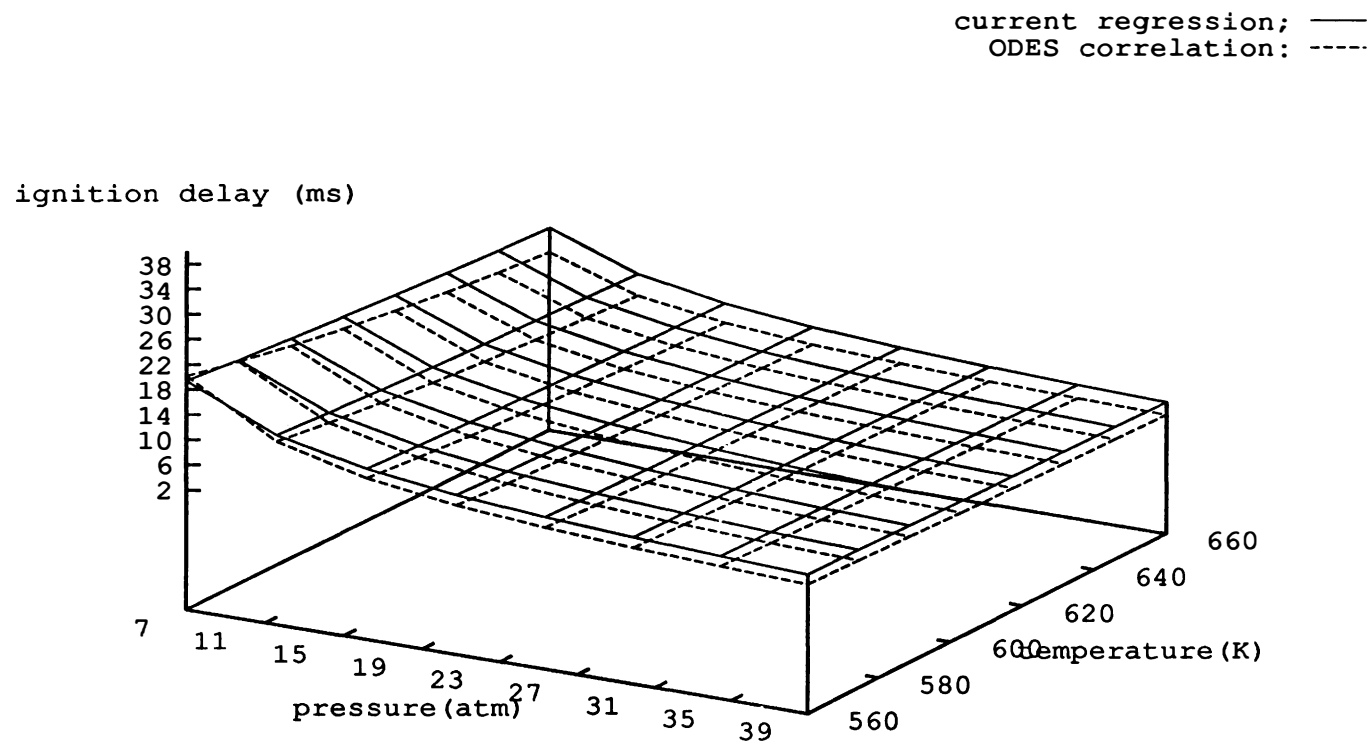


Figure 5.9: Contour Map of Ignition Delay Calculated by Equations 5.40 and 5.41.

5.6 Air Entrainment

5.6.1 Various estimation methods

The process of air entrainment into a burning diesel spray is a complex one involving the transfer of mass, momentum and energy, as well as chemical reaction and diffusion. A full description requires the application of the equations of continuity, momentum, energy, diffusion and reaction, as well as an accurate model of spray structure and spray motion. In phenomenological modelling, various approximations have been proposed in the past. In reviewing of literature, it is found that typical approaches are as follows.

- (1) The entrainment may be calculated according to the distribution of fuel, it being considered that the fuel is distributed in a similar manner to a single phase steady jet. This approach was used in the Cummins model [113].
- (2) Formulae may be obtained from non-reactive turbulent mixing theory such as Eq. 5.15 and 5.16 in the Dent-Metha model.
- (3) Conservation of momentum between the spray and the surrounding air can be applied but an arbitrary coefficient has to be chosen in order to account for the effect of combustion. This approach is used in the Hiroyasu model.
- (4) Entrainment may be calculated according to the volume of the spray and the volume of burned gases, such as in Eq. 5.7.

All of those aforementioned treatments require either much computing effort or many system-related arbitrary coefficients. This makes them not suitable to be used in present study. A method has been developed here based on turbulent mixing theory and the current experimental results of the constant-volume combustion bomb that applies particularly for small spray quantity. This method is discussed in the next section.

5.6.2 Entrainment of air into a spray for small injection quantities

For a spray of small injection quantity such as pilot injection, the injection period is short compared with the entire combustion period. It is therefore reasonable to assume that the entire spray-air mixing process is controlled by the turbulent kinetic energy dissipation. The turbulent mixing can be expressed by Eq. 5.16 in the Dent-Metha's spray mixing model as reviewed in Section 5.3.4. Keeping in mind that the entrainment rate of air, \dot{m}_{ea} , is equal in magnitude to the depletion rate of available air but opposite in sign, then Eq. 5.16 can be rewritten as

$$\dot{m}_{ae} = C_l(m_a/\tau) \quad (5.42)$$

Here C_l is an empirical coefficient, m_a is the mass of remaining unburned air, τ the turbulent mixing time.

In the Dent-Metha turbulent spray model, the coefficient C_l is evaluated by equating the mean timewise entrainment rate over the entire injection period to the right hand side of equation 5.16. The turbulent mixing time τ is given as

$$\tau = (L^2/\varepsilon)^{1/3} \quad (5.43)$$

for a large scale eddy structure where L is the length scale of the eddy structure. In Dent's model, L is taken to be the nozzle orifice equivalent diameter. The quantity ε is the energy dissipation rate. Dent has characterised the turbulent energy dissipation in a quiescent chamber Diesel engine in terms of the injection variables and the engine speed by use of the expression [114], [153]

$$\varepsilon = (C N/\theta_{ip})^3 (V_f/n d_0^2)^2 \quad (5.44)$$

where N is the engine speed, θ_{ip} is the injection angular duration, V_f is the volumetric delivery of fuel, n is the number of holes in the injection nozzle, and d_0 is the injector orifice diameter. C is a constant.

Because equation 5.44 cannot be directly applied for spray combustion in a constant volume combustion bomb, an alternative method to evaluate the rate of air entrainment has been derived by the present author.

From Eq. 5.42, it is noted that if C_l/τ is known, then m_{ae} can be calculated. If the the burning spray is considered as a closed space region with an instantaneous surface $A(t)$, and C_l/τ as a continuous distribution function, $\psi(A)$, on the surface A , the rate of entrainment is obtained by the integration of $\psi(A)$ over the entire surface, at any instant. Eq. 5.42 then becomes

$$\dot{m}_{ae} = C_l(m_a/\tau) = \left(\oint_A \psi(A) \cdot dA \right) \cdot m_a \quad (5.45)$$

Mathematically, a certain function $\Psi(A)$ exists which satisfies

$$\oint_A \psi(A) \cdot dA = \Psi(A) \oint_A dA = \Psi(A) \cdot A$$

The rate of air entrainment is then given as

$$\dot{m}_{ae} = \Psi(A) \cdot A \cdot m_a \quad (5.46)$$

Combining Eq. 5.45 with Eq. 5.46, an entrainment function Ψ is therefore defined as

$$\Psi = \frac{C_l}{\tau} / A(t) \quad (5.47)$$

and the calculation of \dot{m}_{ae} allows the entrainment function Ψ to be found.

5.7 A Model for Diesel Spray Combustion in A Constant Volume Vessel

5.7.1 Model assumptions

The combustion model proposed here for the combustion bomb is based upon these assumptions:

1. For a small quantity pilot fuel injection system, the injection duration is short and evaporation of fuel droplets is faster than the mixing of

the vapour with the air. Pre-mixed burning in the early stage of the combustion only takes a small portion of the fuel and is completed very quickly. Therefore, the entire burning rate is controlled by the rate of vapour mixing with air. It is also assumed that all air will mix with vapour and burn immediately after it is entrained into the burning region.

2. The vaporised fuel is treated as an ideal gas.
3. The burning region is identified with the vapourized spray region. Thus, development of the burning region parameters such as its outer surface area can be calculated by applying spray motion equations.
4. Although the spray expands rapidly during combustion, its surface area and volume can be calculated by considering the spray as a circular jet with an equivalent constant spray angle, as shown on Fig 5.8;
5. The fuel injection in a dual fuel system requires only in a small quantity of pilot injection. Thus no impingement of the spray onto the wall is assumed to occur. The calculation is therefore applied only to the free jet.
6. During the entire combustion process, the instantaneous fuel-air equivalence ratio is equal to the overall fuel-air equivalence ratio.
7. In thermodynamic calculations, conditions are the same as used in Chapter 2.
8. Heat loss from the hot charge to the cool combustion chamber is due to convection only, radiation being negligible.

Using these simplified assumptions, the model equations can be established as in next subsection.

5.7.2 Model equations

Ignition delay

Pressure rise delay is estimated by the empirical correlation obtained from the present combustion bomb experiment as given in Eq. 5.40. This is

$$\tau_{ig}(ms) = AP^n(atm)exp(\frac{C}{T}) \quad (5.48)$$

Here $A = 18.478$, $n = -0.7837$, and $C = 880.8$.

Burning rate

The burning rate of the total mass is the sum of the consumption rate of fuel and consumption rate of air,

$$\dot{m}_b = \dot{m}_{bf} + \dot{m}_{ba} \quad (5.49a)$$

$$\dot{m}_{bf} = \phi_{fa}\dot{m}_{ba} \quad (5.49b)$$

$$\dot{m}_{ba} = \dot{m}_{ea} \quad (5.49c)$$

where ϕ_{fa} is the overall fuel-air equivalence ratio and \dot{m}_{ea} is the rate of air entrainment.

Rate of air entrainment

The rate of air mass entrainment is given by

$$\dot{m}_e = \Psi \cdot A(t) \cdot \dot{m}_a \quad (5.50)$$

Here \dot{m}_a is the mass of the remaining unburned air, Ψ is a turbulent entrainment function about which further discussion is given in a later section. $A(t)$ is the instantaneous surface area of the equivalent circular spray jet, evaluated as

$$A(t) = \pi(\tan^2\theta + 1)S^2(t) \quad (5.51)$$

where θ is the spray angle and $S(t)$ is the spray tip penetration. For a nozzle with n holes, the total spray surface is $n \times A(t)$.

Spray configuration

Spray penetration and angle are calculated by the Hiroyasu correlations:

$$\theta = 0.05 \left(\frac{\rho_a \Delta P d_0^2}{\mu_a^2} \right)^{0.25} \quad (5.52a)$$

$$S(t) = \begin{cases} 0.39 \left(\frac{2\Delta P}{\rho_l} \right)^{0.5} \cdot t & ; \quad \text{if } t < t_b \\ 2.95 \left(\frac{\Delta P d_0^2}{\rho_a} \right)^{0.25} \sqrt{t} & ; \quad \text{if } t_b \leq t \end{cases} \quad (5.52b)$$

$$t_b = 28.65 \frac{\rho_l d_0}{\sqrt{\rho_a \Delta P}} \quad (5.52c)$$

where μ_a, ρ_a are the viscosity and density of air, respectively.

Conservation of mass

Mass conservation for the burned zone and unburned zone is expressed as

$$\frac{V_0}{m_0} = \int_0^{x_b} v_b dx + \int_{x_b}^1 v_u dx \quad (5.53)$$

where x_b is the burned mass fraction at given instant. The above equation can also be written as

$$\bar{v}_0 = x_b \bar{v}_b + (1 - x_b) \bar{v}_u \quad (5.54)$$

where $\bar{v}_b = \int_0^{x_b} v_b dx / x_b$ and $\bar{v}_u = \int_{x_b}^1 v_u dx / (1 - x_b)$

Conservation of energy

For a combustion chamber modelled as a two-zone space, energy conservation can be expressed as

$$\frac{E_0 - W - Q}{m_0} = \int_0^{x_b} e_b dx + \int_{x_b}^1 e_u dx$$

or

$$e_0(T_0) - \frac{W - Q}{m_0} = x_b \cdot \bar{e}_b(T_b) + (1 - x_b) \cdot \bar{e}_u(T_u) \quad (5.55)$$

where $\bar{e}_b(T_b) = \int_0^{x_b} e_b(T_b) dx / x_b$, $\bar{e}_u(T_u) = \int_{x_b}^1 e_u(T_u) dx / (1 - x_b)$, are the mean internal energies for the burned and unburned zone respectively. Also,

$$e_b(T_b) = \sum_B X_i e_i$$

i for all species in the burned zone;

$$e_0(T_0) = \sum_O X_i e_i$$

i for all species appear in initial state;

$$e_u(T_u) = \sum_U X_i e_i$$

i for all species in unburned zone.

W and Q in Eq. 5.55 are the total work and heat loss during combustion, respectively and are given as $W = \int_0^t \dot{w} dt$ and $Q = \int_0^t \dot{q} dt$. For combustion bomb calculations, $\dot{w} \equiv 0$. An expression for \dot{q} is discussed in a later section.

This completes the model equations for the combustion of diesel spray in a constant volume vessel. Numerical computations have been performed by a FORTRAN code in double precision. Calculation results are discussion in later section in comparison with experimental results from the combustion bomb.

5.8 Computational Results Compared with Experimental Records

5.8.1 About the entrainment function Ψ

It is found that the measured pressure traces from the experiment can be well simulated by assuming a constant value of Ψ for each combustion and the value

of Ψ is insensitive to the initial pressure and temperature. From Eq. 5.43, Eq. 5.44 and Eq. 5.47, it can be seen that Ψ is proportional to V_f^2 . That is

$$\Psi = C_e V_f^2$$

where V_f is the volumetric delivery of injected fuel. Fig. 5.10 shows the $\Psi - V_f$ relation obtained from the current experiment. Values of Ψ are obtained by changing Ψ gradually until the computed cylinder dynamic pressure matches the measured results. Values of V_f are calculated from an energy balance for the combustion. These data can be fitted to the equation

$$\Psi = 1.1 V_f^{1.3} \quad (5.56)$$

However, the values of V_f may not be very accurate because of incomplete burning of the fuel, particularly when combustion is at low temperature and pressure, or when injection is in relatively large quantities. Therefore, the precise expression for the entrainment function Ψ is a subject which needs to be further studied.

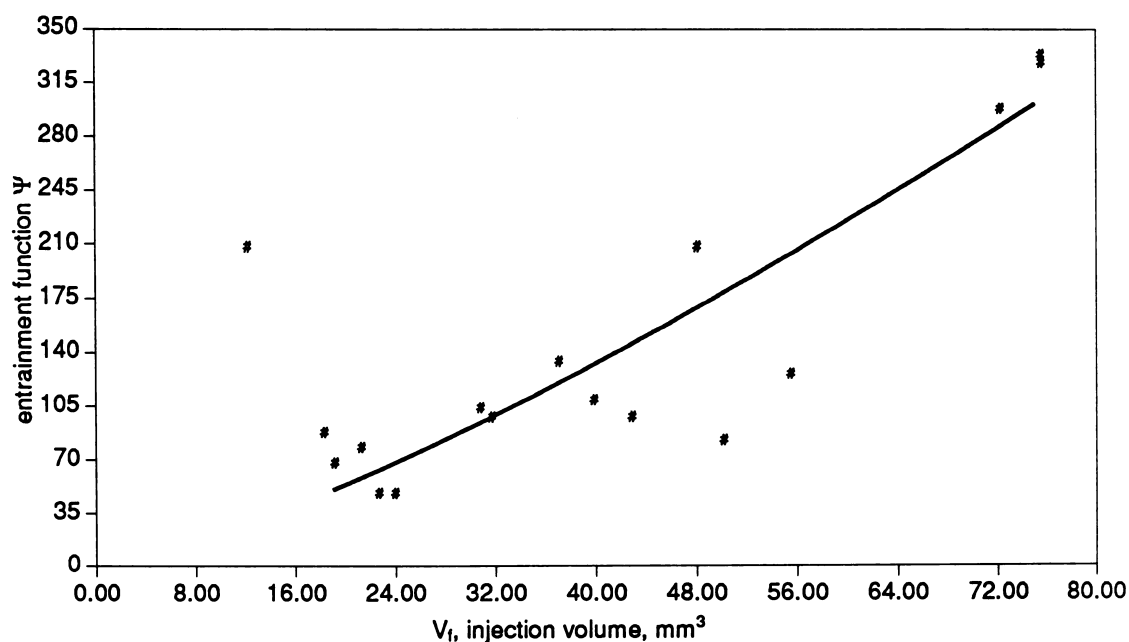


Figure 5.10: Values of the entrainment function

5.8.2 About the heat loss rate \dot{q}

When the combustion pressure and temperature is high, the effect of heat transfer becomes more significant, particularly at the late combustion stage. In an engine calculation, heat transfer from the hot cylinder gas to the cool cylinder wall is usually simplified as convection only and is given as

$$\dot{q} = h_c A_c (T_w - T_m)$$

where h_c is a instantaneous spatial average coefficient of heat transfer , A_c is the total combustion vessel heat transfer area, T_w , T_m are the mean temperature of the cool wall and the cylinder gas, respectively.

Many correlations have been proposed for h_c [142], [19] for engine calculations. In the present study of the combustion bomb, Woschni's correlation for instantaneous heat transfer coefficient has been chosen and has been modified to suit the combustion bomb situation. It is given as follows:

$$h_c (W/m^2 \cdot K) = C_h B(m)^{0.2} P(kPa)^{0.8} T_m(K)^{-0.55} (P - P_0)(kPa)^{0.8} \quad (5.57)$$

where B is the cylinder bore, P is cylinder pressure, P_0 is cylinder pressure before ignition, T_m is a mean cylinder temperature given as $T_m = x_b T_b + (1 - x_b) T_u$. The term $(P - P_0)^{0.8}$ reflects the average gas velocity caused by the combustion pressure rise, and C_h is a an empirical constant.

It has been found from the current experiments that the value of C_h varies substantially according to the various maximum pressures which are achieved during combustion. Thus, in the calculation, different values of C_h are used when the cylinder pressure reaches different ranges, these being

$$C_h = 1.24D - 4 \quad \text{for } 19 \leq P \leq 29 \quad (5.58a)$$

$$C_h = 7.78D - 5 \quad \text{for } 29 < P \leq 45 \quad (5.58b)$$

$$C_h = 3.27D - 5 \quad \text{for } 45 < P \leq 79 \quad (5.58c)$$

Fig. 5.11 to 5.16 show some typical results computed by the current model in comparison with the corresponding measured results.

For the combustion of a small injection quantity at typical engine conditions of initial pressure and temperature, the model gives good prediction of ignition delay time and the dynamic cylinder pressure measured on the combustion bomb, as shown on Fig. 5.11, 5.12 and 5.13

If the injection is so large that abnormal combustion occurs, the model again predicts well until the abnormal combustion occurs but fails after that occurrence, as shown on Fig. 5.15 and 5.14. For combustion at low initial pressures, the prediction is also not very good, as shown on Fig. 5.16 and 5.17.

Prediction failure could be due to several reasons, these being

- (1) For abnormal combustion, the fuel is suddenly burned very rapidly and the heat release predicted by the model is hence slower than the actual value.
- (2) For combustion at low initial pressure and temperature, some prepared fuel-air mixtures may not be able to ignite until the late combustion stage. Therefore, the predicted heat release (and hence the pressure) is first higher than the measured result in the early combustion stage but later becomes lower. This is shown on Fig. 5.16 and Fig. 5.17.
- (3) The value of the entrainment function estimated by Eq. 5.56 may not be very accurate for combustion at large injection or low initial pressure and temperature because some fuel may not be burned. The value of V_{inj} is calculated based on an energy balance by assuming that all injected fuel will take part in the combustion.
- (4) The heat transfer calculation equation Eq. 5.57 was originally derived from engine conditions and may not therefore be suitable for all testing conditions. In particular, the current experiments have been carried out for a range of initial temperatures and pressures outside those for which the correlation was derived.

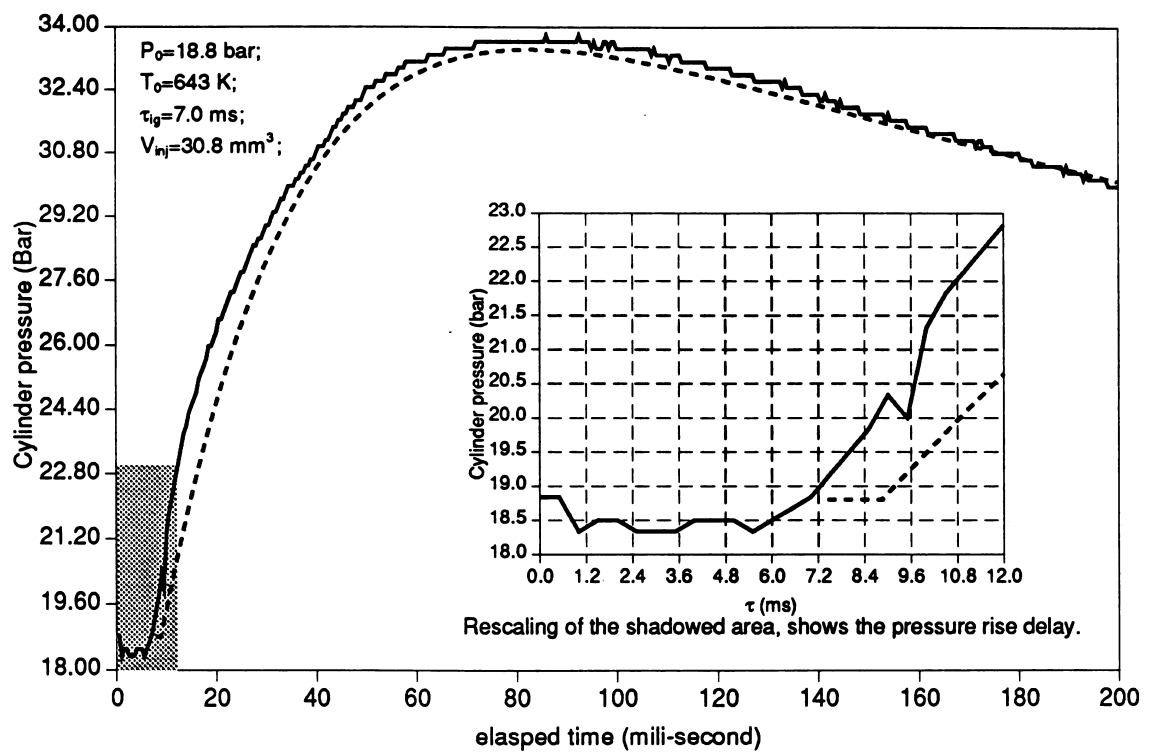


Figure 5.11: Dynamic combustion bomb pressure, computed result (dashed lines) and measured results.

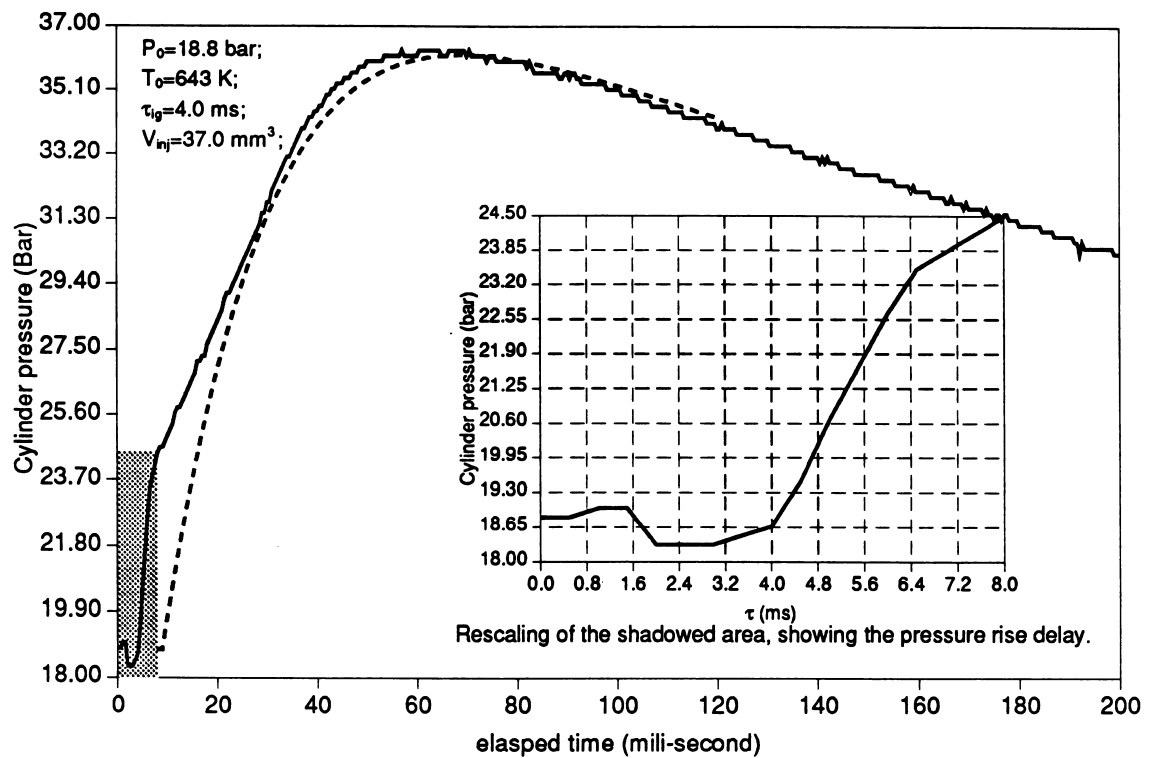


Figure 5.12: Dynamic combustion bomb pressure, computed result (dashed lines) and measured results

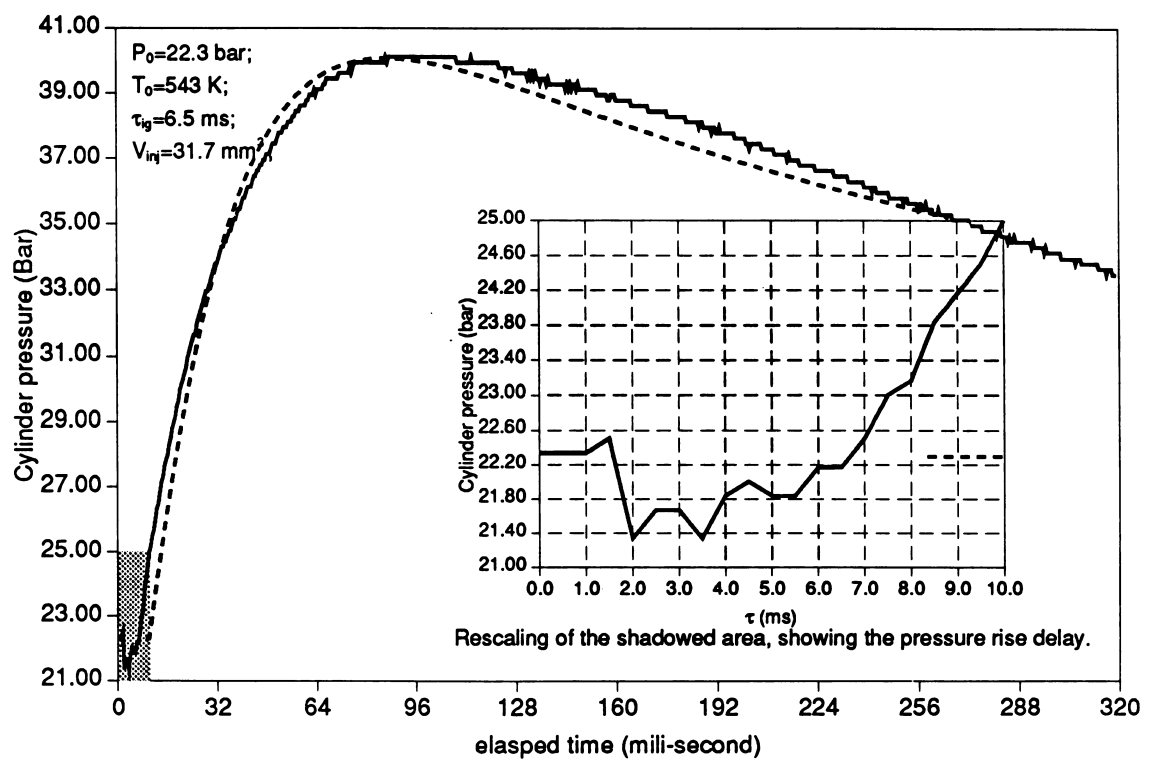


Figure 5.13: Dynamic combustion bomb pressure, computed result (dashed lines) and measured results

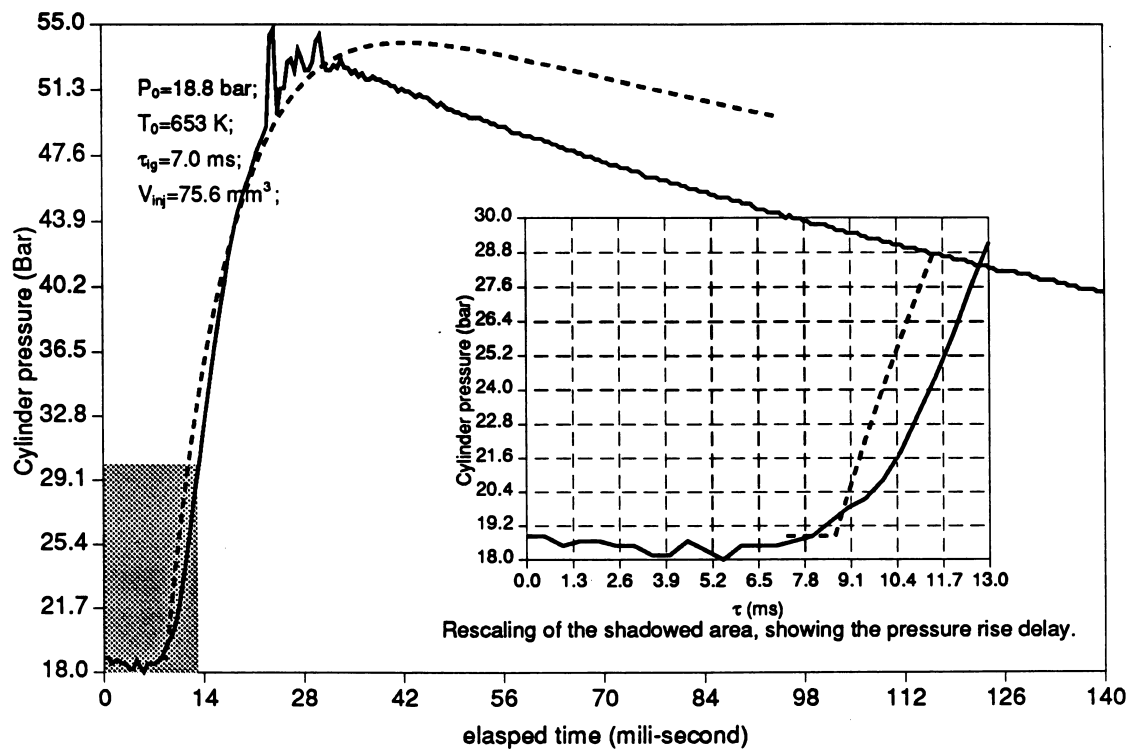


Figure 5.14: Dynamic combustion bomb pressure, computed result (dashed lines) and measured result

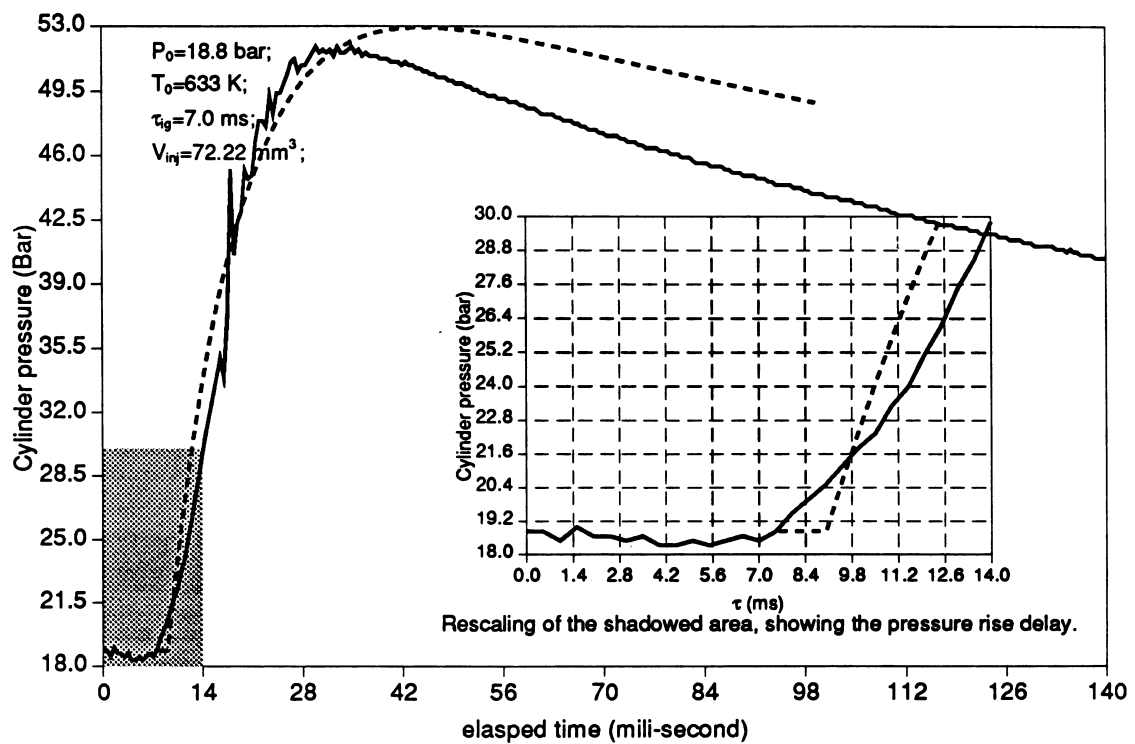


Figure 5.15: Dynamic combustion bomb pressure, computed result (dashed lines) and measured result

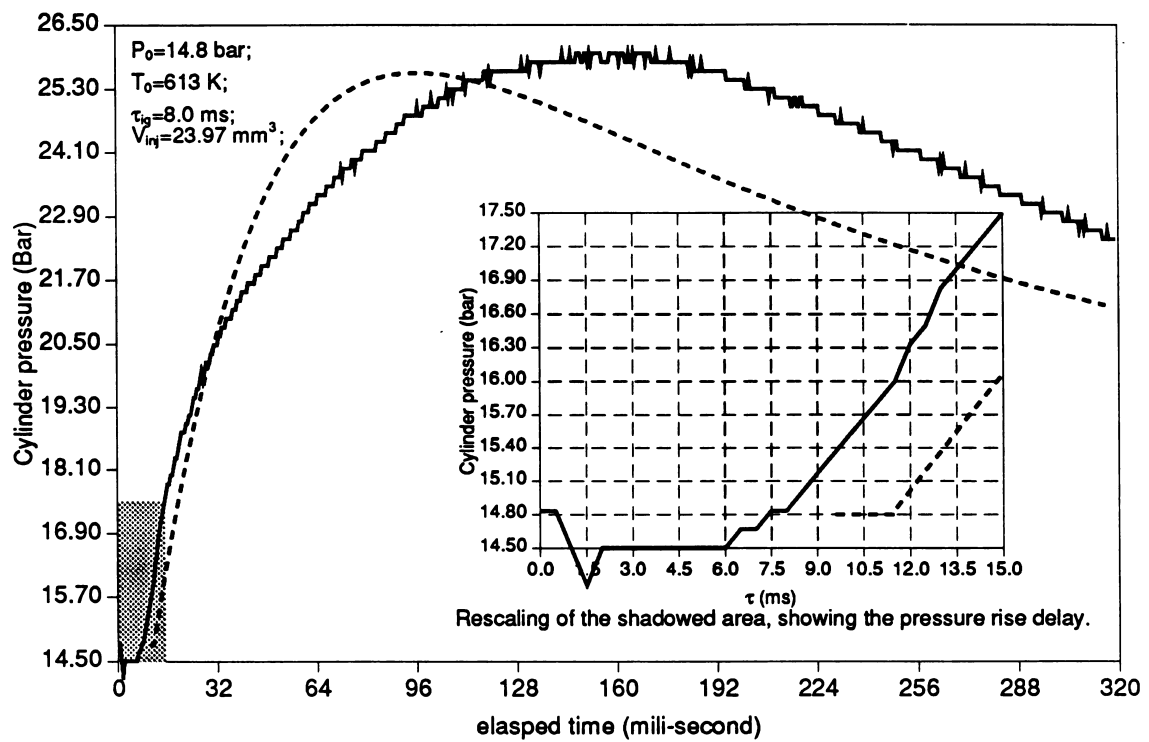


Figure 5.16: Dynamic combustion bomb pressure, computed result (dashed lines) and measured result

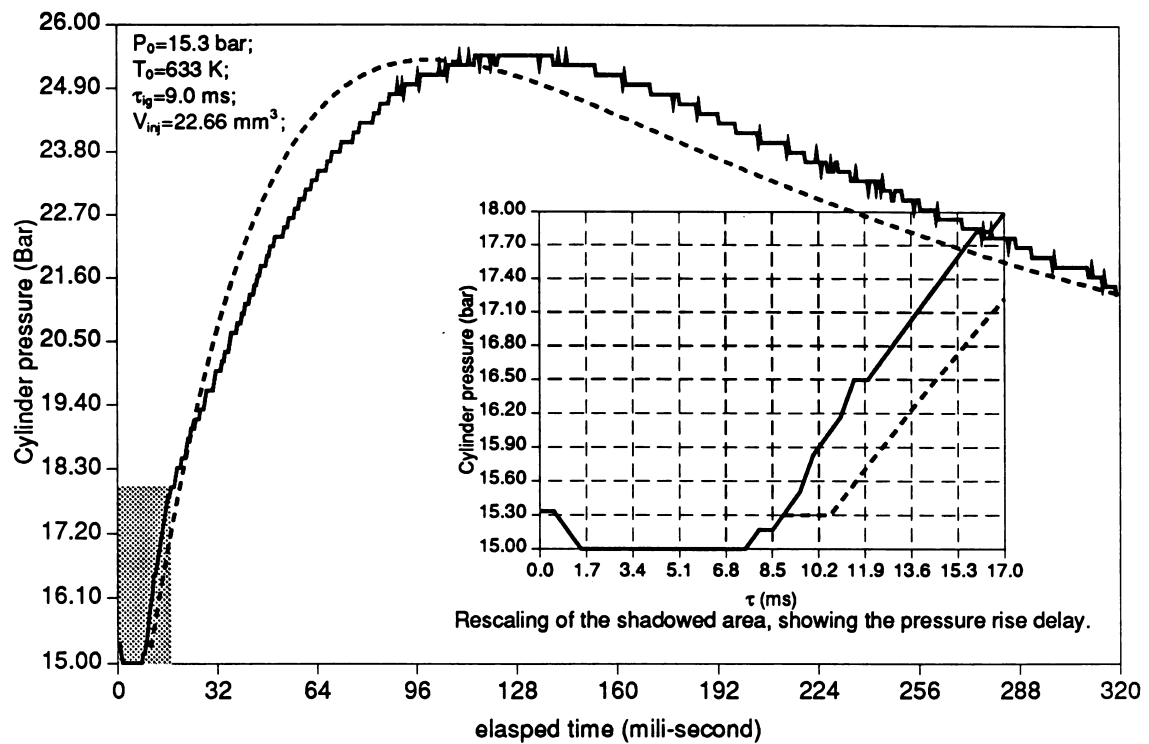


Figure 5.17: Dynamic combustion bomb pressure, computed result (dashed lines) and measured result

Chapter 6

Features of Dual Fuel Combustion Observed From Combustion Bomb Experiments

6.1 Introduction

Though numerous papers have been published related to the various aspects of using gaseous fuel in a diesel engine, all are based on engine data. No report has been found which studies the dual fuel combustion phenomena in a combustion bomb. Knowledge of the details of the fundamental mechanism of the dual fuel combustion process is particularly inadequate. This chapter describes the results of a series of dual fuel combustion experiments which have been conducted using the constant volume combustion bomb which was described in Chapter 4. Emphasis is placed at this stage on the ignition condition, ignition delay and general dual fuel combustion characteristics. However, future projects will consider other phenomena such as flame propagation and quench and knock problems. By analyzing the pressure trace obtained from experiments, previously unreported phenomena of dual fuel combustion have been observed. Explanations are suggested for these phenomena. A correlation for dual fuel ignition delay has been proposed based on the dynamic cylinder pressure diagrams obtained from the dual fuel combustion experiments.

6.2 Literature Review

6.2.1 General Combustion Features Observed in a Dual-Fuel Engine

In a typical dual-fuel combustion system, the homogeneous gas-air mixture is compressed to just below its autoignition condition and is then ignited by an injection of pilot liquid fuel. The injected liquid fuel (usually diesel) vaporises and autoignites promptly to provide a multitude of ignition sites from which turbulent flames develop and propagate to other regions of the combustion chamber hence consuming the homogeneous gaseous fuel-air mixture. The ignition delay of the injected liquid fuel is influenced substantially by the presence of the gaseous fuel to an extent which is in excess of that caused by the reduction of the partial pressure of oxygen or by the lowering of the charge temperature. It is generally believed that gaseous fuel has participated in the pre-ignition chemical processes. Engine tests also indicate that the ignition delay is very sensitive to the intake temperature of the gaseous fuel [8].

At very low gaseous mixture concentrations, the dual-fuel engine is found to have poor efficiency. Also in the engine exhaust, the concentrations of carbon monoxide and unburned gaseous fuel are higher than those of the equivalent “straight” diesel engine. The reason is that, in a very lean fuel mixture, the flame propagation speed is too low to allow the flame front to extend to the extreme regions. Thus only that part of the charge directly in contact with the pilot spray can be fully reacted leaving the remaining homogeneously dispersed gaseous fuel incompletely burned [6], [8], [1].

When the gaseous fuel concentration increases to a point which exceeds a certain limit, the flame fronts can then sweep throughout the mixture resulting in a faster rate of energy release and hence pressure rise. However, further increase in the mixture concentration may lead to uncontrolled combustion, or engine knock as shown in engine tests [8], [15], [14].

It has been observed that increasing the quantity of liquid fuel injection

improves the combustion. This has been explained by three reasons: (1) the increase of injection quantity provides more ignition sites and a larger combustion region for the gaseous mixture; (2) more pilot fuel provides a greater energy release resulting in higher pressures and local temperatures which improve flame propagation in the gaseous mixture; (3) in the case of methane as the gaseous fuel, the mixture of diesel-air is more flammable than the methane-air mixture. The presence of diesel vapour will therefore modify the local composition and hence alter the lean flammability limit in a favourable direction.

6.2.2 Ignition Delay Observed in a Dual-fuelled Engine

Most of the investigations on dual-fuel ignition delay have been for engine dual fuel operation. It has long been noticed that the presence of lean gaseous fuel in the mixture substantially prolongs the ignition delay period of the pilot fuel. Increasing the gaseous concentration leads to first a reduction of the ignition delay to a minimum value, followed by a rapid increase in the delay until ultimately ignition failure occurs[4]. Typical results obtained by Karim are shown on Fig. 6.1 [154]. This phenomenon has also been noticed by some other researchers in dual fuel engine tests with various combinations of gaseous and liquid fuels, including methane, carbon monoxide and propane as the gaseous fuel and diesel, cetane and heptane as the pilot fuel [9]. On some occasions, this decrease of ignition delay does not occur when gaseous concentration changes from low to high [10].

The ignition delay period in a dual fuel engine is much longer than that of a conventional diesel engine. This prolongation exceeds that caused by the reduction of the oxygen partial pressure or the reduction in the temperature of the charge around TDC resulting from the addition of gaseous fuels in the mixture which changes the isentropic index for the compression process. It is therefore believed that the gaseous fuel has participated in the pre-ignition chemical process [8].

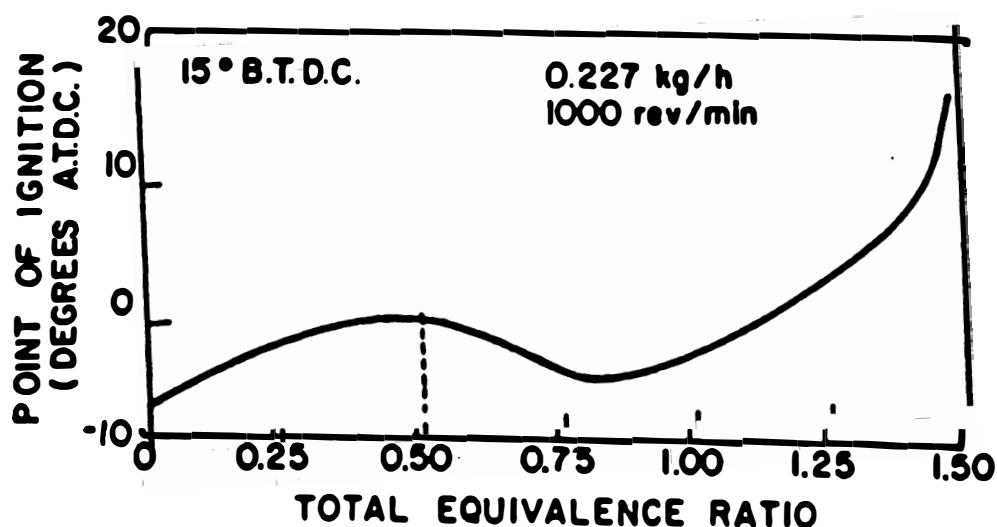


Figure 6.1: Typical variations of the ignition point of a dual fuel engine operating at constant speed and constant pilot quantity with methane. Reproduced from reference [154].

Based on their dual fuel engine experiments with various combinations of pilot and gaseous fuels, Nielsen et al [9] pointed out that ignition delay is primarily dependent on the charge temperature, pilot injection quantity and the concentration of gaseous fuel in the mixture. Karim further noted that the severity of the variation in the ignition delay period depends markedly on the quantity of liquid pilot fuel. As can be seen in Fig 6.2, more pilot fuel results in a smaller change to the delay while relatively smaller pilot fuel quantity, especially at low intake temperature, can bring about such an extension to the ignition delay that ignition actually fails.

In regard to factors affecting the dual fuel ignition delay, Karim et al [154] noted that (1) logarithmic plots of ignition delay versus the inverse of the calculated mean compression temperature do not exhibit a single curve for all equivalence ratios. Thus, taking ignition delay to be a simple exponential function of the inverse mean temperature is inappropriate; (2) the change in the oxygen concentration of the charge due to the added gas cannot be considered to be the major factor in the behaviour of the ignition delay; (3) the reactive environment around the pilot fuel jet is modified by the gaseous fuel. Consequently, both the reaction zone and the thickness of the reaction

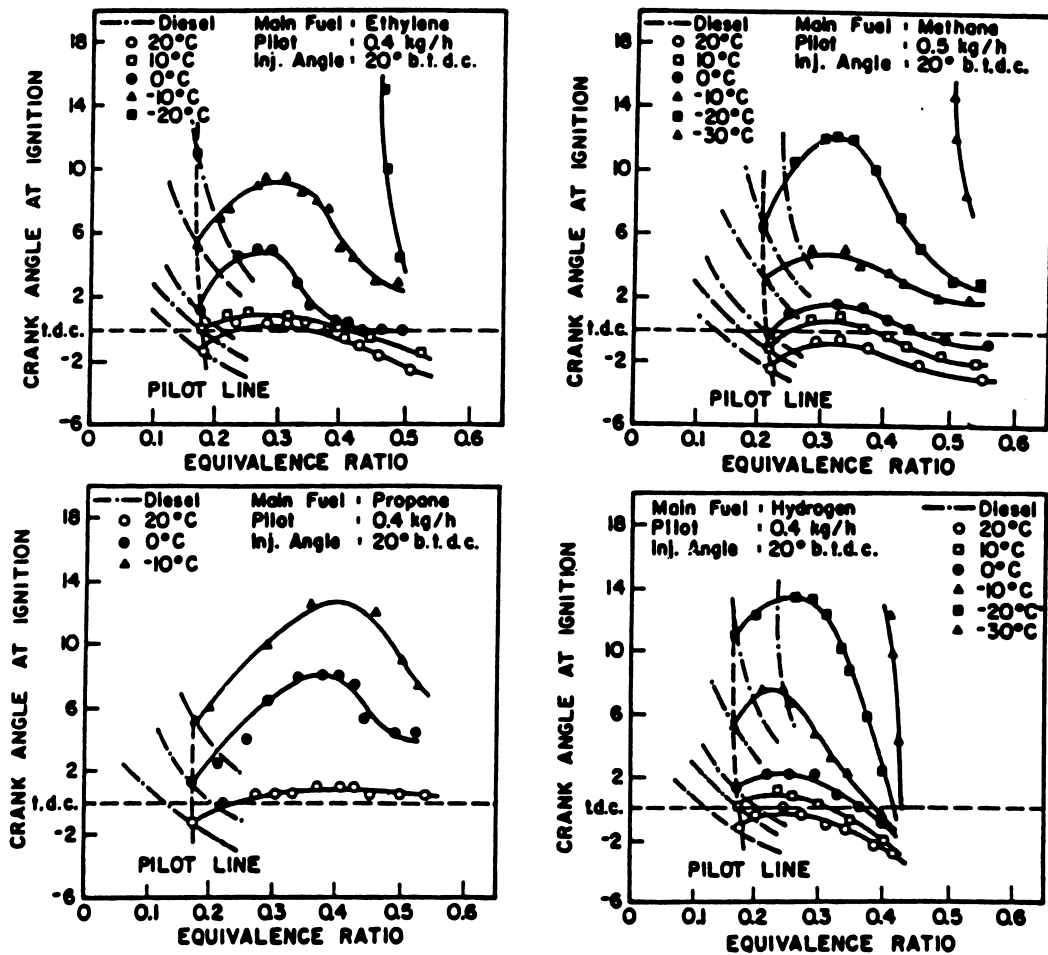


Figure 6.2: Typical variation in the ignition point with the total equivalence ratio of a dual fuel engine fuelled with different fuels at different intake temperatures and constant pilot quantity. Reproduced from reference [154].

zone expand widely so that the energy release rate increases. This feature may explain in part the reduction in the ignition delay observed on further fuel addition; (4) dual fuel ignition delay is sensitive to the charge intake temperature. This implies that chemical effects are a prominent factor in the delay.

6.2.3 Chemical Kinetic Model of Dual Fuel Ignition Delay

Nielsen et al evaluated several reported single fuel kinetic combustion models in order to construct a dual fuel ignition model [13]. The ignition criterion is set to $[H_2O] > 0.002$ mole/liter. Dual fuel ignition models are obtained from combining corresponding single fuel models. Though their combination model is able to predict the increase of ignition delay of the hydrocarbon/hydrogen reaction and the hydrocarbon/hydrogen/carbon monoxide reaction, it failed to predict the tendency in ignition delay to decrease for higher concentrations of gaseous fuel.

6.3 Ignition Conditions Observed from the Current Experiments

A series of diesel and dual fuel combustion experiments have been carried out in which special emphasis has been placed on the ignition conditions, particularly on the minimum temperature necessary and the minimum injection quantity required for the dual fuel combustion to be initiated. Diesel was used as the pilot fuel and natural gas (which is assumed to be methane, CH_4) as the gas substitute. The experimental setup has been described in Chapter 4.

6.3.1 Minimum Temperature for Ignition

The minimum ignition temperature T_{min} was studied as a function of the injection quantity m_{inj} , the initial pressure P_0 , and the gas-air equivalence ratio ϕ_{gas} . T_{min} was determined for each test condition by gradually reducing the initial temperature until the point where further reduction of the cylinder temperature led to ignition failure. Ignition was considered to have failed if no significant pressure rise occurred on the pressure trace and no obvious temperature rise was observed within the cylinder.

For low pilot fuel injection, as in the present experiments, it was observed that the minimum ignition temperature for dual fuel combustion was lower than that of “straight” diesel combustion, as shown on Fig. 6.3. This could be due to various reasons, these being the fact that some combustion with very long ignition delay has a different ignition mechanism to that of “straight” diesel combustion (this will be further discussed in later section), that the presence of the gaseous fuel increased the local fuel-air ratio compared to the fuel-air ratio of the “straight” diesel combustion with the same pilot injection quantity, and that the pre-ignition chemical reaction may change the combustion characteristics of the mixture so that ignition can occur at a lower temperature.

It should be pointed out that data for T_{min} for Fig. 6.3 was obtained from the “optimum” condition of m_{inj} and ϕ_{gas} . The term “optimum” here means that the data obtained were not for a constant m_{inj} and ϕ_{gas} . Rather, they were for the lowest T_{min} for the corresponding P_0 , regardless of the value of m_{inj} and ϕ_{gas} .

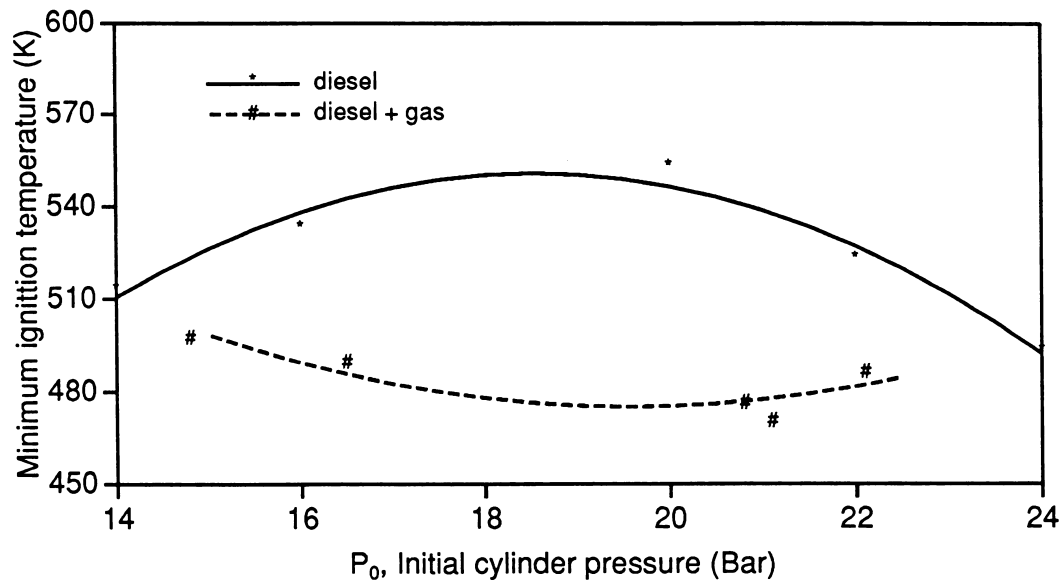


Figure 6.3: Minimum ignition temperature at “optimum” condition of pilot injection and gas-air ratio. For dual fuel combustion, $P_0 = pp_{air} + pp_{gas}$.

For dual fuel combustion at a particular initial pressure ($P_0 = pp_{air} + pp_{gas}$, for example, $P_0 = 20.5$ as shown on Fig. 6.4), the minimum ignition temperature reduces slightly with the gas-air equivalence ratio increase until a point near $\phi_{gas} = 1.0$. Further increase in ϕ_{gas} beyond this point will lead to an increase in the value of T_{min} . This phenomenon is more obvious for larger pilot injection than for the smaller pilot injection. Because the pilot diesel fuel only takes a small portion in the total energy, a similar change of T_{min} can be seen as a function of the total fuel-air equivalence ratio ϕ_{total} , as shown on Fig. 6.5. Also, as shown on Fig. 6.4, a combustion with a larger pilot injection requires a higher ignition temperature. These phenomena are due to the fact that the minimum ignition temperature is affected by the local fuel-air ratio and temperature. When the pilot fuel is delivered to the mixture, a decline in the temperature in the region surrounding the spray occurs because of droplet vaporization. The greater the pilot quantity, the more heat it absorbs for vaporizing with a consequent decline of in the local temperature. If the mixture is at a temperature which is at or near the minimum ignition temperature, when the injection quantity exceeds a certain level, ignition failure occurs because either the temperature declines too severely, or insufficient pilot fuel can be vapourized.

Despite the fact that more pilot fuel injection is usually favoured as a means of obtaining better dual fuel combustion, this result implies that increasing the injection quantity may cause ignition failure if the pilot fuel is delivered to a gas-air mixture which is at or near the minimum ignition temperature.

Also shown on Fig. 6.4, a mixture near stoichiometric has the lowest ignition temperature as T_{min} increases slightly for a rich fuel mixture when ϕ_{gas} increases.

6.3.2 Effects of P_0 and ϕ_{gas} on ignition

Effects of the initial pressure P_0 and the gas-air equivalence ratio ϕ_{gas} on the ignition and ignition delay are as shown on Fig. 6.6 and Fig. 6.7. Data for

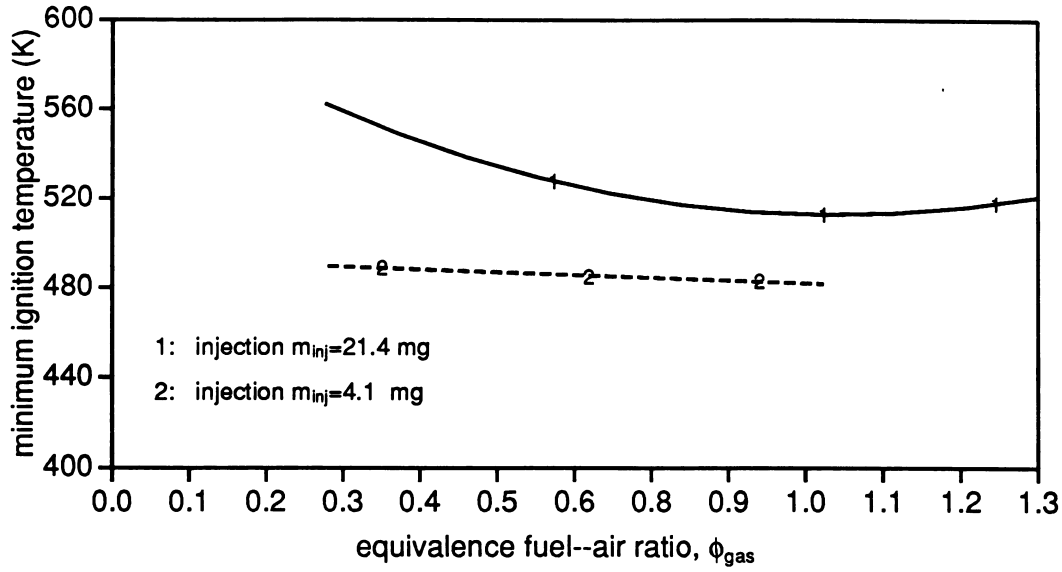


Figure 6.4: Minimum ignition temperature of dual fuel combustion as a function of gas-air equivalence ratio at initial pressure ($pp_{air} + pp_{gas}$) $P_0 = 20.5$ bar.

these diagrams are taken from experiments with $m_{inj} = 21.4$ (the maximum injection quantity for the current experiments) and $m_{inj} = 4.1$ (the minimum) respectively because more tests have been carried out under these injection conditions than under other values. Regions have been outlined with different ranges of ignition delay and occurrence of ignition failure. In both diagrams, ignition delay can be extremely long (for example, 200 ms) in the region between ignition failure and the next ignition delay range. Because the current research concentrates on the maximum use of gaseous fuel, experiments were carried out at $\phi_{gas} > 0.3$.

It can be seen that for fixed conditions of T_0 , m_{inj} , and P_0 , the ignition delay τ_{ig} can reach a local minimum at a certain value of ϕ_{gas} . Increasing or reducing ϕ_{gas} from this point results in a prolongation of the ignition delay. This phenomenon is consistent with previous observations by Karim et al [154] on a dual fuel engine. Similar trends can also be seen from the T_0 - ϕ_{gas} diagram (Fig. 6.9).

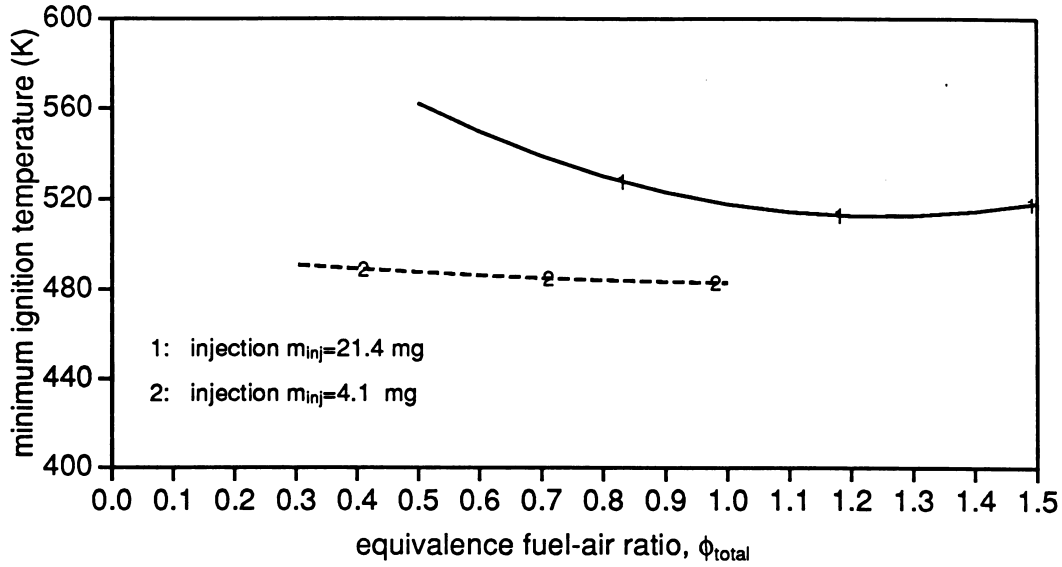


Figure 6.5: Minimum ignition temperature of dual fuel combustion as a function of total fuel-air equivalence ratio at initial pressure ($pp_{air} + pp_{gas}$) $P_0 = 20.5$ bar.

Two constant ϕ_{gas} lines ($\phi_{gas} = 0.7$ and $\phi_{gas} = 0.8$) have been drawn on Fig. 6.6. They show that the ignition delay is approximately a geometric function of P_0 when ϕ_{gas} remains constant, if T_0 and m_{inj} are also approximately constant. Therefore, when T_0 , ϕ_{gas} and m_{inj} remain unchanged, it is reasonable to evaluate the ignition delay τ_{ig} as a geometric function of P_0 . However, the power index in the geometric functional equation varies with ϕ_{gas} . That is

$$\tau_{ig} \approx A \cdot P^{f(\phi_{gas})}$$

if the initial temperature T_0 , the pilot injection quantity m_{inj} and the gas-air equivalence ratio ϕ_{gas} are all constants respectively.

Fig. 6.6 and Fig. 6.7 also show that ignition in the very low ϕ_{gas} region is very sensitive to initial conditions. Slight changes of the initial conditions (value of T_0 , P_0 or m_{inj}) cause the ignition delay to change substantially and may cause ignition failure. This phenomenon also can be seen in the T_0 - ϕ_{gas} diagram Fig. 6.9.

As data for Fig. 6.6 and Fig. 6.7 were taken from experiments with the same pilot injection quantity respectively ($m_{inj}=21.4$ mg at Fig. 6.6 and $m_{inj}=4.1$ mg at Fig. 6.7), diagrams plotted against the total fuel-air equivalence ratio ϕ_{total} instead of ϕ_{gas} will also show similar trends for dual fuel ignition.

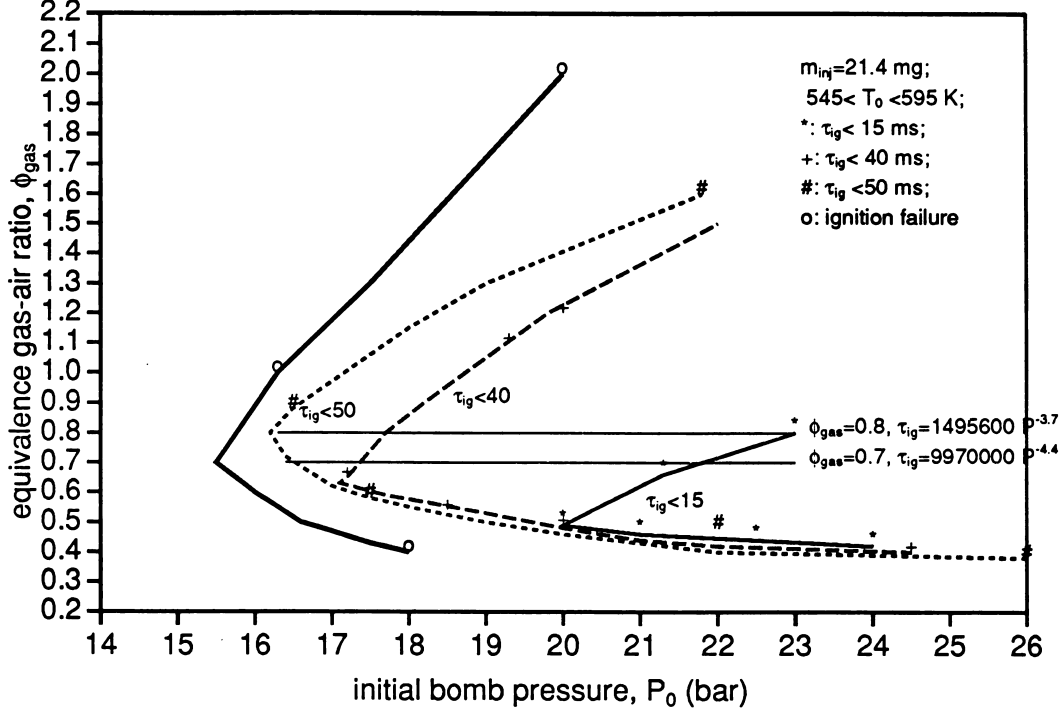


Figure 6.6: Effects of pressure P_0 and gas-air equivalence ratio ϕ_{gas} on dual fuel ignition.

6.3.3 Effects of P_0 and m_{inj} on ignition

Effects of the initial pressure P_0 and the pilot fuel injection quantity m_{inj} on ignition delay and ignition failure are shown on Fig. 6.8. Data for the diagram are taken from experiments with $0.8 \leq \phi_{gas} \leq 1.0$ and $545 \leq T_0(K)$. Regions of different ignition delay and ignition failure are approximately outlined. In the region between ignition failure and $\tau_{ig}(ms) \leq 50$, the ignition delay can be extremely long (for example, 200 ms). Three constant m_{inj} lines ($m_{inj}=14.5$, 18, 20 respectively) are drawn which again show that ignition delay is an

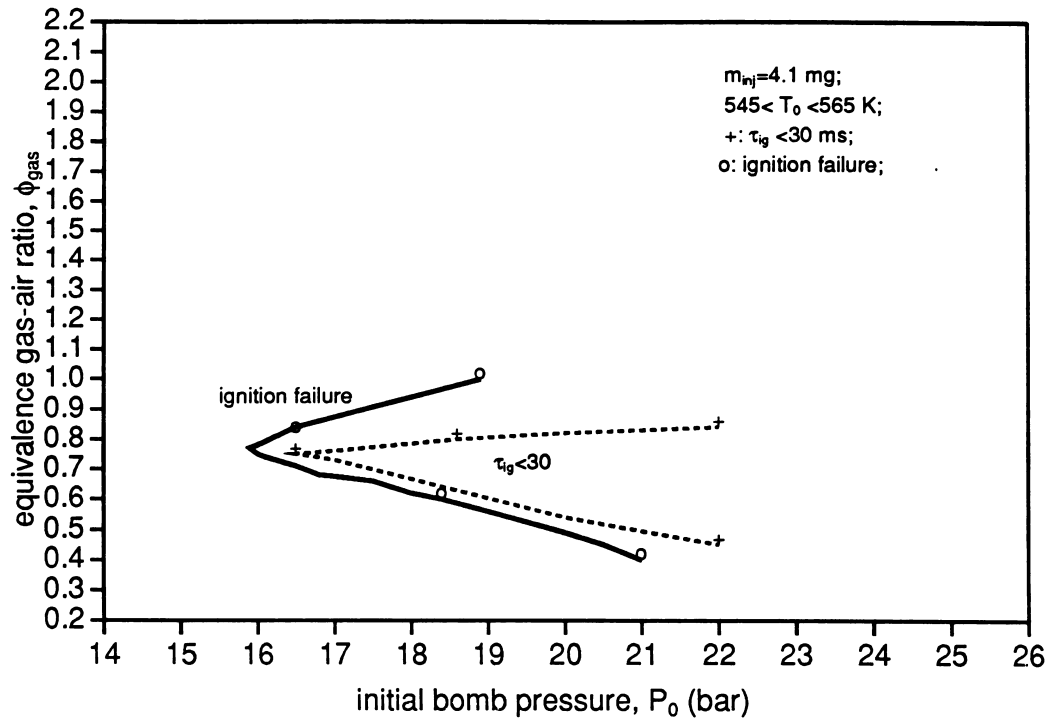


Figure 6.7: Effects of pressure P_0 and gas-air equivalence ratio ϕ_{gas} on dual fuel ignition.

approximate geometric function of P_0 when m_{inj} remains constant, if T_0 and ϕ_{gas} are also approximately unchanged. Therefore, when T_0 , ϕ_{gas} and m_{inj} remain unchanged, it is reasonable to evaluate the ignition delay τ_{ig} as a geometric function of P_0 . It shall be noted that the power index in the geometric function equation is almost unchanged for various m_{inj} values. It indicates that the power index in the equation can be assumed to be independent of the injection quantity m_{inj} .

Fig. 6.8 also shows that, when the pilot fuel quantity is small, the dual fuel ignition delay can be very long at low initial pressure although ignition may still occur. Therefore, the minimum pilot injection required for dual fuel engine application is controlled by the ignition delay rather than by ignition failure.

6.3.4 Effects of T_0 and ϕ_{gas} on ignition

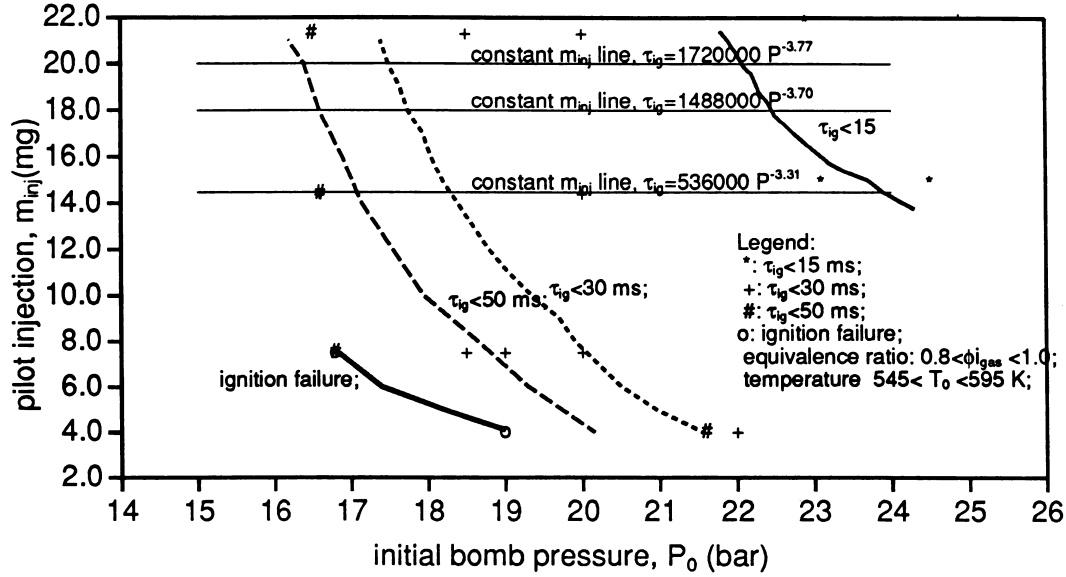


Figure 6.8: Effects of pressure P_0 and pilot quantity m_{inj} on ignition.

Fig. 6.9 approximately outlines various ignition regions on a $\phi_{gas}-T_0$ diagram. Data for the diagram were taken from experiments with pilot injection $m_{inj} = 21.4$ mg and initial pressure P_{0i} 20 bar.

Similarly to Fig. 6.6, ignition delay at fixed conditions of T_0 , P_0 and m_{inj} can reach a local minimum at a certain value of ϕ_{gas} from where increasing or reducing ϕ_{gas} causes τ_{ig} to prolong. A short ignition delay also appears at the region of very low ϕ_{gas} and high initial temperature T_0 . Fig. 6.9 also shows that dual fuel ignition becomes very unsteady in the region where ignition delay exceeds about 30 ms. In this region, ignition delay and ignition failure seem to become random or at least extremely sensitive to the initial conditions. As will be seen in a later section, dynamic pressure traces of the combustion with long ignition delay are also essentially different from those of combustion with short ignition delay. This indicates that the ignition mechanism of a dual fuel combustion with very long ignition delay (approximately over 30 ms) is different from that of a combustion with a short ignition delay. For

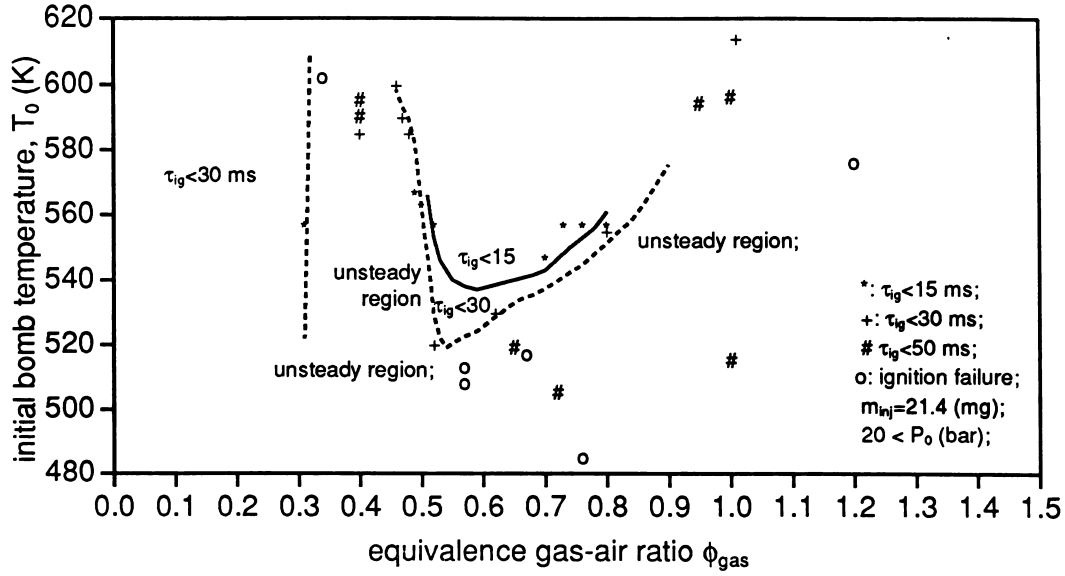


Figure 6.9: Effects of temperature T_0 and equivalence gas-air ratio ϕ_{gas} on ignition

combustion after a short ignition delay, ignition nuclei start at the pilot fuel jet region and then propagate to the gas-air mixture. The initial ignition process is similar to that in a conventional diesel engine. In the case of very long ignition delay as observed from the current combustion bomb experiments, the pilot fuel has sufficient time to vaporise and fully mix with the gas-air mixture. Therefore, ignition starts in the pre-mixed mixture making the initial ignition process for this case similar to that of spontaneous ignition of gas. This could be the reason for the fact that ignition in a dual fuel bomb can occur at some low temperature-pressure conditions at which ignition fails for sole diesel combustion, as described previously in section 6.3.1.

6.3.5 Minimum pilot fuel quantity

The minimum pilot fuel injection quantity m_{inj} for dual fuel combustion has been studied in the current experiments. Emphasis has been placed on the relationship of m_{inj} to the gas conditions P_0 , T_0 and ϕ_{gas} . The experimental results were obtained by changing the fuel injection quantity gradually while other working parameters such as P_0 , T_0 and ϕ_{gas} remained unchanged. As shown on Fig. 6.6, the minimum pilot quantity required for dual fuel combustion varies with the initial condition of ϕ_{gas} , P_0 and T_0 . Also, for some ranges of ϕ_{gas} , T_0 and P_0 , low pilot quantity prolongs the ignition delay substantially to such an extent that no ignition is possible in actual engine operation. Therefore, the minimum pilot injection is controlled by the ignition delay rather than by the occurrence of ignition.

It was also observed that, at low initial charge temperatures such as those near the minimum ignition temperature, a large pilot injection exceeding certain limits can also cause ignition failure. This is due to the fact that a larger pilot quantity requires a higher temperature for ignition, as described previously in Section 6.3.1.

6.4 Dual Fuel Ignition Delay

Ignition delay in a dual-fuelled diesel engine had been studied by many researchers. However, no correlation formula has been found in the literature. It is believed that the ignition delay in a dual fuel combustion is a complex combined result of the effect of many factors. The relation of ignition delay τ_{ig} with cylinder pressure P_0 , temperature T_0 , gas-air equivalence ratio ϕ_{gas} and pilot fuel quantity m_{inj} has been discussed primarily in last section. In attempts to obtain a calculation formula for the dual fuel ignition delay, regression of the current experimental results has been performed with many various functional forms of T_0 , P_0 , ϕ_{gas} and m_{inj} . However, no satisfactory result has been obtained which can be applied to the entire range of experimental conditions. This may

be because the fact that long and short ignition delay are actually caused by different ignition mechanisms, as discussed previously. Nevertheless, very long ignition delay is virtually equivalent to ignition failure in application. For the purpose of engine simulation, calculation is essentially needed for cases with short ignition delay. It was found that experimental results of dual fuel ignition delay under 30 ms can be fitted to the equation

$$\tau_{ig} = 19.3 P_0^{f(\phi_{gas})} g(\phi_{gas}, m_{inj}) \exp\left(\frac{500}{T_0}\right) \quad (6.1)$$

Here

$$f(\phi_{gas}) = -1.0174 + 0.7119\phi_{gas} \quad (6.2a)$$

$$g(\phi_{gas}, m_{inj}) = g_1(m_{inj}) + g_2(m_{inj})\phi_{gas} + g_3(m_{inj})\phi_{gas}^2 + g_4(m_{inj})\phi_{gas}^3 \quad (6.2b)$$

$$g_1(m_{inj}) = (3.70 + 0.28855m_{inj}) \quad (6.2c)$$

$$g_2(m_{inj}) = (-5.8236 - 0.9640m_{inj}) \quad (6.2d)$$

$$g_3(m_{inj}) = (7.869 + 0.8761m_{inj}) \quad (6.2e)$$

$$g_4(m_{inj}) = (-4.2668 - 0.22235m_{inj}) \quad (6.2f)$$

Here P_0 is the initial cylinder pressure (16.5 – 24.3 bar), m_{inj} is the total pilot fuel quantity (4.1 – 21.4 milligram), ϕ_{gas} is the equivalence ratio of the gaseous fuel/air (0.3 – 1.1), T_0 is the initial temperature (450 – 600 K) of the mixture in the cylinder and τ_{ig} is the ignition delay ($\tau_{ig} \leq 30ms$) Fig. 6.10 to Fig. 6.13 are a comparison of the correlation and experiments. It can be seen that the correlation gives not only correct trends but also quite accurate quantitative estimations of the ignition delay in dual fuel combustion. Fig. 6.14 to Fig. 6.17 are further demonstration of the functional relations implied by Eq. 6.1.

It is noted that the ignition delay correlation indicates that the affect of the gas/air equivalence ratio (therefore also the total fuel/air equivalence ratio as the pilot fuel only contributes a small proportion of the total fuel) no the ignition delay occurs in two different ways. At very low pilot fuel injection level, ignition delay τ_{ig} continuously increases with increasing ϕ_{gas} . However, when the pilot injection quantity exceeds a certain amount, there is a range within

which τ_{ig} decreases with increasing ϕ_{gas} . This could be the explanation of the fact, as has been reviewed in Chapter 1, that some different observations exist in previous reports about this phenomenon. Further experiment is needed to clarify this question.

It is also noted that while increase of the pilot quantity can usually reduce the ignition delay period, it can also prolong the ignition delay when the pre-mixed mixture is at very low fuel/air equivalence ratio. This is because of the fact that at low gas/air ratios, pilot fuel constitutes a significant proportion of the total fuel so that larger pilot injection increases the total fuel/air ratio significantly resulting in the increase in the ignition delay.

It should be pointed out that the regression result obtained here is limited by the available computing capacity. A better solution can be obtained by increasing the regression parameters. For example, regression results can be improved by introducing an equivalence fuel/air ratio function ϕ_{total} and then modifying the temperature term $\exp(\frac{2200}{T_0})$ so that it becomes $\exp(\frac{f(\phi_{total})}{T_0})$. However, the increase of the regression parameter substantially aggravates the overflow problem in performing non-linear multi-dimensional regression. For the time being, regression has been performed with a limiting maximum of 12 parameters. Improvement can be achieved when better computing facilities and algorithms are available.

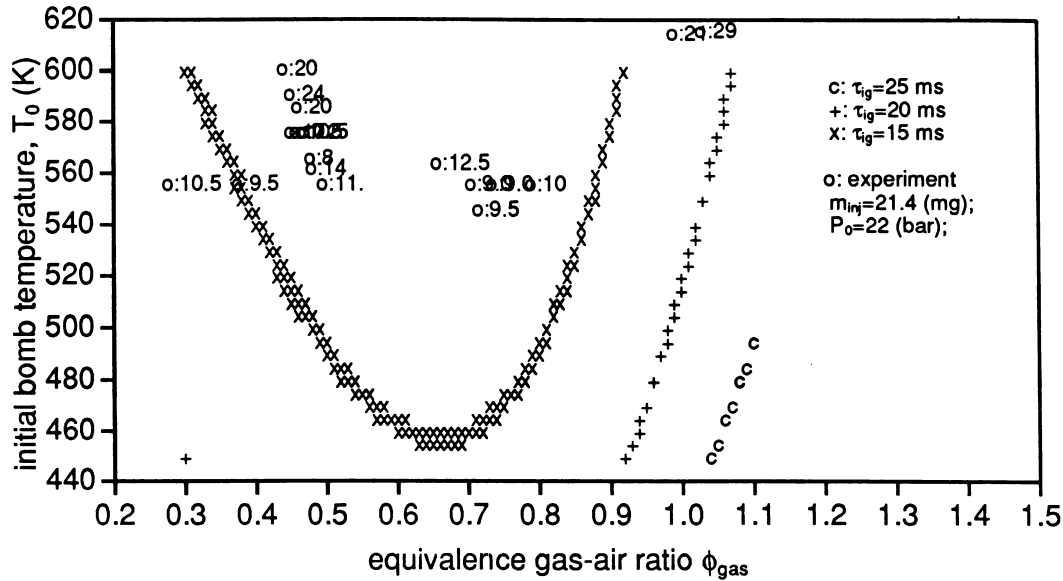


Figure 6.10: Affects of $T_0 - \phi_{gas}$ on dual fuel ignition delay

6.5 General Dual Fuel Combustion Features

Experiment shows that the ignition delay and heat transfer have a strong affect on dual fuel combustion features. Dual fuel combustion which follows a long ignition delay is distinct from that which follows a short ignition delay period. A long ignition delay is usually followed by a very rapid burning, represented by a very sharp pressure rise immediately following the ignition delay period. Combustion pressure can then reach a very high level as the heat release rate is much faster than the heat loss rate.

There are several reasons which causes rapid combustion following a long ignition delay. These are:

- (1) During a long ignition delay period, a large portion or even all of the pilot fuel may have vaporised and will be well mixed with the air. Pre-mixed burning of the pilot fuel then occurs which is very fast.

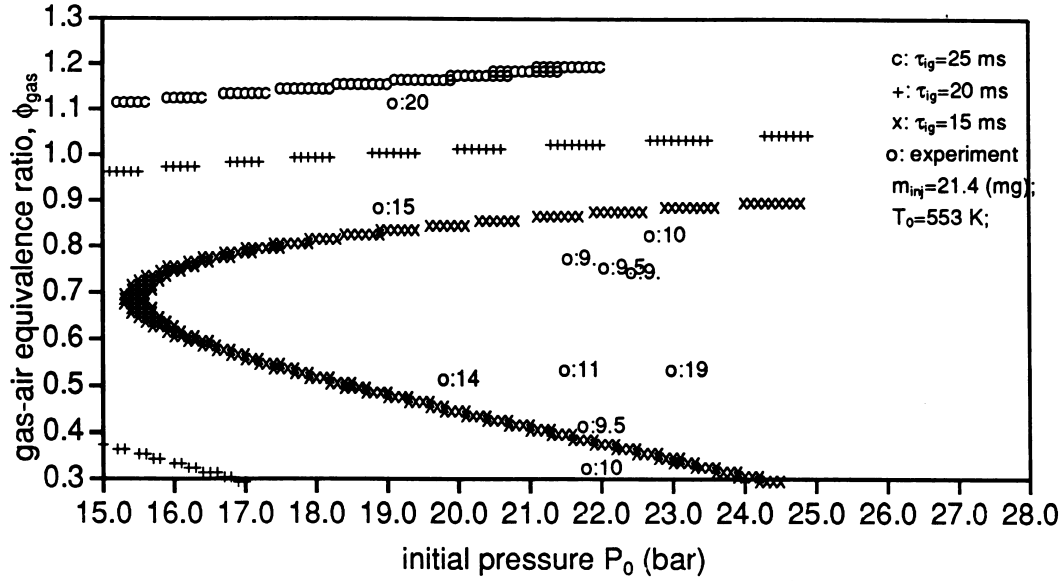


Figure 6.11: Affects of $P_0 - \phi_{gas}$ on dual fuel ignition delay

- (2) During a long ignition delay, a large portion or all of the gas-air mixture will have been entrained into the pilot spray region. Multiple ignition points are likely to occur simultaneously in the spray region igniting the gas over a wide volume. Hence, the gas-air mixture will be consumed quickly.
- (3) The long dual fuel ignition delay is usually caused by a high gas ratio. The laminar flame speed is higher for high equivalence ratio mixtures and the flame front once ignited moves quickly.

In contrast, following a short ignition delay, less pilot fuel is vaporised and mixed with the gas-air mixture, a lower portion of the gas-air mixture is entrained into the spray region and the flame speed is lower. These all reduce the burning rate. As the burning rate is low, heat loss rate is comparatively high. The maximum combustion pressure is therefore lower. Also, as the gas ratio affects the dual fuel ignition delay substantially, a shorter ignition delay usually means that less gaseous fuel has been used and the combustion pressure

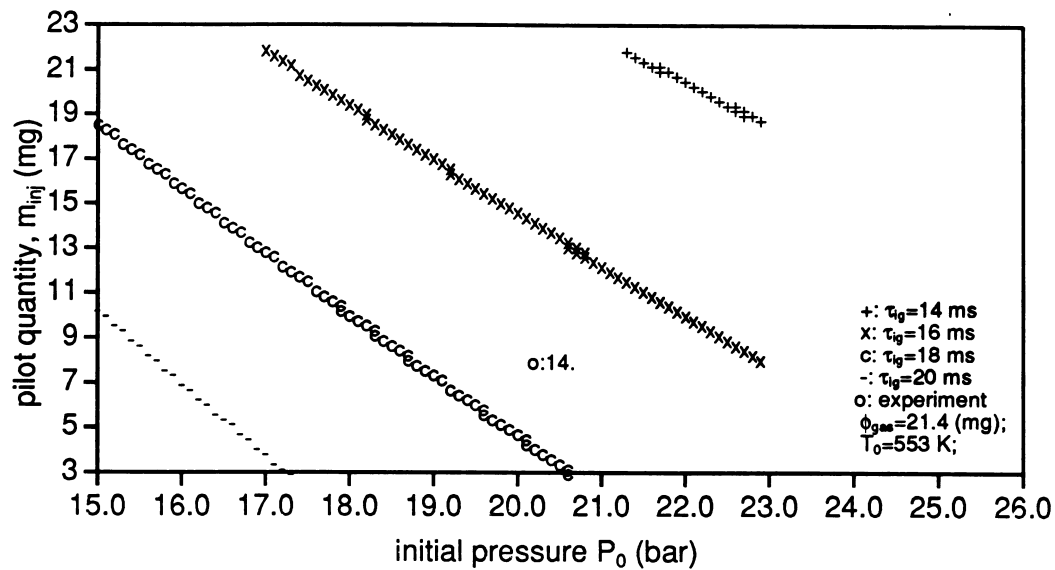


Figure 6.12: Affects of $P_0 - m_{inj}$ on dual fuel ignition delay

is therefore lower.

Figures 6.18, 6.19, and 6.20 are some typical pressure traces of dual fuel combustion with a short ignition delay and Figures 6.21, and 6.22 are those for a long ignition delay. It can be seen that the pressure trace in the burning with long dual fuel ignition delay combustion is rather simple. It appears to be similar to that of the combustion of a homogeneous mixture. This is because the injected pilot fuel has had sufficient time to vaporize and mix to some extent with the gas-air mixture. The long ignition delay period could in fact give sufficient time for the formation of a homogeneous vapour-gas-air mixture. On the other hand, the pressure trace of the combustion with a short dual fuel ignition delay tends to be complex. This reflects the complex nature of the combustion. Here, because part of the injected fuel may still have not yet vaporised, there could be fuel liquid or vapour not fully mixed with the gas and air to form a combustible mixture. After the start of the principal ignition, further ignition could still occur in regions beyond the principal flame

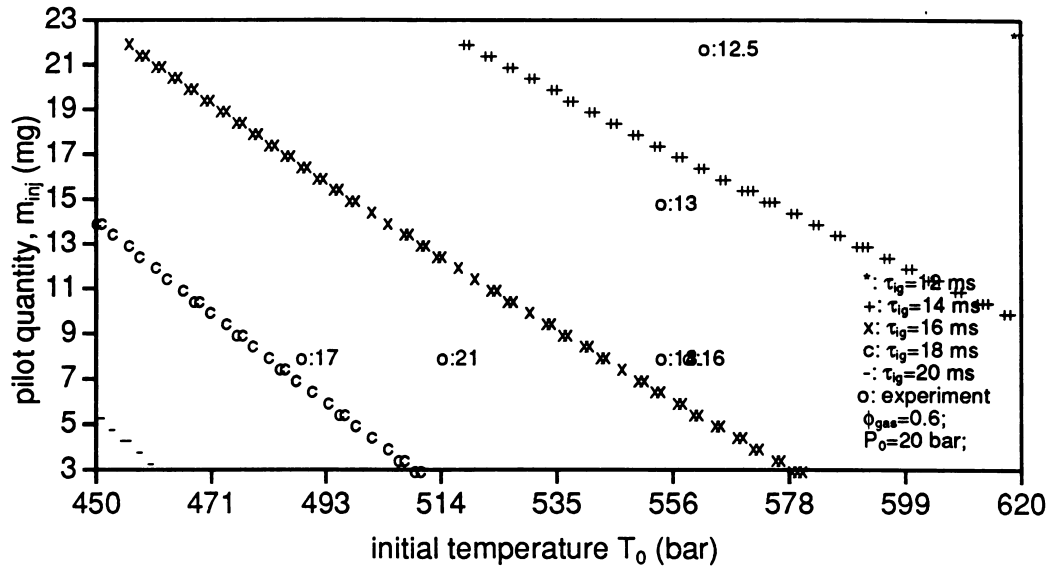
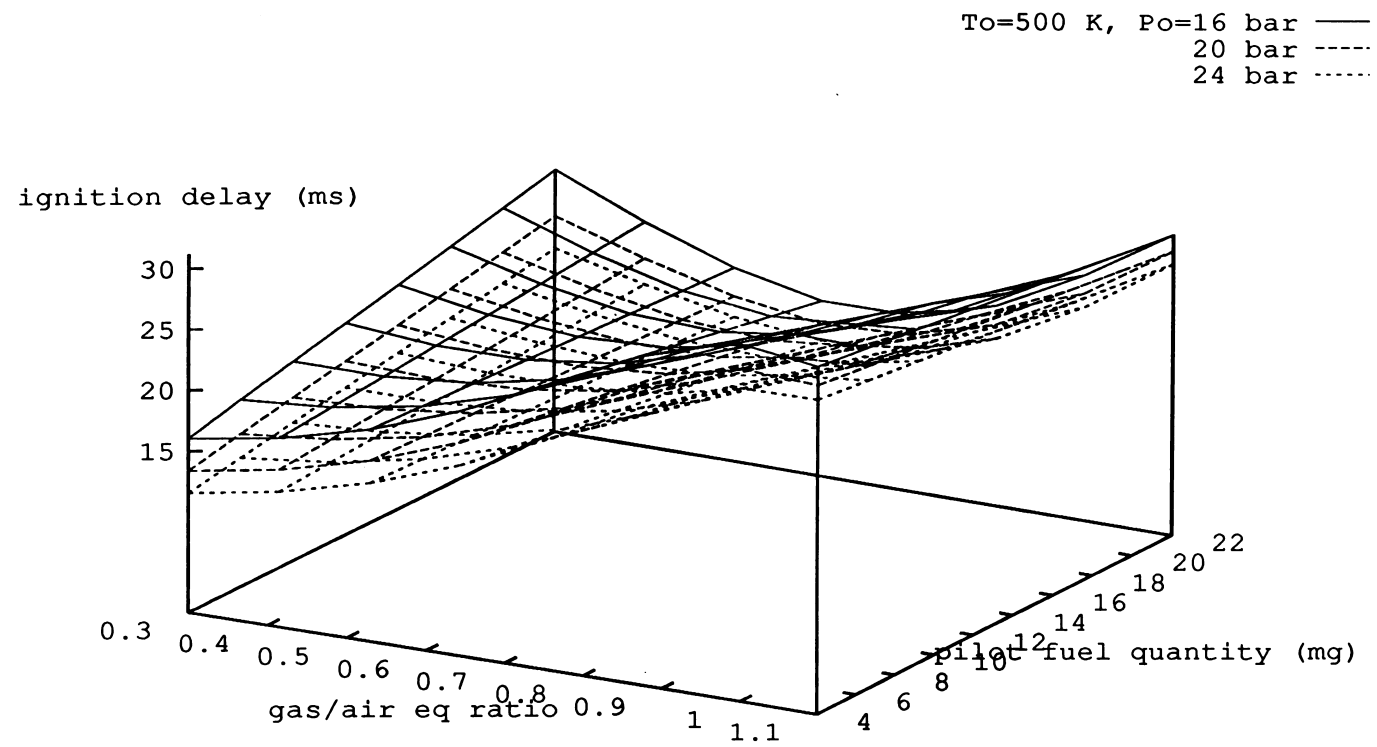


Figure 6.13: Affects of $T_0 - m_{inj}$ no dual fuel ignition delay

but within the spray. This is because the non-uniform distribution of vapour could generate ignition sites at different times in different spray regions. All these factors contribute to the complex nature of the dual fuel combustion process following a short ignition delay period.

In the next chapter, a phenomenological model is established based on these experimental observations.

Figure 6.14: Dual fuel ignition delay as a function of the initial conditions



T=600 K, gas/air eq ratio: 1.0 —
0.7 ----
0.4 -.-.-

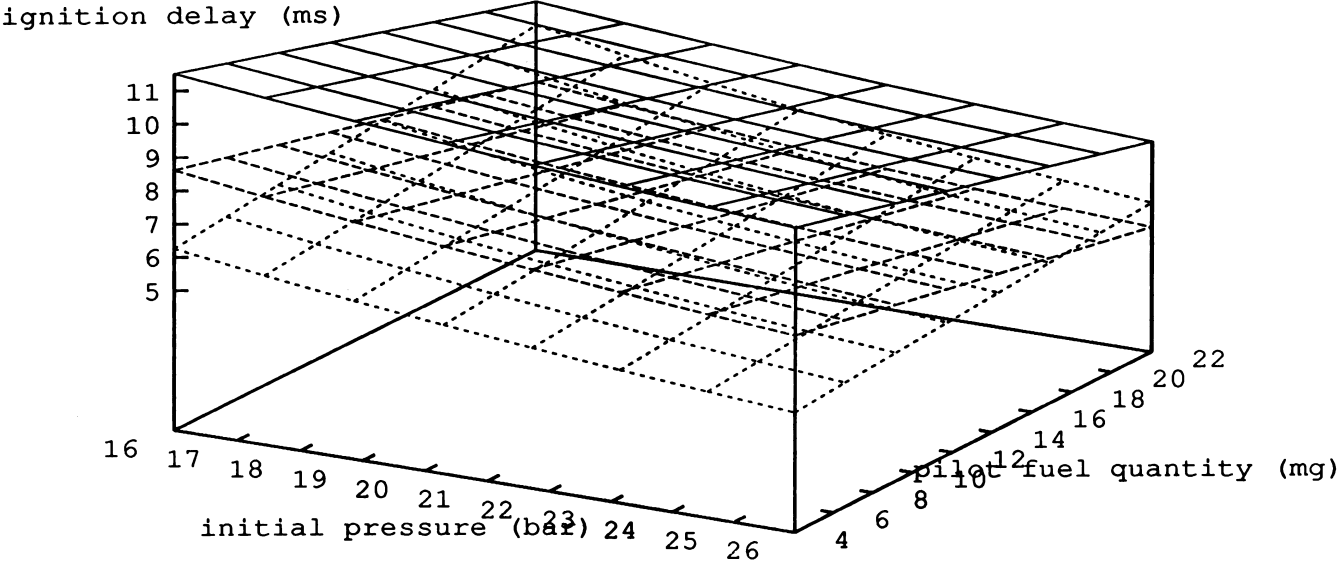
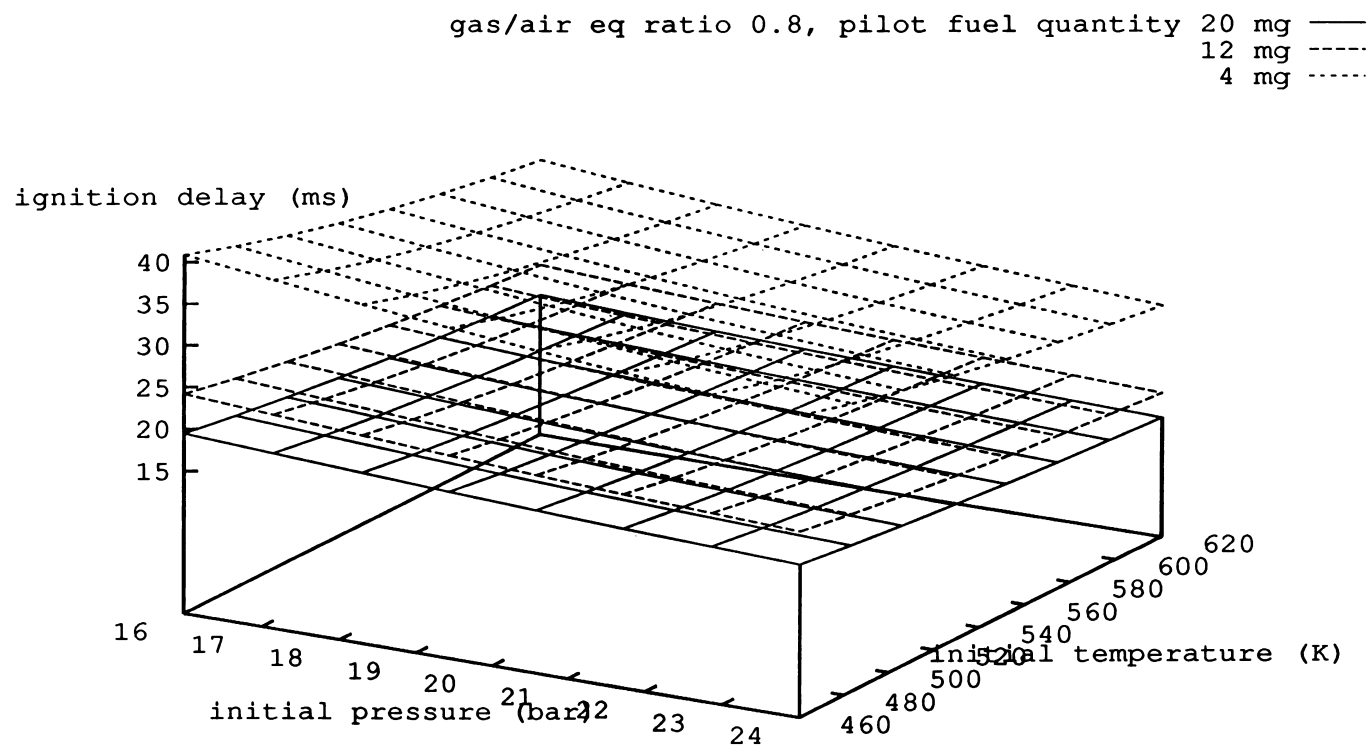


Figure 6.15: Dual fuel ignition delay as a function of the initial conditions

Figure 6.16: Dual fuel ignition delay as a function of the initial conditions



Po=20 bar, gas/air eq ratio: 1.0 —
0.7 ----
0.4 -.-.-

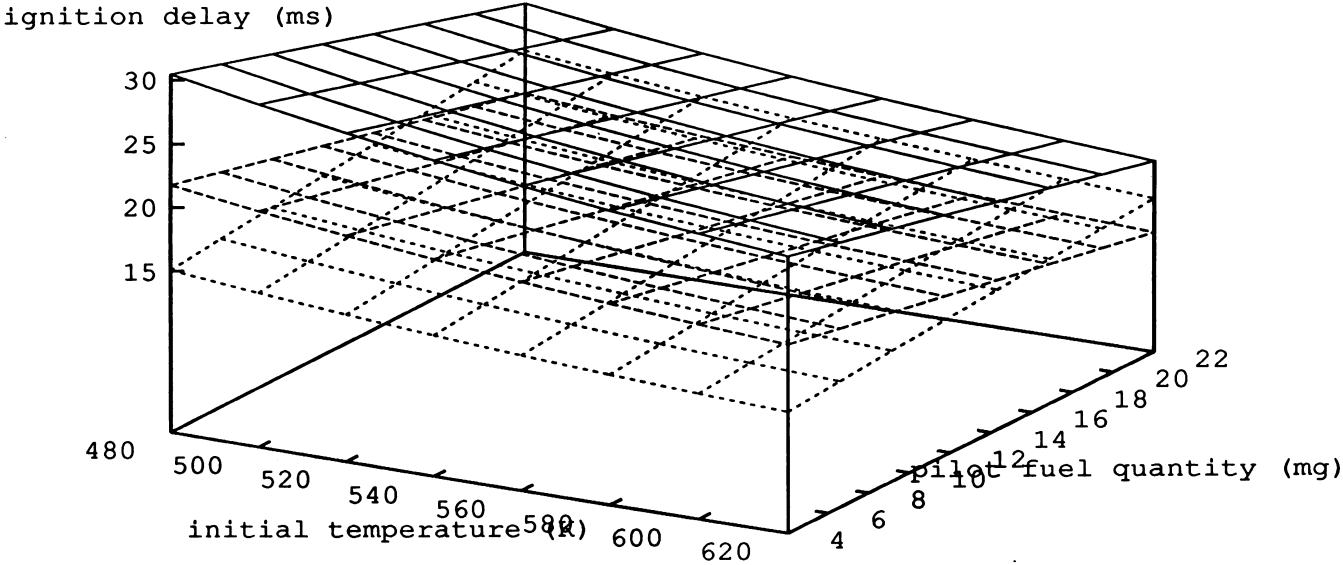


Figure 6.17: Dual fuel ignition delay as a function of the initial conditions

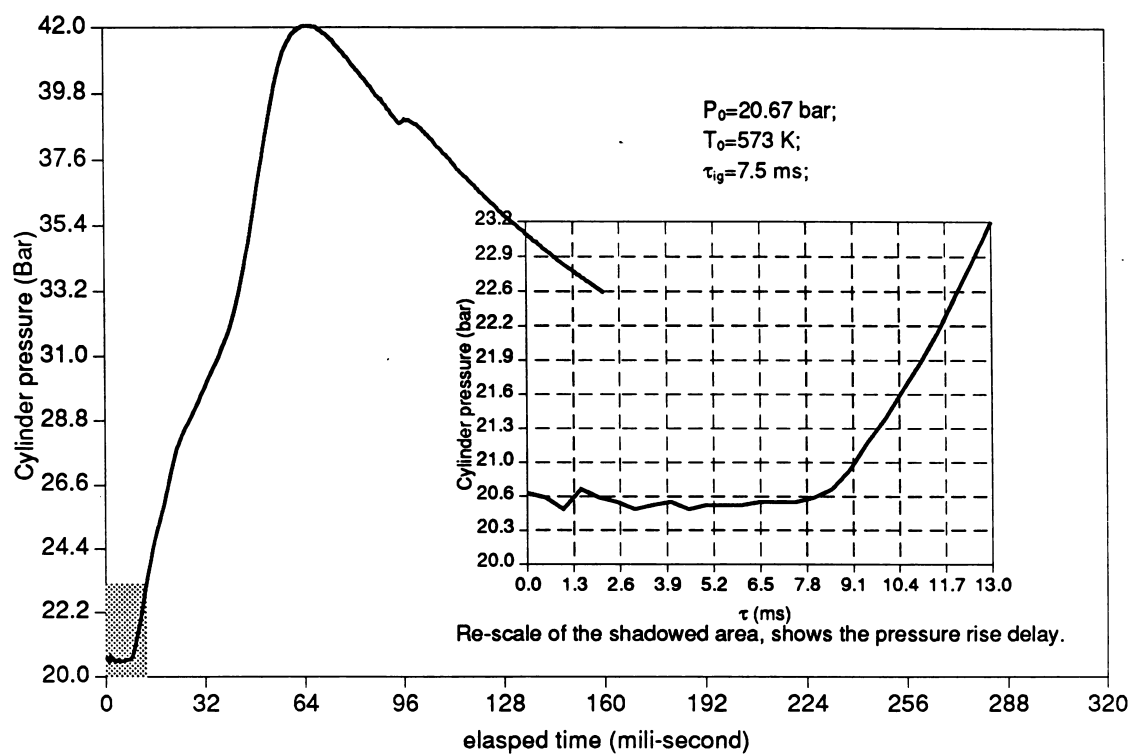


Figure 6.18: Typical pressure trace of dual fuel combustion with short ignition delay.

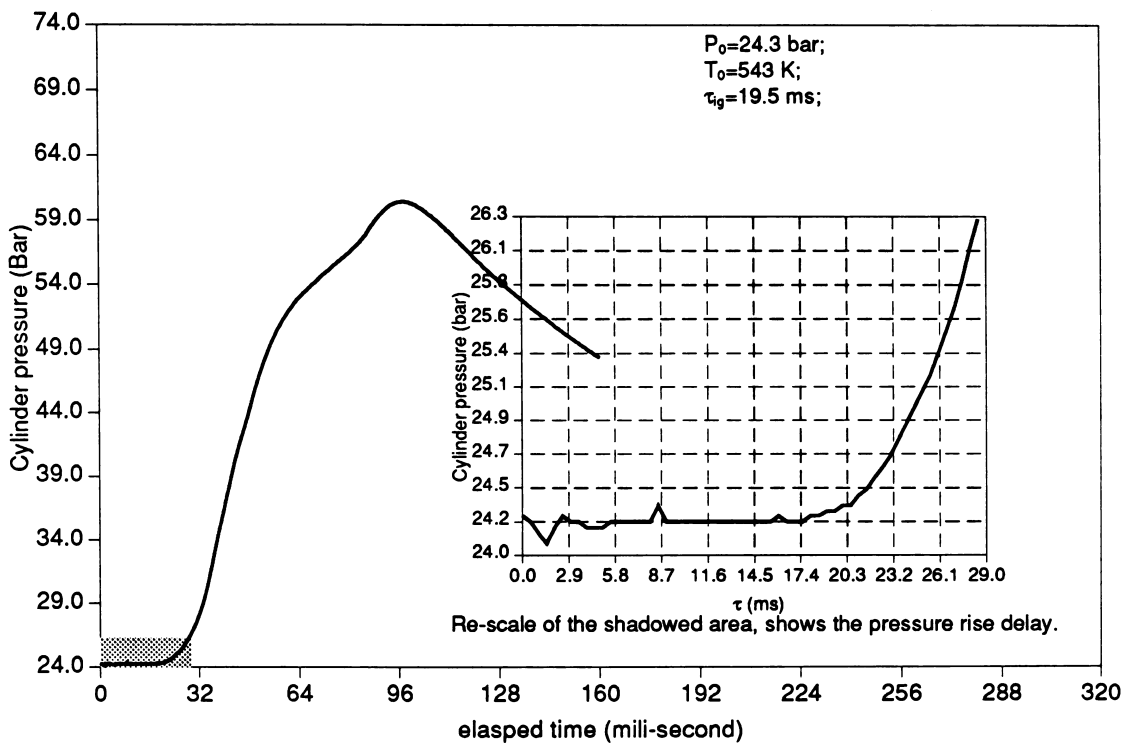
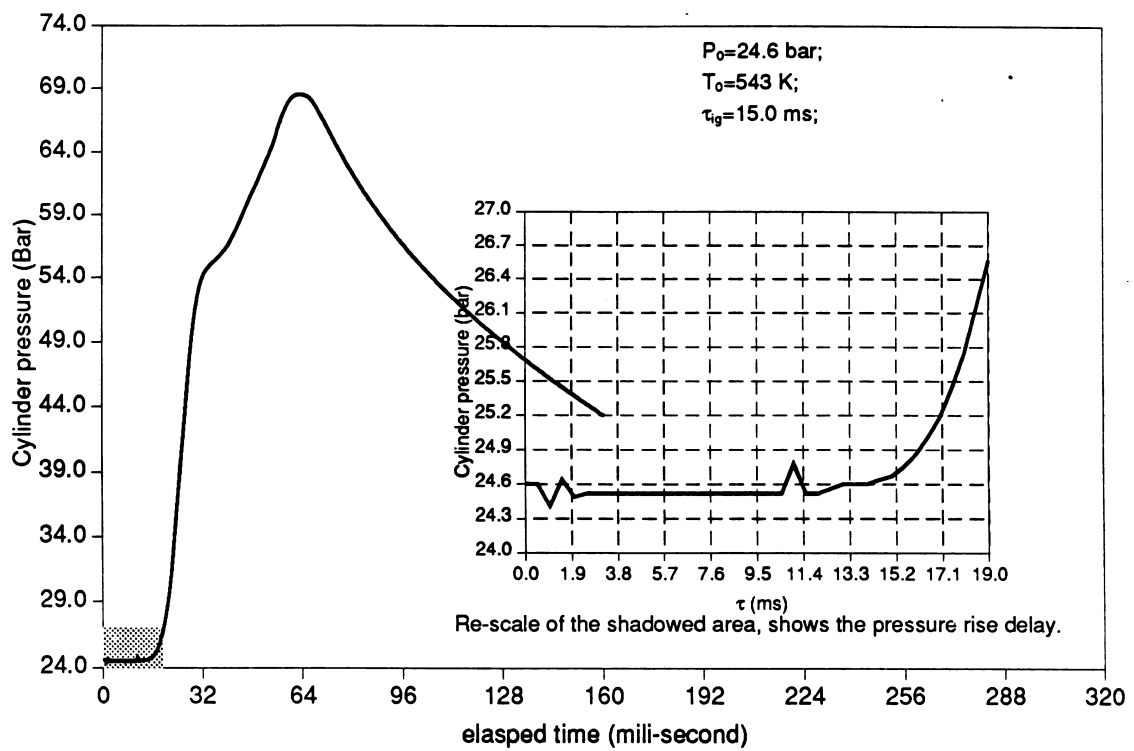


Figure 6.19: Typical pressure trace of dual fuel combustion with short ignition delay.

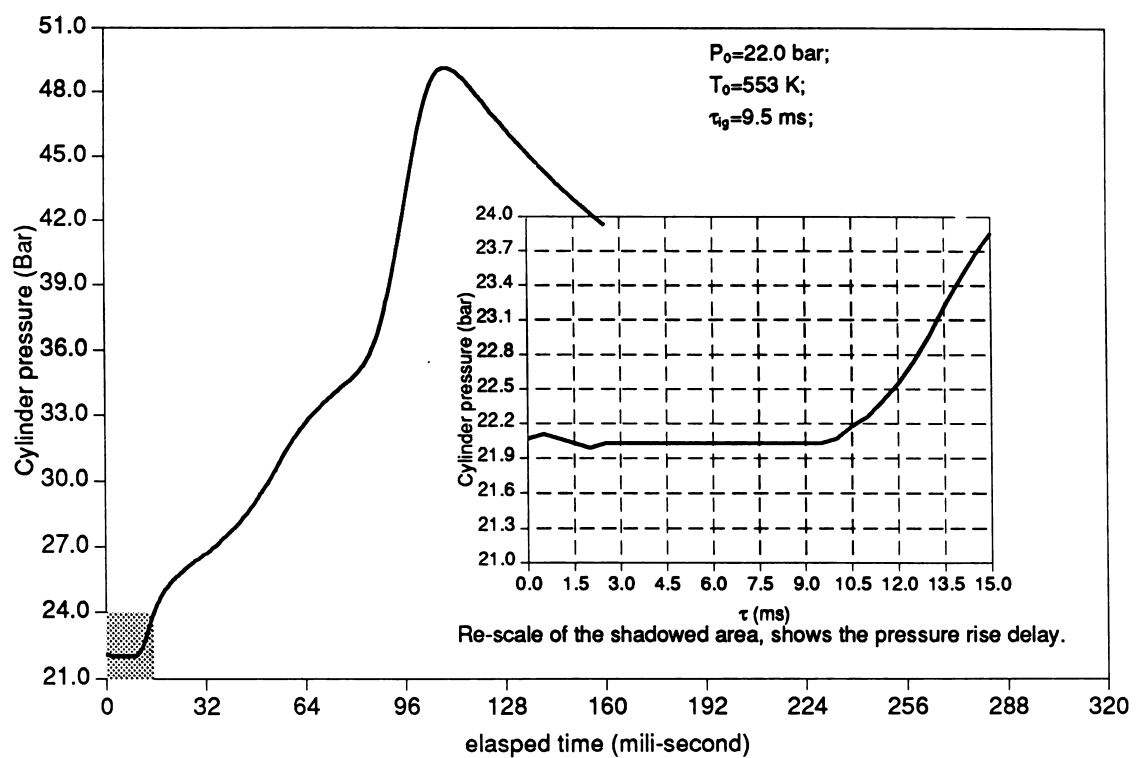


Figure 6.20: Typical pressure trace of dual fuel combustion with short ignition delay.

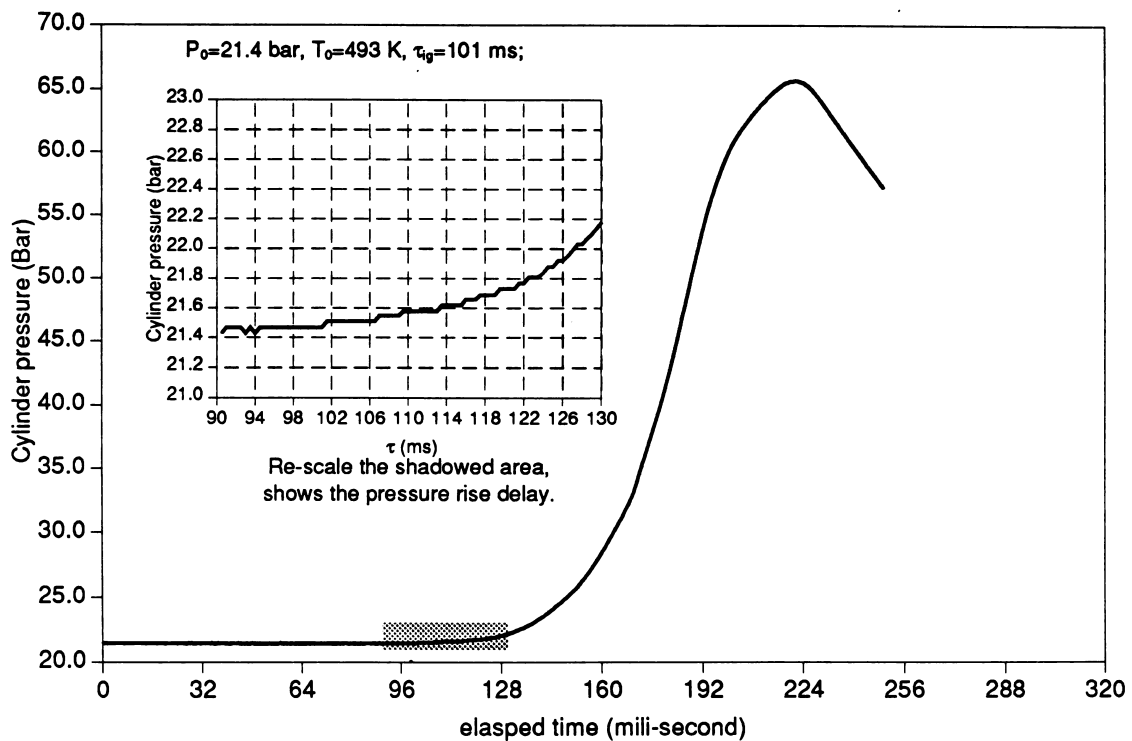
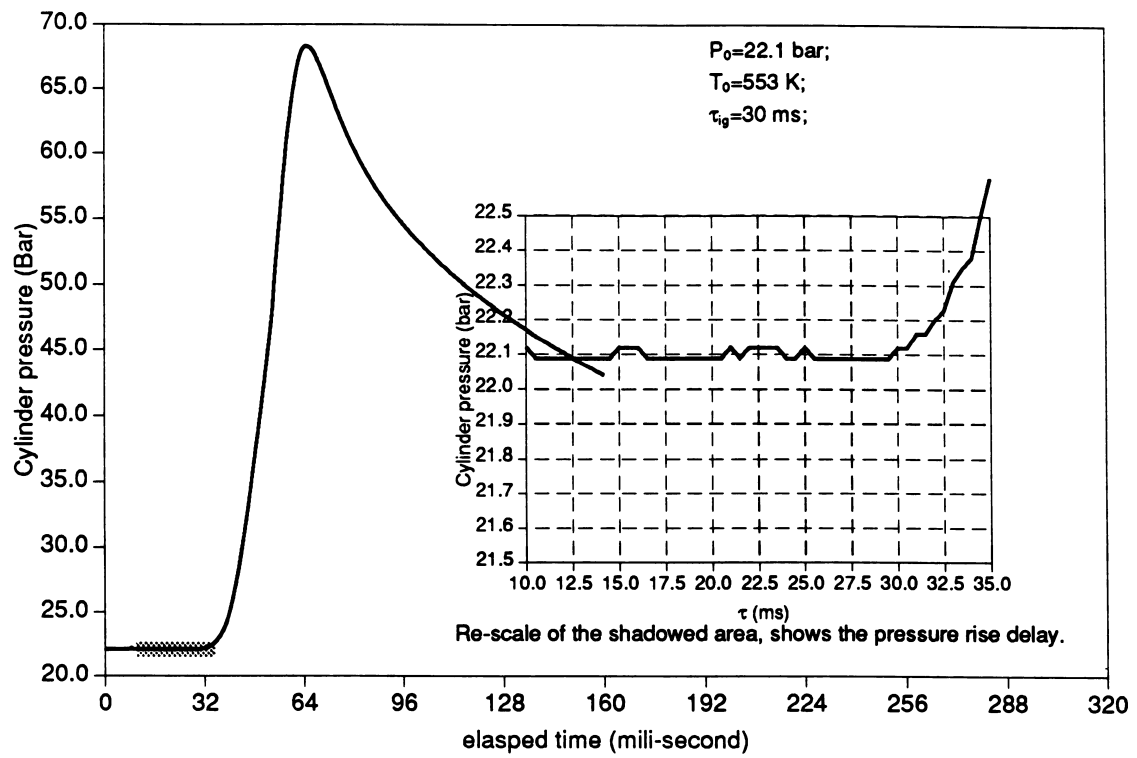


Figure 6.21: Typical pressure trace of dual fuel combustion with long ignition delay.

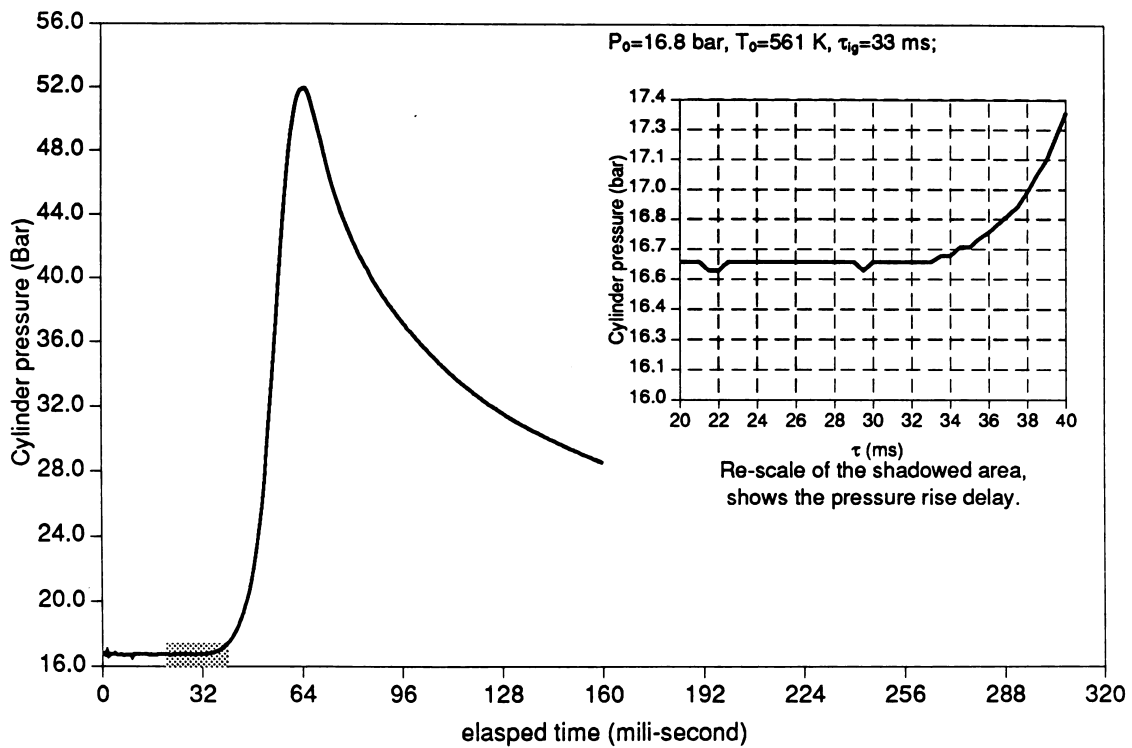
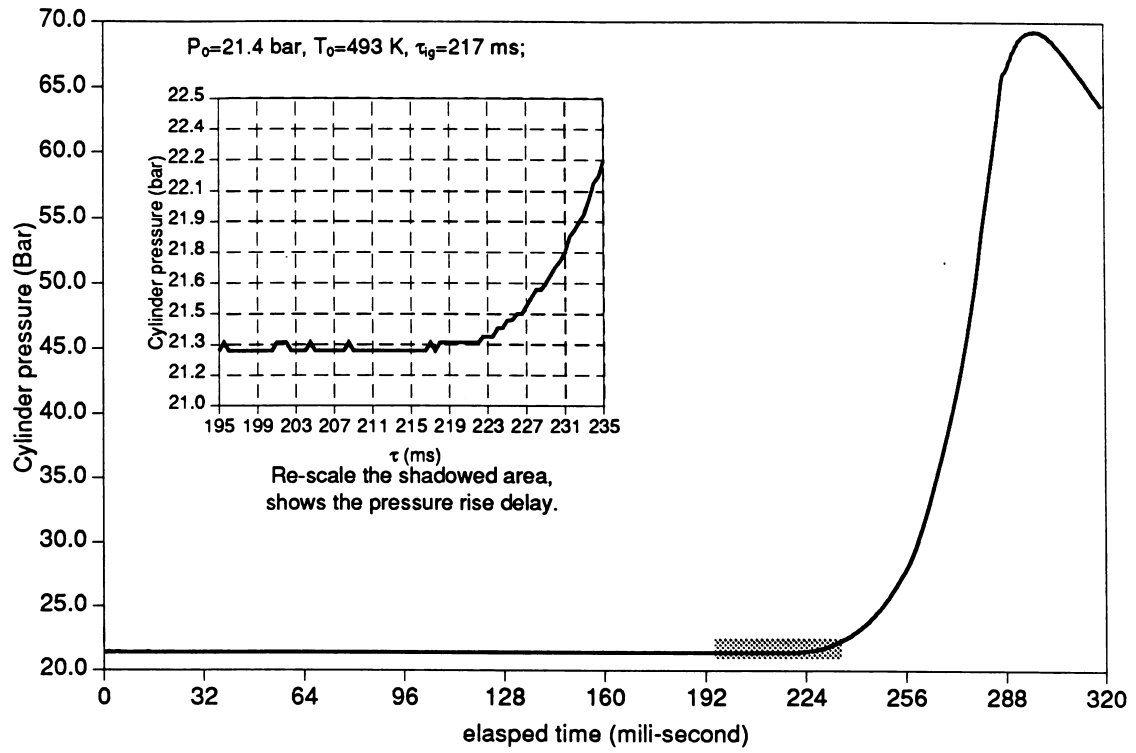


Figure 6.22: Typical pressure trace of dual fuel combustion with long ignition delay.

Chapter 7

Phenomenological Modelling of Diesel-Gas Dual Fuel Combustion

NOMENCLATURE

- a empirical constant, -
- act index constant in Whitehouse heat release model, -
- A area, area of spray, area of flame front, m^2
- B constant, -; cylinder bore, m
- c, C, C' constant, -
- C_h, C_r empirical constant, -
- c_p specific heat at constant pressure, $J/kg \cdot K$
- cr compression ratio, -
- d, d_0, d_n diameter of nozzle orifice, cm, m
- D diameter, m
- D_0 equivalent orifice diameter, m
- e internal energy of unit mass, J/kg, kJ/kg
- E internal energy, activation energy, J, kJ
- \mathcal{F}_1 premixed-burning function in Watson heat release model
- \mathcal{F}_2 mixing-controlled function in Watson heat release model
- h_c, h_i coefficient of convective heat transfer, $W/m^2 \cdot K$

h_r coefficient in radiant heat transfer, $W/m^2 \cdot K$
 k, k' coefficient constant, -
 l length, m
 m, M mass, kg
 M_p Preparation rate of mass in Whitehouse-Way model
 M_R molecular weight, kg/mol
 n number of nozzle hole, number of droplet, -
 P pressure, Pa, kPa
 P_r preparation rate of fuel
 p_O partial pressure of oxygen, kPa, MPa, Bar
 \mathcal{P} rate of preparation of fuel, kg/deg crank
 ΔP pressure drop across nozzle orifice, Pa, MPa
 Q heat transfer, J, kJ
 \dot{q}, \dot{Q} heat transfer rate, W/sec
 \dot{Q} fuel injection rate, m^3/s
 R ideal gas constant, radius of combustion bomb
 R_b rate of burning in Whitehouse-Way model
 R_L Reynold number, -
 s, S spray tip penetration, cm
 S speed, m/sec
 S_L laminar flame speed, m/s, cm/s
 T temperature, K, $^{\circ}C$
 t, t' time, second, mili-second
 t_{ig} ignition delay, ms
 u speed, m/sec
 u' turbulent intensity, m/sec
 V Volume, m^3
 v specific volume, m^3/kg ; velocity, m/sec
 \bar{v} average specific volume, m^3/kg

W work, J, kJ
 x, X mass fraction, kg/kg; spray penetration, cm
 x_b, X_b burned mass fraction, kg/kg
 X_j molar fraction of ideal gas species j, -
 β fraction coefficient in Watson heat release model
 γ adiabatic process index, -
 ϕ, Φ fuel/air equivalence ratio, -
 ρ density, kg/m^3
 θ crank angle, degree
 τ ignition delay time, turbulent mixing time, sec, ms
 τ_{id} ignition delay, degree crank, ms

Subscripts:

0 initial state
 a air
 b burned zone state, burned
 c convective heat transfer
 e entrainment
 f, F fuel
 fl flame
 g, G gas
 i ignition, ignition delay, injection
 ig ignition, ignition delay
 inj injection of pilot fuel
 j injection
 l, L liquid fuel
 m mean average value
 O, O_2 oxygen
 sp spray

- T turbulence
- u unburned, unburned zone
- v fuel vapour
- w wall, wall impingement

7.1 Introduction

This chapter describes a phenomenological model for diesel–gas dual fuel combustion. The model is based on knowledge from SI and CI engine combustion and from dual fuel combustion, particularly from the experimental results obtained from the dual fuel combustion bomb described in previous chapters. It includes the flame propagation model discussed in Chapter 3, the spray combustion model developed in Chapter 5 and the dual fuel ignition delay correlation in Chapter 6. Computational results of this model are compared with measurements from the constant volume dual-fuelled combustion bomb.

7.2 Literature Review

Very few attempts at analytical modelling for dual fuel combustion have been reported. All reported phenomenological models have been based on a single-zone (zero-dimensional) diesel combustion model and engine data. These are discussed below.

7.2.1 Sumbally heat release model [156]

The heat release model for the dual fuel DI diesel engine proposed by Sumbally et al is based on a single zone spray combustion model and a cosine burning law function for the homogeneous gas-air mixture.

In this model, the burning of the diesel spray was described by the Whitehouse-Way single zone model [107] in which the preparation rate (kg/deg)

was given as

$$Pr = kM_i^{1/3}M_u^{2/3}P_{O_2}^m$$

and the burning rate was given as

$$Rb = \frac{k'P_{O_2}}{n\sqrt{T}} \exp\left(\frac{-act}{T}\right) \int (Pr - Rb)d\theta$$

Constants k , k' , act and m were obtained by matching the calculation result to the engine data.

Burning of the gaseous mixture was calculated by the Lavoie cosine burning law [155] as

$$X_b = 0.51 - \cos\left[\frac{\pi}{1.16} \frac{\theta - \theta_{0.05}}{\theta_{0.95} - \theta_{0.05}}\right]$$

where $\theta_{0.95}$, $\theta_{0.05}$ is the crank angle at $X_b = 0.95$ and $X_b = 0.05$, respectively.

This model was applied to calculate the dual fuel operation performance of a DI diesel engine with vaporised ethanol as the gaseous fuel and gas energy substitution percentages from 0% to 40%. Obviously, this model is a simple approximation for a complex phenomena. Its accuracy depends on the choice of many empirical constants.

7.2.2 Thyagarajan model [11]

The combustion model for a dual fuel DI diesel engine proposed by Thyagarajan et al in 1985 is essentially a zero-dimensional model and is again based on engine test data. It assumes a uniform pressure and temperature distribution throughout the entire cylinder and that the total heat release rate is the sum of those given by the burning of diesel and gas respectively obtained by separate calculations.

The burning of the diesel spray is calculated by the Whitehouse-Way model [107] as

$$M_p = CM_i^{1/3}M_u^{2/3}P_{O_2}^{0.4}$$

and

$$M_b = \frac{C'P_{O_2}}{N T^{0.5}} \exp\left(\frac{-ACT}{T}\right) \int (M_p - M_b)d\theta$$

where M_p, M_b are the rate of preparation and rate of burning, respectively; empirical constants C, C' , and ACT are obtained by matching the calculated results to the engine data.

The burning rate of gaseous fuel is assumed to be equal to an entrainment rate given by the turbulent jet entrainment model which was used in Dent's spray combustion model (Section 5.3.4 in Chapter 5) and is

$$\dot{m}_e = \dot{m}_i \left(\frac{0.32 S}{D_0 - 1} \right)$$

for the free jet. For the wall jet, if $S/D_0 > 6.8$, it is

$$\dot{m}_e = \dot{m}_i \left(\frac{0.86 S}{D_0 - 1} \right)$$

Here \dot{m}_i is the mass rate of liquid fuel injection, D_0 is the equivalent orifice diameter given by $D_0 = D \sqrt{\frac{\rho_L}{\rho_a}}$. S is the spray tip penetration given by the Hiroyasu's correlation [112] as described in Section 5.3.5 of chapter 5.

The model was used in engine simulation of a DI diesel engine in dual fuel operation with bio-gas as its gaseous fuel. Because it neglects the interference between gas fuel and diesel, particularly because it assumes that the burning rate of gas equals its entrainment rate, this combustion model obviously gives only an approximate estimation.

7.2.3 Rafiquillslam combustion model for dual fuel IDI diesel engine

In a dual fuel combustion model for a divided chamber diesel engine, Rafiquillslam et al [12] applied the Watson IDI diesel engine combustion model to calculate the burning rate of both diesel and gaseous fuel, the latter being bio-gas. The total burning rate of gas and diesel is

$$X_b = \beta f_1(t) + (1 - \beta) f_2(t)$$

The phase proportionality factor β is given by

$$\beta = 1 - a \phi^b / t_{ig}^c$$

with empirical constants a , b , and c are given as

$$0.8 < a < 0.95$$

$$0.25 < b < 0.45$$

$$0.25 < c < 0.5$$

The function f_1 and f_2 are given as

$$f_1(t) = 1 - (1 - t^{k_1})^{k_2}$$

$$f_2(t) = 1 - \exp(-k_3 t^{k_4})$$

where t is normalized by the total combustion duration t_{comb} which is estimated by

$$t_{comb} = 3.52 \exp\left(\frac{2100}{T_p}\right) / P^{1.022}$$

Empirical constants k_1 , k_2 , k_3 , and k_4 are obtained by matching the cylinder pressure data from engine experiment.

This model was applied to the calculation of an IDI divided chamber diesel engine operated with bio-gas. Since this model directly applied a correlation which was originally obtained from a diesel engine to dual fuel operation without any modification except the empirical constants, it is obviously a very rough approximation.

7.2.4 A Comparison of the Existing Models

The common link between the three existing models of dual fuel combustion reviewed here is that they are all based on a simple single-zone assumption of the combustion chamber and all directly apply correlations obtained from conventional diesel engines or SI engines with only minor modifications in the matching of the value of the empirical constants. The RafiquiIslam approach to the dual fuel divided chamber diesel engine is a particularly very rough estimation as it did not separate the combustion of gaseous fuel from that of diesel fuel.

The Sumbally and Thyagarajan models are relatively more detailed as the burning of the gas was separated from the burning of diesel. However, inherent in the single-zone assumption is that the effect of flame propagation in the mixture cannot be estimated in either of these models. The Sumbally model also was not able to relate the combustion to the injection characteristics such as spray configuration and motion. While Thyagarajan et al had took the injection characteristics into account, its affect was limited to the combustion of the gaseous fuel only leaving the combustion of diesel fuel unrelated to the spray characteristics. Furthermore, Thyagarajan et al estimated that the burning rate of gas being equals the rate at which the gas-air mixture is entrained into the fuel spray but neglected the fact that combustion can take place beyond the spray region as the flame propagates into the mixture.

7.3 Thermodynamic Sub-model for the Current Dual Fuel Combustion Model

The thermodynamic sub-model used here for dual fuel combustion is a modification of that described in Chapter 2. The modifications are to allow it to cope with the burning of two fuels simultaneously.

7.3.1 Model Assumptions

The thermodynamic model for dual fuel combustion is based on the following assumptions:

- (1) The entire mixture inside the combustion bomb is divided into a burned zone to which an average burned zone temperature applies and an unburned zone to which an average unburned zone temperature applies, respectively. The volume of the reaction region which divides the burned zone and unburned zone is always negligible. Before ignition, both the volume and mass of the burned zone is zero. When combustion is complete, the volume and mass of the unburned zone is zero.

- (2) No heat transfer takes place between the burned zone and the unburned zone. The only energy exchange between the mixture and the cylinder is heat loss from the burned zone. Heat transfer from the unburned zone is negligible. Thus the unburned zone undergoes an adiabatic compression during combustion and its composition remains identical to that which existed before the combustion started.
- (3) Although there is insufficient time to reach thermodynamic equilibrium during the combustion, the burned zone mixture is assumed to be in thermodynamic equilibrium throughout the combustion. This is because the purpose here is not to determine the combustion products. Calculation of the equilibrium composition in the burned zone follows Weinberg's rapid convergent method [25], [24] which is described in Chapter 2.
- (4) The gaseous mixture including the vaporised diesel fuel and the air in the unburned zone and the combustion products in the burned zone, are all considered as ideal gases but the specific heat of each species is a function of the temperature. In calculating the thermodynamic properties, mixtures in the initial state, burned zone and unburned zone are all considered to be homogeneous mixtures, respectively.
- (5) The total mass and volume inside the combustion chamber remains unchanged during the combustion.
- (6) The pressure is spatially homogeneous inside the combustion chamber during the entire combustion process.
- (7) The overall heat transfer from the cylinder charge to the cool wall during combustion is due to convection and radiation only.

7.3.2 Conservation of mass

The total combustion chamber volume V_0 consists of a burned zone and an unburned zone, volume of reaction region being negligible, thus

$$V_0 = m_b \cdot \bar{v}_b + m_u \cdot \bar{v}_u$$

Since $m_u = m_0 - m_b$, this becomes

$$V_0 = m_b \cdot \bar{v}_b + (m_0 - m_b) \cdot \bar{v}_u$$

where \bar{v}_b and \bar{v}_u are the mean specific volumes of the burned zone and unburned zone, respectively, and are given as

$$P\bar{v}_b = R_b \cdot T_b \quad , \text{ and } \quad P\bar{v}_u = R_u \cdot T_u \quad (7.1)$$

Defining the total burned mass fraction as $x_b = m_b/m_0$, the equation of mass conservation can also be expressed as

$$\frac{V_0}{m_0} = x_b \bar{v}_b + (1 - x_b) \bar{v}_u \quad (7.2)$$

7.3.3 Conservation of energy

At any instant, the energy conservation equation for a two-zoned model of the combustion chamber can be expressed as

$$e_0(T_0) - \frac{W}{m_0} - \frac{Q}{m_0} = x_b \bar{e}_b(T_b) + (1 - x_b) \bar{e}_u(T_u) \quad (7.3)$$

For a combustion bomb of fixed volume, $W \equiv 0$. Because it has been assumed that the mixture in the initial state, unburned zone, and burned zone are all ideal gases, their internal energies can be calculated as functions of temperature only. Hence:

$$e_0(T_0) = \sum_0 X_i e_i(T_0) \quad (7.4a)$$

$$e_u(T_u) = \sum_U X_i e_i(T_u) \quad (7.4b)$$

$$e_b(T_b) = \sum_B X_i e_i(T_b) \quad (7.4c)$$

Here X_i is the mass fraction for species i and the notation 0, U, B in the above equations means that the summations are taken for all species in the mixture

for the initial state, the unburned zone and the burned zone, respectively. For each species, internal energy is given as

$$e_i = h_i(T_i) - R_i T_i \quad (7.5)$$

For species in the mixture in the initial state or the unburned zone, enthalpies $h_i(T_i)$ are calculated by polynomial functions given as Eq. 2.4 and Eq 2.5 in Chapter 2; for species in the burned zone, enthalpies are calculated using a linear function as given by Eq. 2.3 in Chapter 2.

7.3.4 Adiabatic compression of the unburned zone mixture

As it has been assumed that the unburned zone mixture undergoes an adiabatic compression, its temperature is therefore given by

$$T_u = T_0 \left(\frac{P}{P_0} \right)^{\frac{(\gamma_u-1)}{\gamma_u}} \quad (7.6)$$

7.3.5 Heat transfer

It is always difficult to precisely predict heat transfer in a combustion device. In engine calculations, a common practice is to use a convection type correlation which is based on an instantaneous spatial average heat transfer coefficient to estimate the overall heat transfer. A typical example of this approach is the Woschni correlation, which, with modification for the combustion bomb situation, has been applied in Chapter 5 for heat transfer in diesel combustion. However, experimental results of the current dual fuel combustion bomb show that convective heat transfer alone tends to underestimate the heat loss, particularly during the high pressure and high temperature combustion period. Therefore, a radiant heat transfer term is necessary. The overall heat transfer rate from the hot combustion chamber charge to the cool wall is therefore

estimated here by

$$\dot{q} = h_i A_c (T_m - T_w) + h_r \cdot \sigma A_c (T_m^4 - T_w^4) \quad (7.7)$$

where $\sigma = 5.66961 \times 10^{-8} W \cdot m^{-2} K^{-4}$ is the Stephan-Boltzman constant and $T_m = x_b T_b + (1 - x_b) T_u$ is the mean temperature of the cylinder charge. The convective heat transfer coefficient h_i is estimated by the correlation described in Chapter 5, and is:

$$h_i (W/m^2 \cdot K) = C_h B(m)^{0.2} P(kPa)^{0.8} T_m(K)^{-0.55} (P - P_0)(kPa)^{0.8} \quad (7.8)$$

Because well-accepted formula for radiant heat flux in an engine are not available, the radiant heat transfer coefficient h_r is estimated here by an equation with the same format as Eq. 7.8 but with a different coefficient constant. The equation is:

$$h_r (W/m^2 \cdot K^4) = C_r B(m)^{0.2} P(kPa)^{0.8} T_m(K)^{-0.55} (P - P_0)(kPa)^{0.8} \quad (7.9)$$

Both C_h and C_r are empirical constants. Detail of evaluating the value of C_h and C_r is discussed in a later section. This constructs the appropriate thermodynamic sub-model.

7.4 The Combustion Model

7.4.1 Model assumptions

In dual fuel combustion, if it is considered that the pilot spray region remains the same as in the conventional diesel engine when no combustible gas is present and since the gaseous fuel and diesel fuel exist simultaneously in the burning zone, the total burning rate is affected by both the flame propagation of the gaseous-air mixture and the entrainment of air into the diesel spray. Therefore, the burning zone will not be limited to the spray jet region only. Contribution to the total combustion are partly by the flame propagation outside the spray region and partly by the combustion within the spray itself. However, because

a portion of the gas is entrained into the spray jet region together with the air, burning in the spray region is not diesel fuel alone. On the other hand, because the ignition delay is long in dual fuel combustion, a portion of the diesel fuel should be well mixed with the air-gas mixture before ignition, Therefore, the flame-propagation controlled burning may also include some diesel fuel.

The following assumptions have been made in constructing the present dual fuel combustion model:

- (1) The presence and burning of the gaseous fuel do not affect the pilot jet's configuration and motion. Thus, the 'spray jet' region and spray tip penetration can be calculated by correlations obtained from conventional diesel engine research.
- (2) A dual fuel combustion consists of two parts and the burning has to be extended beyond the diesel spray region. These two parts are the burning outside the spray jet region which is controlled by the flame propagation and the burning within the diesel spray which can be assumed to be controlled by the air entrainment into the spray, as previously described in Chapter 5. However, burning outside the 'spray jet' region is not necessary limited to the gaseous fuel only and burning within the 'spray jet' region is not confined to diesel fuel. That is, a portion of the gaseous fuel combustion is controlled by the burning rate within the diesel 'jet region' while a portion of the diesel is burned outside the 'jet region' where it is controlled by the flame propagation. These two kinds of combustion start at the same instant immediately following the ignition delay but are not necessary completed at the same time.
- (3) Pilot fuel injection is in such a small quantity that the effect of wall jet formation is negligible.
- (5) During combustion, diesel fuel and gaseous fuel consume the air proportionally according to their chemical composition. This means that the burning of diesel and gas takes place at the same fuel/air equivalence ratio which is always equal to its initial value before the combustion. This

is

$$\Phi_G \equiv \Phi_L \equiv \Phi_0 \quad (7.10)$$

This assumption simplifies the calculation. However, its validation is a subject which needs further investigation in later projects.

7.4.2 Model equations

The rate of burning

The burning rate, given in terms of the mass fraction x is

$$\frac{dx_b}{dt} = \mathcal{F} \cdot \left(\frac{dx_{b1}}{dt}\right)_{fl} + (1 - \mathcal{F}) \cdot \left(\frac{dx_{b2}}{dt}\right)_{sp} \quad (7.11)$$

where \mathcal{F} is a weighting factor which is a function of the ignition delay and is

$$\mathcal{F} = a_f \cdot \tau_{ig}^{b_f} \quad (7.12)$$

Here a_f and b_f are empirical constants which can be determined from experiment.

The term $\left(\frac{dx_{b1}}{dt}\right)_{fl}$ is a burning rate controlled by the flame propagation, as described in Chapter 3, and is

$$\frac{dx_{b1}}{dt} = \frac{x_e - x_{b1}}{\tau} \quad (7.13a)$$

$$\frac{dx_e}{dt} = \frac{\rho_u A_{fl}}{m_0} (C_T u' + S_L) \quad (7.13b)$$

and $\left(\frac{dx_{b2}}{dt}\right)_{sp}$ is the entrainment controlled burning rate described in chapter 5, and is:

$$\left(\frac{dx_{b2}}{dt}\right)_{sp} = C_e A_{sp} (1 - x_{b2}) \quad (7.14)$$

Here C_e is a function of the injection volume m_{inj} as discussed previously in Chapter 5 and is expressed as:

$$C_e = a \cdot v_{inj}^b \quad (7.15)$$

A_{fl} in equation 7.13b is a flame front area estimated by considering a sector of a sphere and the cylinder wall as in Chapter 3. Also, A_{sp} in Eq. 7.14 is a spray area estimated from the diesel jet configuration as in chapter 5.

Equation 7.11 can be understood as follows. The burned zone in dual fuel combustion consists of two parts, one part having a surface area $\mathcal{F}A_{fl}$ in which burning is controlled by flame propagation, the other part is with a surface area of $(1 - \mathcal{F})A_{sp}$ in which burning is controlled by air entrainment. As will be seen from Equation 7.12 and Equation 7.20 later in this section, the weighing factor \mathcal{F} for the dual fuel combustion burning rate increases with the ignition delay τ_{ig} . Equation 7.11 also indicates that the longer the ignition delay, the more the dual fuel combustion burning rate is dominated by the flame propagation. This is because more pilot fuel has mixed with the air-gas mixture during the ignition delay period.

The ignition delay

The ignition delay is calculated by the correlation obtained from combustion bomb experiments as discussed in Chapter 6, and is

$$\tau_{ig} = 19.3P_0^{f(\phi_{gas})}g(\phi_{gas}, m_{inj})\exp\left(\frac{500}{T_0}\right) \quad (7.16)$$

Here

$$f(\phi_{gas}) = -1.0174 + 0.7119\phi_{gas} \quad (7.17a)$$

$$g(\phi_{gas}, m_{inj}) = g_1(m_{inj}) + g_2(m_{inj})\phi_{gas} + g_3(m_{inj})\phi_{gas}^2 + g_4(m_{inj})\phi_{gas}^3 \quad (7.17b)$$

$$g_1(m_{inj}) = (3.70 + 0.28855m_{inj}) \quad (7.17c)$$

$$g_2(m_{inj}) = (-5.8236 - 0.9640m_{inj}) \quad (7.17d)$$

$$g_3(m_{inj}) = (7.869 + 0.8761m_{inj}) \quad (7.17e)$$

$$g_4(m_{inj}) = (-4.2668 - 0.22235m_{inj}) \quad (7.17f)$$

Here P_0 is the initial pressure (bar) of the mixture, ϕ_{gas} is the equivalence ratio of the mixture when there is gaseous fuel only, m_{inj} is the pilot injection quantity (mg) and T_0 is the initial temperature (K) of the mixture. The ignition delay τ_{ig} is in ms.

7.4.3 Empirical coefficients and correlations for the combustion model

coefficients of heat transfer

Values of C_h and C_r for the current combustion model are obtained by the following method. For a particular dual fuel combustion experiment, calculations were repeated by gradually changing the values of C_h and C_r until the calculation matched the experimental result of pressure trace. A pair of particular values of C_h and C_r were therefore obtained. While values of these coefficients vary slightly for each particular experiment, their average values can be applied to all experiments and these average values can be expressed as follows:

The coefficient for radiant heat transfer:

$$C_r = 4.94 \times 10^{-8} \quad (7.18)$$

The coefficient for convective heat transfer:

$$C_h = 11.2 \times 10^{-5} \quad (7.19)$$

The calculation results presented in later section of this chapter were obtained by using these average values. Fig. 7.1 and Fig. 7.2 show the effects of the radiant coefficient C_r and the convective coefficient C_h respectively. It can be seen that while the convective coefficient C_h is the dominant factor in heat transfer, use of C_h alone could not represent the data throughout the whole range of the combustion, particularly in the high pressure and high temperature region. The radiant heat transfer term C_r is therefore necessary.

It should be noted that, in the sole diesel combustion as described in Chapter 5, the radiant heat transfer term is not required as the combustion is usually at lower pressure and temperature.

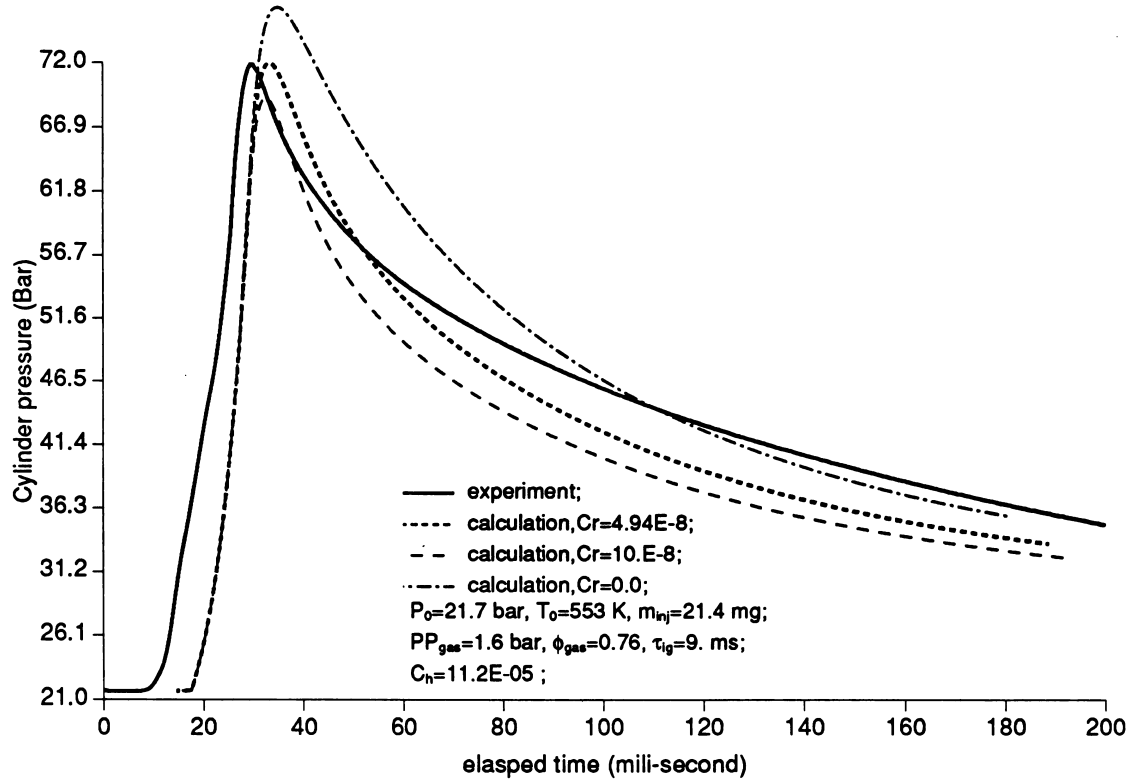


Figure 7.1: Effects of radiant heat transfer coefficients

The weighting factor of the burning rate

By using a similar method as in evaluating the heat transfer coefficients, the weighting factor of the burning rate can be obtained and expressed as

$$\mathcal{F} = 0.206 \tau_{ig}^{0.368} \quad (7.20)$$

where τ_{ig} is the ignition delay calculated by equation 7.16.

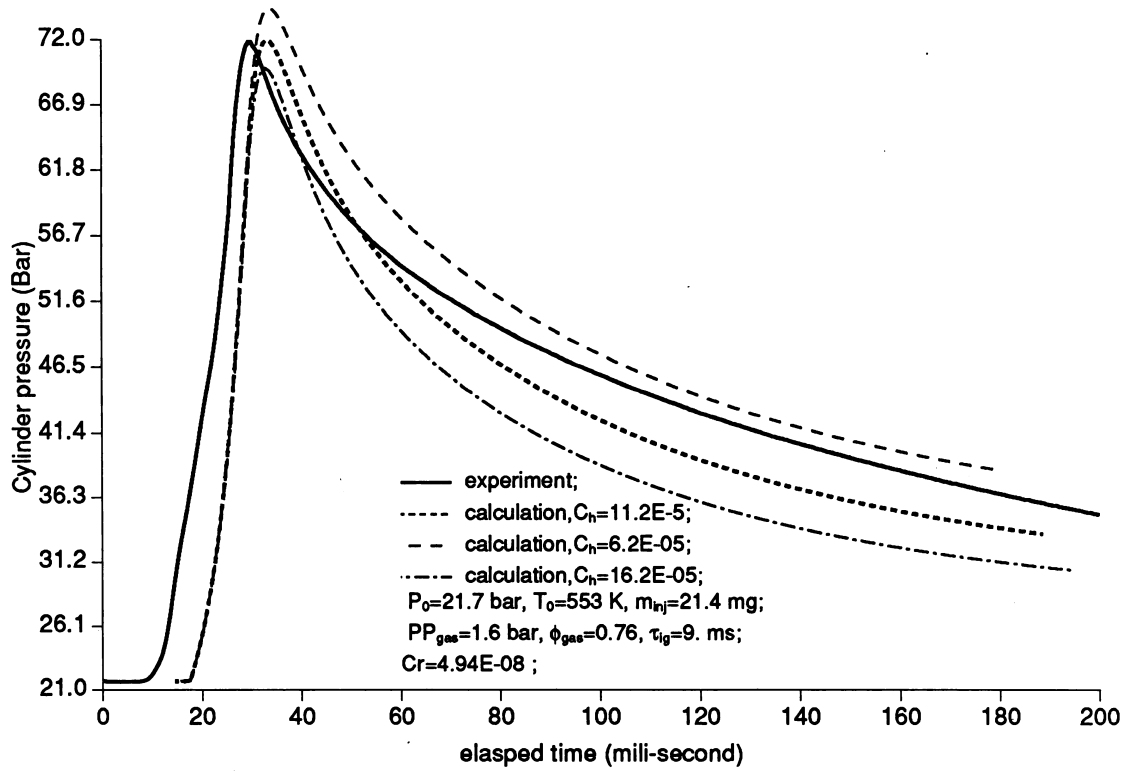


Figure 7.2: Effects of convective heat transfer coefficients

The coefficient of entrainment

Also by a similar method, the coefficient for entrainment is evaluated as

$$C_e = 33.33 v_{inj}^{0.52} \quad (7.21)$$

where v_{inj} is the volume of diesel injection in mm^3 .

These coefficients and correlations are obtained from experimental data with the conditions of

1. initial pressure

$$18.1 \leq P_0(\text{bar}) \leq 24.8$$

2. initial temperature of the mixture

$$513 \leq T_0(K) \leq 573$$

3. ignition delay

$$9.0 \leq \tau_{ig}(ms) \leq 22.0$$

4. pilot fuel injection quantity

$$4.1 \leq m_{inj}(mg) \leq 21.4$$

5. and the energy ratio

$$0.778 \leq (E_{gas}/E_{total}) \leq 0.951$$

7.5 Computational Results of the Model

Figures 7.3 to 7.20 are calculated results of the current combustion model compared with corresponding experimental results. In all these figures, dynamic pressure traces are presented from the moment of pilot injection till 200 ms after the injection. In all cases, according to the calculation, more than 98% of the total fuel has been burned within this period.

It can be seen that the model predicts both an ignition delay time and the entire combustion pattern. However, the calculated ignition delay period is usually slightly longer than that of the measurement. Also, the model gives a faster burning rate than that measured during the rapid pressure rise period because the actual dual fuel combustion process is much more complex than the model's assumption, particularly in the initial stage. In the late combustion stage, the calculated pressure is usually lower than that measured. This could be caused by a few reasons: (1) as the model gives too fast a burning rate during the early combustion stage, it must then give too slow a burning rate at a later stage; (2) correlations for convective and radiant heat loss used in this model give too high a value; (3) the cool wall temperature is assumed to be unchanged in the calculation but it actually increases slightly during combustion.

7.6 Total Engine Simulation

Primary work for incorporating the current dual fuel combustion model into a total engine simulation package has been carried out. The original package (ODES) is a general purpose, 'filling and emptying' type code which, with calibration from an engine, is able to perform the simulation of conventional diesel and gasoline engines. In order to incorporate the current dual fuel combustion model into the package so that it will also be able to simulate the perform of a dual fuel engine, the package has been converted to a double precision Fortran code from its original single precision code. This is because the dual fuel combustion simulation requires a higher accuracy in its calculations. This modification improves the accuracy of the calculations and reduces the machine dependency of the package.

Modification has also been made at the user interface of the package. The original ODES program required a very strictly structured input data file in which all data must be in the correct order and no comment line is allowed. As data files for engine simulation are usually very large, such a data file without any comment is very inconvenient for users. Furthermore, any mistake (for instance, a typographical error) in the data will be very difficult to detect. After the modification, various forms of comment can be inserted into the data file. The program will now itself also try to locate any possible mistake in the data file.

After these modifications, the engine simulation package has become more user friendly. The dual fuel combustion model has been inserted and its further development can proceed with relative ease.

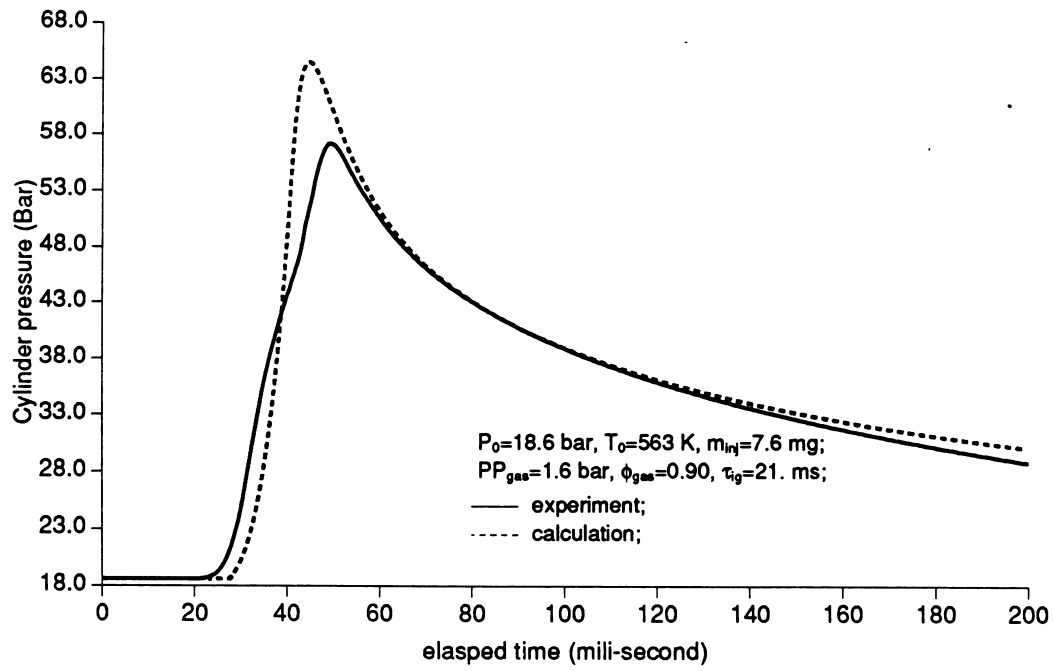


Figure 7.3: NG+Diesel dual fuel combustion dynamic pressure trace.

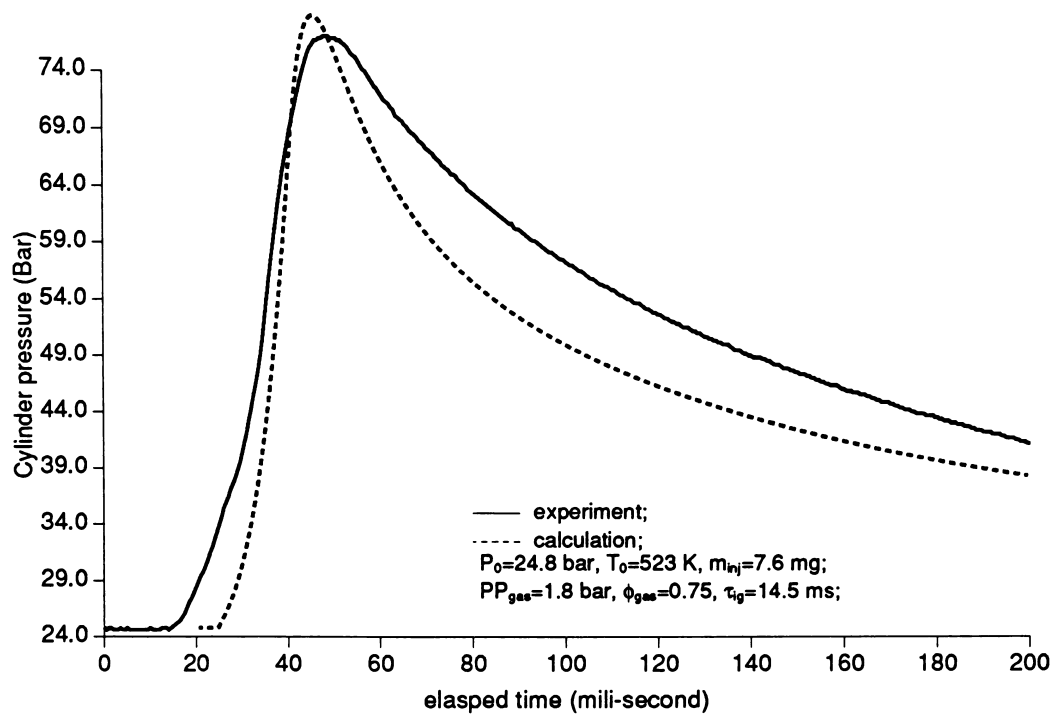


Figure 7.4: NG+Diesel dual fuel combustion dynamic pressure trace.

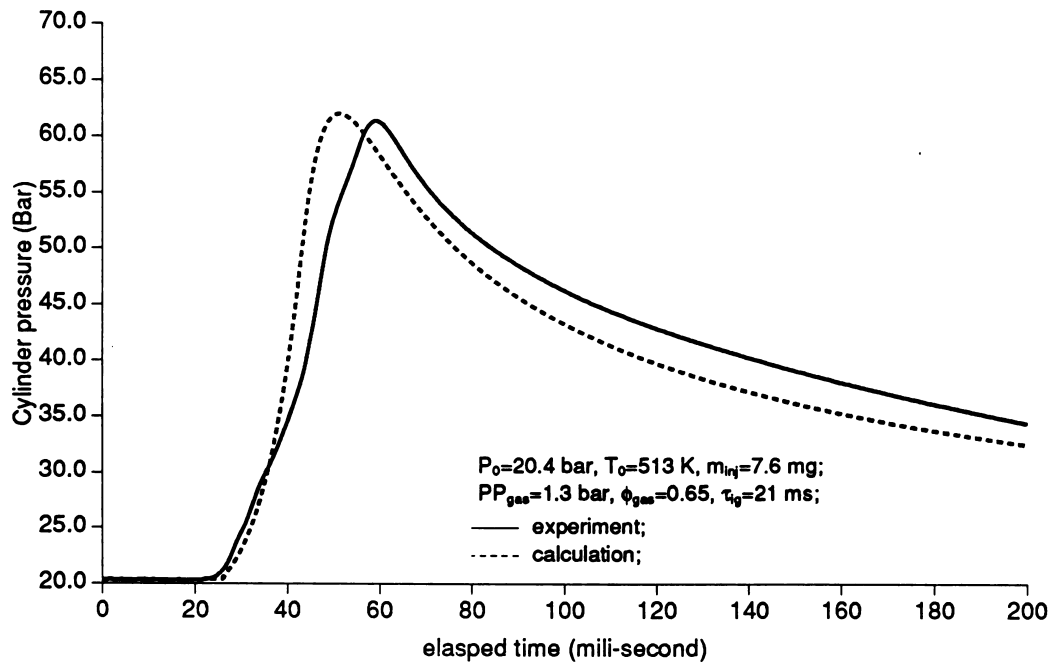


Figure 7.5: NG+Diesel dual fuel combustion dynamic pressure trace.

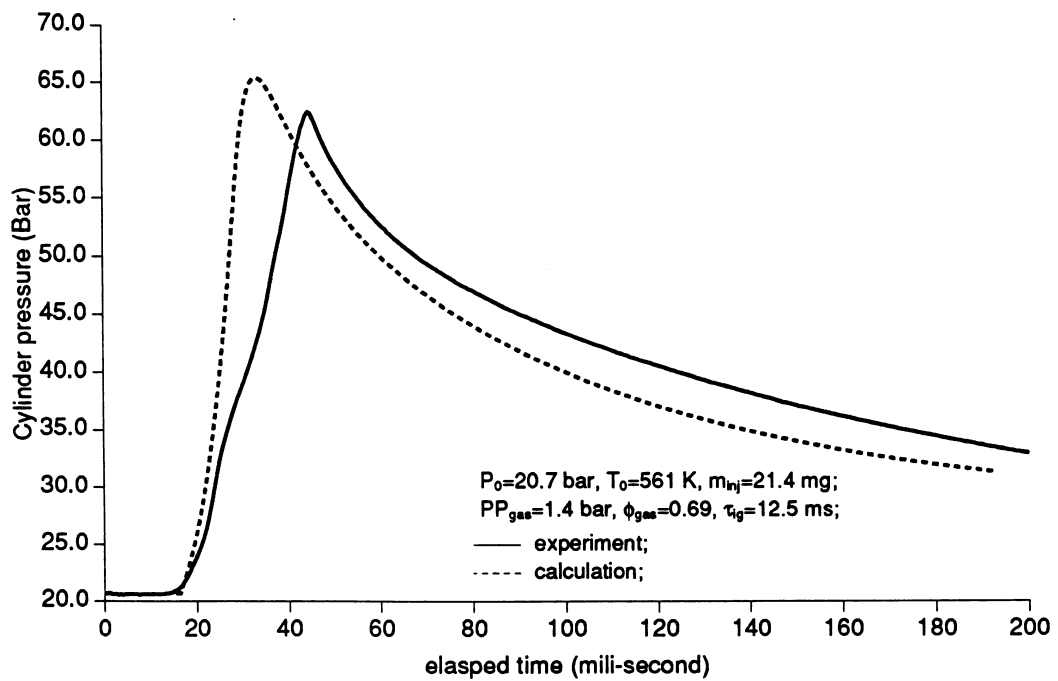


Figure 7.6: NG+Diesel dual fuel combustion dynamic pressure trace.

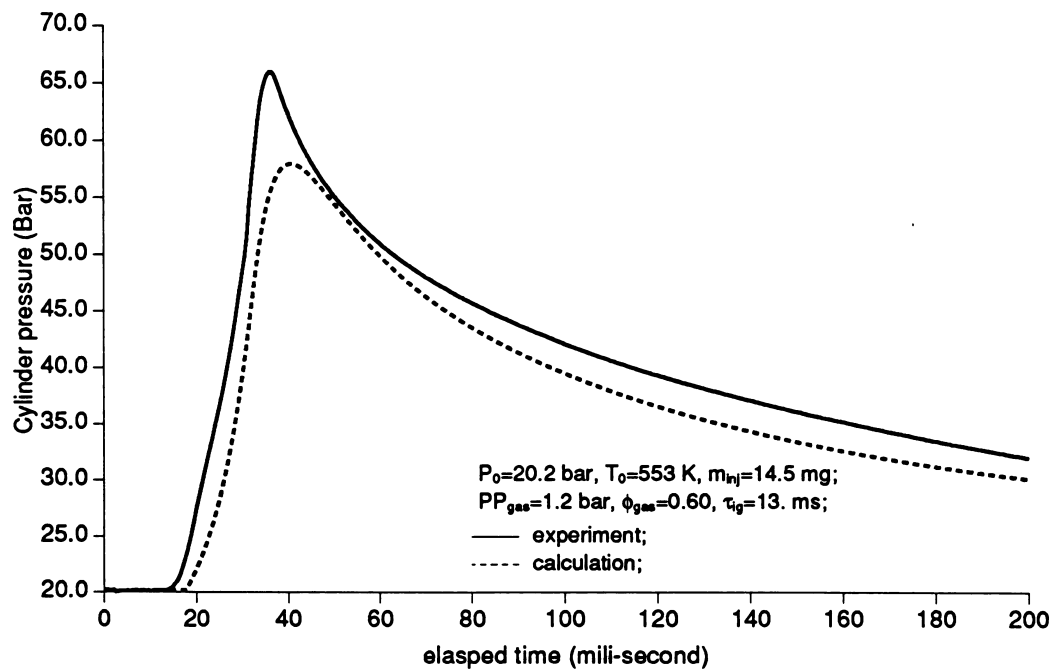


Figure 7.7: NG+Diesel dual fuel combustion dynamic pressure trace.

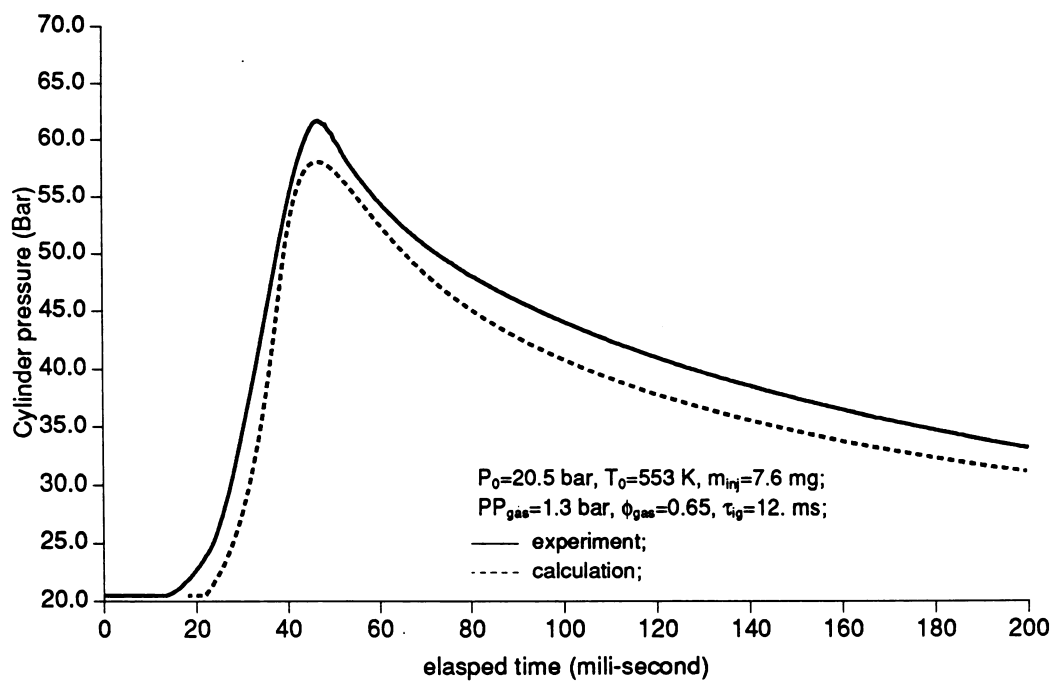


Figure 7.8: NG+Diesel dual fuel combustion dynamic pressure trace.

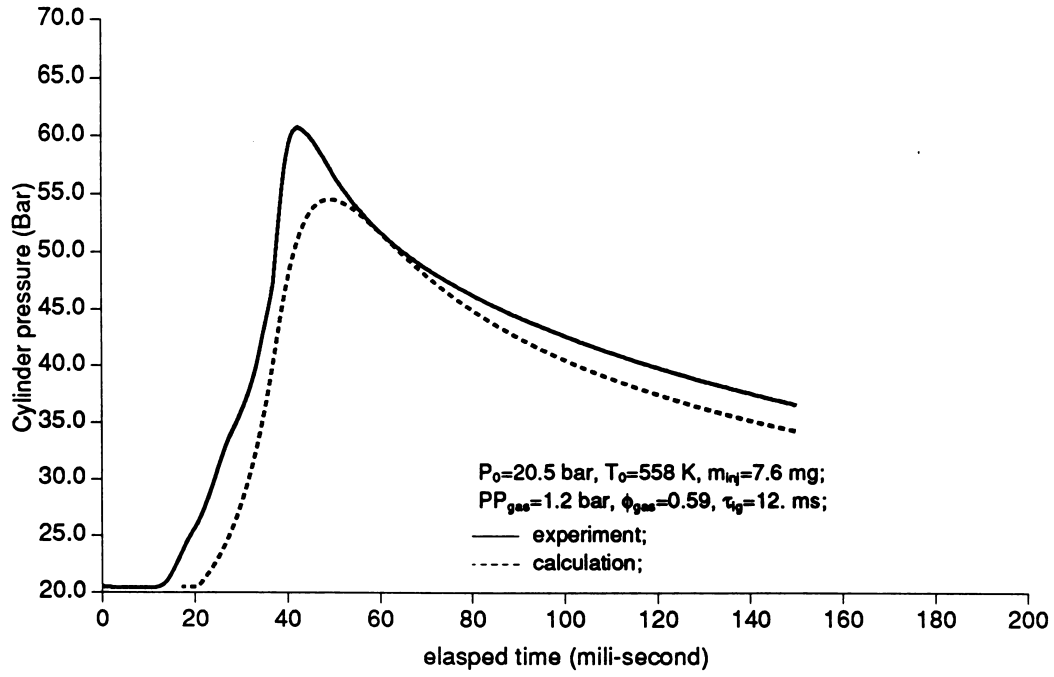


Figure 7.9: NG+Diesel dual fuel combustion dynamic pressure trace.

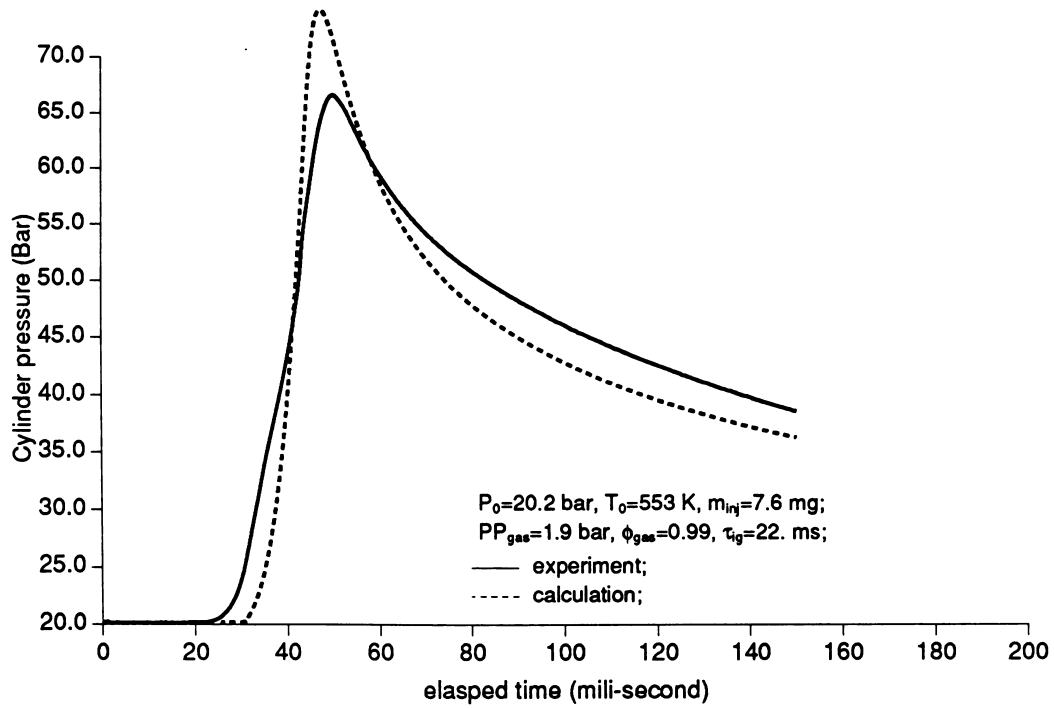


Figure 7.10: NG+Diesel dual fuel combustion dynamic pressure trace.

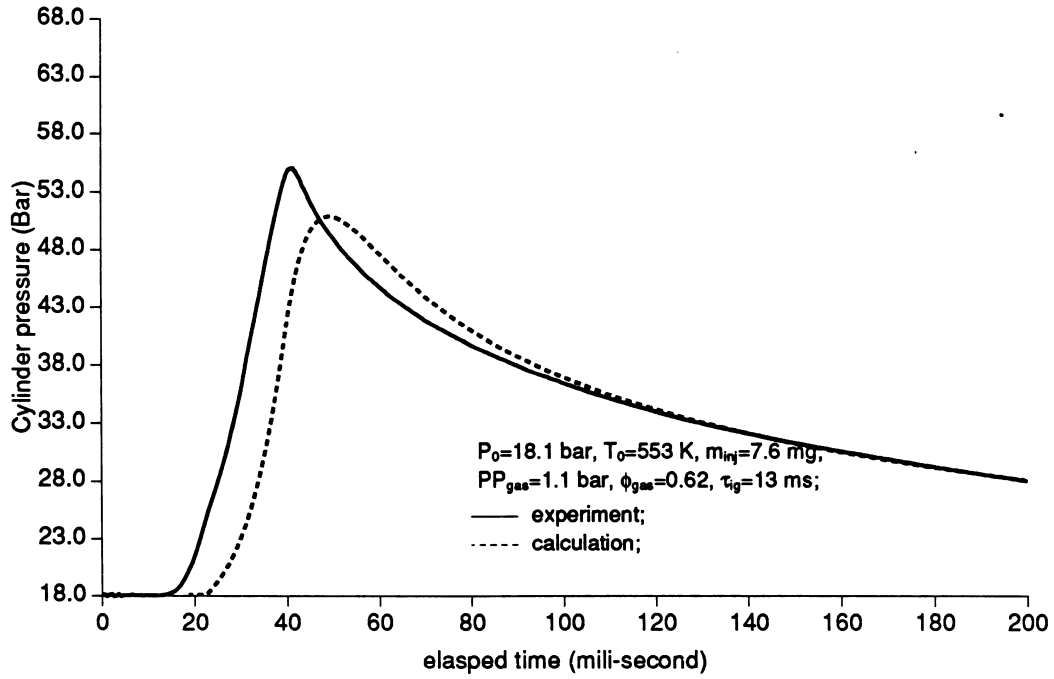


Figure 7.11: NG+Diesel dual fuel combustion dynamic pressure trace.

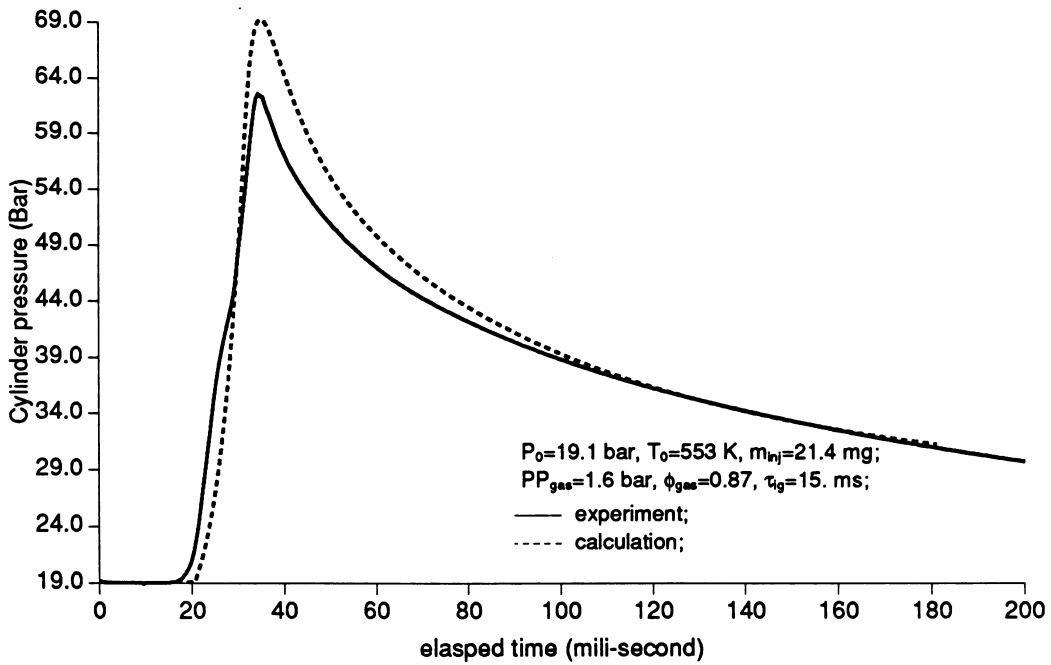


Figure 7.12: NG+Diesel dual fuel combustion dynamic pressure trace.

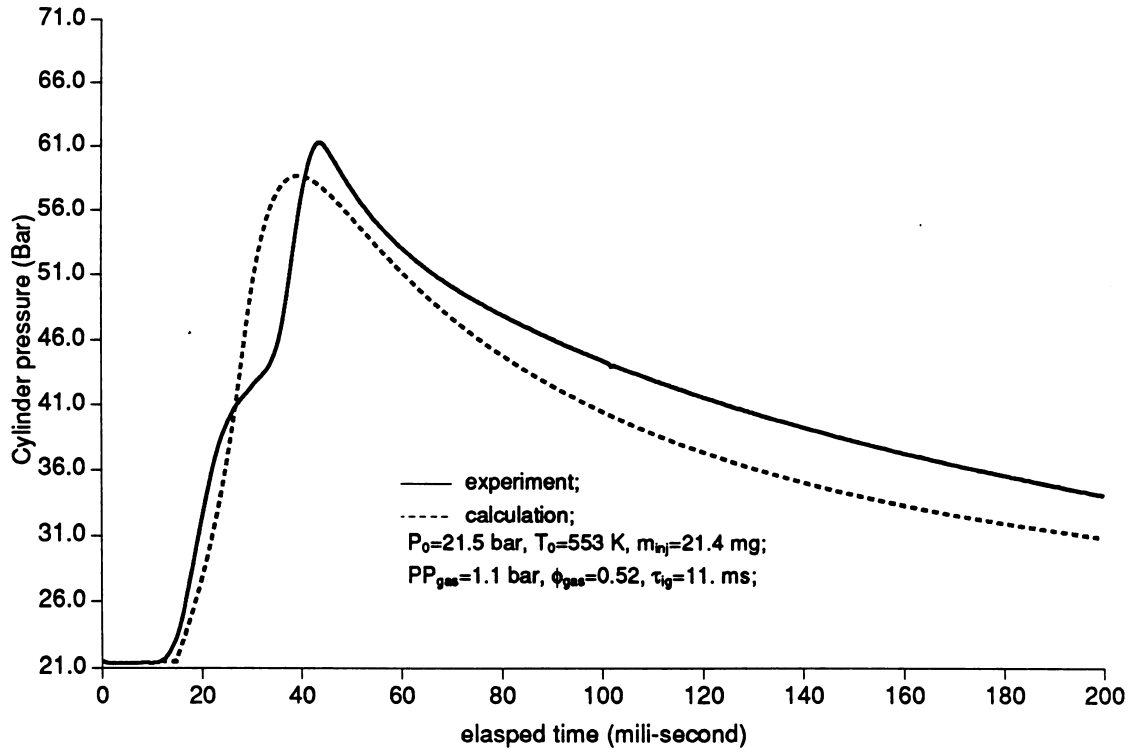


Figure 7.13: NG+Diesel dual fuel combustion dynamic pressure trace.

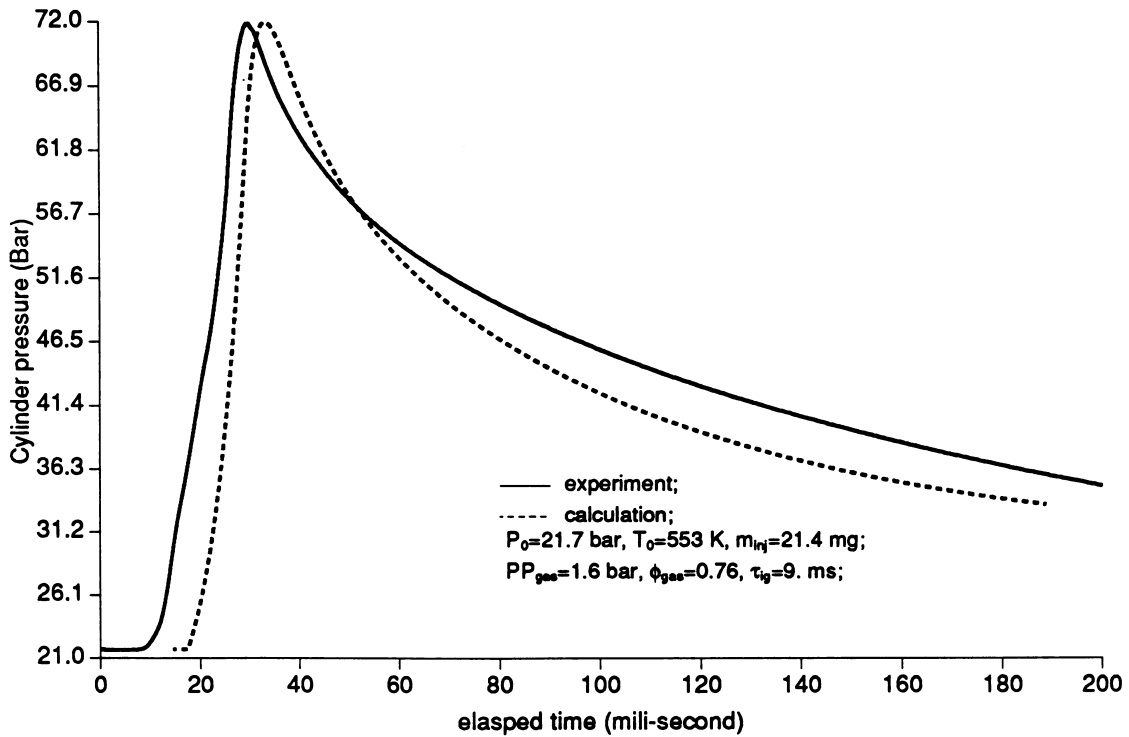


Figure 7.14: NG+Diesel dual fuel combustion dynamic pressure trace.

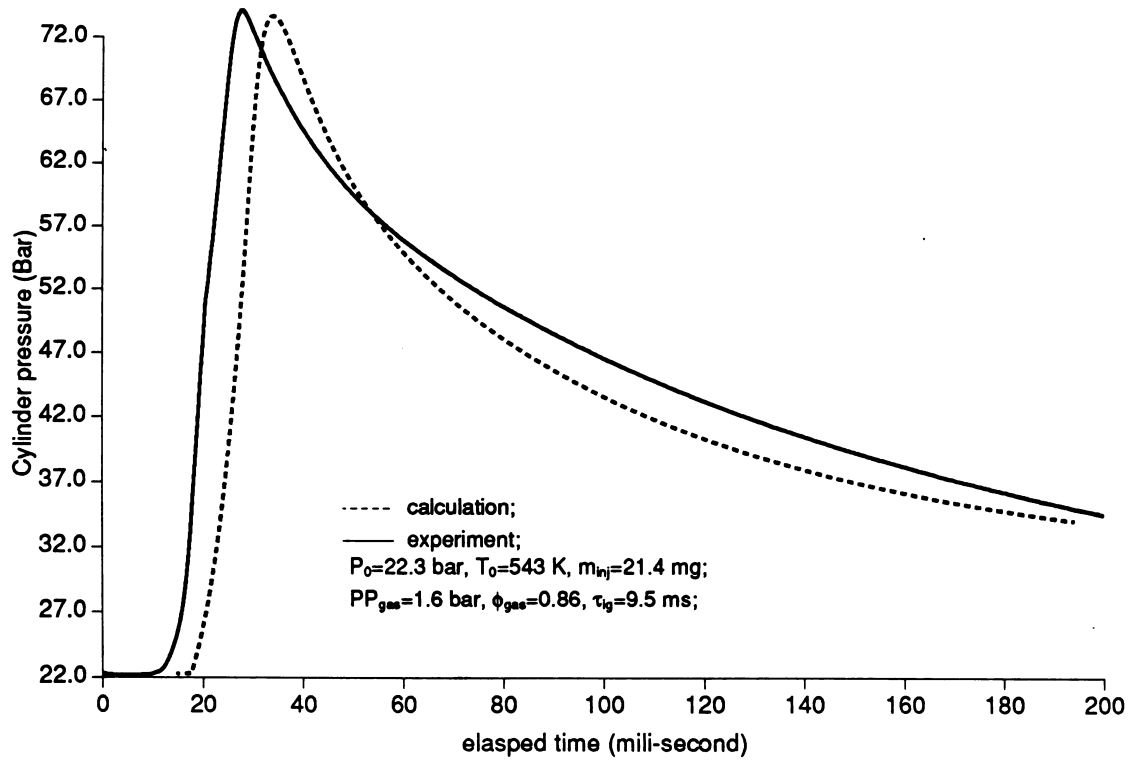


Figure 7.15: NG+Diesel dual fuel combustion dynamic pressure trace.

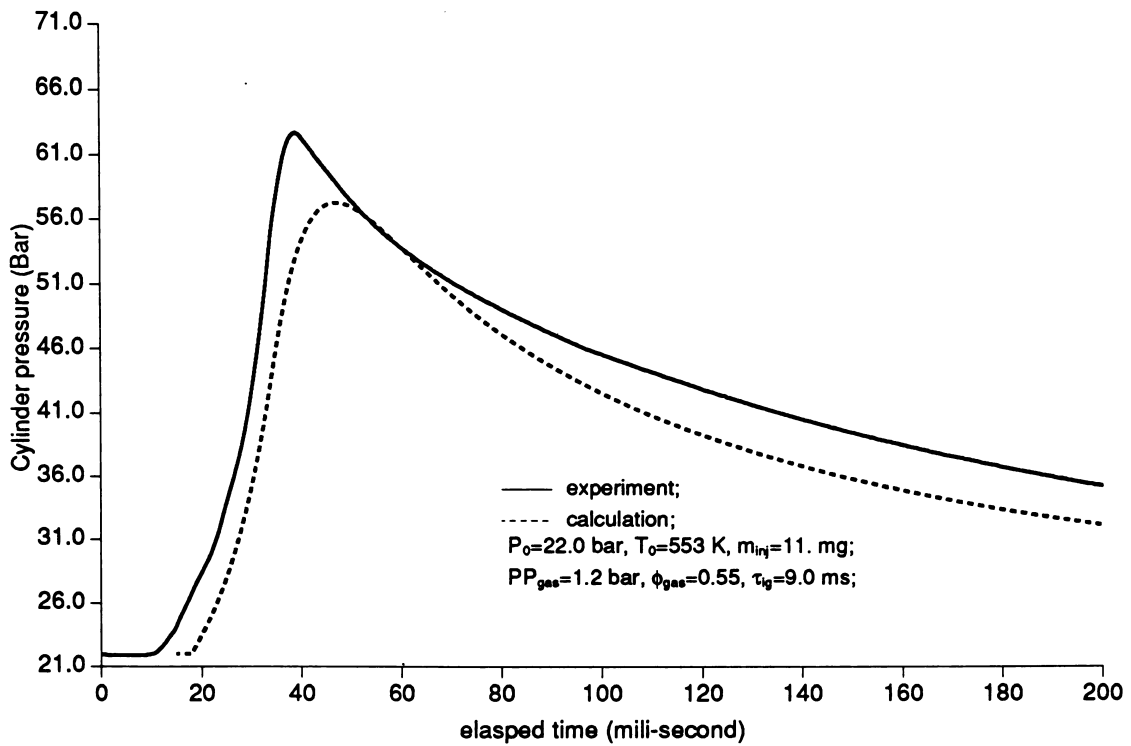


Figure 7.16: NG+Diesel dual fuel combustion dynamic pressure trace.

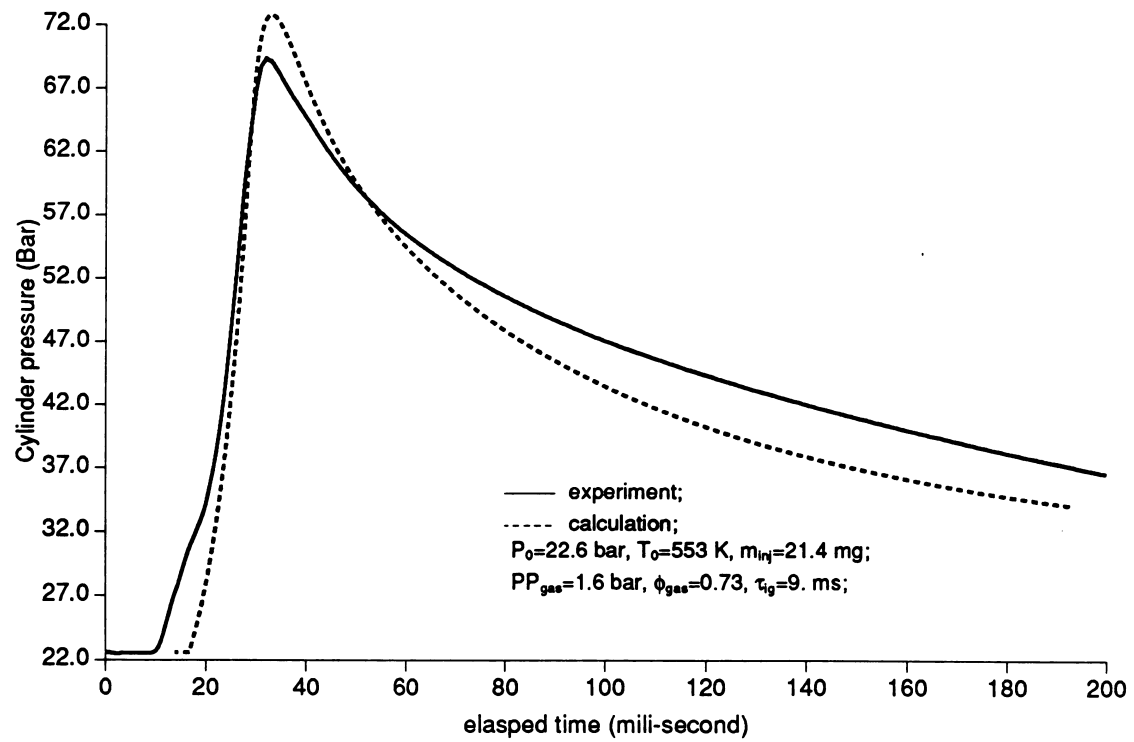


Figure 7.17: NG+Diesel dual fuel combustion dynamic pressure trace.

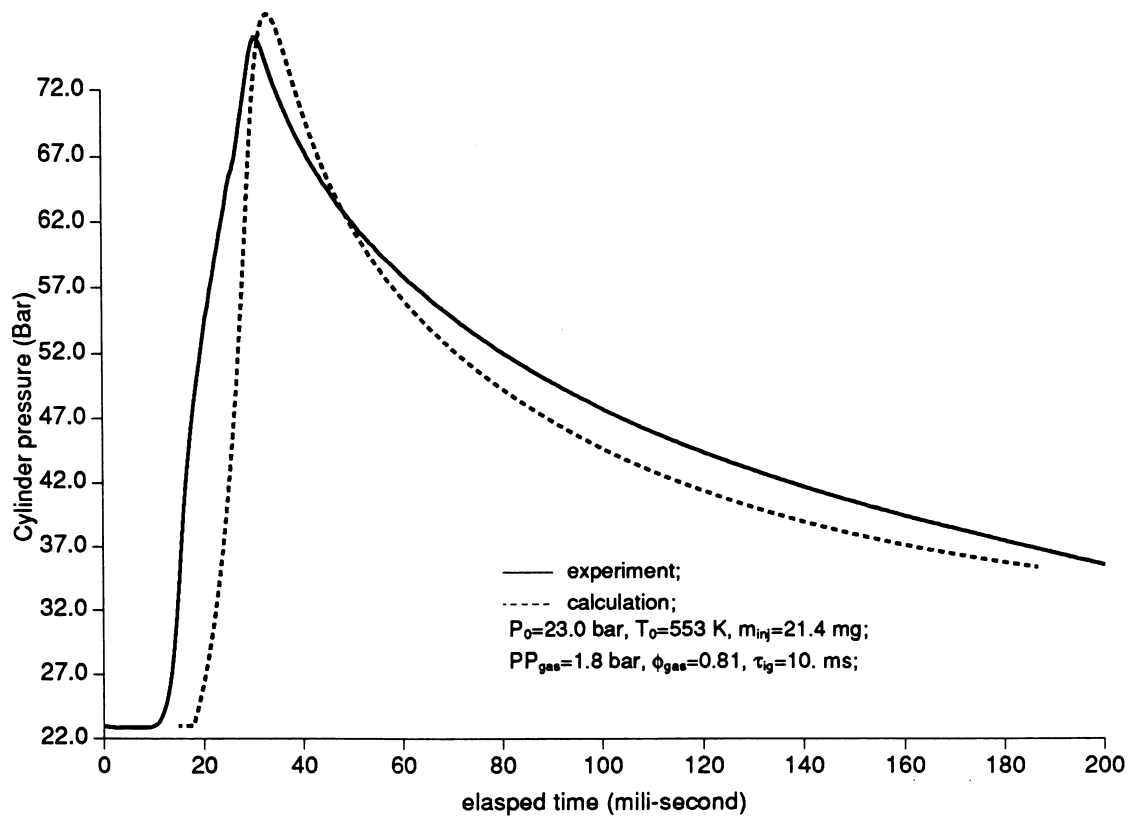


Figure 7.18: NG+Diesel dual fuel combustion dynamic pressure trace.

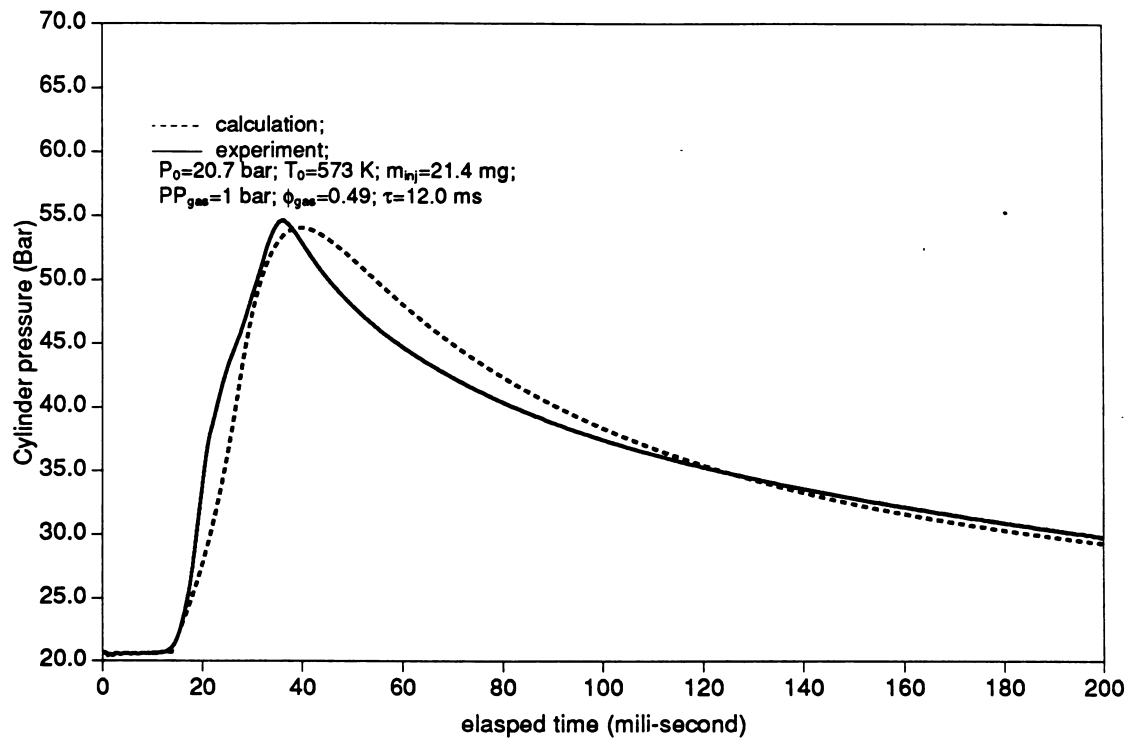


Figure 7.19: NG+Diesel dual fuel combustion dynamic pressure trace.

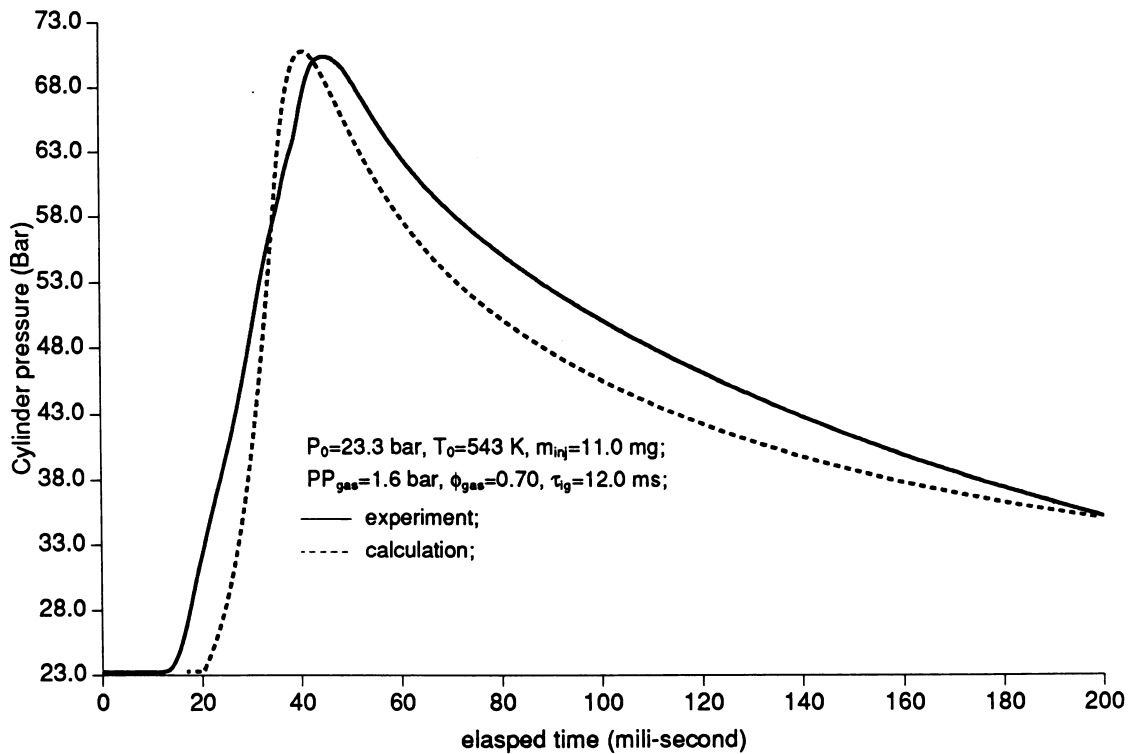


Figure 7.20: NG+Diesel dual fuel combustion dynamic pressure trace.

Chapter 8

Conclusions, Discussion and Recommendation for Further Research

8.1 Conclusions

- (1) A new quasi-dimensional phenomenological model including the ignition delay and heat transfer for a dual fuel combustion engine has been developed. This model is constructed based on a sub-model of turbulent flame propagation and a sub-model of air entrainment controlled combustion of low quantity spray. Data has been obtained from experiments using a constant volume dual fuel combustion bomb. That is, this model describes the dual fuel combustion in term of a turbulent flame propagation controlled premixed burning plus a turbulent air entrainment controlled pilot spray burning. The total burning rate for the dual fuel combustion is given as a weighted sum of the two aforementioned burning rates. The weighting factor is a function of the dual fuel ignition delay. Values of empirical coefficients for the correlation of this combustion model have been determined from combustion bomb experimental data. The physical meaning of these coefficients and correlations are also given. This combustion model has a clear physical base.
- (2) A computer code to perform the calculation of the dual fuel combustion

model has been developed. Calculation results are in good agreement with the experimental data of the dynamic pressure trace from the constant volume dual fuel combustion bomb. Despite the fact that the current model is a quasi-dimensional model which treats the combustion process in more detail than does a zero-dimensional model, it requires less empirical coefficients than do existing zero-dimensional models. This allows the model to be relatively easily applied to a total engine simulation calculation. The primary work of incorporating the current combustion model into an engine simulation computer program, ODES, has been carried out.

- (3) A constant volume combustion bomb experimental rig has been developed particularly for dual fuel combustion experiments. Extensive experimental work has been carried out on both sole diesel operation and diesel-NG dual fuel operation. No previous research work on a dual fuel combustion bomb is available. Despite the fact that many difficulties have been encountered in developing the experimental rig and in performing the dual fuel experiments, a large amount of experimental data has been obtained and is used in developing the current phenomenological combustion models, particularly the diesel and dual fuel pressure rise ignition delay, the value of the air entrainment coefficient, the value of the burning rate weighting factor for dual fuel combustion, and values of convective and radiant heat transfer coefficients.
- (4) The affects of initial conditions on the dual fuel combustion have been investigated experimentally in the combustion bomb. The factors being investigated include the initial pressure and temperature of the cylinder charge, the quantity of pilot injection, and the ratio of pilot to gaseous fuel. Emphasis is placed on investigating the ignition conditions and the minimum pilot injection for the dual fuel combustion. Experiment shows that good dual fuel combustion can still be achieved for pilot diesel fuel contributing as little as 5% of the total energy.
- (5) The dual fuel ignition delay can be considered as the parameter which indicates the general status of the initial conditions of dual fuel combus-

tion. This is because the experimental observation shows that the dual fuel ignition delay period is strongly affected by the initial pressure and temperature of the cylinder charge, the quantity of pilot fuel injection and the relative amount of gaseous fuel in the mixture. The dual fuel ignition delay also has a strong affect on the combustion pattern and the heat release rate.

- (6) A mathematical formula has been proposed to calculate the dual fuel ignition delay as a function of initial pressure, initial temperature, gas/air equivalence ratio and pilot injection quantity. Data on pressure rise delay is obtained by a simple graphical analysis method from the dynamic pressure trace of the combustion bomb experiment. The correlation of the ignition delay is then obtained by a multi-dimensional non-linear regression of the data for the pressure rise delay. No similar correlation which considers the dual fuel ignition delay as a function of initial pressure, temperature, amount of pilot injection and gas has been found in the literature despite the fact that much research on ignition delay for dual fuel engines has been reported.
- (7) A new two-zone combustion model particularly for small quantities of diesel injection has been developed based on the dynamic pressure trace obtained from the combustion bomb experiment. The physical meaning of model's coefficient is given and a correlation for calculating the coefficient is also obtained from experiments on diesel combustion in the constant volume combustion bomb. A computer code based on this model has been developed and the computational results are in good agreement with the experimental observations of normal combustion.
- (8) A correlation for ignition delay for sole diesel fuel combustion has also been obtained. Regression data for this correlation is obtained by the same graphical analysis method used for dual fuel ignition delay. Results of this correlation are found to be very close to those of other researchers which are based on actual diesel engine data. This further confirms the validity of using the constant volume combustion bomb to simulate an actual

engine. It also confirms the validity of the graphical analysis method used in this research.

- (9) Experiments on the combustion bomb show that the heat transfer effect is significant in dual fuel combustion and convection alone cannot estimate this effect sufficiently. Both convective and radiant heat transfer have been therefore taken into account in calculating the heat transfer effect.
- (10) Because no correlation for calculating the laminar flame speed of methane at $T=298$ K and $P=1$ atm over a range of equivalence ratio values is available in spite of much research has been reported, regression data from the literature has been performed and a correlation formula has been obtained. This correlation has been used in the turbulent flame propagation sub-model.
- (11) In performing the thermodynamic calculation, the current research applies a simple linear temperature function to estimate enthalpies of the combustion products. This simple approach gives almost identical results to that of more sophisticated methods used by other researchers for a wide range of combustion conditions. Coefficients of this linear function for common combustion products have been calculated.

8.2 Discussion and Recommendations for Further Research

Detail discussion of the computational and experimental results have been carried out previously in the appropriate chapters. The discussion here concerns the general method of approach being used in this research, the conclusions described in the last section and aspects on which further research effort is recommended.

- (1) **Phenomenological Modelling.** In general, the PM approach provides a reasonably accurate method to simulate the combustion process in an IC engine. This can be seen from the fact that phenomenological models

developed in this research can correctly predict the development trends of cylinder dynamic pressure with a reasonable level of accuracy for both sole diesel combustion and diesel-NG dual fuel combustion. This method can be very useful for various applications such as total engine calculations and the general analysis of engine performance. However, when there is concern at a more detailed level, such as the onset of abnormal combustion (engine knock) and ignition failure, phenomenological modelling seems to be incapable of giving a correct prediction. This can also be seen from the fact that the no sudden abrupt change of the pressure trace can be obtained from the current calculation although it often is in the measurements. Neither are the current calculation models able to predict ignition failure. Therefore, when the problem under consideration is at such a detailed level, fluid-dynamic based dimensional modelling seems to be inevitable.

- (2) **Numerical method.** In performing the discretization of the model's governing differential equations, the burned mass fraction x_b rather than the time t is chosen as the variable to be differenced so that a fixed boundary of $0 \leq x_b \leq 1$ for all combustion is obtained for discretization. In order to improve the accuracy of the numerical solution, a Runge-Kutta fourth order algorithm has been used in the discretization, and the entire combustion process is divided into 20,000 mesh points. That is, the computing step for the algebraic finite difference equations is as small as $\Delta x_b = 5.0E - 5$.
- (3) **Language and machine dependency.** All calculations are computed by double precision FORTRAN code in the VAX 6000-520 machine under the VAX/VMS V5.4-3 system. Computational results have also been checked against those computed in the IBM 3090 system. It was found that results of the double precision Fortran code were identical in both systems while results of single precision could have significant diversity. Double precision is therefore more appropriate. However, it has been also noted that a double precision Fortran code for the total engine simulation may not be possible in a DOS machine because the program may exceed

DOS memory capacity.

- (4) **The dual fuel ignition delay.** Dual fuel ignition delay has been noted as an important factor in determining the combustion pattern. Although a correlation has been proposed, further investigation of the dual fuel ignition delay is recommended. In particular, further experimental studies of the affects of initial pressure, temperature, pilot injection and gaseous fuel concentration no the ignition delay are required.
- (5) **Further experimental study.** So far, dual fuel experiments have been carried out for NG only. Other common gaseous fuels such as LPG can also be used for further experiments in order to have a better understanding of the dual fuel combustion phenomenon. Also, measurement and visualization experiments of the premixed flame propagation in a vaporised diesel-air mixture and diesel-gas-air mixture could be very useful.
- (6) **Improvement of the experimental rig.** Although the present experimental setup can successfully record the entire pressure trace of a combustion with excellent accuracy, some parts of the setup still need to be improved. These include an improved injection device to obtain precise control of the pilot injection, a better heating system so that the temperature of the cylinder charge can be precisely controlled and a uniform temperature distribution can be obtained and a better method to introduce the gaseous fuel so that the gaseous fuel concentration can be controlled more precisely.
- (7) **Total engine simulation.** As the primary work for incorporating the current combustion model into a total engine simulation package has been carried out, including converting the original single precision Fortran code to a double precision code and modifying the input procedure so that it can be used in dual fuel combustion and becomes more user friendly, further incorporation of the combustion model can therefore proceed with relative ease.

REFERENCE

- [1] Karim, G. A., "Some measures towards enhancing the performance of methane fuelled diesel engine at light road". Paper 59, Int. Assoc. NGV Conf. Buenos Aires, Oct., 1990
- [2] Wood, J., "The natural gas company offers efficient options". *Energy Focus*. (Edited by Dept. Minerals and Energy). vol 2/No 1, Sept. 1990
- [3] Boyer, R. L., "Status of dual-fuel engine development". SAE FL 1949 **57**,46
- [4] Karim, G. A., "Knock in dual-fuel engines". *Proc Instn Mech Engrs* 1966-67, vol 181 pt 1 No 20 pp453-466
- [5] Elliot, M. A. ,and Davis,R. M., " Dual-fuel engine combustion in diesel engines",*Ind. Engng Chem. ind.(int.)* Edn 1951 **64**, 2854
- [6] Moore, N. P. W. and Lewis, J. D. " An investigation of combustion in dual -fuel engines",IV Congres International du Chauffage Industriel (10/3/1952)
- [7] Felt, A. E. and Steel, W. A., " Combustion control in dual-fuel engine", S.A.E. Trans 1962, **70**,644
- [8] Karim, G. A., and Burn, K. S., "The combustion of gaseous fuels in a dual fuel engine of the compression ignition type with particular reference to cold intake temperature condition", SAE 800263
- [9] Nielsen, O. B., Qvale, B., and Sorenson, S. , " Ignition delay in the dual fuel engine", SAE 870589

- [10] Milton, B. E., "Improving the performance of small dual-fuelled engines". paper 22, First NGV International Conf. and Exhibition, Oct.1988 Sydney Australia
- [11] Thyagarajan V., Gajendra Babu, M. K., " A combustion model for a dual fuel direct injected diesel engine". Pro. int. Symposium on Diagnostics & Modelling of combustion in reciprocating engines, 1985, Tokyo
- [12] Rafiqul, I., Subrahmanyam, J. P., Gajendra Babu, M. K., " Combustion modelling of a dual-fuel indirect injection compression ignition engine", C-5, Proc. vol I, IX National Conf. on IC engines and combustion, Dehra Dun, India, Nov. 1985
- [13] Nielsen, O. B., and Sorenson, S. C., "The interaction of liquid and gaseous fuels in the dual fuel engine", C49/88, *Proceeding of IMechE Conf 1988*
- [14] Karim, G. A., " The dual fuel engine of the compression ignition type- prospects, problems and solutions - A review", SAE 831073
- [15] Karim, G. A., " A review of combustion processes in the dual fuel engine - the gas diesel engine", *Prog. Energy Combust. Sci. Vol6, pp.277-285*
- [16] Walker, I., " Australia NGV research and development", paper 9, Int. Assoc. NGV conf., Buenos Aires, Oct 1990
- [17] Blumberg, P. N., Lavoie, G. A., Tabaczynski, R. J., " Phenomenological Models for Reciprocating Internal Combustion Engines", *Prog. Energy Combust. Sci., 1979, Vol. 5, pp.123-167*
- [18] Heywood, J. B., *Combustion Modeling in Reciprocating Engine* , Plenum Press. New York. 1980, p.1.
- [19] Heywood, J. B., *Internal Combustion Engine Fundamentals* , McGraw-Hill. New York. 1988.
- [20] Lavoie, G. A., Heywood, J. B., and Keck, J. C., " Experimental and Theoretical Study of Nitric Oxide Formation in Internal Combustion Engines", *Combustion Science and Technology* 1970, vol. 1, pp.313-326.

- [21] Chase, M. W., et al. *JANAF Thermochemical Tables*, 3rd Edition, National Bureau of Standards Publication (1985).
- [22] Campbell, A. S., *Thermodynamic Analysis of Combustion Engines*, John Wiley & Sons, Inc. (1979).
- [23] Svehla, R. A., and McBride, B. J., :“Fortran IV Computer Program for Calculation of Thermodynamic and Transport Properties of Complex Chemical Systems”, NASA Technical Note TND - 7056, NASA Lewis Research Center, 1973.
- [24] Strehlow, R. A.,: *Combustion Fundamentals*, McGraw - Hill, Inc., 1984, pp. 517-527.
- [25] Weinberg, F. J., :“ Calculation of Equilibrium Gas Compositions”, Proc. R. Soc., London, **241A**: 132 (1957).
- [26] Gordon, S., and McBride, B. J.:“ Computer Program for the Calculation of Complex Chemical Equilibrium Composition , Rocket Performance, Incident and Reflected Shocks, and Chapman-Jouguet Detonations,” NASA publication SP-273,1971(NTIS number N71-37775).
- [27] Svehla, R. A., and McBride, B. J.:“ Fortran IV Computer Program for Calculation of Thermodynamic and Transport Properties of Complex Chemical System,” NASA technical note TND 7056, 1973(NTIS number N73-15954).
- [28] Press, W. H., Flannery, B. P., Teukolsky, S. A., and Vetterling W. T. : *Numerical Recipes in C - the Art of Scientific Computing* , Cambridge Univesiry Press (1988),pp517-558.
- [29] Gosman, A. D., Johns R. J. R. and Watkins, A. P.“ Assessment of a Prediction Method for in-cylinder Processes in Reciprocating Engines,” General Motors Research Laboratories Symposium on Combustion Modeling in Reciprocating Engines, Warren, Michigan, November 1978.

- [30] Reynolds, W. C.(1980), Modelling of Fluid Motions in Engines: An Introductory Overview, in *Combustion Modelling in Reciprocating Engines* (Ed., J.N. Mattavi and C.A. Amann). Plenum Press, New York.
- [31] Rubesin, M.W. and Rose, W. C.: “ The Turbulent Mean-flow, Reynolds-stress and Heat-flux Equations in Mass-averaged Dependent Variables,” NASA TMX 62,248, March 1973.
- [32] Watkins, A.P., “ Flow and Heat Transfer in Piston / Cylinder Assemblies,” Ph.D Thesis, Univ. London,1977.
- [33] ElTahry, S., “ k- ϵ Equation for Compressible Reciprocating Engine Flows,” *Journal of Engery*, Vol.7. No. 4,pp. 345-353,1983.
- [34] Morel, T. and Mansour, N. N. ,“ Modeling of Turbulence in Internal Combustion Engines,” SAE paper No.820040, 1982.
- [35] Ahmadi-Befrui, B., Gosman, A. D., and Watkins, A. P., “ Prediction of In-cylinder Flow and Turbulence with Three Versions of k- ϵ Turbulence Model and Comparison with Data,” in T.Uzkan(Ed.) *Flows in Internal Combustion Engines -II,FED-* vol. 20,p.27, ASME, New York 1984.
- [36] El Tahry, S. H.:“Application of a Reynolds Stress Model to Engine Flow Calculations,” in T.Uzkan(Ed.),*Flows in Internal Combustion Engines - II,FED* - vol. 20, pp.39-46, ASME, New York, 1984.
- [37] Ferieger, J.H.:“Large Eddy Simulations of Turbulent Flows,” AIAA paper 76-347,1976.
- [38] Clark, R. A., Ferziger, J. H. and Reynolds, W. C.:”Evaluation of Subgrid-Scale Turbulence Models Using a Fully Simulated Turbulent Flow,” Jour. of Fluid Mech.,Vol.91,pp. 1-16,1979.
- [39] Kwak, D., Reynolds, W. C. and Ferziger, J. H.:“ Three-Dimensional ,Time-Dependant Computation of Turbulent Flows,” Report TF-5, Dept. of Mech. Engrg., Stanford Univ.,1975.

- [40] Shaanan, S., Ferziger, J. H. and Reynolds, W.C.: "Numerical Simulation of Turbulence in the Presence of Shear," Report TF- 6, Dept. of Mech. Engrg., Stanford Univ., 1975.
- [41] Mansour, N. N., Moin, P., Reynolds, W. C. and Ferziger, J. H.: "Improved Methods for large-Eddy Simulation of Turbulence," *Proc. Symp. on Turbulent Shear Flows*, Pennsylvania State Univ., 1977.
- [42] Mansour, N. N., Ferziger, J. H. and Reynolds, W.C.: "Large Eddy Simulation of a Turbulent Mixing Layer," Report TF-11, Dept. of Mech. Engrg., Stanford Univ., 1978.
- [43] Amsden, A. A., Butler, T. D., O'Rourke, P. J. and Ramshaw, J. D.,: "KIVA - A Comprehensive Model for 2-D and 3-D Engine Simulations ," SAE paper 850554, 1985.
- [44] Bulter, T. D., Cloutman, L. D., Dukowicz, J. K. and Ramshaw, J. D.: "Multidimensional Numerical Simulation of Reactive Flow in Internal Combustion Engines," in *Prog. Energy Combust.*, Vol.7, pp.293-315, 1981.
- [45] Gosman, A. D., Johns, R. J. R. and Watkins, A. P., "Development of Prediction Methods for In-cylinder Processes in Reciprocating Engines," in *Combustion Modelling in Reciprocation Engines* , Mattavi, J. N. and Amann, C. A. Eds., Plenum Press, pp. 69-124, 1980
- [46] Gosman, A. D. and Johns, R. J. R.: " Developments of a predictive Tool for In-cylinder Gas Motion in Engines," SAE paper No. 780315, 1978.
- [47] Ramos, G. I. and Sirignano, W. A.: "Axisymmetric Flow Model with and Without Swirl in a Piston-cylinder Arrangement with Idealized Valve Operation," SAE paper No. 800284, 1980.
- [48] Markatos, N. C. and Mukerjee, T.: "Three-Dimensional Computer Analysis of Flow and Combustion in Automotive Internal Combustion Engines," IMACS, Vol. XXIII, No. 4, 1981.
- [49] Butler, T. D., Cloutman, L. D., Dukowicz, J. K. and Ramshaw, J. D., "COHCHAS: An Arbitrary Lagrangian-Eulerian Computer Code for

Multi-Component Chemically Reactive Fluid Flow at All Speeds," Los Alamos Scientific Laboratories Report No. LA-8129-MS,1979.

- [50] Raithby, G. D.: "Skew Upstream Differencing Schemes for Problems Involving Fluid Flow," in *Computer Methods in Applied Mechanics and Engineering*, Vol 9, p153,1975.
- [51] Sirignano, W. A.: " One-Dimensional Analysis of Combustion in Spark-Ignition Engine," *Combustion Science and Technology*, vol. 70, pp 99-108,1973.
- [52] Westbrook, C. K.: " Fuel Motion and Pollutant Formation in Stratified Charge Combustion," SAE International Congress and Exposition, Detroit, Michigan. SAE paper No. 790248,1979.
- [53] Singh, T. and Surakomol, K.: " Mathematical Modeling of Combustion Process in a Spark-Ignition Engine," SAE International Congress and Exposition, Detroit, Michigan, SAE paper No. 790354,1979.
- [54] Bellan, J. R. and Sirignano, W. A., " A Theory of Tubulent Flame Development and Nitric Oxide Formation in Stratified Charge Internal Combustion Engines," *Combustion Science and Technology* vol. 8, pp.51-68,1973.
- [55] Bellan, J. R. and Sirignano, W. A.: " Combustion and NO Formation in a Stratified - Charge Engine: A Two-Turbulent Equations Model," *Combustion Science and Technology* ,vol.12, pp.75-104,1976.
- [56] Wallis, G. B., *One-Dimensional Two-Phase Flow*, McGraw-Hill ,New York,1969.
- [57] Shimamoto, Y., Oka, M. and Tanaka, Y.: "A Research on Inertia Charging Effect of Intake System in Multi-cylinder Engines." Bull. JSME 21, No.153, 1978.
- [58] Kurkov, A. P. and Mirsky, W.: "An analysis of the mechanism of flame extinction by a cold wall." *Twelfth Symposium (International) on Combustion*. The Combustion Institute. 1969

- [59] Bracco, F. V.: "Theoretical Analysis of Stratified, Two-Phase Wankel Engine Combustion," *Combustion Science and Technology*, vol.8, pp.69-84, 1973.
- [60] Reitz, R. D. and Bracco, F. V.: "Studies Toward Optimal Charge Stratification in a Rotary Engine", *Combustion Science and Technology*, vol.12, pp. 63-74, 1976.
- [61] Przekwas, A.: "Modeling of Fluid Flow Heat Transfer and Flame Propagation in Reciprocating Engines," in *Flow in Internal Combustion Engines*, ed. T. Uzman, pp.73-79, ASME. New York, 1982.
- [62] Smith, J. R., "Turbulent Flame Structure in a Homogeneous- Charge Engine," SAE International Congress and Exposition, Detroit, Michigan, SAE paper No.820043, 1982.
- [63] Hakberg, B. and Gosman, A. D., "Analytical Determination of Turbulent Flame Speed from Combustion Models," *Twentieth Symposium (International) on Combustion*. pp.225-232, The Combustion Institute, Pittsburgh, Pennsylvania, 1984.
- [64] Ahmadi-Befrui, B., Gosman, A. D., Lockwood, F. C. and Watkins, A. P., "Multidimensional Calculation of Combustion in an Idealised Homogeneous Charge Engine: A Progress Report," SAE International Congress and Exposition, Detroit, Michigan, SAE Paper No 810151, 1981.
- [65] Abraham. J., Bracco, F. V. and Reitz, R. D., "Comparisons of Computed and Measured Premixed Charge Engine Combustion," *Combustion and Flame* vol.60, pp.309-332, 1985.
- [66] Bracco, F.V. and O'Rourke, P. J., "A Review of Initial Comparisons of Computed and measured Two-Dimensional Unsteady Flame Fields," *Progress in Energy and Combustion Science*, vol.7, pp.103-124, 1981.
- [67] Markatos, N. C. and Mukerjee, T., "Three-Dimensional Computer Analysis of Flow and Combustion in Automotive Internal Combustion Engines",

Mathematics and Computers in Simulation, vol. XXIII, no. 4, pp.354-366,1981.

- [68] Griffin, M. D., Diwakar, R., Anderson, J.D. and Jones, E.,“ Computational Fluid Dynamics Applied to the Flow in an Internal Combustion Engine,” AIAA 16th Aerospace Sciences Meeting,Huntsvill, Alabama,Paper No.78-57,1978.
- [69] Griffin, M. D., Anderson, J. D. and Jones, E.,“Computational Fluid Dynamics Applied to Three-Dimensional Nonreacting Inviscid Flows in an Internal Combustion Engine”, *ASME Journal of Fluid s Engineering*, vol.101, pp. 367-372,1979.
- [70] Oppenheim, A. K. and Rotman, D. A.,“Fundamental Features of Ignition and Flame Propagation in Engines,” Energy-Sources Technology Conference and Exhibition, Dallas, Texas, Paper No.87-ICE-21,ASME New York 1978.
- [71] Gosman, A. D.,:“Multidimensional Modeling of Cold Flows and and Turbulence in Reciprocating Engines,” SAE paper 850344,1985.
- [72] Bray, K. N. C., Libby, P. A., Masuya, G. and Moss, J. B.,“Turbulence Production in Premixed Turbulent Flames,” *Combustion Science and Technology*, vol.25,pp.127-140,1981.
- [73] Sirignano, W. A.,“The Formulation of Spray Combustion Models:Resolution Compared to Droplet Spacing,” *ASME Journal of Heat Transfer*, vol.108, pp.633-639,1986.
- [74] Gupta, H. C. and Bracco, F. V.,“Numerical Computations of Two-Dimensional Unsteady Sprays for Application to Engines,” AIAA Journal, vol.16, no.10, pp.1053-1061,1978.
- [75] Westbrook, C. K.,“Three-Dimensional Numerical Modeling of Liquid Fuel Sprays,” *Sixteenth Symposium(International) on Combustion*, pp.1517-1526, The Combustion Institute, Pittsburg, Pennsylvania, 1977.

- [76] Prakash, S. and Sirignano, W. A., "Theory of Convective Droplet Vaporization with Unsteady Heat Transfer in the Circulating Liquid Phase," *International Journal of Heat and Mass Transfer*, vol.23, no.3, pp.253-268, 1980.
- [77] Sirignano, W. A., "Fuel Droplet Vaporization and Spray Combustion Theory," *Progress in Energy and Combustion*, vol.9, pp.291-322, 1983.
- [78] Aggarwal, S. K., Tony, A. Y. and Sirignano, W. A., "A Study of Inter-Phase Exchange Laws in Spray Combustion Modeling," AIAA 21st Aerospace Sciences meeting. Reno, Nevada, paper No.AIAA-83-0152,1983.
- [79] Gosman, A. D. and Johns, R. J. R., "Computer Analysis of Fuel-Air Mixing in Direct-Injection Engines," SAE International Congress and Exposition, Detroit, Michigan, SAE paper No.800091,1980.
- [80] Gosman, A. D., and Harvey, P. S., "Computer Analysis of Fuel-Air Mixing and Combustion in an Axisymmetric D.I. Diesel Engine," SAE International Congress and Exposition, Detroit, Michigan. SAE paper, No. 820036, 1982.
- [81] Nguyen, H. L, Schock, H. J., Carpenter, M. H. and Ramos, J. I. and Stegeman, J. D., "Numerical Simulation of the Flow Field and Fuel Sprays in an IC Engine," SAE International Congress and Exposition, Detroit, Michigan, SAE paper No.870599, 1987.
- [82] Dukowicz, J.K., "A Particle-Fluid Numerical Model for Liquid Sprays," *Journal of Computational Physics*, vol. 35, pp 229-253, 1980.
- [83] Grasso, F. and Bracco, F. V., "Evaluation of a Mixing-Controlled Model for Engine Combustion," *Combustion Science and Technology*, vol.28, pp.185-210,1982.
- [84] Blumberg, P. N., Lavoie, G. A., and Tabaczynski, R. J.,: " Phenomenological Models for Reciprocating Internal Combustion Engines," *Prog. Energy Combust. Sci.*, 1979, vol.5 , pp.123-167.

- [85] Patterson, D. J. and Van Wylen, G., " Digital Computer Simulation for Spark Ignition Engine Cycles," SAE paper 633F(1962)
- [86] Blumberg, P. N. and Kummer, J., "Prediction of Nitric Oxide Formation in Spark Ignited Engines - an Analysis of Methods of Control, " *Comb. Sci. Tech*, 4, 73-95(1971).
- [87] Komiyama, K. and Heywood, J., "Prediction NO Emissions and Effects of Exhaust Gas Recirculation in Spark-ignition Engines," Paper 730475 presented at SAE National Automobile Engineering Meeting, Detroit, 1973.
- [88] Lucas, G. G. and Varde, K. S., "Analysis of nitric oxide formation in spark ignition with heat transfer and effect of ignition point." Paper 740189 presented at SAE Automotive Engineering Congress and Exposition, Detroit, 1974.
- [89] Chen, K. K., and Krieger, R. B., " A statistical analysis of the influence of cyclic variation on the formation of nitric oxide in spark ignition engines," *Combust. Sci. Tech.* ,12, 125-134, 1976.
- [90] Sakai, Y., Miyazaki, H. and Mukai, K., " The effect of combustion chamber shape on nitrogen oxides," SAE Paper 730154(1973).
- [91] Annand, W. J. D., Daneshyar, H. and Watfa, M., "Calculation of nitric oxide and carbon monoxide concentrations in spark-ignited engine, " *Proc. Inst. Mech. Engrs.* 188, 41/74 (1974).
- [92] Watfa, M. and Daneshyar, H., "Formation of nitric oxide, carbon monoxide and unburnt hydrocarbons, in spark ignited engines," Institute of Mechanical Engineers, Paper C99/75 (1975).
- [93] Keck, J. C. and Gillespie, D., "Rate Controlled Partial Equilibrium Method for Treating Reacting Gas Mixtures," *Combust. Flame*, 17, 237 (1971).

- [94] Sherman, K. H. and Blumberg, P. N., "The Influence of Induction and Exhaust Processes on Emissions and Fuel Consumption in the Spark Ignited Engine," Paper
- [95] Bension, R. S., Annand, W. J. and Baruah, P. C., "A Simulation Model Including Intake and Exhaust Systems for a Single Cylinder Four-stroke Cycle Spark Ignition Engine," *Int. J. Mech. Sci.* 17,97-124, 1975.
- [96] Blizard, N. C. and Keck, J. C., "Experimental and Theoretical Investigation of Turbulent Burning Model for Internal Combustion Engines", Paper 740191 presented at SAE Automotive Engineering Congress and Exposition, Detroit 1974.
- [97] Tabaczynski, R. J., Ferguson, C. R. and Radhakrishnan, K., "A Turbulent Entrainment Model for Spark-Ignition Engine Combustion," SAE paper 770647, 1977.
- [98] Hires, S. D., Tabaczynski, R. J. and Novak, J. M., "The Prediction of Ignition Delay and Combustion Intervals for a Homogeneous Charge Spark-ignition Engine," SAE 780232, 1978.
- [99] Heywood, J. B., Tabaczynski, R. J., Higgins, J. M. and Briggs, M. "A Modeling Study of the Fuel Consumption and NO_x Emissions of Spark-ignition Engines over a Range of Design and Operating Conditions," ERDA Contract E(11-1)-2881, 1976.
- [100] Lavoie, G. A. and Blumberg, P. N., "A Fundamental Model for Predicting Emissions and Fuel Consumption for the Conventional Spark-ignition Engine," Paper presented at the Fall Technical Meeting, Eastern States Section, The Combustion Institute, Hartford, Connecticut, 1977.
- [101] Huls, T. A., Myers, P. S. and Uyehara, O. A., "Spark Ignition Engine Operation and Design for Minimum Exhaust Emission," *SAE Progress in Technology Series*, Vol.12, Vehicles Emission Part II, p.71; originally in SAE Trans. 75(1976).

- [102] Strange, F. M. " An Analysis of the Ideal Cycle,including the Effects of Heat Transfer, Finite Combustion rates, Chemical Dissociation, and Mechanical Losses," *SAE Progress in Technology Series*, Vol. TP-7 (1964).
- [103] Trumphy, D. K., Uyehara, O. A. and Myers, P. S., "The Pre-knock Kinetics of Ethane in a Spark Ignition Engine," SAE690518,1969.
- [104] Jain, B. C., Rife, J. M. and Keck, J. C., " A Performance Model for the Texaco Controlled Combustion Stratified Charge Engine," SAE paper 760116, 1976.
- [105] Whitehouse, N. D., Stotter. A., Goudie, G. O. and Prentice, B. W., "Method of Predicting Some Aspects of Performance of a Diesel Engine Using a Digital Computer," *Proc. Inst. Mech. Eng.(London)*, 176, No.9 (1962).
- [106] Benson, R. S., " A Comprehensive Digital Computer Program to Simulate a Compression Ignition Engine including Intake and Exhaust System ," SAE paper 710173, 1971.
- [107] Whitehouse, N. D. and Way, R. J. B., "A Simple Method for the Calculation of Heat Release Rates in Diesel Engines Based on the Fuel Injection Rate," SAE paper 710134, 1971.
- [108] Whitehouse, N. D. and Sareen, B. K., "Prediction of Heat Release in a Quiescent Chamber Diesel Engine Allowing for Fuel/Air Mixing ," SAE Paper 740084(1974).
- [109] Watson, N., Pilley, A. D. and Marzouk, M.: "A Combustion Correlation for Diesel Engine Simulation," SAE paper 800029,1980.
- [110] Lyn, W.-T. : "Study of Burning Rate and Nature of Combustion in Diesel Engines," in *Proceedings of Ninth International Symposium on Combustion*, pp. 1069-1082, The Combustion Institute, 1962.
- [111] Kumar, K., Babu, M. K. G., Gaur, R. R. and Garg, R. D., "A Thermodynamic Simulation Model for a Four Stroke Medium Speed Diesel Engine,"

- SAE International Congress and Exposition, Detroit, Michigan, SAE paper No.840516, 1984.
- [112] Hiroyasu, H., Kadota, T. and Arai, M., "Development and Use of a Spray Combustion Modeling to Predict Diesel Engine Efficiency and Pollutant Emissions. Part 1: Combustion Modelling," *Bulletin of the JSME*, vol. 26, No 214, pp569-575, 1983.
 - [113] Chiu, W. S., Shahed, S. M. and Lyn, W. T., "A Transient Spray Mixing Model of Diesel Combustion," SAE paper 760128.
 - [114] Dent, J. C. and Meththa, P. S.,: "Phenomenological Combustion Model for a Quiescent Chamber Diesel Engine," SAE 811235, 1981.
 - [115] Kamimoto, T., Chang, Y. T. and Kobayashi, H., "Rate of Heat Release and Its Prediction of a Diesel Flame in a Rapid Compression Machine," SAE International Congress and Exposition, Detroit, Michigan, SAE Paper No. 841076, 1984.
 - [116] Kau, C. J., Tyson, T. J. and Heap, M. P., "A Study of Oxides of Nitrogen from DDiesel Engines," EPA-CRC Report P-76-16, (March 1976).
 - [117] Wilson, R. P., Jr., Waldeman, C. H. and Muzio, L. J., "Foundation for Modeling NO_x and Smoke Formation in Diesel Flames. Final Report for Phase I," EPA-460/3-74-002a (January 1974).
 - [118] Bastress, E. K., Chng, K. M. and Dix, D. M., (Northern Research and Engineering Corporation), " Modeling of Combustion and Nitric Oxide Formation in Direct and Indirect Injection Compression-ignition engines," 1971 Inter Society Energy Conversion Conference. Boston, SAE Paper 719053 (1971).
 - [119] Shahed, S. M., Chiu, W. and Yumlu, V. S., " A Preliminary Model for the Formation of Nitric Oxide in DI Diesel Engines and Its Application in Parametric Studies," SAE Paper 730083 (1973).
 - [120] Khan, I. M., Greeves, G. and Probert, D. M., "Prediction of Soot and Nitric Oxide Concentration in Diesel Engine Exhaust," Conference on Air

Pollution Control in Transport Engines, Institute of Mechanical Engineers z(1971).

- [121] Witze, P. O.: "The Effect of Spark Location on Combustion in a Variable-Swirl Engine," SAE paper 820044, SAE Trans., vol.91, 1982.
- [122] Keck, J. C.: "Turbulent Flame Structure and Speed in Spark-Ignition Engines," *Proceeding of the Nineteenth International Symposium on Combustion*, The Combustion Institute, pp. 1451-1466, 1982.
- [123] Ramos, J. I., lectures on Mathematics Models of Spark-ignition Engines, in *Computer Simulation of Fluid Flow, Heat and Mass Transfer, and Combustion in Reciprocating Engines*, ed. N.C. Markatos, Hemisphere Publishing Corporation, New York, 1989.
- [124] Tabaczynski, R. J., Trinker, F. H. and Shannon, B. A., "Further Refinement and Validation of a Turbulent Flame Propagation Model for Spark-Ignition Engines," *Combust. Flame* **39**, 111-121 (1980).
- [125] Beretta, G. P., Rashidi, M. and Keck, J. C.: "Turbulent Flame Propagation and Combustion in Spark Ignition Engines," *Combust. Flame*, vol.52, pp.217-245, 1983.
- [126] Keck, J. C., Heywood, J. B., and Noske, G.: "Early Flame Development and Burning Rates in Spark-Ignition Engines," SAE paper 870164, 1987.
- [127] Egolfopoulos, F. N., CHO, P. and Law, C. K.: "Laminar Flame Speeds of Methane-Air Mixtures Under Reduced and Elevated Pressures," *Combustion and Flame*, **76**, pp. 375-391, 1989.
- [128] Yu, G., Law, C. K. and Wu, C. K.: "Laminar Flame Speeds of Hydrocarbon + Air Mixtures with Hydrogen Addition," *Combustion and Flame*, **63**, pp. 339-347, 1986.
- [129] van Oostendorp, D.L. and Levinsky, H. B.: "The Effects of Fuel and Non-Fuel Gases on the laminar Burning Velocity of Methane-Air Flames," *Journal of the Institute of Energy*, **63**, pp. 160-166, Decembr 1990.

- [130] Annand, W. J. D.; "The Estimation of Flame Propagation Rates in Routine Computer Synthesis of Spark-Ignition Engine Combustion," *Combustion in Engineering*, vol. 1, C48/83, pp. 125-134, IMechE 1983.
- [131] Ohyagi, S., Harigaya, Y., Kakaizaki, K., and Toda, F.; "Estimation of Flame Propagation in Spark-Ignition Engine by Using Turbulent Burning Model," *Proceeding of International Symposium on Diagnostic and Modeling of Combustion in Reciprocating Engines*, COMODIA 85, Tokyo 1985.
- [132] Daneshyar, H. and Hill, P. G.; "The Structure of Small-Scale Turbulence and Its Effect on Combustion in Spark Ignition Engines," *Prog. Energy Combust. Sci.* Vol.13, pp. 47-73, 1987.
- [133] Hill, P. G.; "Cyclic Variations and Turbulence Structure in Spark-Ignition Engines," *Combustion and Flame*, Vol.72, pp. 73-89, 1988.
- [134] Lilly, L. C. R. (Ed) : "Diesel Engine Reference Book," Butterworth and Co (Publishers) Ltd (1984).
- [135] Whitehouse, N. D., and Baluswamy, N.: "Calculation of Gaseous Products During Combustion in a Diesel Engine Using Four Zone Model," SAE paper, SAE770410, 1977.
- [136] Hiroyasu, H., Kadota, T. and Arai, M.: "Supplementary Comments: Fuel Spray Characterisation in Diesel Engines," *Combustion Modelling in Reciprocating Engines*, Plenum Press, 1980.
- [137] Abramovich, G. N.: "The Theory of Turbulent Jets," The M.I.T. Press, Mass., 1963.
- [138] Ricou, F. P. and Spalding, D. B.: "Measurements of Entrainment by Axisymmetrical Turbulent Jets," *J. Fluid Mechanics*, vol. 11, 1961.
- [139] Dent, J. C.: "A Basis for the Comparison of various Experimental Methods for Studying Spray Penetration," S.A.E. Paper SAE710571, 1971.

- [140] Hardenberg, H. O. and Hase, F. W.: "An Empirical Formula for Computing the Pressure Rise Delay of a Fuel from its Cetane Number and from the relevant Parameters of Direct-Injection Diesel Engines," SAE paper 790493, 1979.
- [141] Shahed, S. M., Flynn, P. F. and Lyn, W. T.: "A Model for Formation of Emission in A Direct-Injection Diesel Engine," in *Combustion Modeling in Reciprocation Engines*, Eds. Mattavi, J.N. and Amann, C.A. pp. 345-368. Plenum Press, New York 1980.
- [142] Hiroyasu, H.: "Diesel Engine Combustion and Its Modeling," in *Proc. Int. Symposium on Diagnostics and Modeling of Combustion in Reciprocation Engines*, Tokyo, 1985.
- [143] Sareen, B. K.: "Relationship between Fuel Injection and Heat Release in a Quiescent Chamber Diesel Engine," Ph.D. thesis, Univ. of Manchester, Institute of Science and Technology, England, 1972.
- [144] Reitz, R. D. and Bracco, F. B., "On the Dependence of Spray Angle and Other Spray Parameters on Nozzle Design and Operating Conditions," SAE paper 790494, 1979.
- [145] Kou, T., Yu, R. C., and Shahed, S. M.: "A Numerical Study of the Transient Evaporation Spray Mixing Process in the Diesel Environment," SAE paper 831735, *SAE Trans.*, vol.92, 1983.
- [146] Elkotb, M. M.: "Fuel Atomization for Spray Modelling," in *Prog. Energy Combust Sci.*, 1982, Vol.8, pp. 61-91.
- [147] Faeth, G. M.: "Evaporation and Combustion of Sprays," in *Prog. Energy Combust. Sci.*, 1983, vol.9, pp. 1-76.
- [148] Bracco, F. V.: "Modeling of Engine Sprays," SAE paper 850394, 1985.
- [149] Pischinger, F., Reuter, U. and Scheid, E.: "Self-Ignition of Diesel Sprays and Its Dependence on Fuel Properties and Injection Parameters," , *Journal of Engineering for Gas Turbines and Power*, Vol. 110, pp.399-404. July 1988.

- [150] Wolfer, H. H.: "Ignition Lag in Diesel Engines," VDI-Forschungsheft 392, 1938; Translated by Royal Aircraft Establishment, Farnborough Library No. 358, UDC 621-436.047, August 1959.
- [151] Fujimoto, H., et al.: "Illumination Delay in Diesel Spray," JSAE Paper No. 800-13, 1980, 149.
- [152] Balles, E. N. and Heywood, J. B.: "Spray and Flame Structure in Diesel Combustion," in *Journal of Engineering for Gas Turbines and Power*, Vol.111, pp.451-457, July 1989.
- [153] Dent, J. C.: "Turbulent Mixing Rate - Its Effect on Smoke and Hydrocarbon Emissions from Diesel Engines," S.A.E. paper 800092, 1980.
- [154] Karim, G. A., Jones, W. and Raine, R. R.: "An Examination of the Ignition Delay Period in Dual Fuel Engines," SAE International Fuel & Lubricants Meeting & Exposition, Baltimore, Maryland, SAE Paper 892140, 1989.
- [155] Lavoie, G. A. and Blumberg, P. N.: "A fundamental model for prediction fuel consumption, NO and NC emissions of the Conventional spark ignition engine," *Combustion Science and Technology*, vol.21 (1980).
- [156] Sumbally, R., Subrahmanm, J. P, and Gajendra Babu M. K.: "A combustion model for a dual fuel direct injection compression ignition engine," in *Proc. IX National Conf. on I.C.engine and Combustion*, Dehra Dun, India, Nov 1985.
- [157] The National Algorithms Group Limited : " The NAG Fortran Library Manual,," Mark 14, Vol3, E02. 1990.
- [158] Karim, G. A., Rain, R. R., and Jones, W.: "An Examination of Cyclic Variations in a Dual Fuel Engine," SAE paper, SAE881661, 1988.
- [159] Tanaka, Y.: "Numerical Simulations for Combustion of Quiescent and turbulent Mixtures in Confined Vessels," *Combustion and Flame*, 1988.

- [160] Spalding, D. B.: "The PHOENICS Computer Code," lectures in *Computer Simulation of Fluid Flow, Heat and Mass Transfer, and Combustion in Reciprocating Engines*, pp.383-396. ed. N.C. Markatos, Hemisphere Publishing Corporation, New York, 1989.
- [161] AMSDEN, A.: "KIVA: A Computer Program for Two- and Three- Dimensional Fluid Flows with Chemical Reactions and Fuel Sprays," lectures in *Computer Simulation of Fluid Flow, Heat and Mass Transfer, and Combustion in Reciprocating Engines*, pp.239-344. ed. N.C. Markatos, Hemisphere Publishing Corporation, New York, 1989.
- [162] Fujimoto, H., Shimoda, T. and Sato, T.: "Investigation on Combustion in Diesel Engines using a Constant Volume Combustion Chamber (Effects of Initial Temperature)", Bulletin of the JSME, vol. 22, No. 174, December 1979, Paper No.174-15.
- [163] Jackson, S. R.: "The Development of a Diesel Combustion Bomb," thesis of Bachelor of Engineering, the University of New South Wales, October, 1989.
- [164] Kuehl, D. K.: "Laminar burning velocities of propane-air mixture," *8th Symposium(international) on Combustion*, 1962, p510.
- [165] Fraser, R. A., Felton, P. G., Bracco, F. V. and Santavicca, D. A. : "Preliminary turbulence length scale in a motored engine," S.A.E paper No.860021(1986).
- [166] Batchelor, G. K.: *The theory of homogeneous turbulence*, Cambridge University Press(1982).
- [167] Kadota, T. and Hiroyasu, H., Trans. JAME., 42-365(1971), 1216,(in Japanese).
- [168] Hamamoto, Y., Izumi, M., Tomita, E. and Miyamoto, O. : "Direct Measurement of Burning Velocity of Flame Propagating in Fuel-Air Homogeneous Mixtures in a Closed Vessel," *JSME International Journal, Series II*, Vol.34, No.2, 1991.

- [169] Milton, B. E. and Keck, J. C. :“ Laminar Burning Velocities in Stoichiometric Hydrogen and Hydrogen-Hydrocarbon Gas Mixtures,” *Combustion and Flame*, **58**: 13-22 (1984).
- [170] Milton, B. E. :“Fundamental Problems in Minimising Pilot Distillate in Dual Fuel Engines,” *Progress Report* on NERDDC project. March 1991.
- [171] Metghalchi, M., and Keck, J. C.: “Laminar Burning Velocity of Propane-Air Mixtures at High Temperature and Pressure,” *Combust. Flame*, vol. 38, pp.143-154 ,(1980).
- [172] Ko, Y., Anderson, R. W., and Arpaci, V.S. :“Spark Ignition of Propane-Air Mixture Near the Minimum Ignition Energy: Part I. An Experimental Study,” *Combustion and Flame*, **83**: 75-87 (1991).
- [173] Ko, Y., Arpaci, V.S. and Anderson, R. W. :“Spark Ignition of Propane-Air Mixture Near the Minimum Ignition Energy: Part II. An Model Development,” *Combustion and Flame*, **83**: 88-105 (1991).
- [174] Hamamoto, Y., Izumi M., and Tomita E. :“ Effects of Swirl and Air-Fuel Ratio on Premixed Combustion in a Closed Vessel,” *JSME International Journal*, Series II, Vol.33, No. 2. 1990.
- [175] Nishida, K., Murakami, N. and Hiroyasu, H. :“ A Pulsed-Laser Holography Study of the Evaporating Diesel Spray in a High Pressure Bomb,” in *Proc. Int. Symposium on Diagnostics and Modeling of Combustion in Reciprocation Engines*, Tokyo, 1985.
- [176] Nishida, K., Murakami, N. and Hiroyasu, H.:“Holographic Measurement of Evaporating Diesel Sprays at High Pressure and Temperature,” *JSME International Journal*, Vol. 30, No. 259, 1987.
- [177] Hurn, R. W. and Hughes, K. J. :“ Combustion Characteristics of Diesel Fuels as Measured in a Constant-Volume Bomb,” *SAE Quarterly Transaction*, vol. 6, No. 1, January 1952.

- [178] Hiroyasu, H. and Kadota, T.: "Evaporation and Spontaneous Ignition Delay of a Fuel Droplet and Spray in High Pressure Gaseous Environments," Dept. of Mech. Eng., Hiroshima University, Automobile Exhaust Clarification Study Group, Feb., 1977.
- [179] Elkotb, M. M., Aly, S. L., and Elsalmawy, H. A. : "Evaporation of fuel and Multifuel Droplets", *Combustion and Flame*, 85: 300-308 (1991).
- [180] Tanaka, Y. and Milton, B. E. : "Three-Dimensional Analysis of Flames Ignited at Double Spark Locations," *Computers & Fluid* , Vol. 18, No. 4, pp. 347-359, 1990.
- [181] Bradley, D. and Lung. K. K.: "Spark Ignition and the Early Stages of Turbulent Flame Propagation," *Combustion and Flame* 69: pp. 71-93 (1987).

Appendix A

Coefficients of linear enthalpy function

Under the assumption an of ideal gas, the enthalpy values are functions of temperature only. Polynomial approximations of enthalpy for many species have been calculated by NASA [26],[27] as:

$$\frac{\tilde{h}}{\tilde{R}T} = a_1 + \frac{a_2}{2}T + \frac{a_3}{3}T^2 + \frac{a_4}{4}T^3 + \frac{a_5}{5}T^4 + \frac{a_6}{T} \quad (\text{A.1})$$

For an in-cylinder combustion, the temperature range of the unburnt and burnt zone are usually within 500 - 1000 K and 1000 - 3500 K, respectively. It is possible to find a good linear approximation, for both the unburnt and burnt zone respectively, to ease the thermodynamic analysis. By using a least squares linear regression program [28], modelling coefficients for a linear enthalpy equation as expressed in Table A.1 are obtained by fitting data to the function $h(T) = c_m T + [h_m + h_f^0]$. Data for ideal gases CH_4 , O_2 , O , N_2 , C , CO_2 , H_2O , H_2 , OH , NO , H , CO , N and NO_2 are from JANAF [21], while data for C_3H_8 , C_6H_{14} , C_8H_{18} , CH_3OH , C_2H_5OH , $C_{8.26}H_{15.5}$ and $C_{10.8}H_{18.7}$, not available from JANAF tables, are calculated by a polynomial function from [19]. In the table, h_f^0 is the enthalpy of formation (standard enthalpy) of the species and ϵ is the maximum relative error of the linear function to data. This usually only occurs at the boundary of the temperature range while inside the temperature range, it is much lower. Figures .1, .2, .3, and .4 compare the linear

Linear Enthalpy Function: $h(T) - h_f^0 = c_m T + h_m$							
		500 - 1000 K			1000 - 3500 K		
species	h_f^0 (kJ/mol)	c_m (kJ/mol.K)	h_m (kJ/mol)	ϵ (%)	c_m (kJ/mol.K)	h_m (kJ/mol)	ϵ (%)
CH_4	-74.873	0.57325E-01	-0.20429E+02	6.36	0.95092E-01	-0.63688E+02	17.75
N_2	0.000	0.30804E-01	-0.94994E+01	5.01	0.36087E-01	-0.15614E+02	4.61
O_2	0.000	0.32835E-01	-0.10323E+02	7.08	0.38238E-01	-0.16726E+02	5.25
O	249.170				0.20868E-01	-0.60157E+01	0.09
C_3H_8	-103.909	0.14715E+00	-0.53177E+02	6.61			
C_6H_{14}		0.35626E+00	-0.12314E+03	4.53			
C_2H_5OH	-234.6	0.90779E-01	-0.33541E+02	7.98			
C_8H_{18}	-224.1	0.35506E+00	-0.12830E+03	6.57			
CH_3OH	-201.2	0.84164E-01	-0.29344E+02	5.11			
$C_{8.26}H_{15.5}$	-259.28	0.43046E+00	-0.14897E+03	4.55			
$C_{10.8}H_{18.7}$	-394.20	0.46814E+00	-0.16781E+03	6.15			
CO	-110.53				0.36330E-01	-0.15541E+02	4.15
CO_2	-393.52				0.60554E-01	-0.28923E+02	5.29
H	218.00				0.20784E-01	-0.61920E+01	0.13
H_2	0.00				0.34868E-01	-0.15933E+02	8.44
H_2O	-241.86				0.51925E-01	-0.29441E+02	13.5
N	472.68				0.20846E-01	-0.62975E+01	0.28
NO	90.29				0.36735E-01	-0.15284E+02	3.50
NO_2	33.1				0.56478E-01	-0.25252E+02	3.45
OH	38.99				0.35033E-01	-0.15599E+02	7.17

Table A.1: Linear Model of Enthalpy Function for Unburnt and Burnt Zone

function to the original data from which the high ϵ species can be seen.

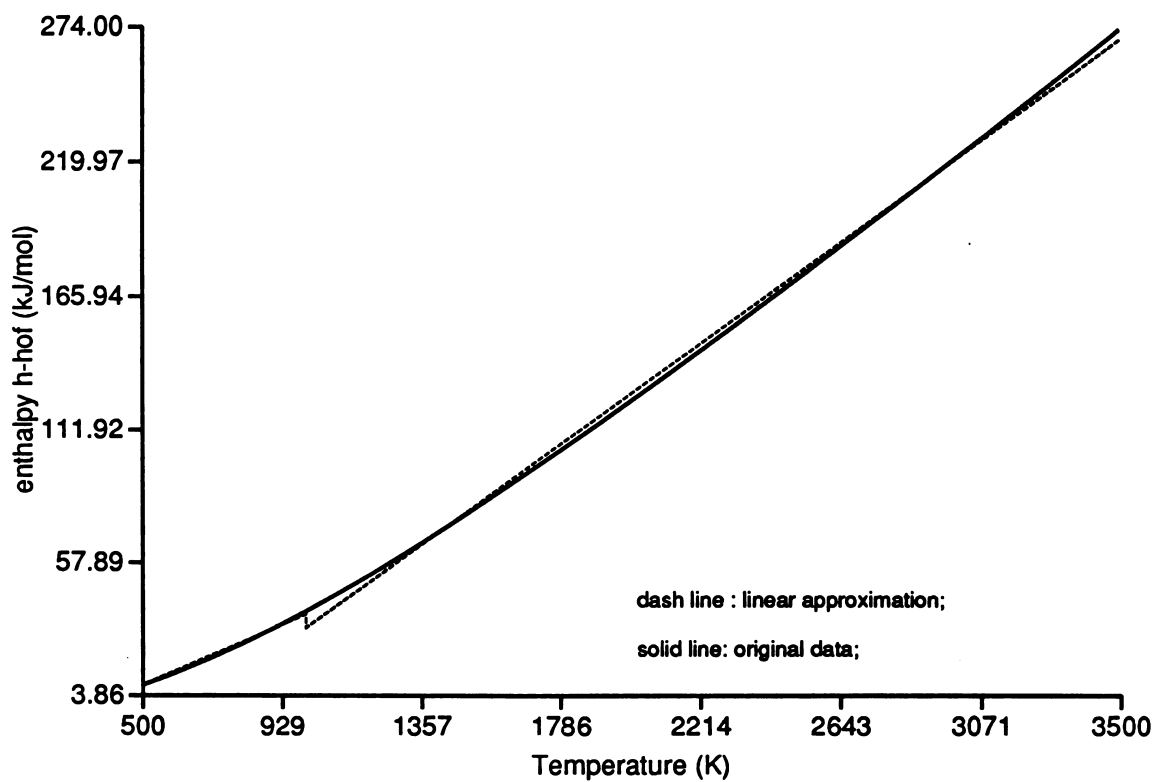


Fig .1 Enthalpy of Methane $\text{CH}_4(\text{G})$

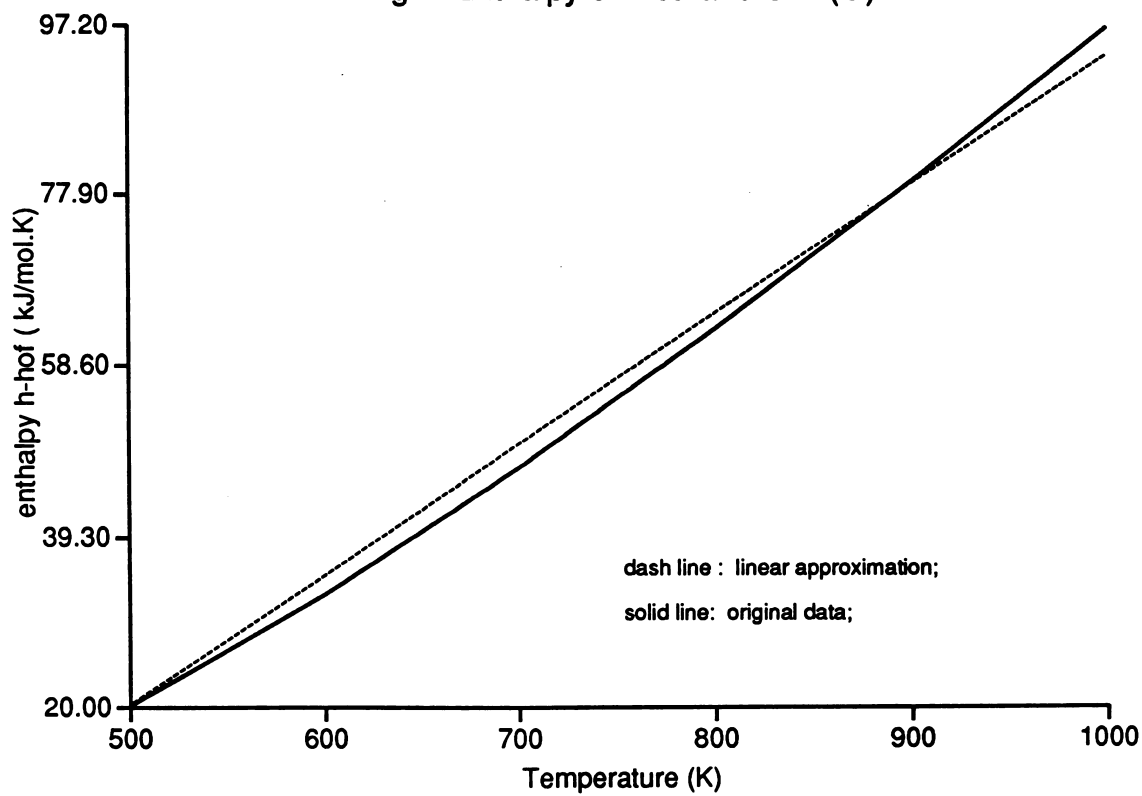


Fig .2: Enthalpy of Propane $\text{C}_3\text{H}_8(\text{G})$

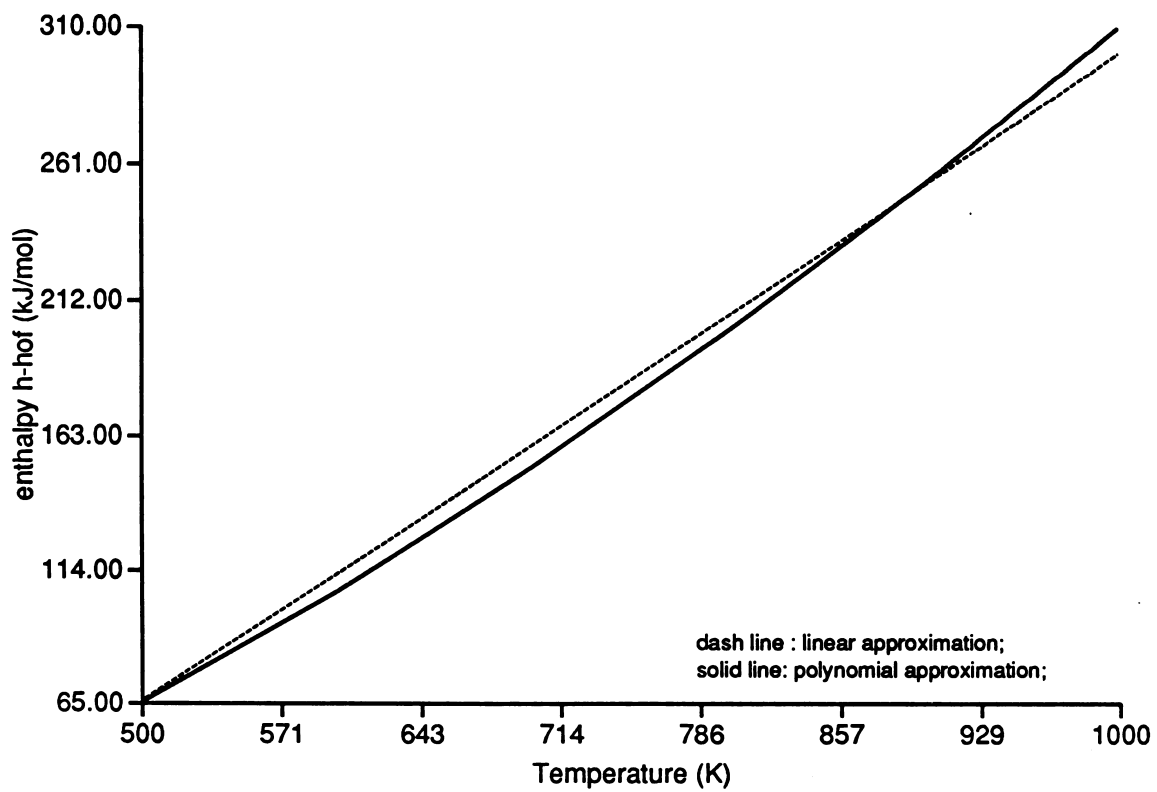


Fig .3 Enthalpy of Diesel C10.8H18.7(vapour)

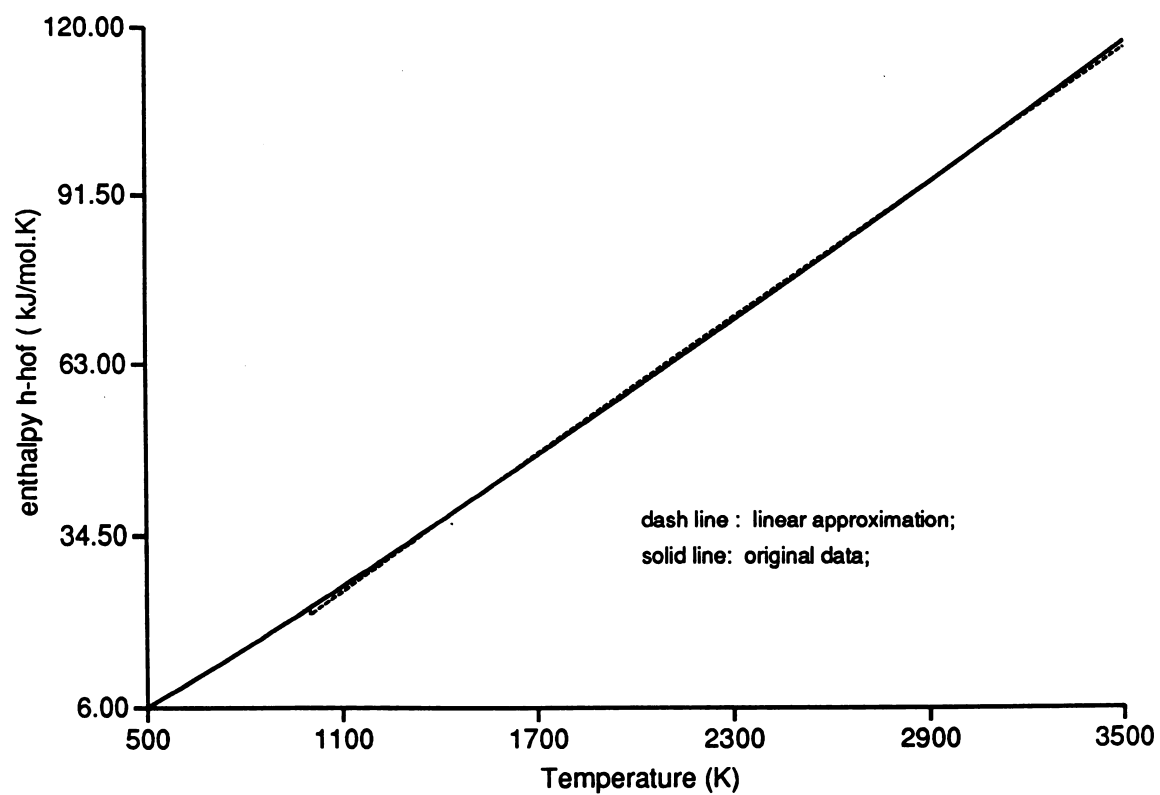


Fig .4: Enthalpy of Oxygen O2(G)

Appendix B

Properties of fuels used in the current model

Data are taken from following references:

- (1) Heywood, J. B. : “ Internal Combustion Engine Fundamentals” McGraw-Hill, Inc. 1988.
- (2) JANAF “Thermochemical Tables,” Document PB 168-370, Clearinghouse for Federal Scientific and Technical Information, 1965.
- (3) Vargaftik, N. B.:“Table on the Thermophysical Properties of Liquids and Gases, ” 2nd Edition. Hemisphere Publishing Corporation.

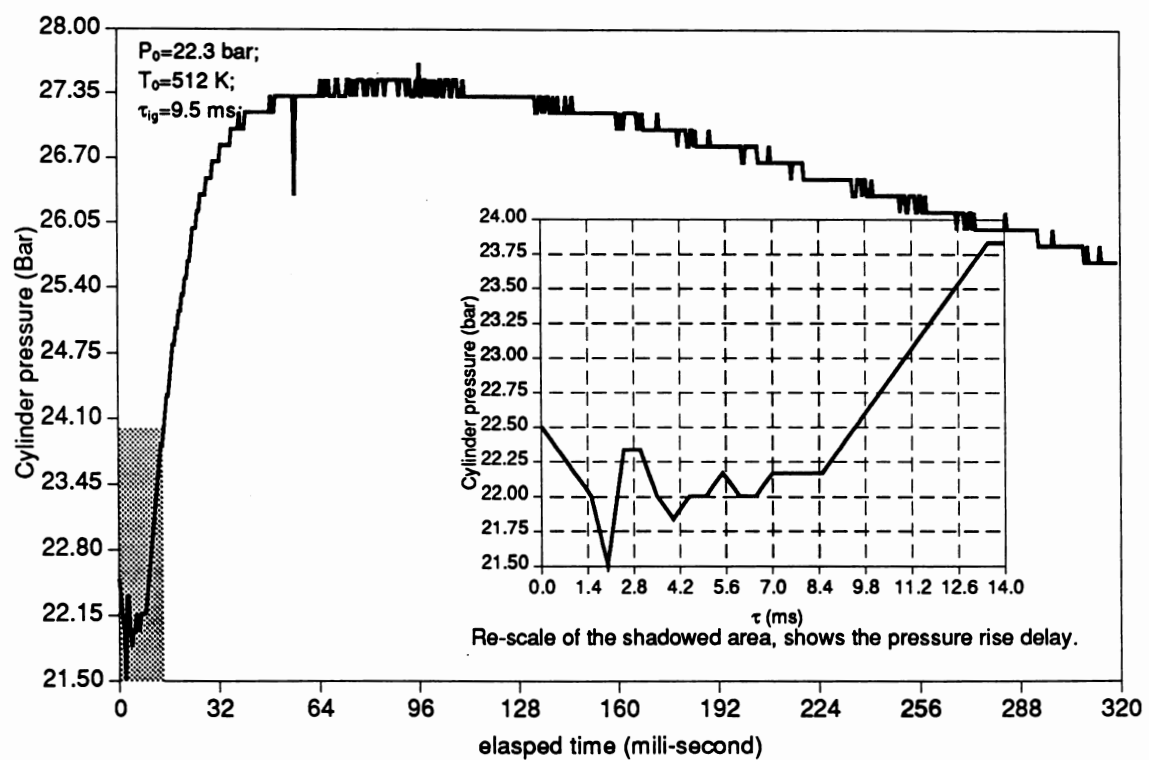
Fuel:	NG(assumed to be methane)	propane	Diesel
Formula	$CH_4(g)$	$C_3H_8(g)$	$C_{10.8}H_{18.7}(l)$
Molecular mass	16.04	44.10	148.6
lower heating value(kJ/kg)	50,005	46,346	42,500
Enthalpy of formation [@] (kJ/kmol)	-74,873	-103,909	-394,199*
Density [@] (kg/m ³)	0.72	2.0	840
Stoichiometric fuel/air ratio	0.0580	0.0638	0.0694

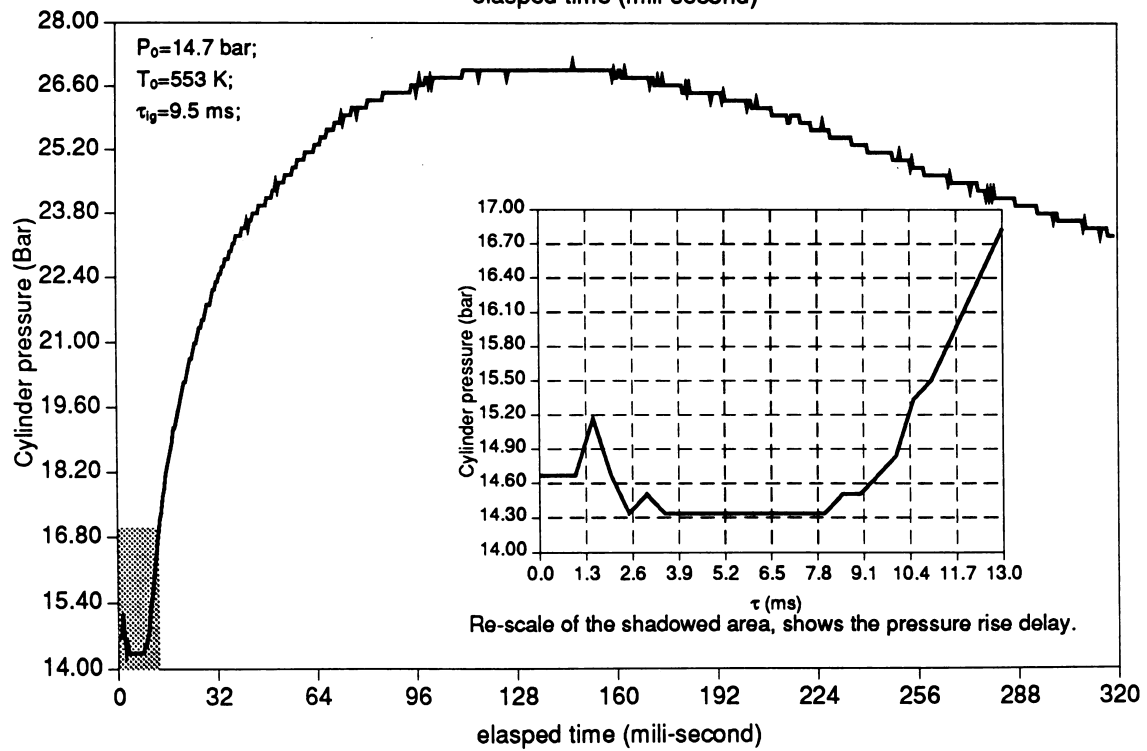
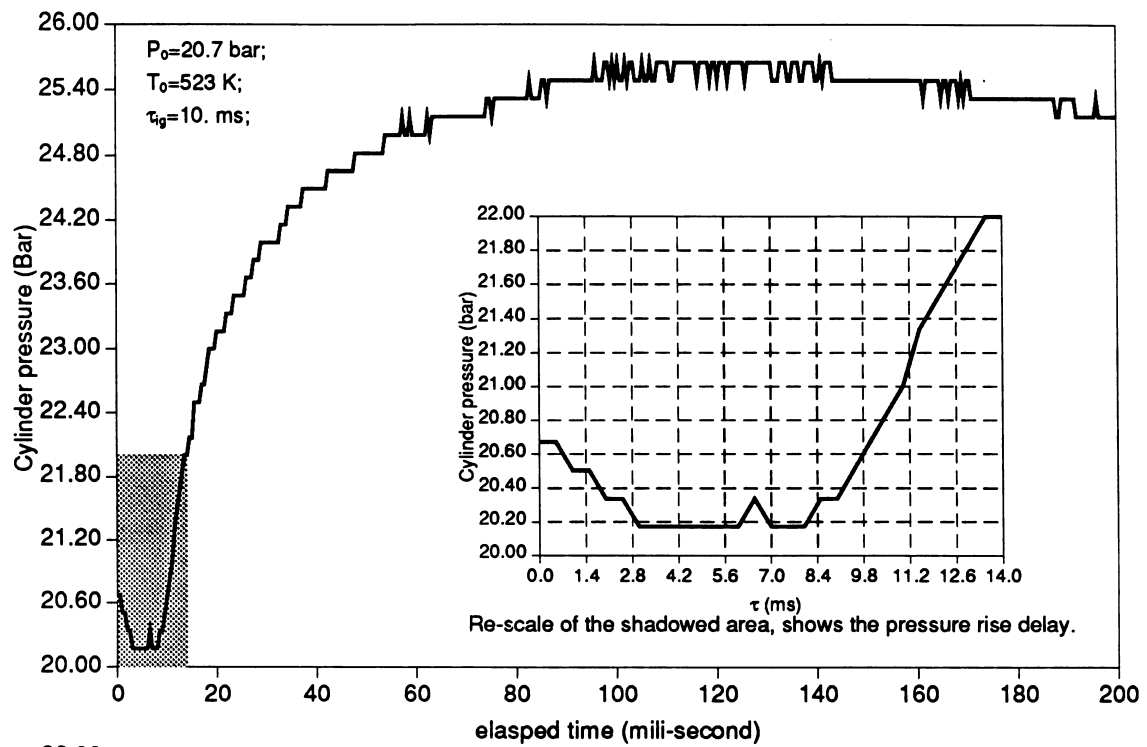
*: Data are for the liquid dodecane.

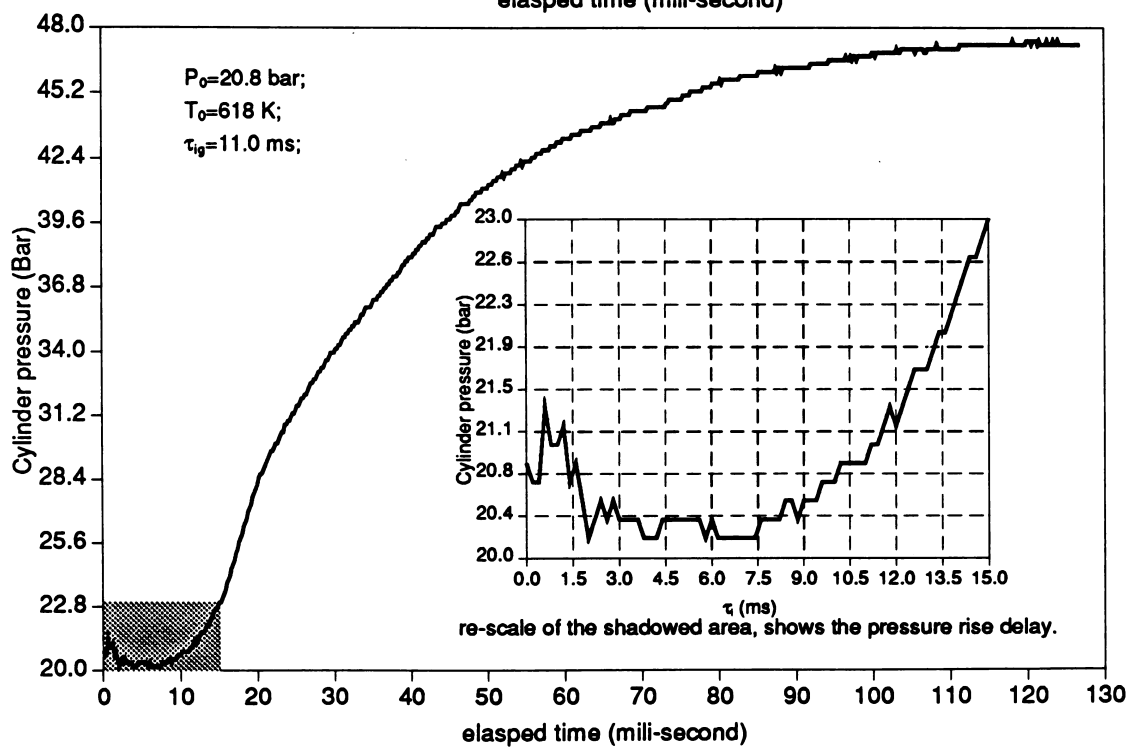
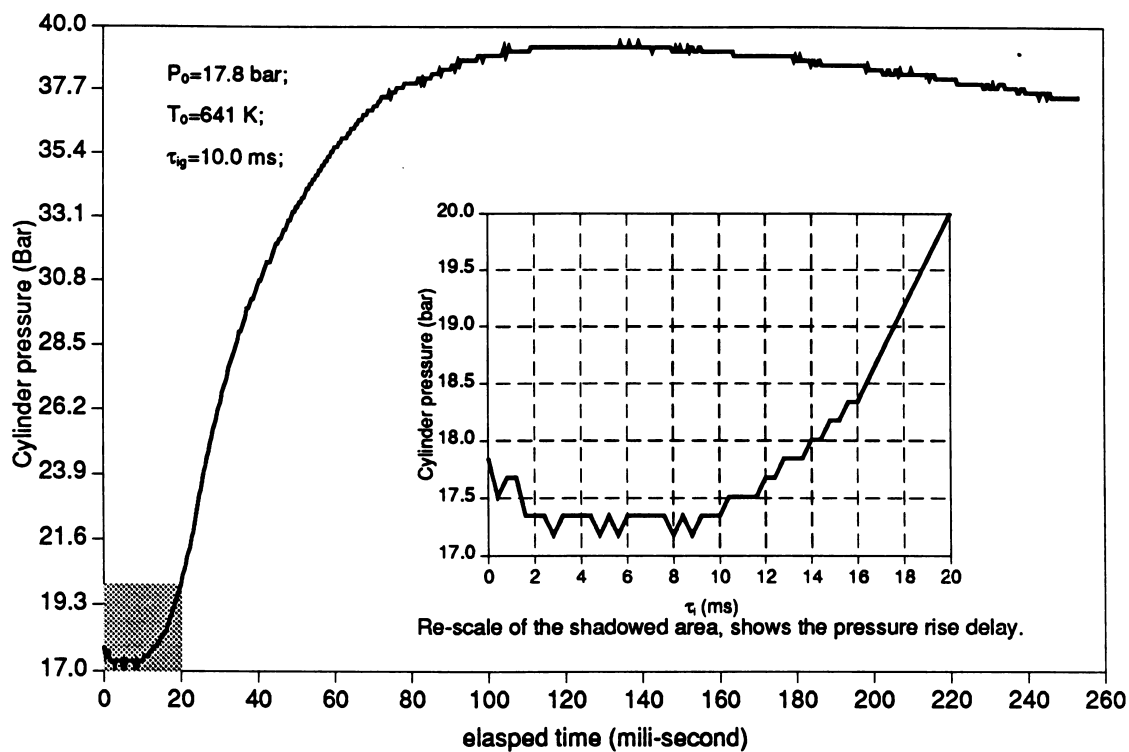
@: Data are for the standard state defined as T=298.15 K, P=0.1 MPa.

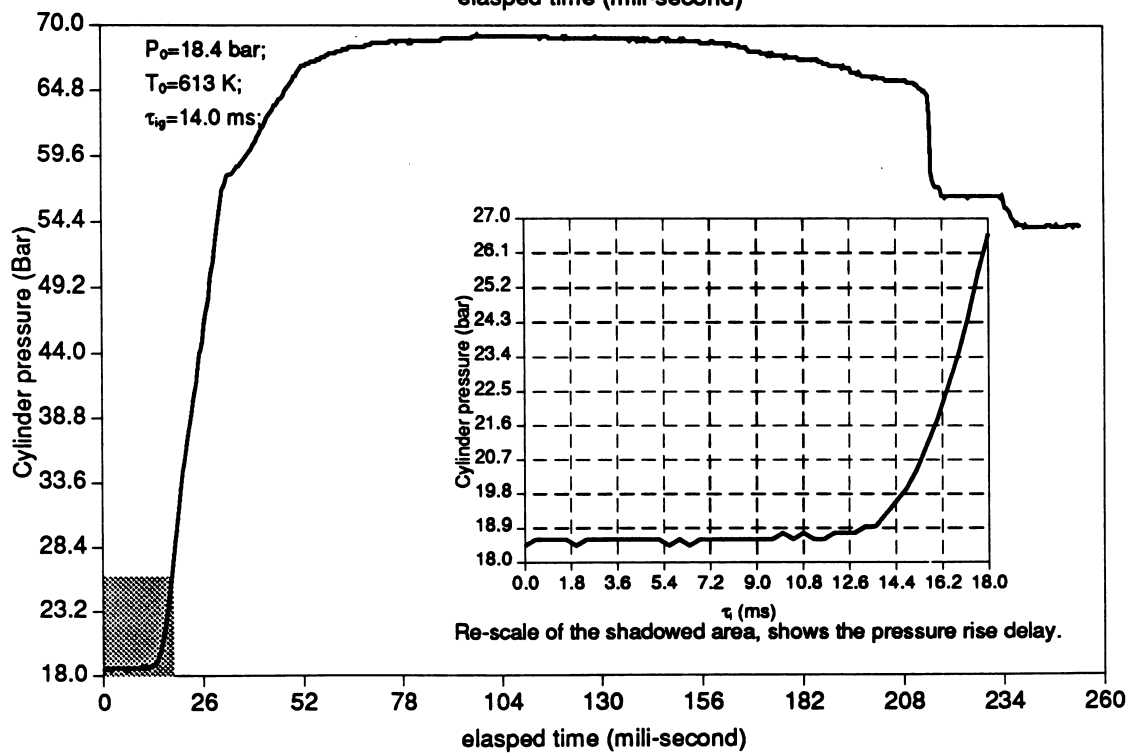
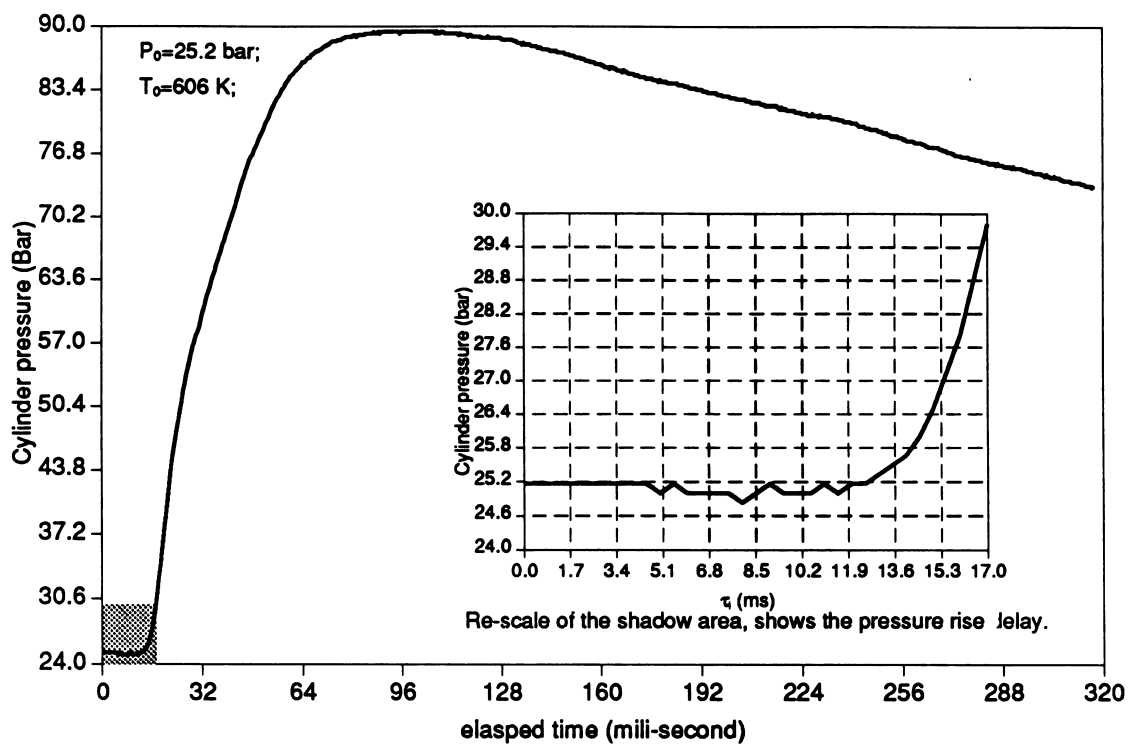
Appendix C

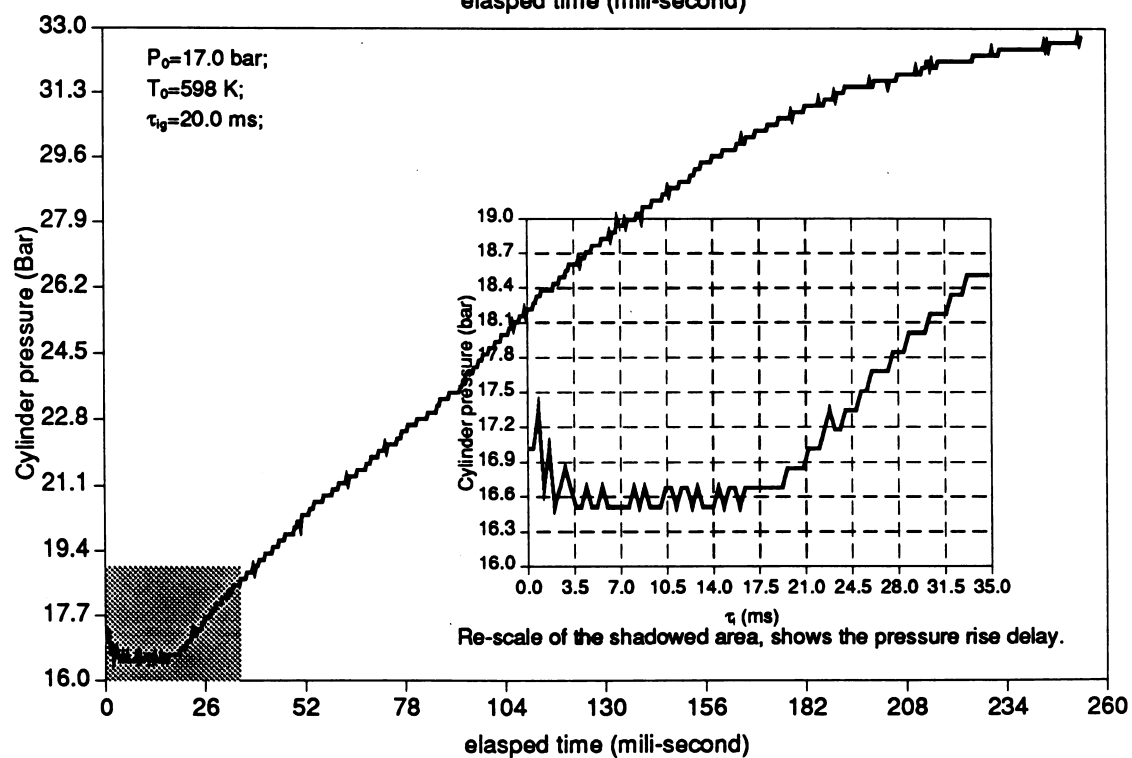
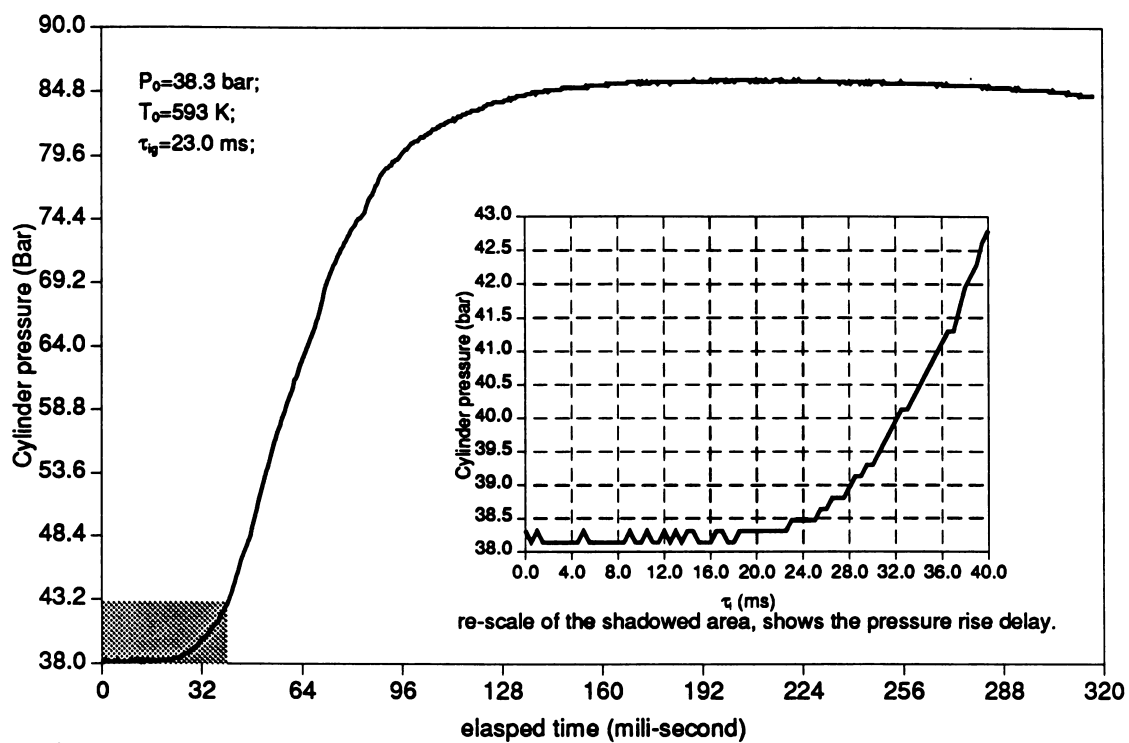
**Experimental results of dynamic
pressure trace of diesel
combustion in constant volume
bomb**

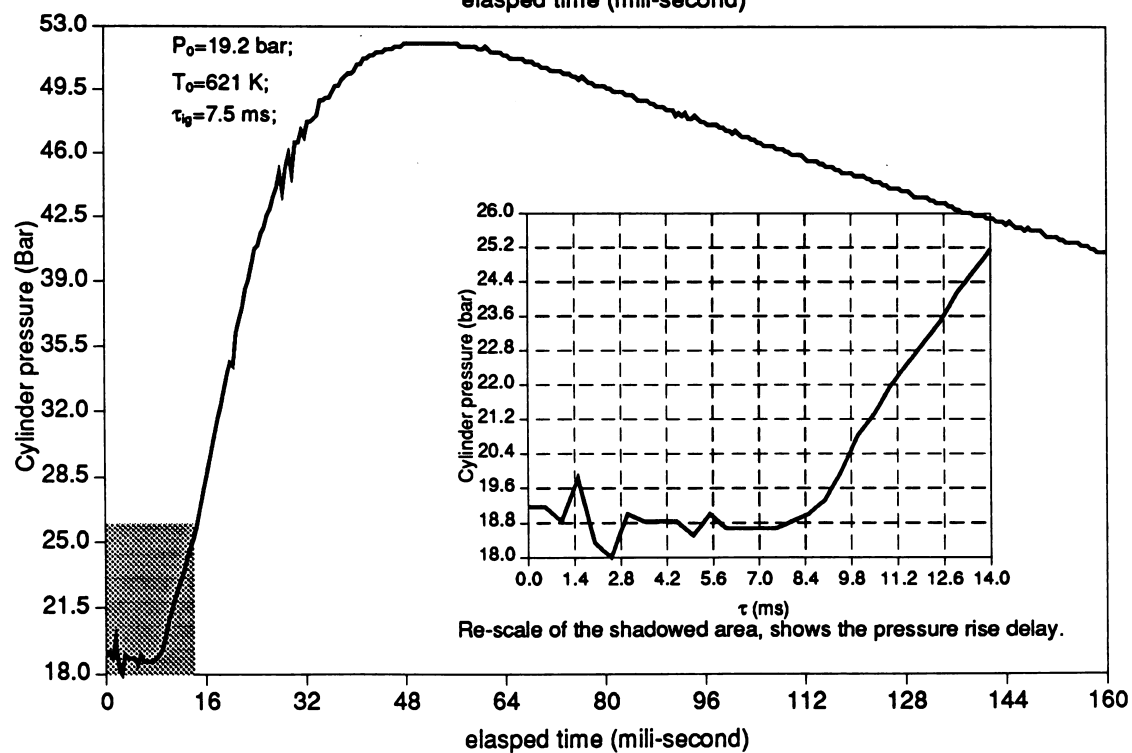
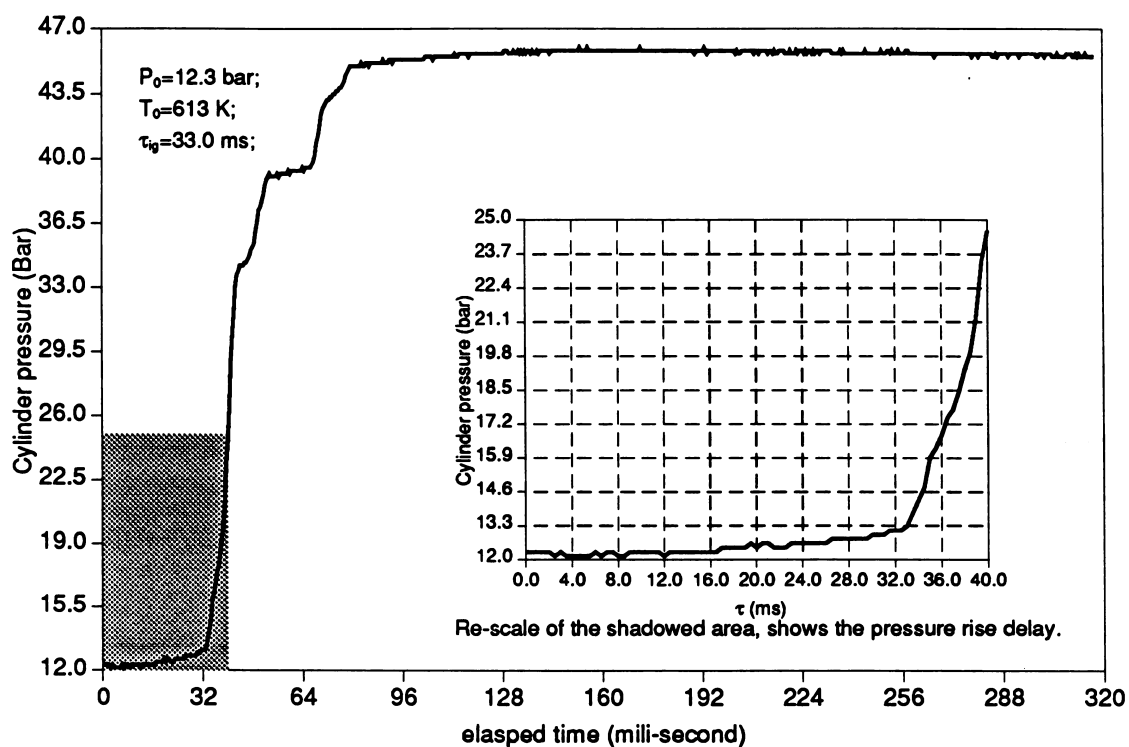


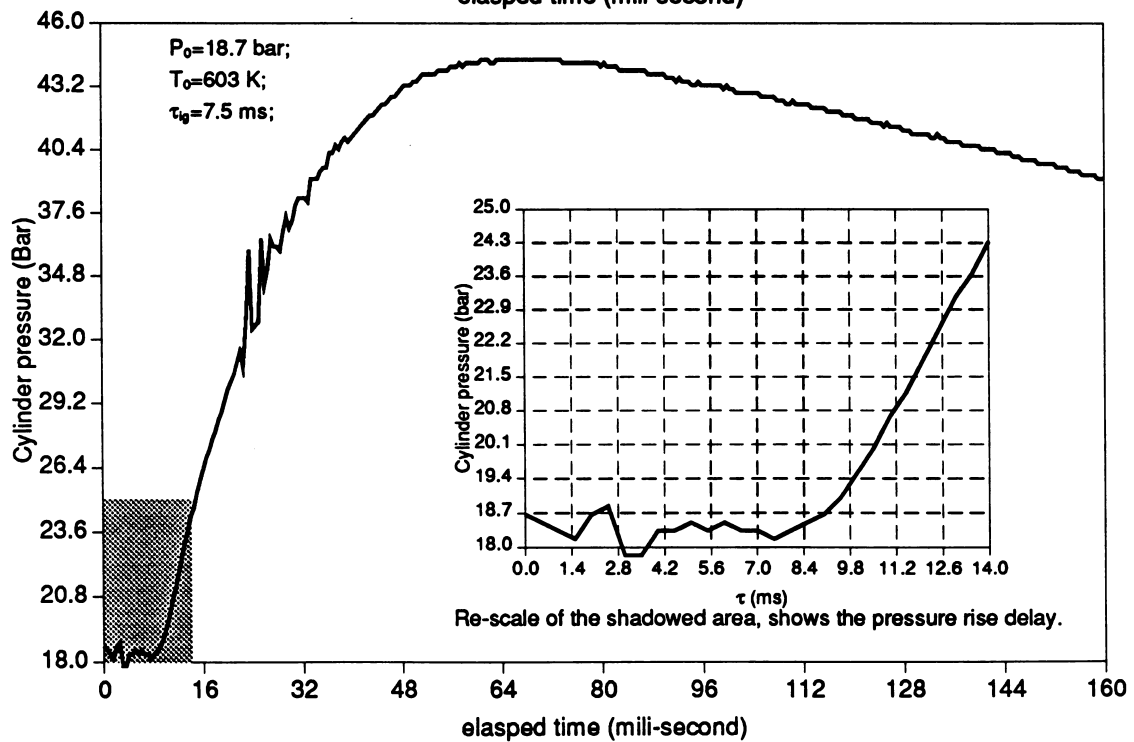
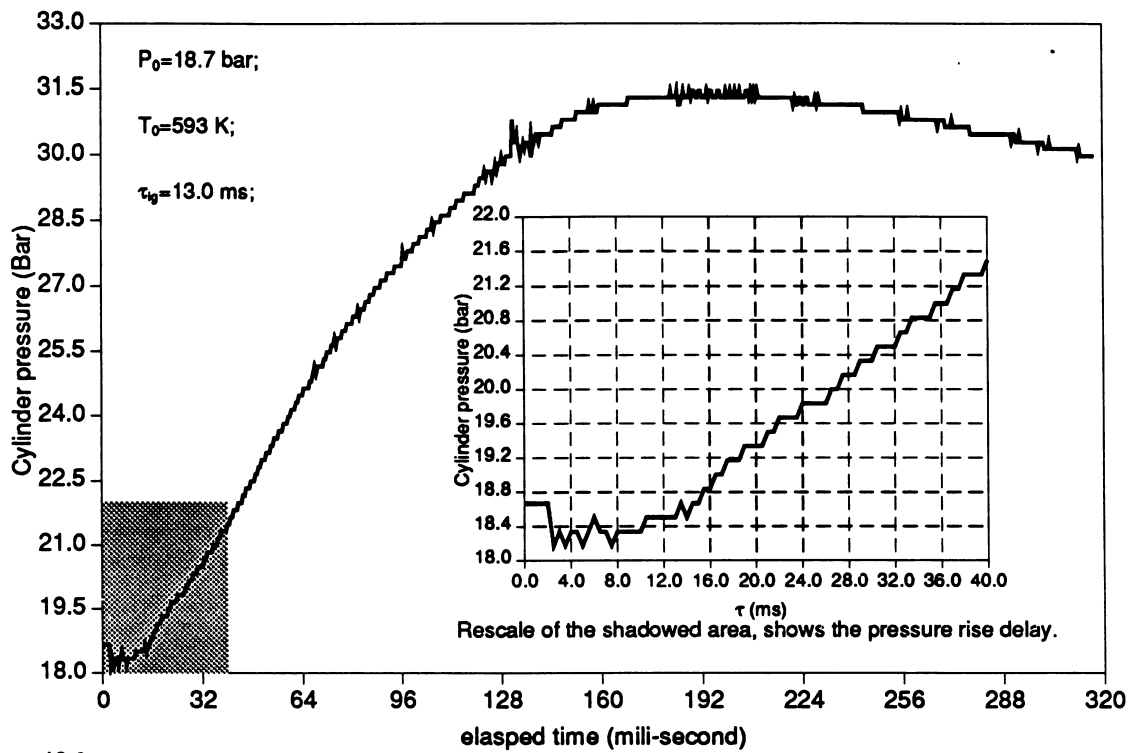


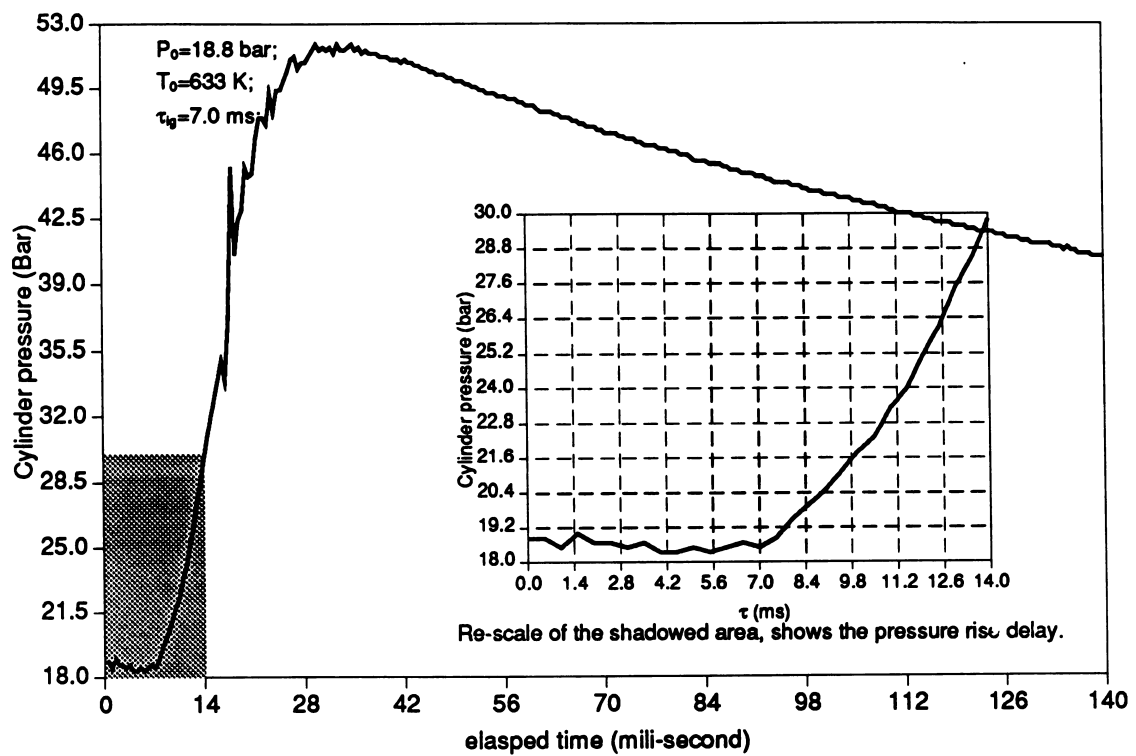


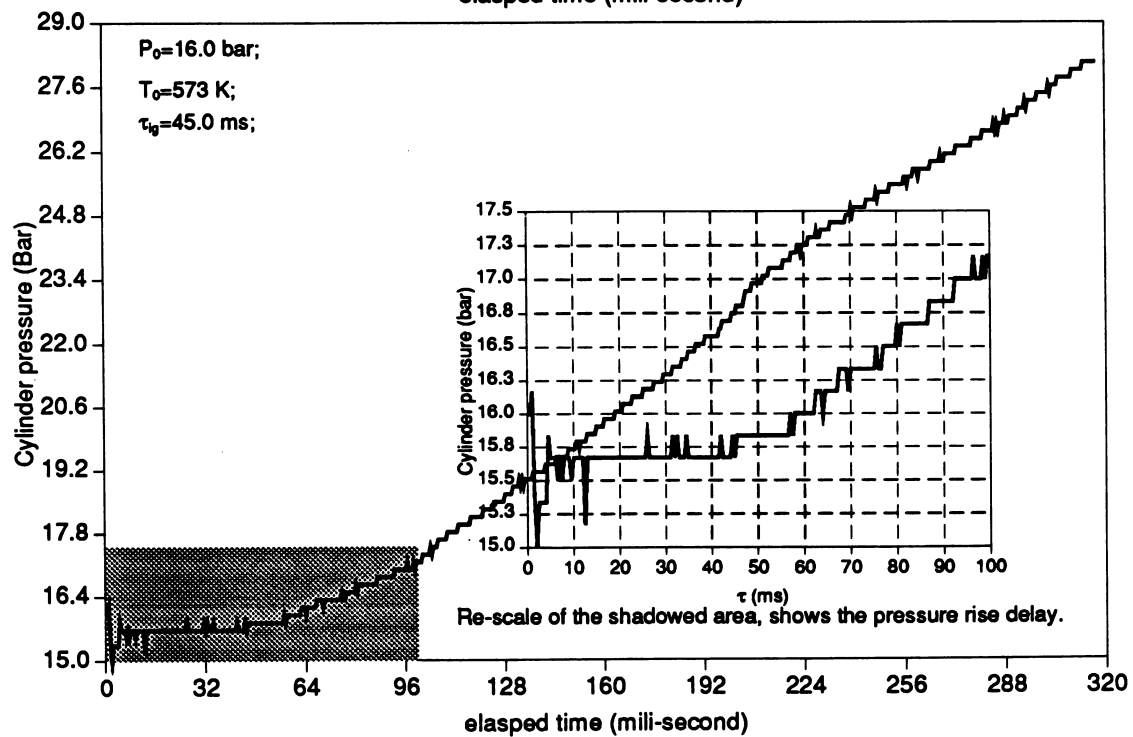
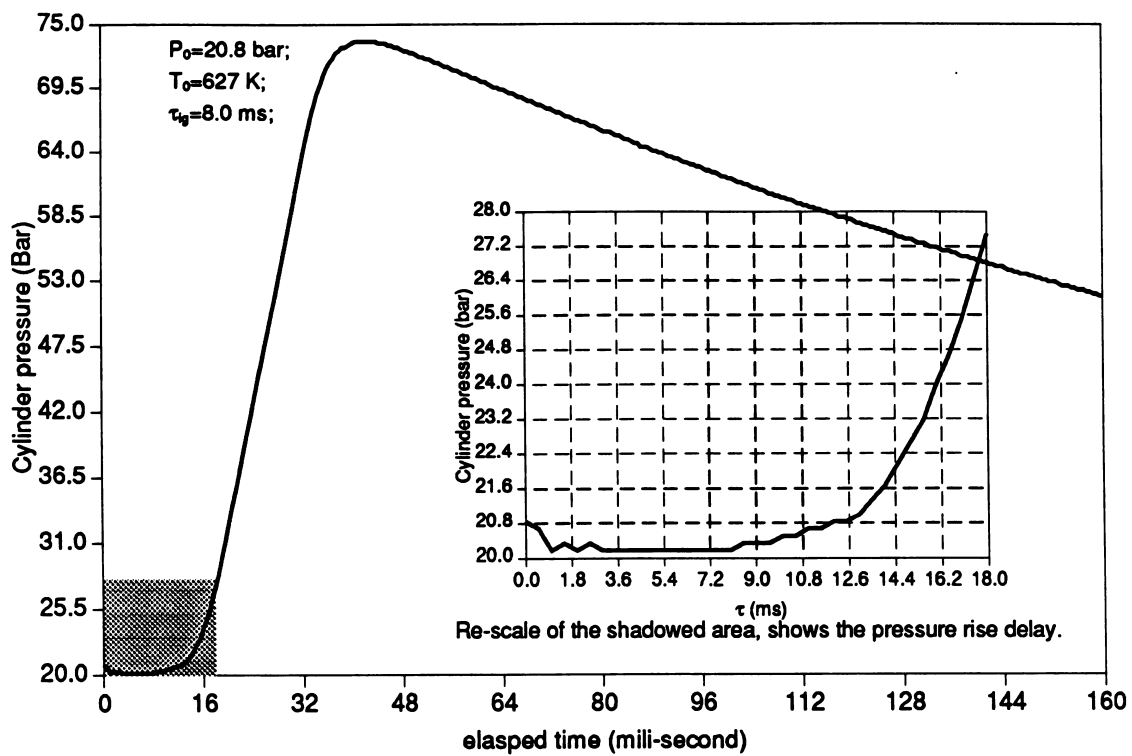


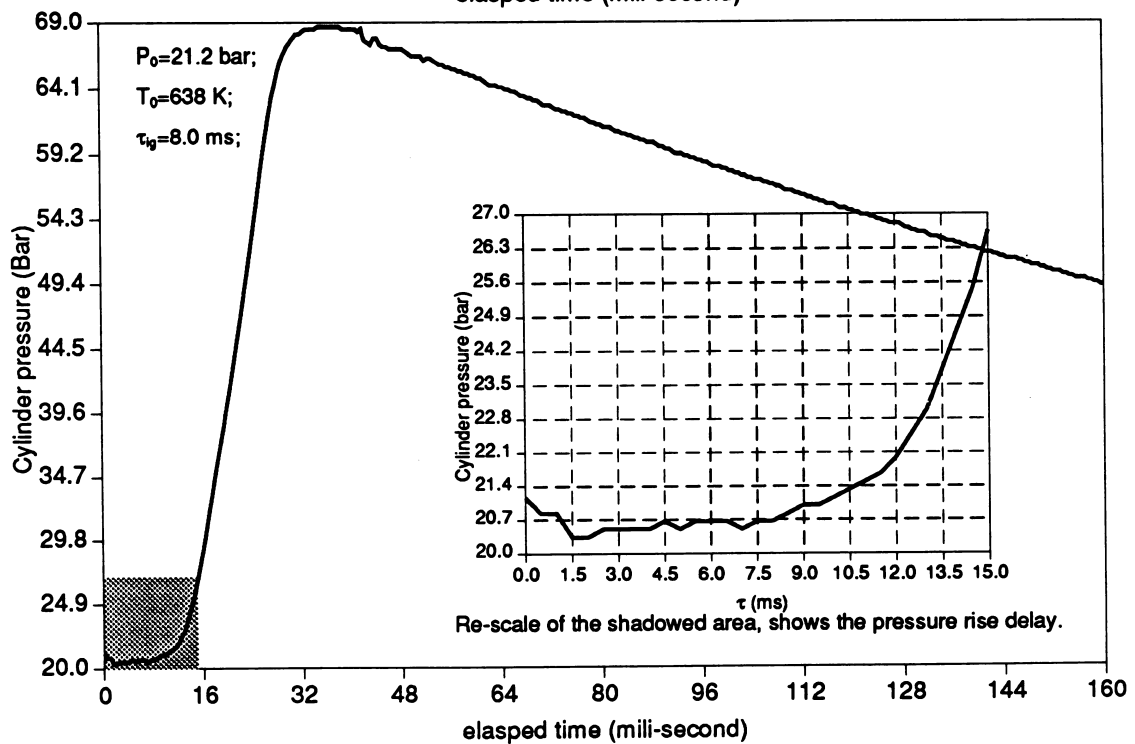
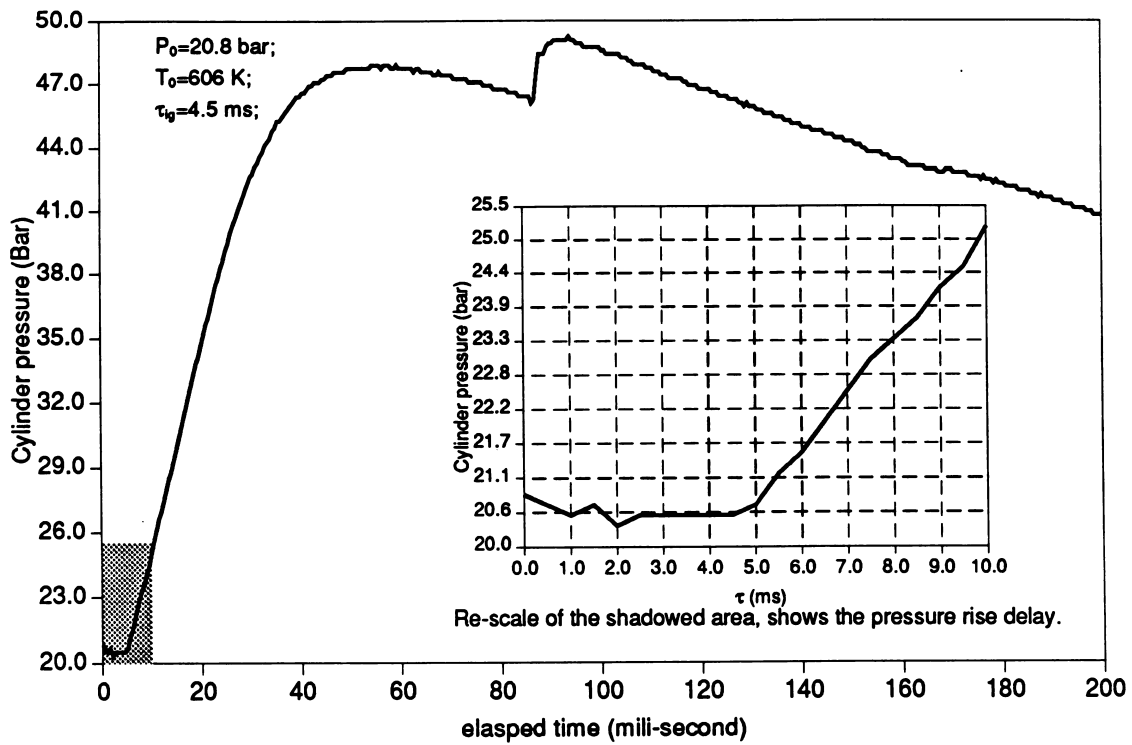


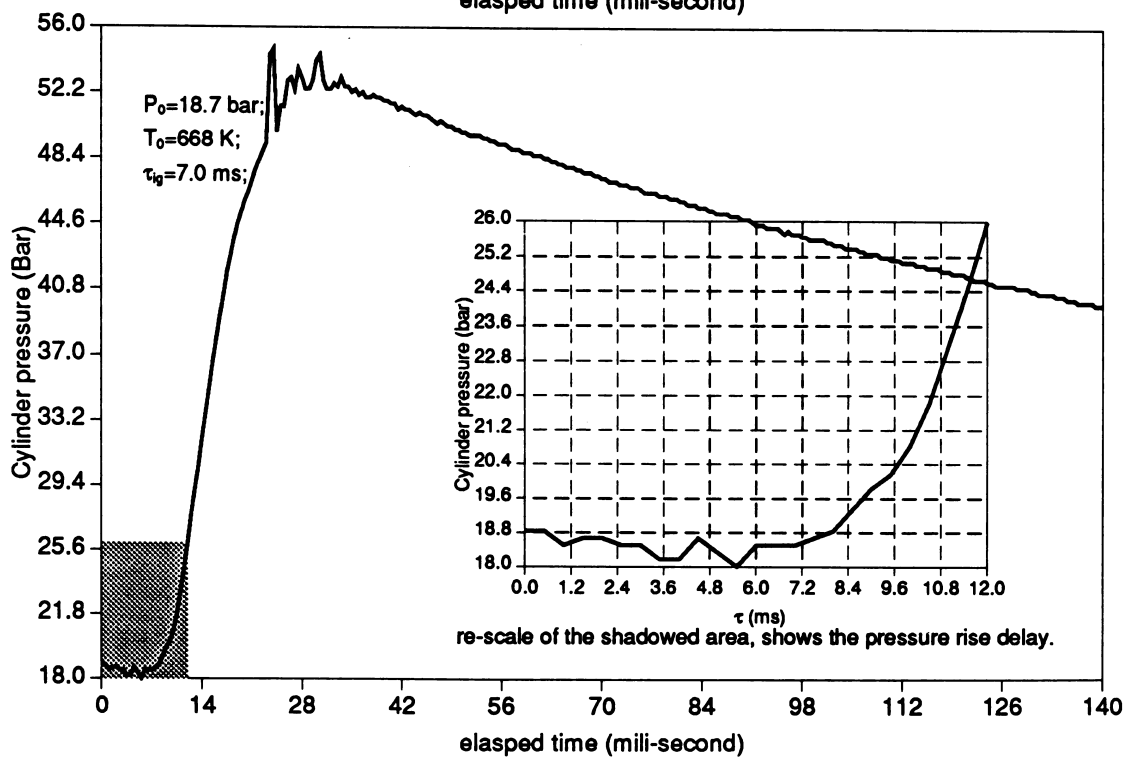
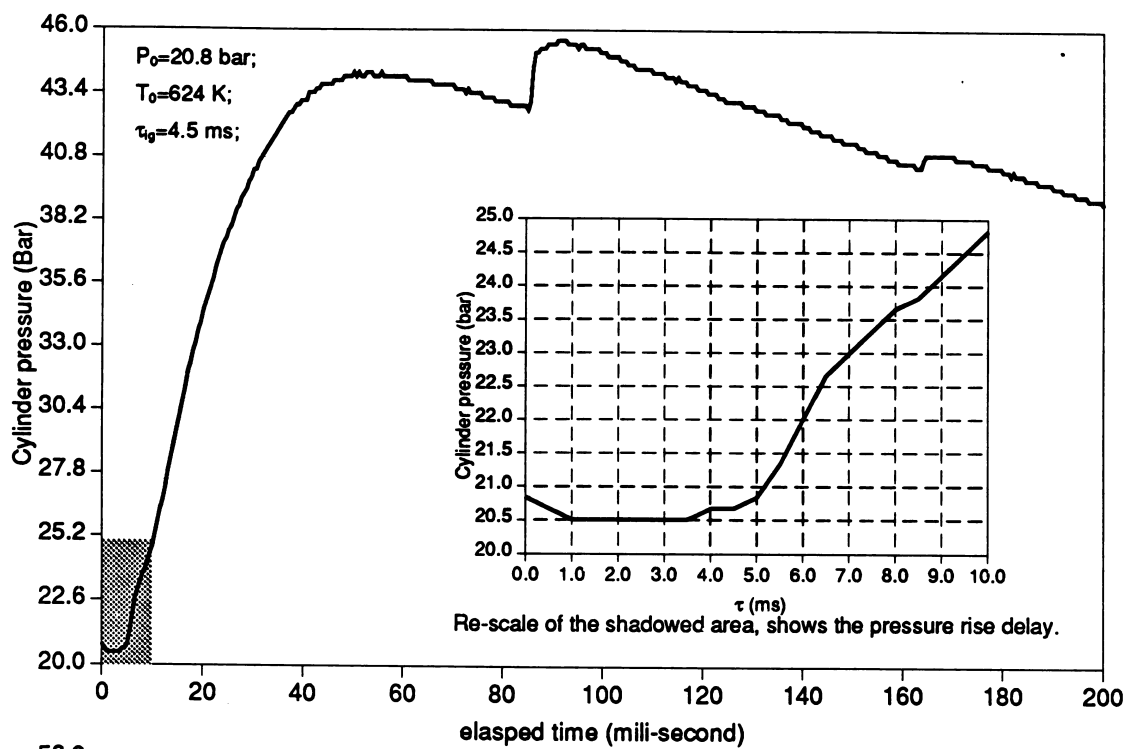


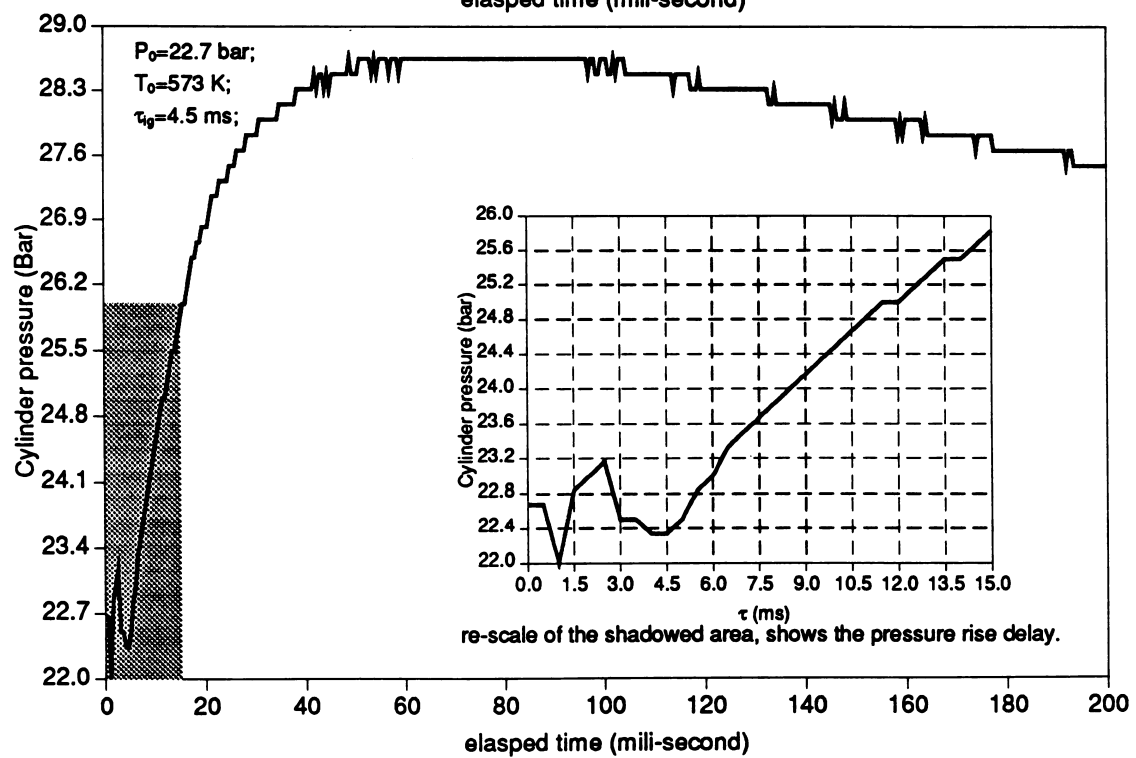
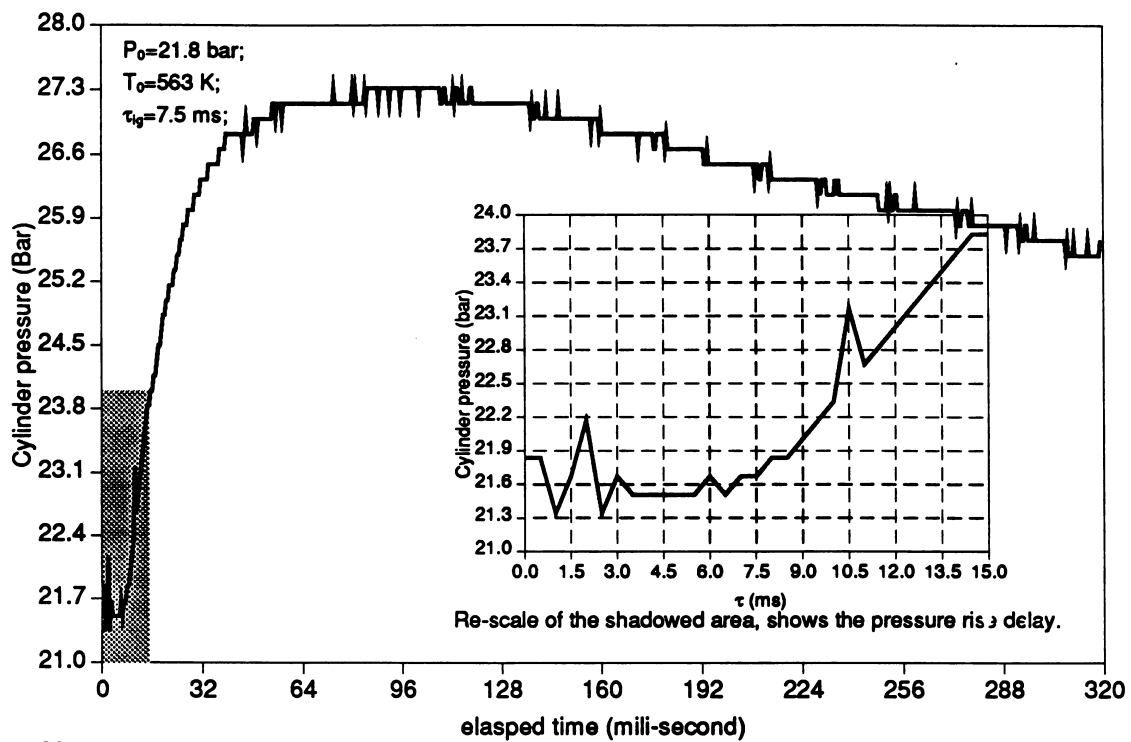


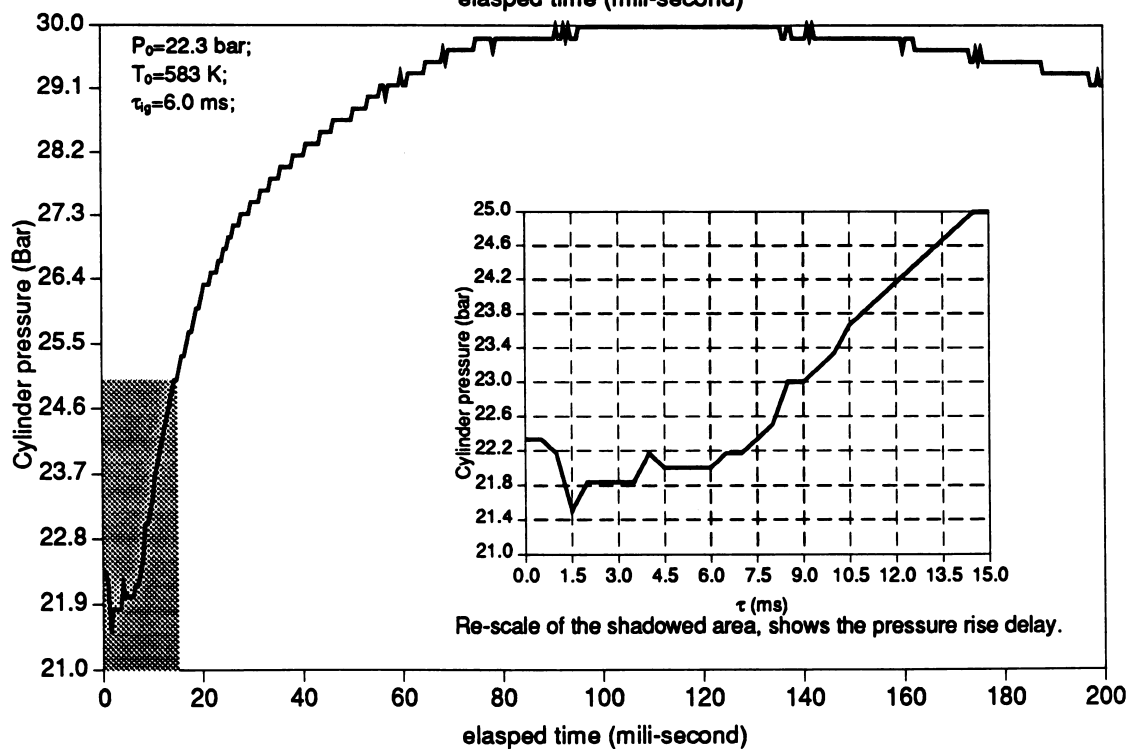
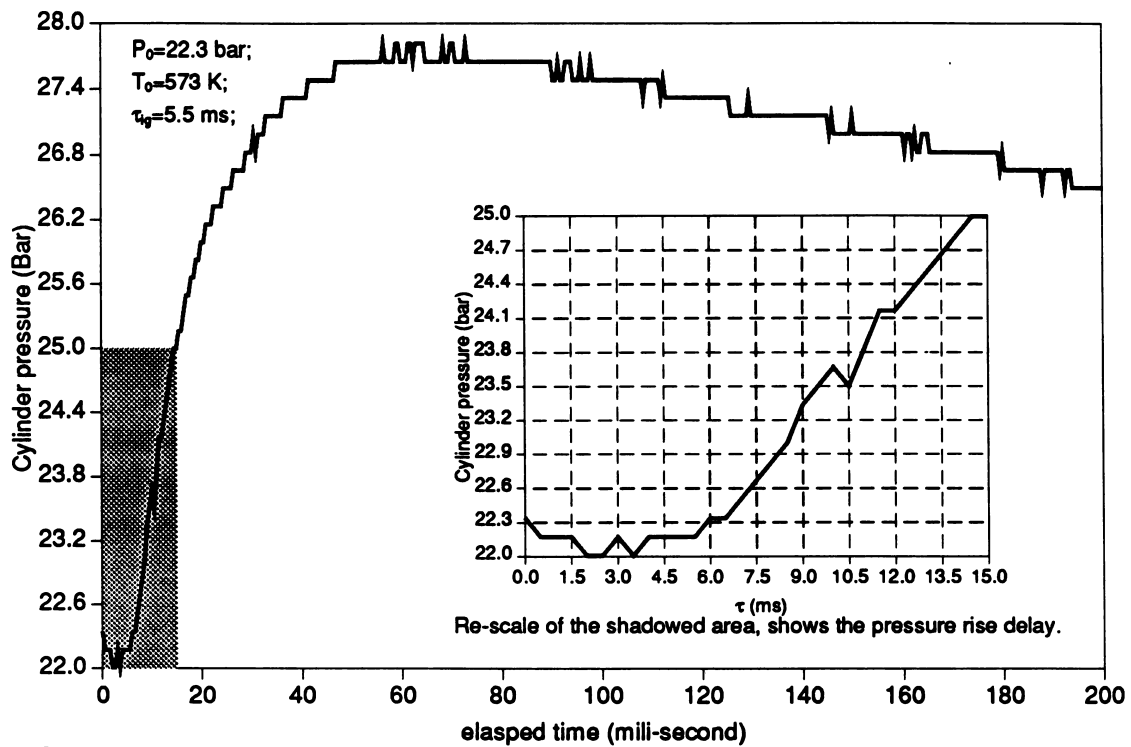


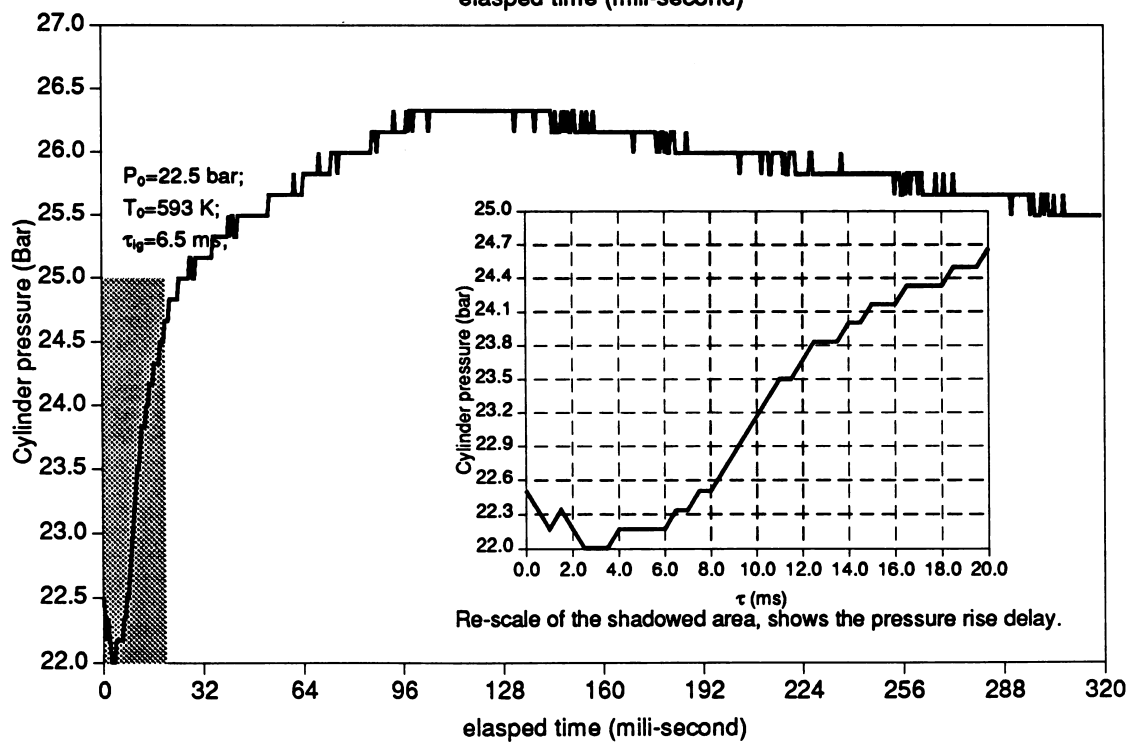
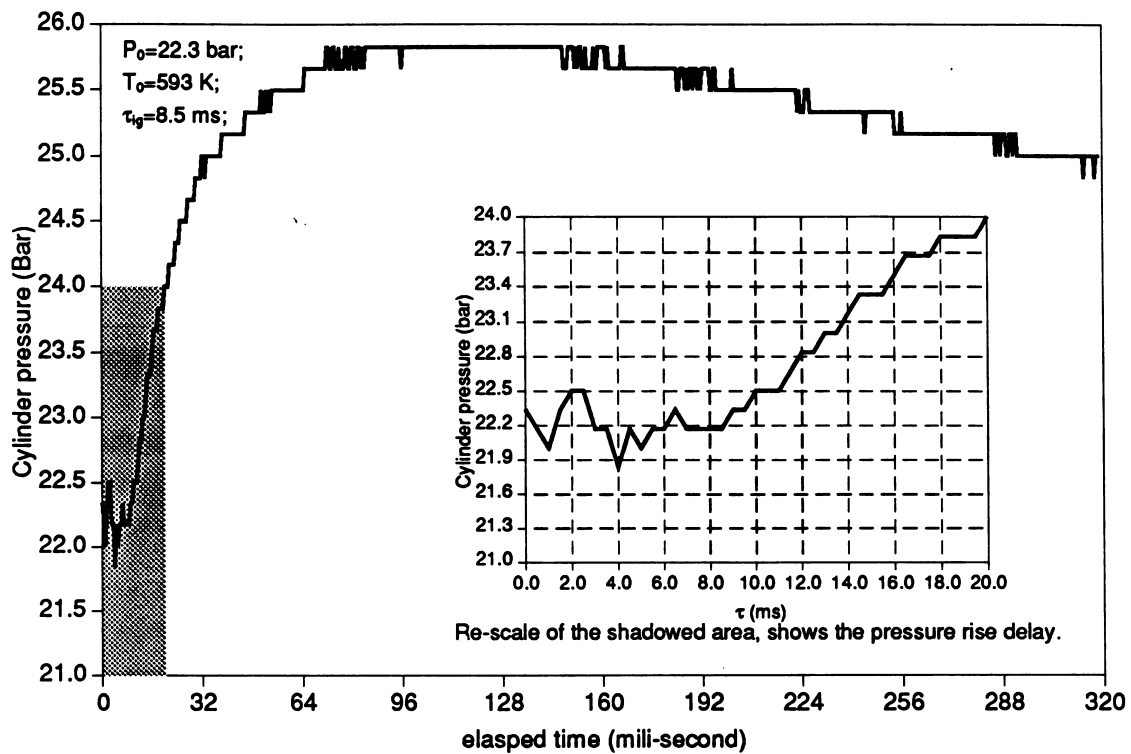


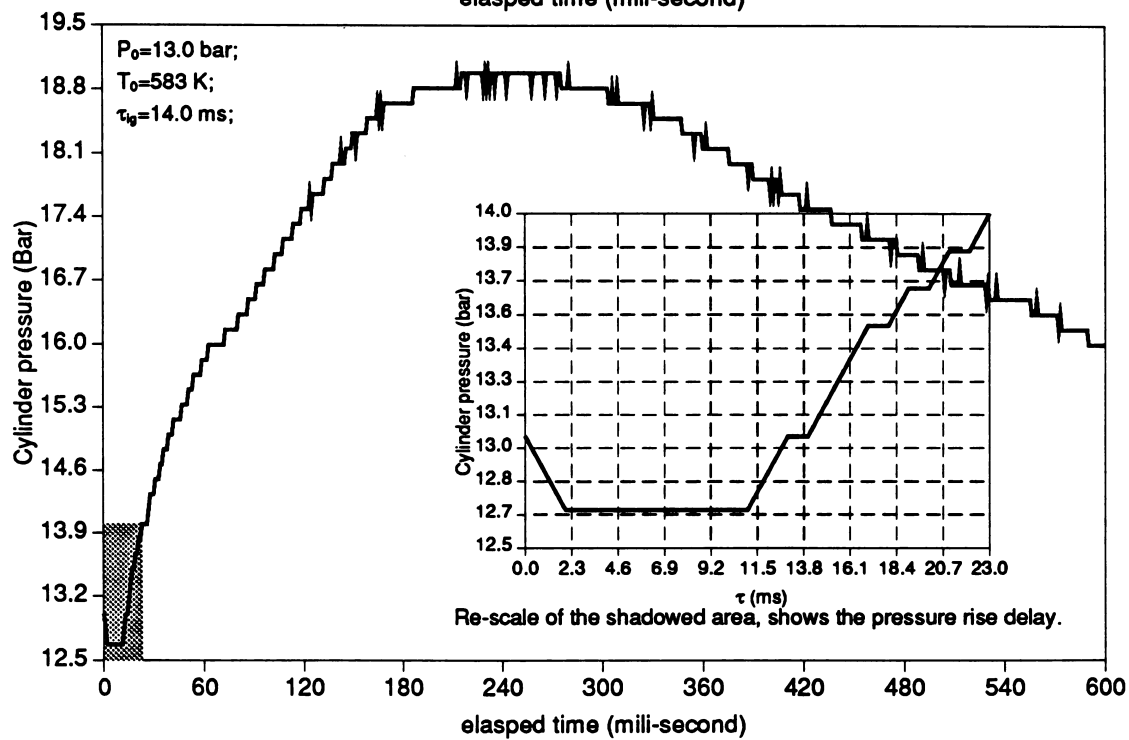
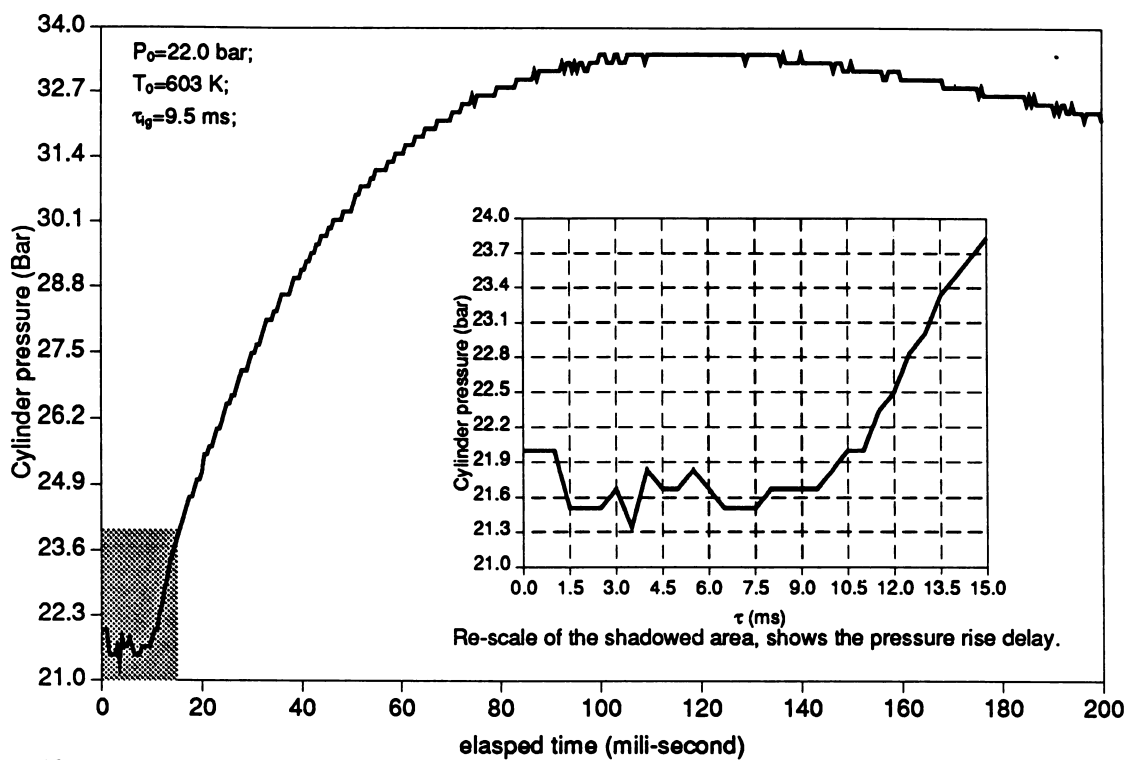


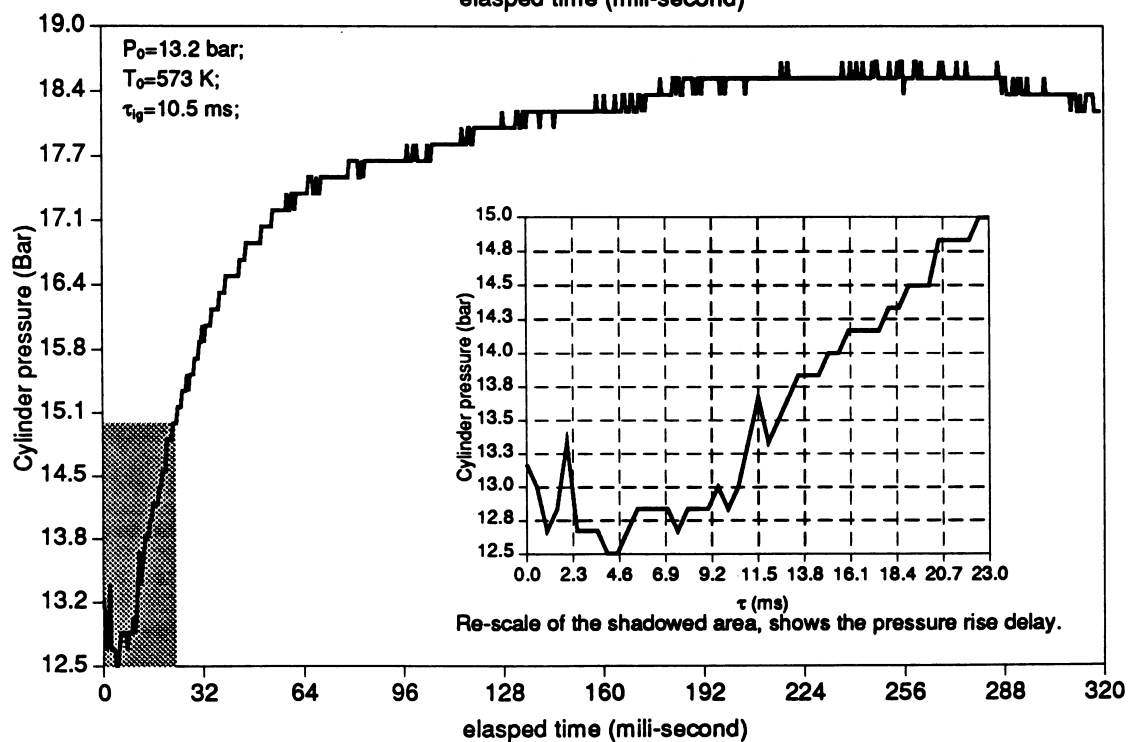
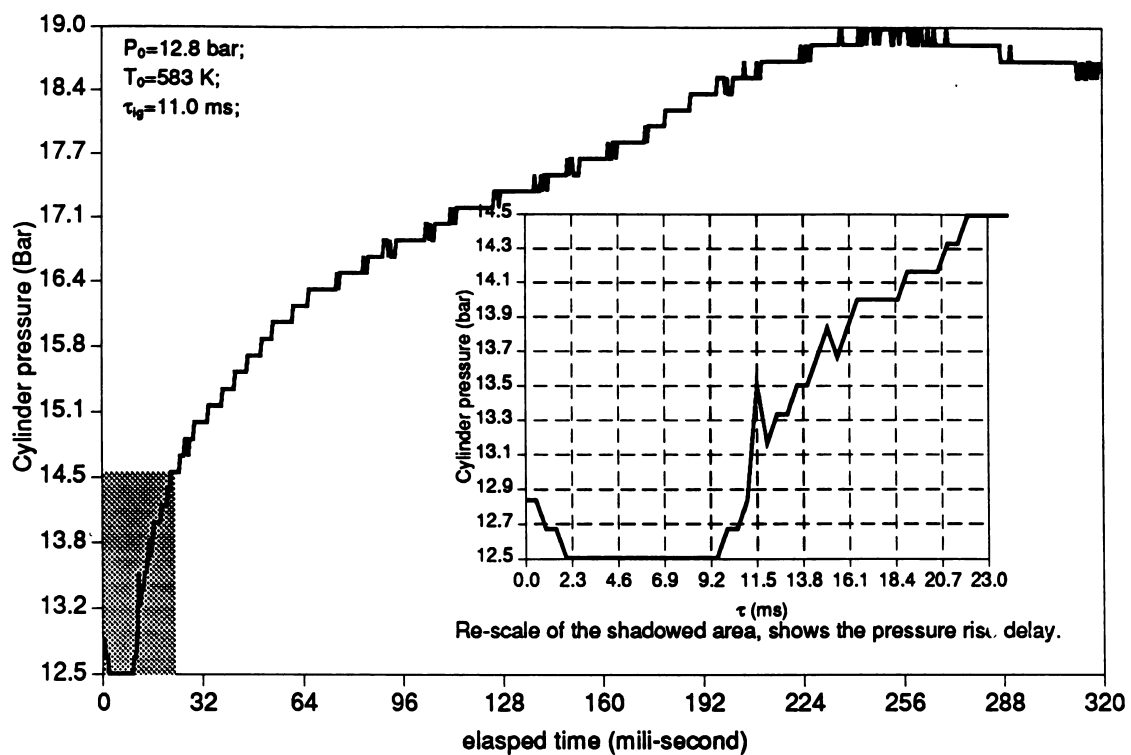


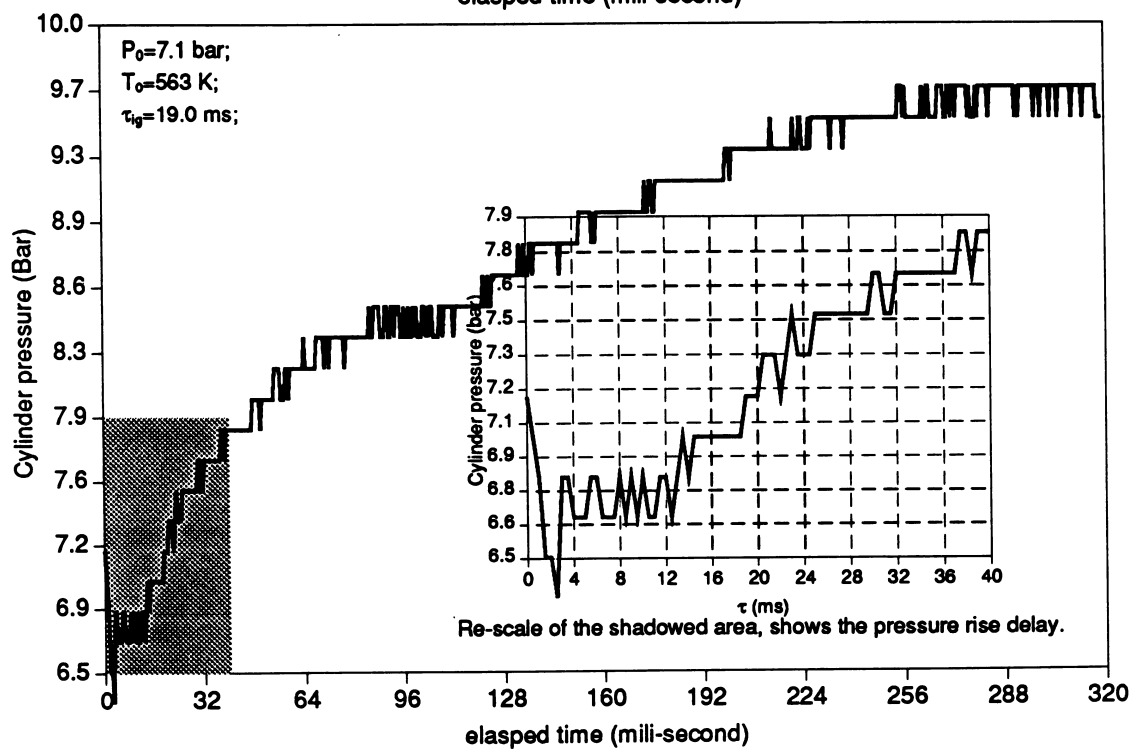
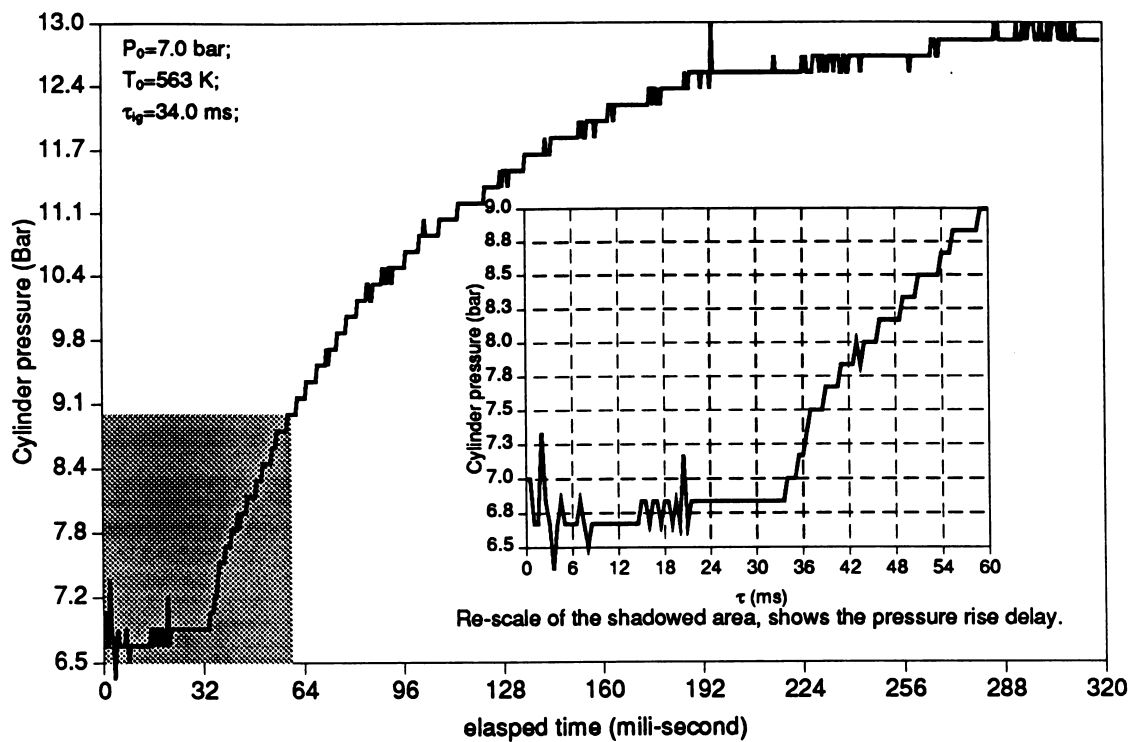


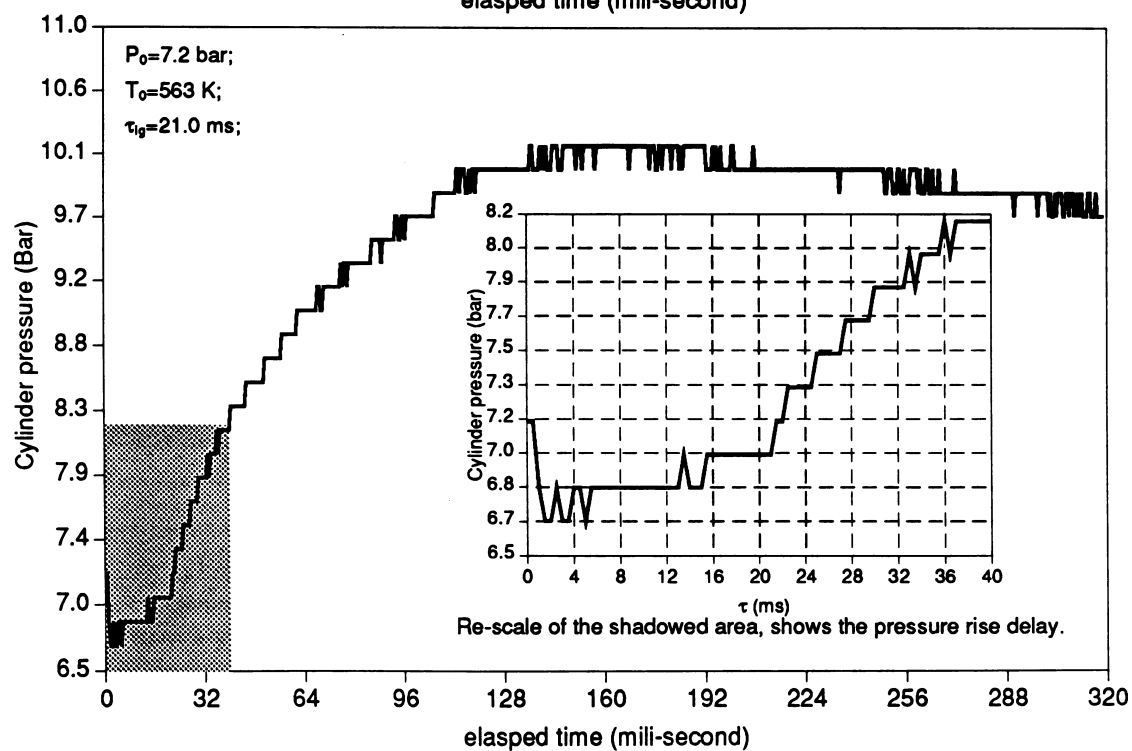
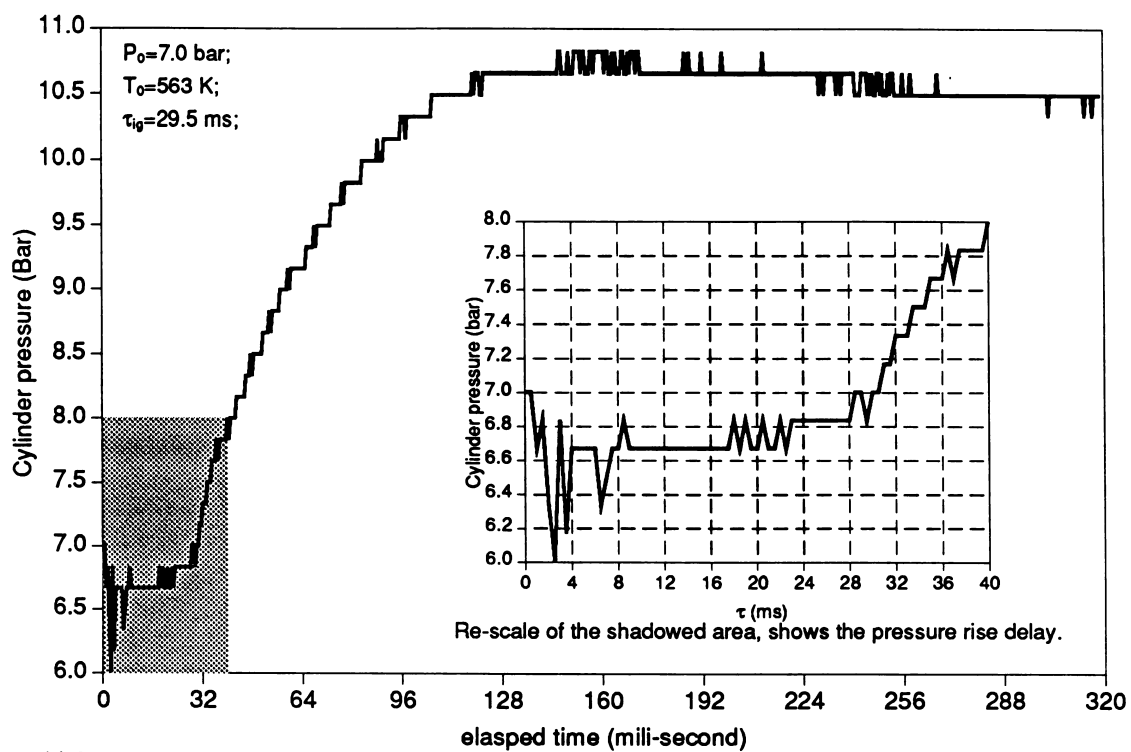


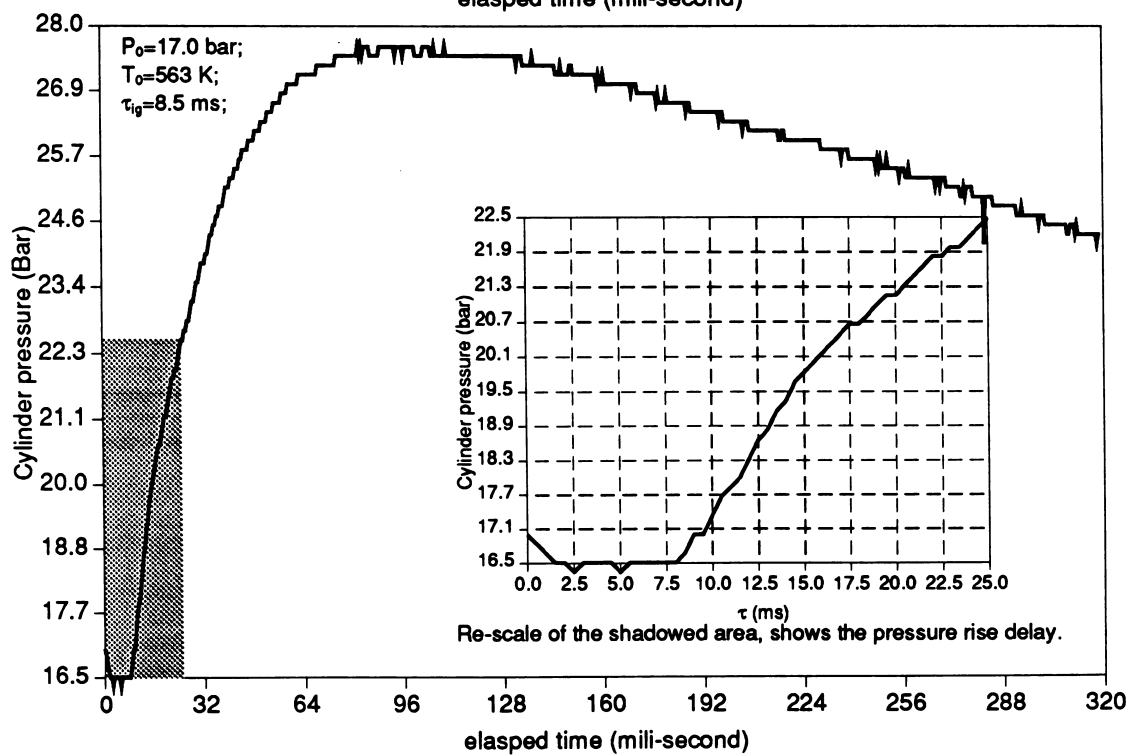
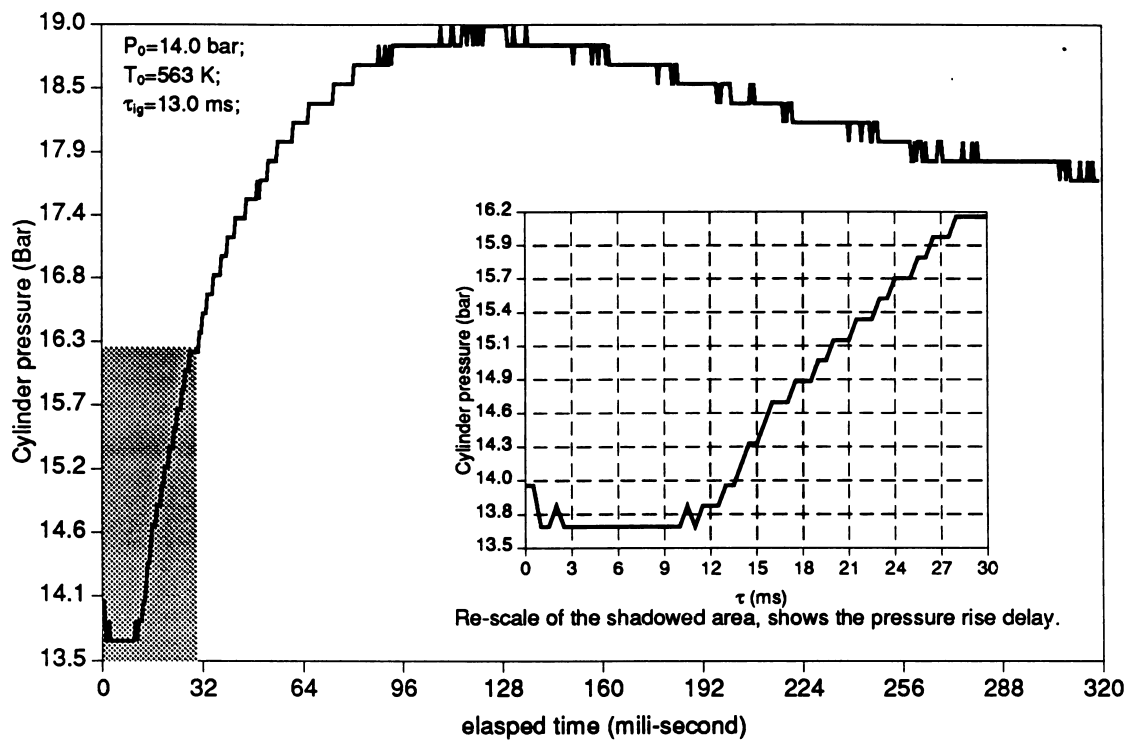


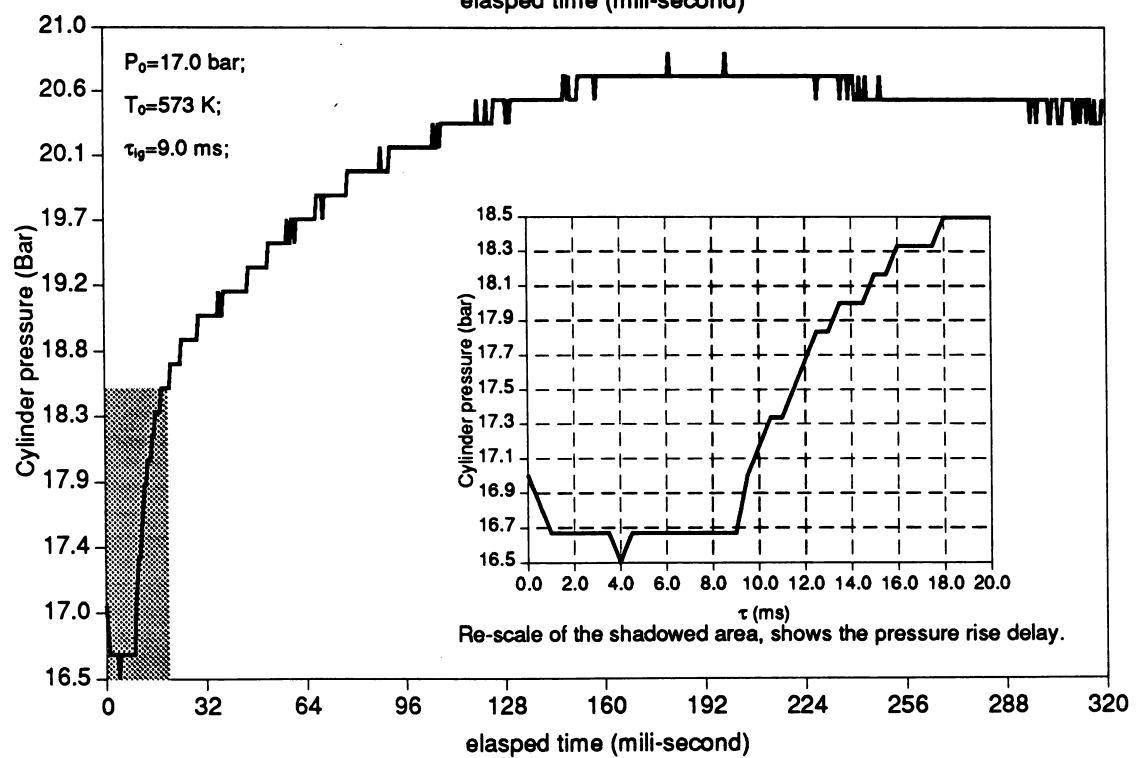
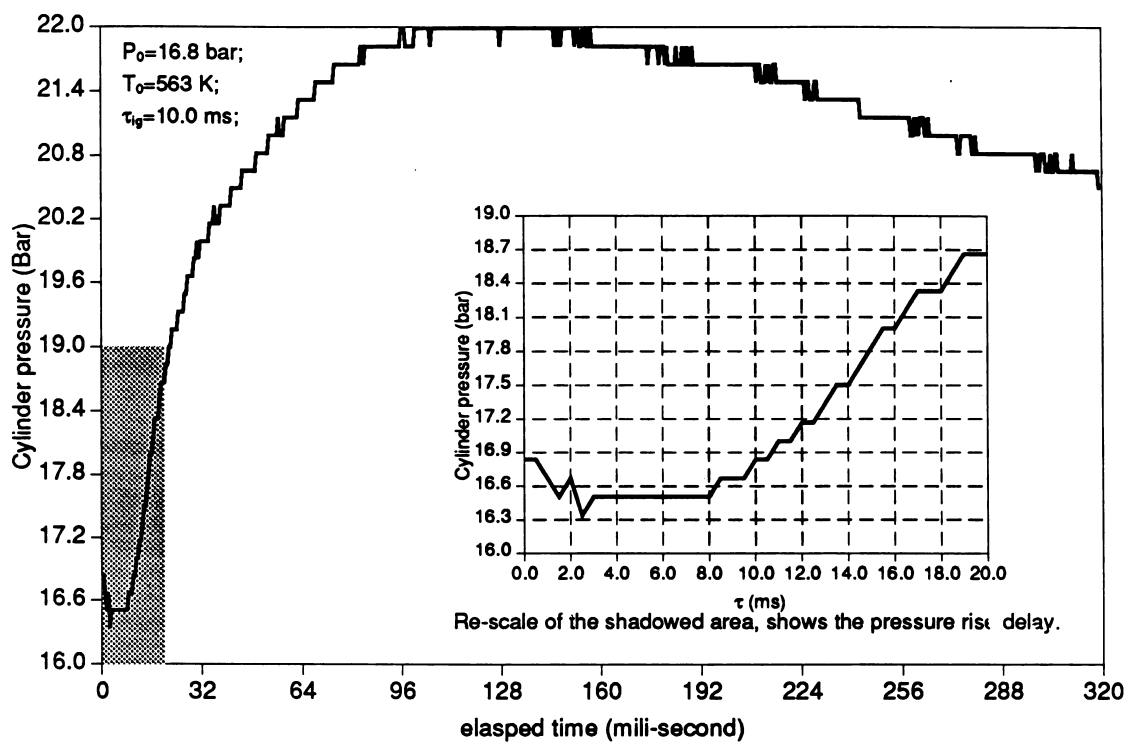


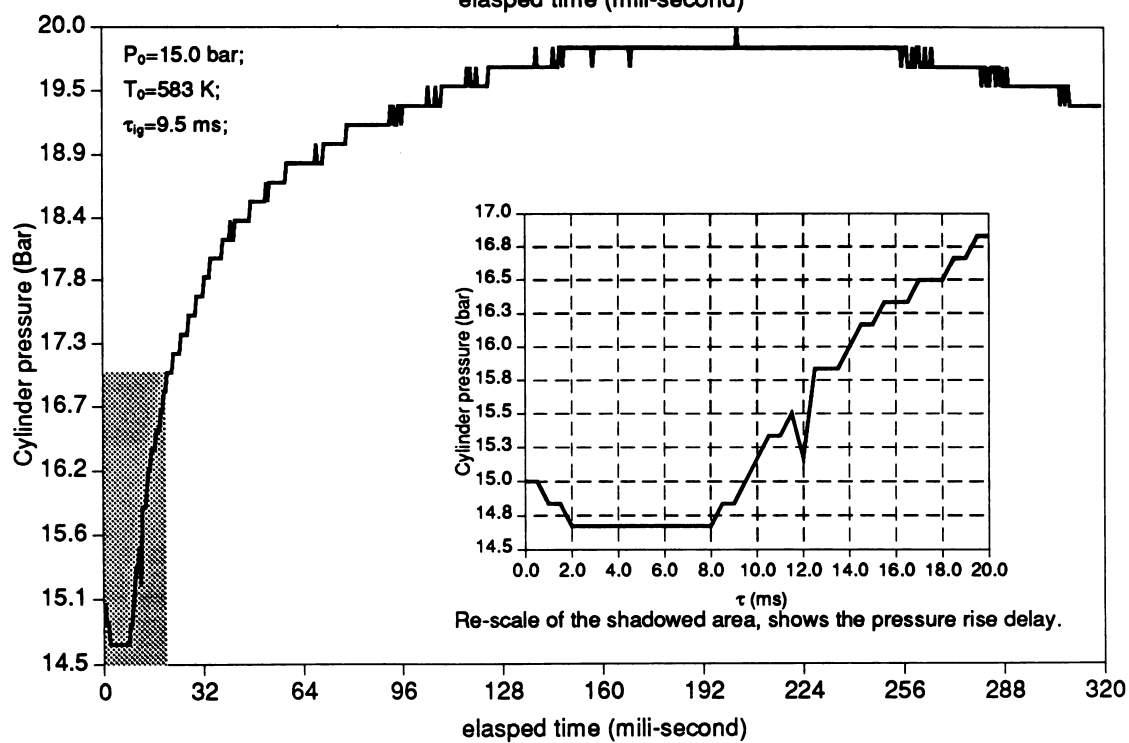
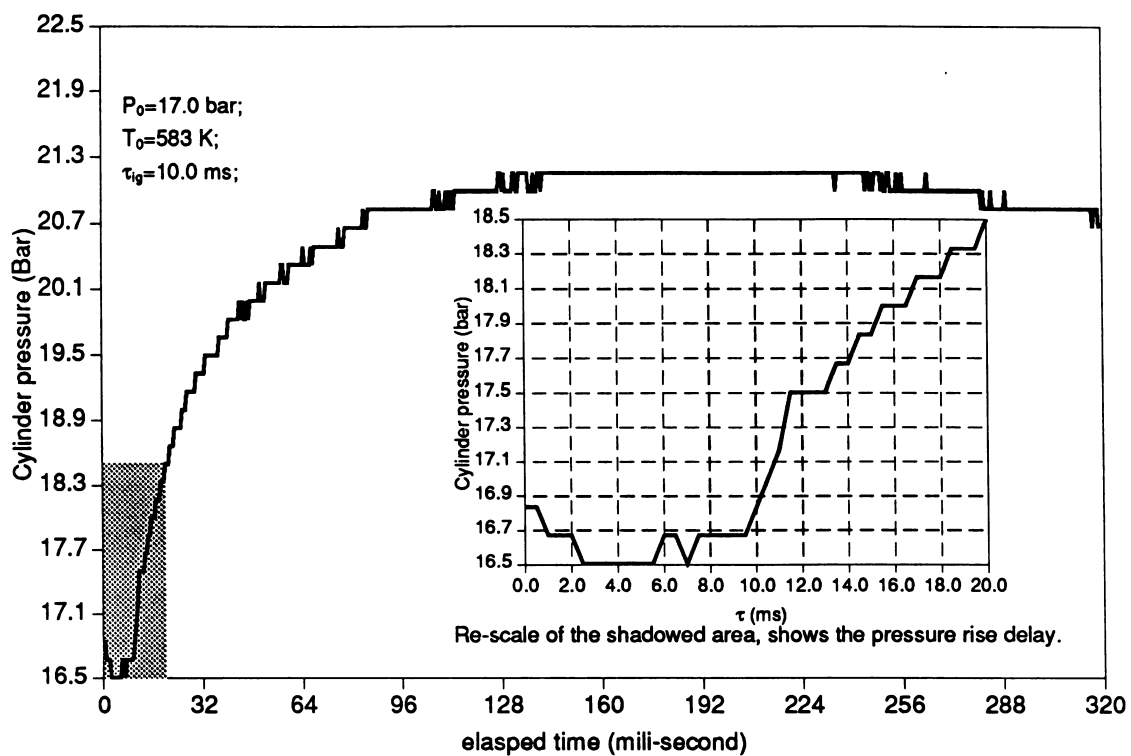


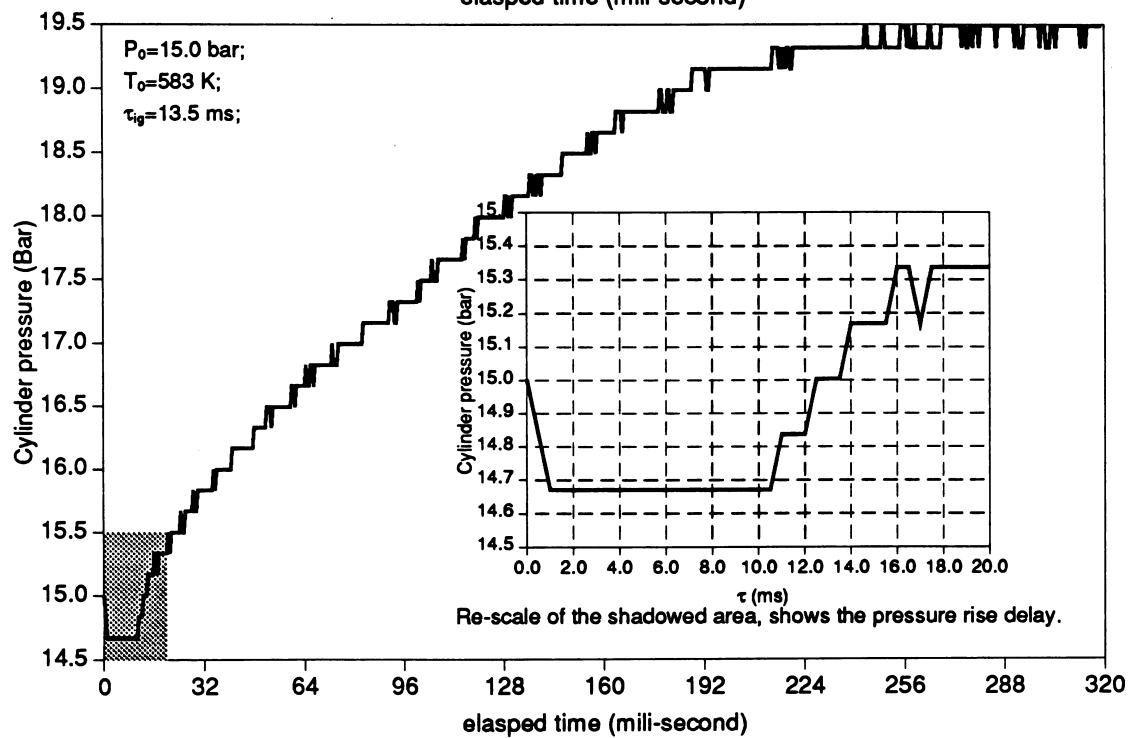
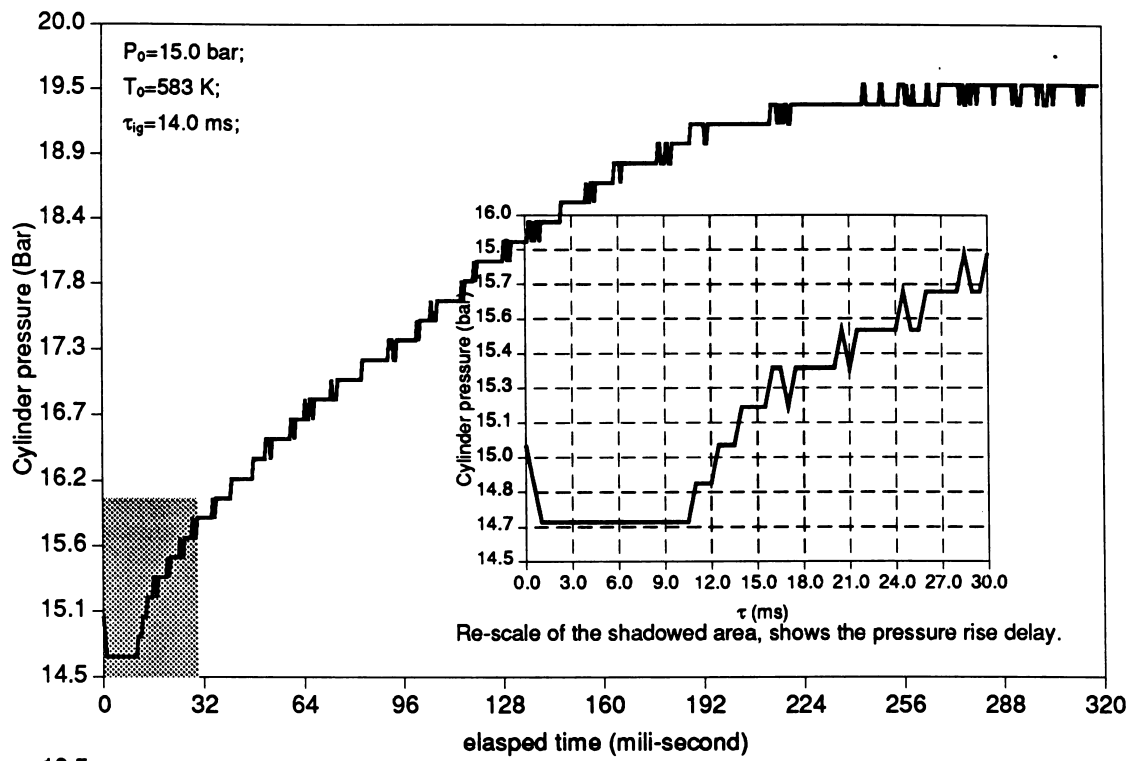


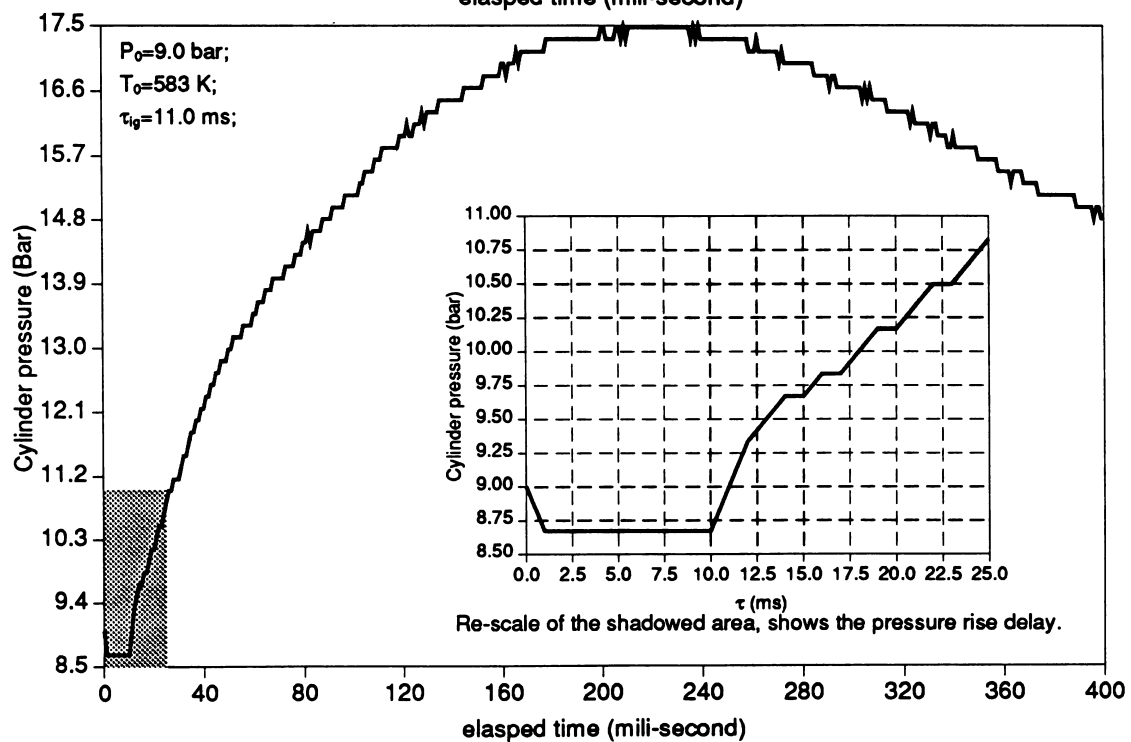
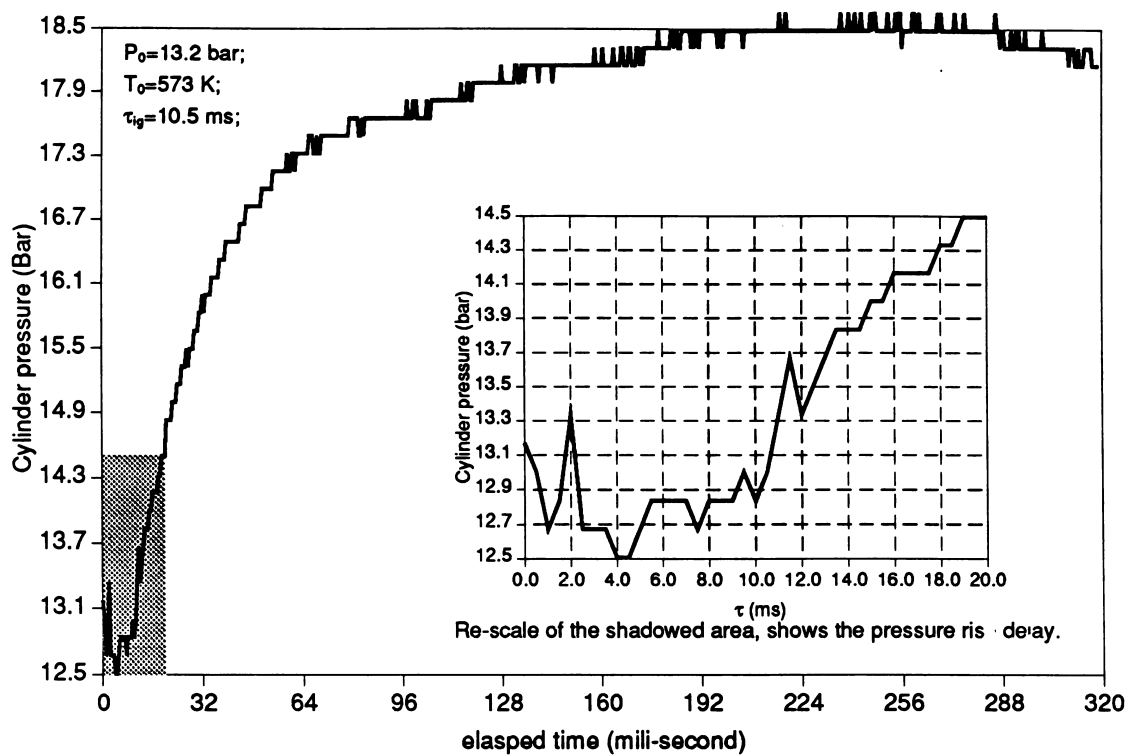


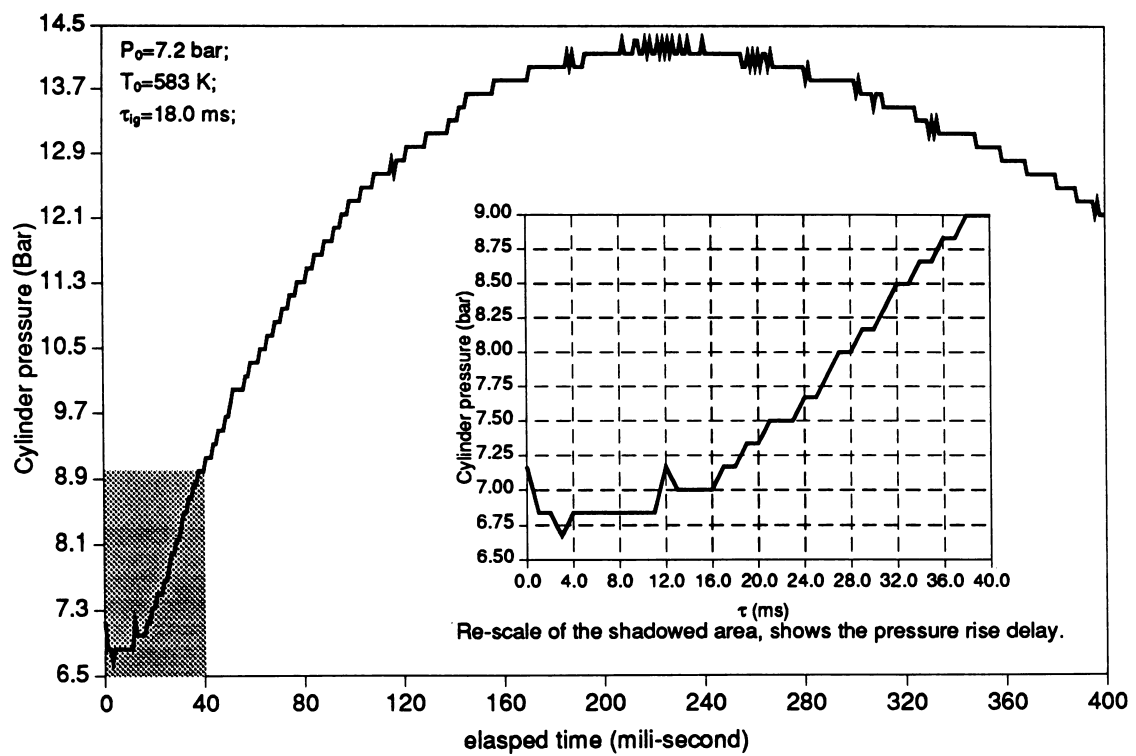


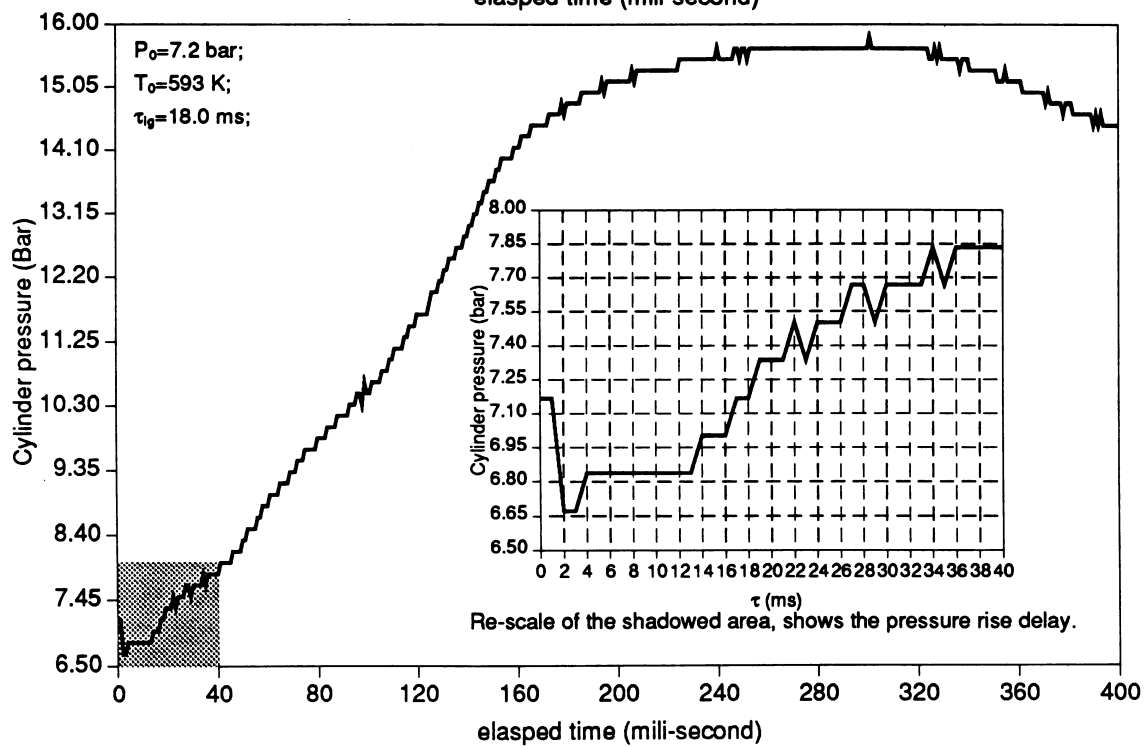
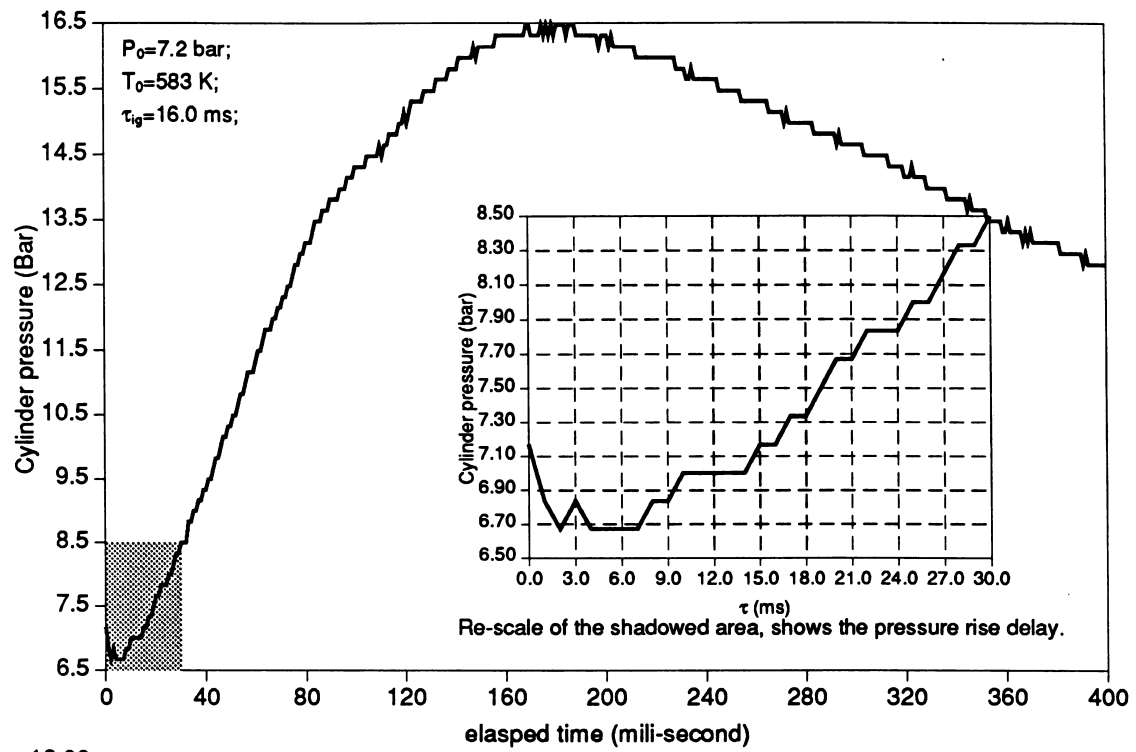


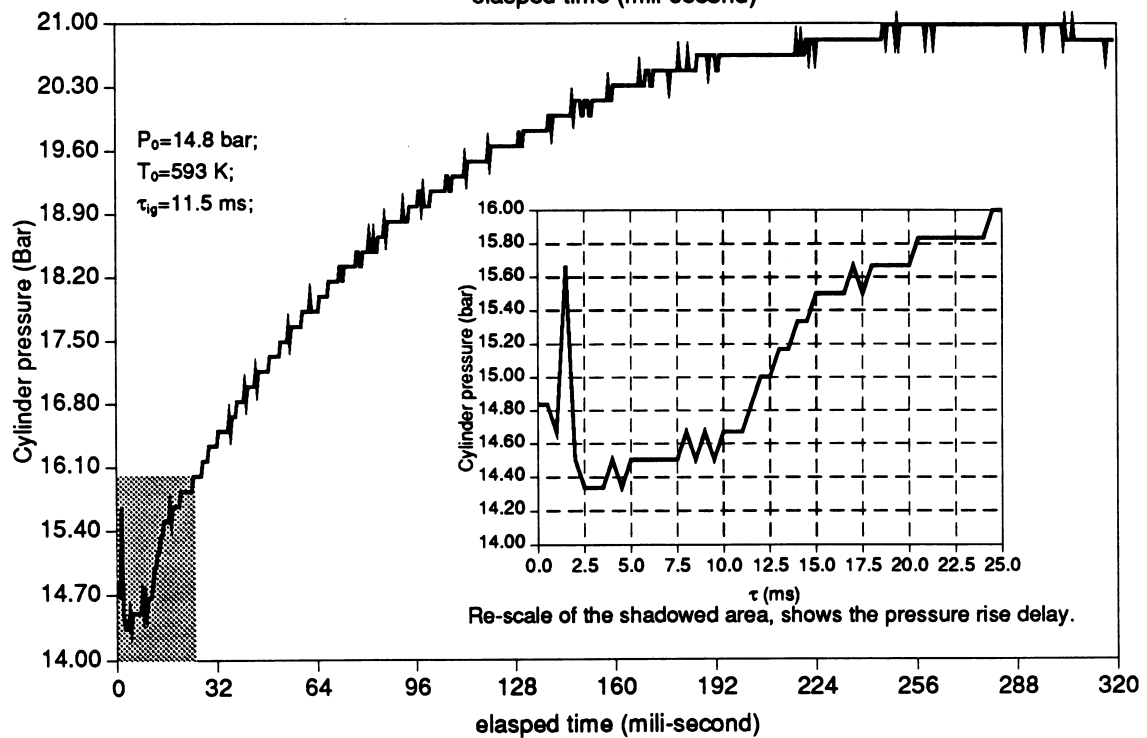
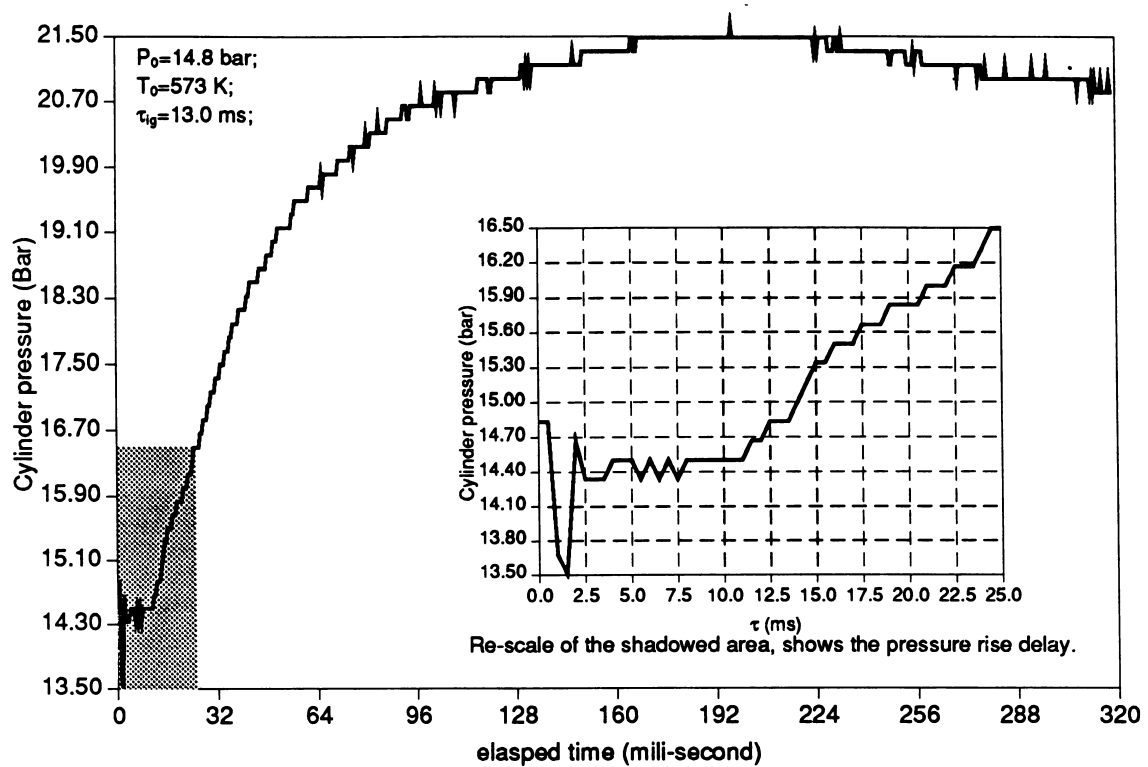


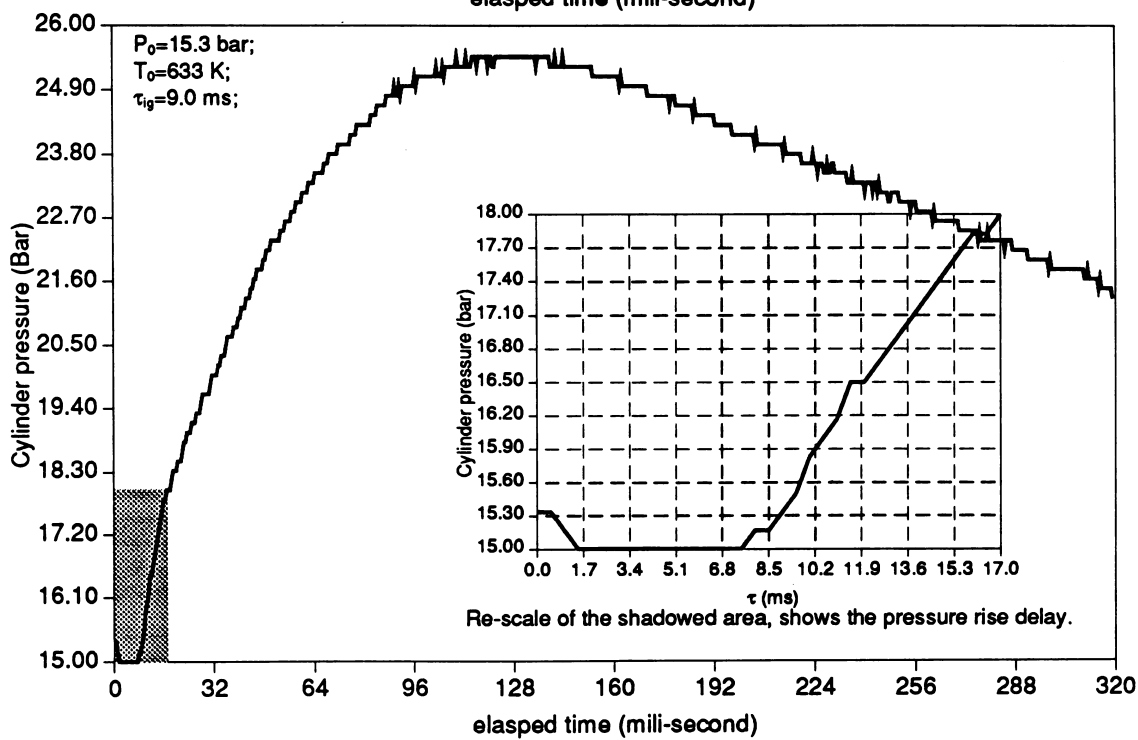
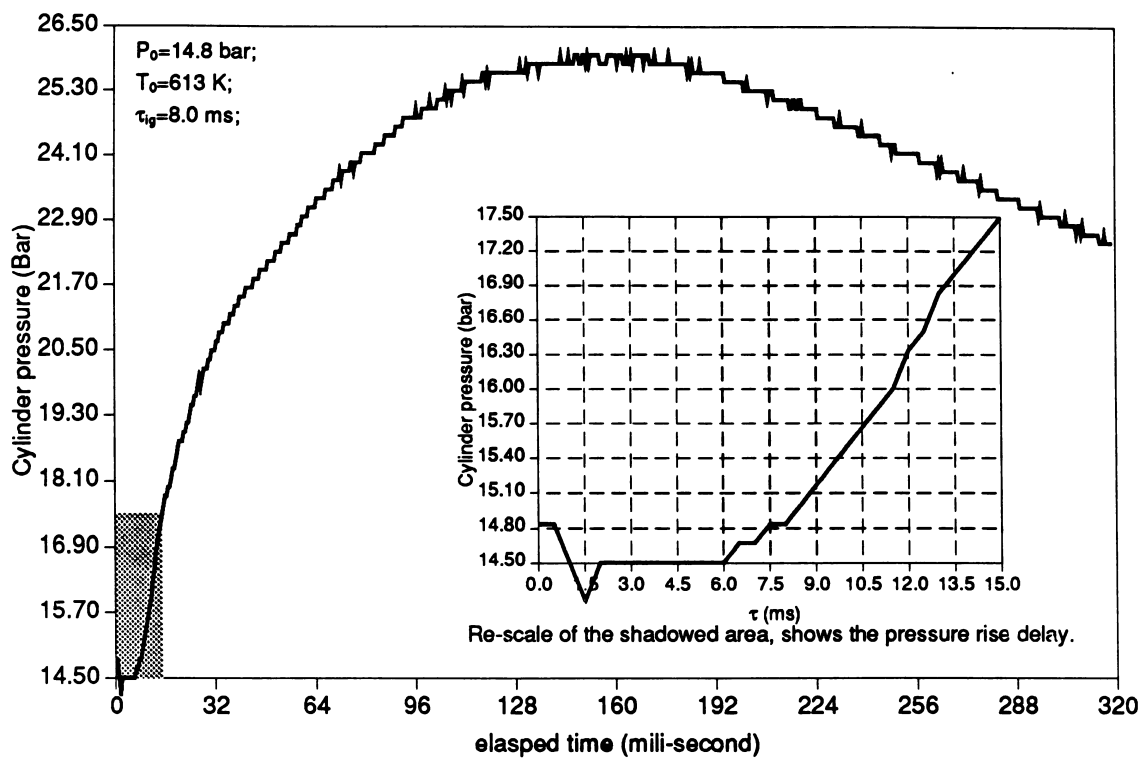


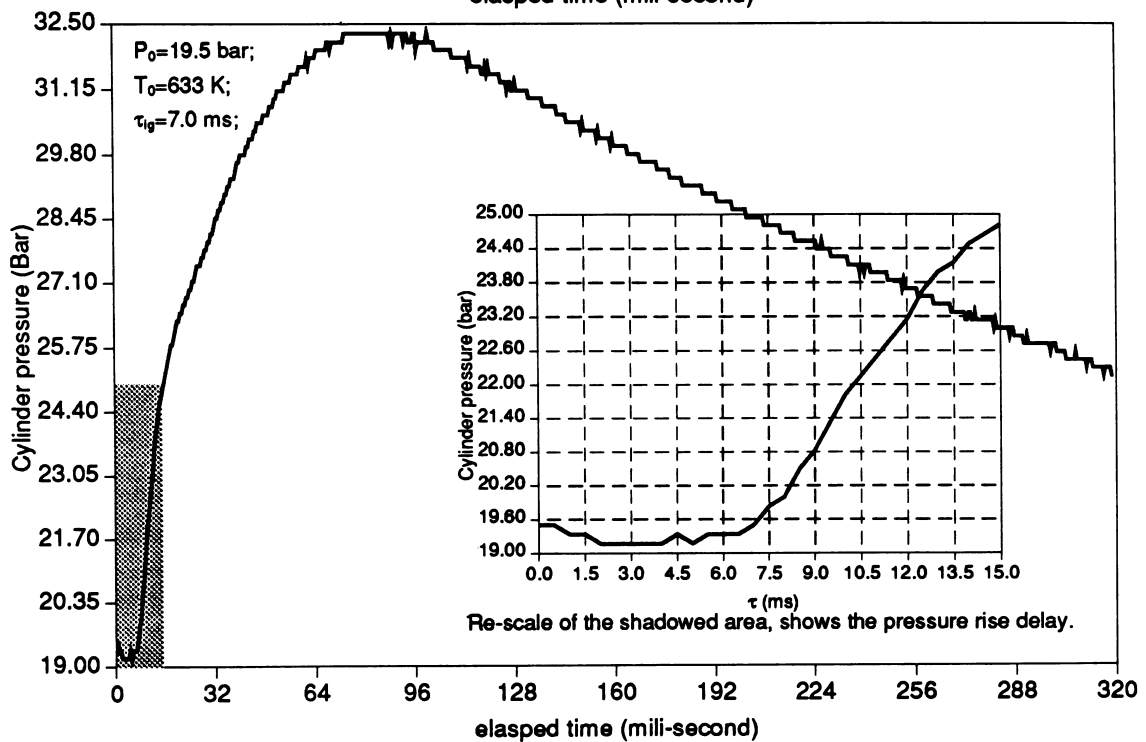
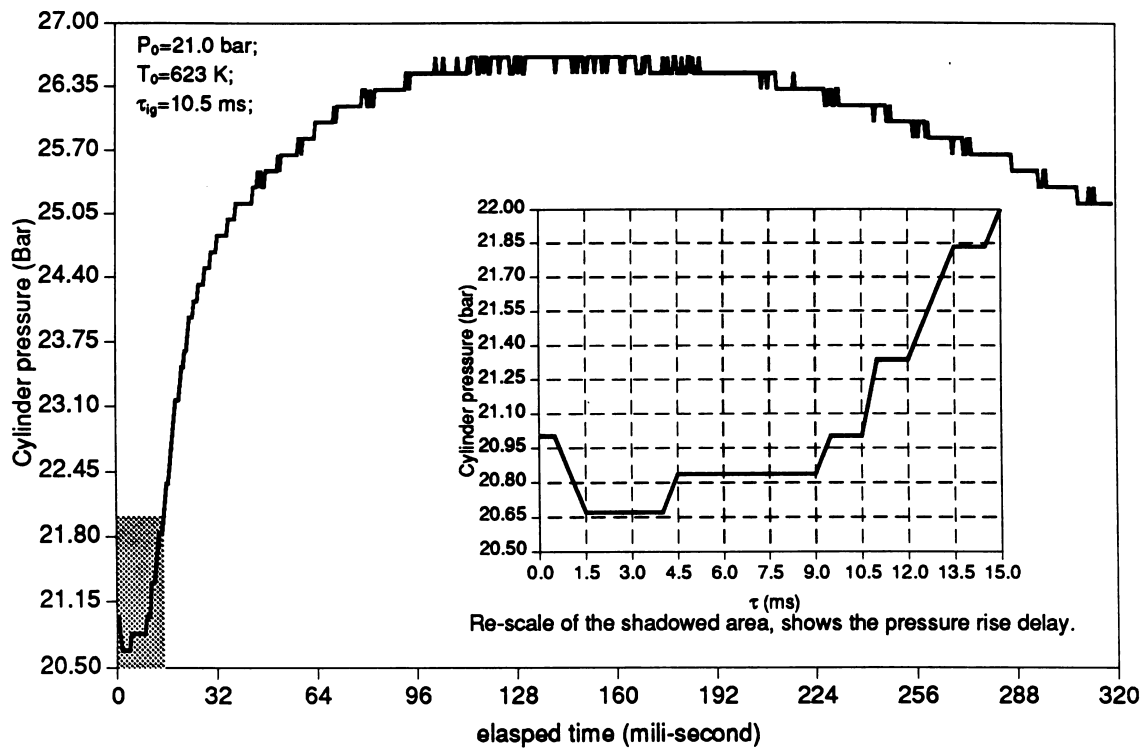


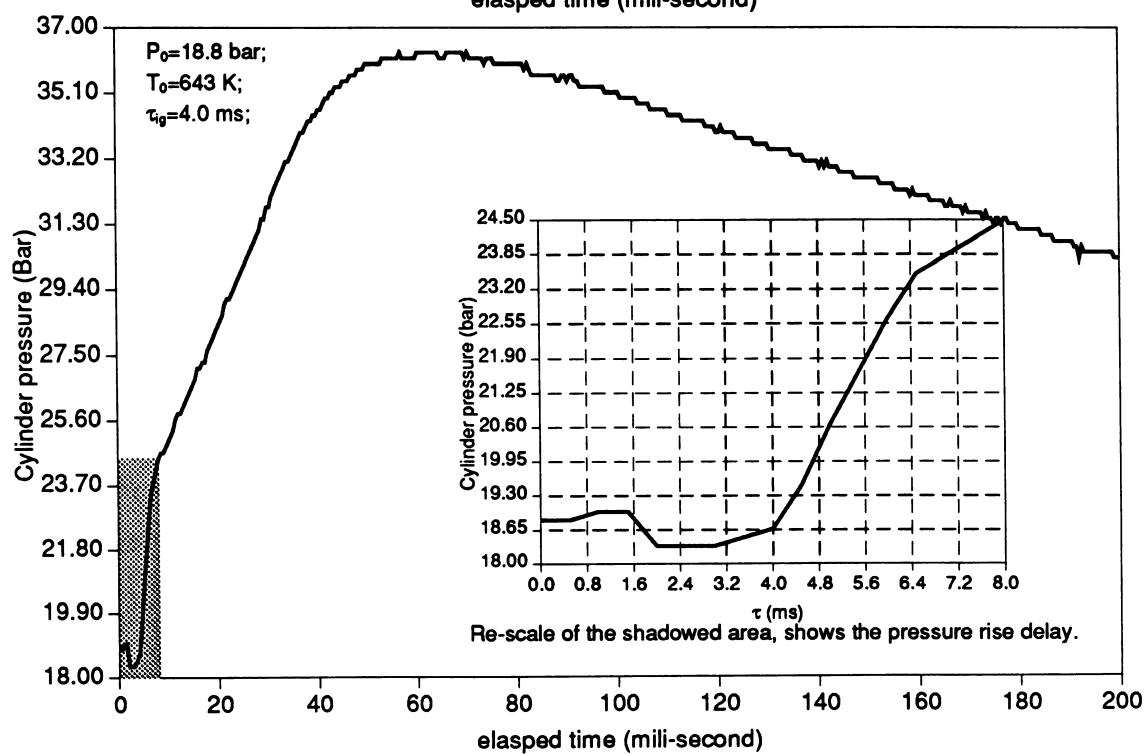
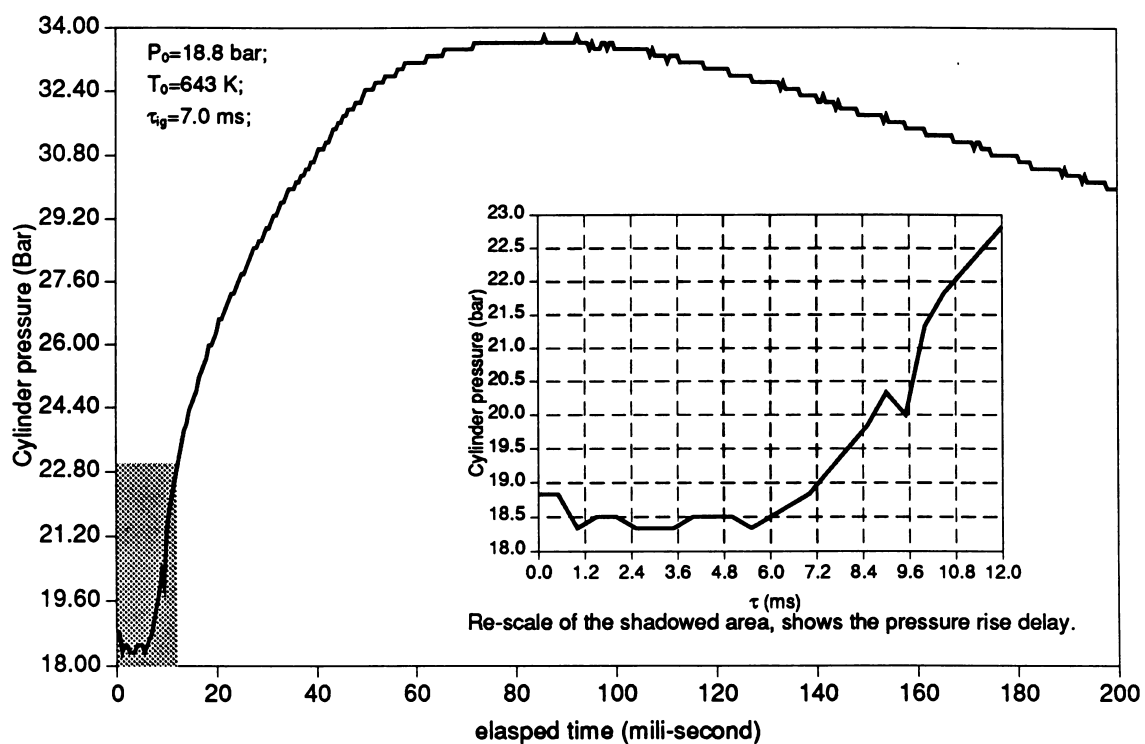


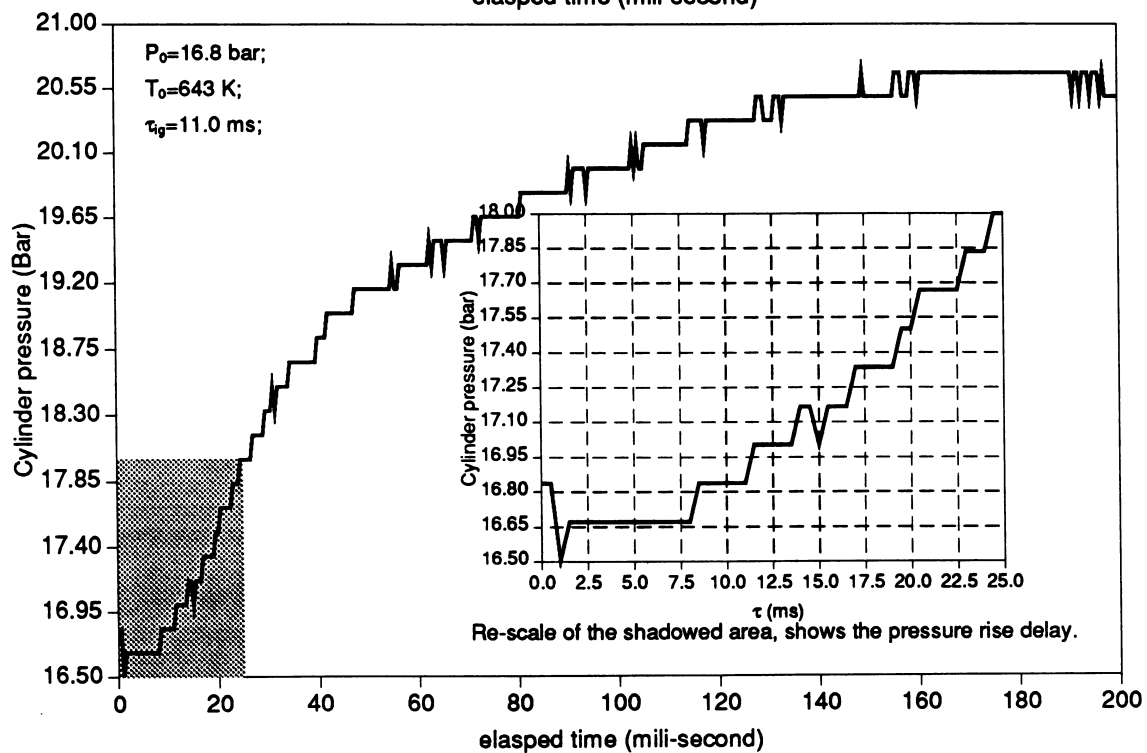
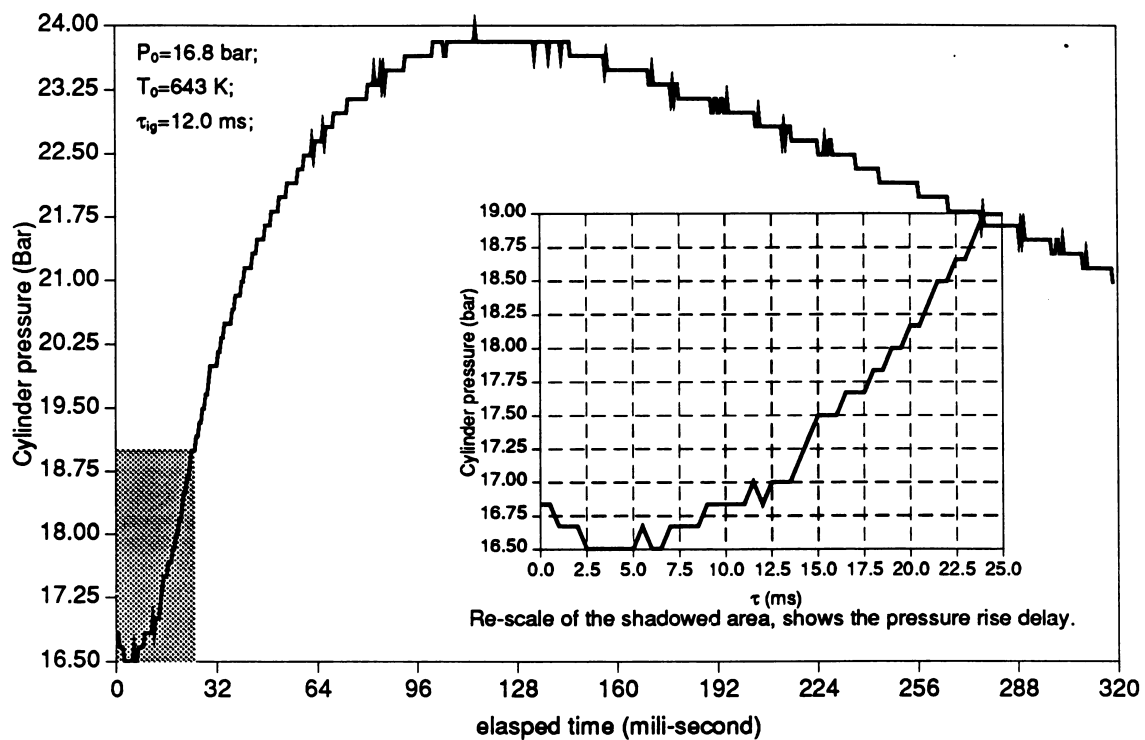


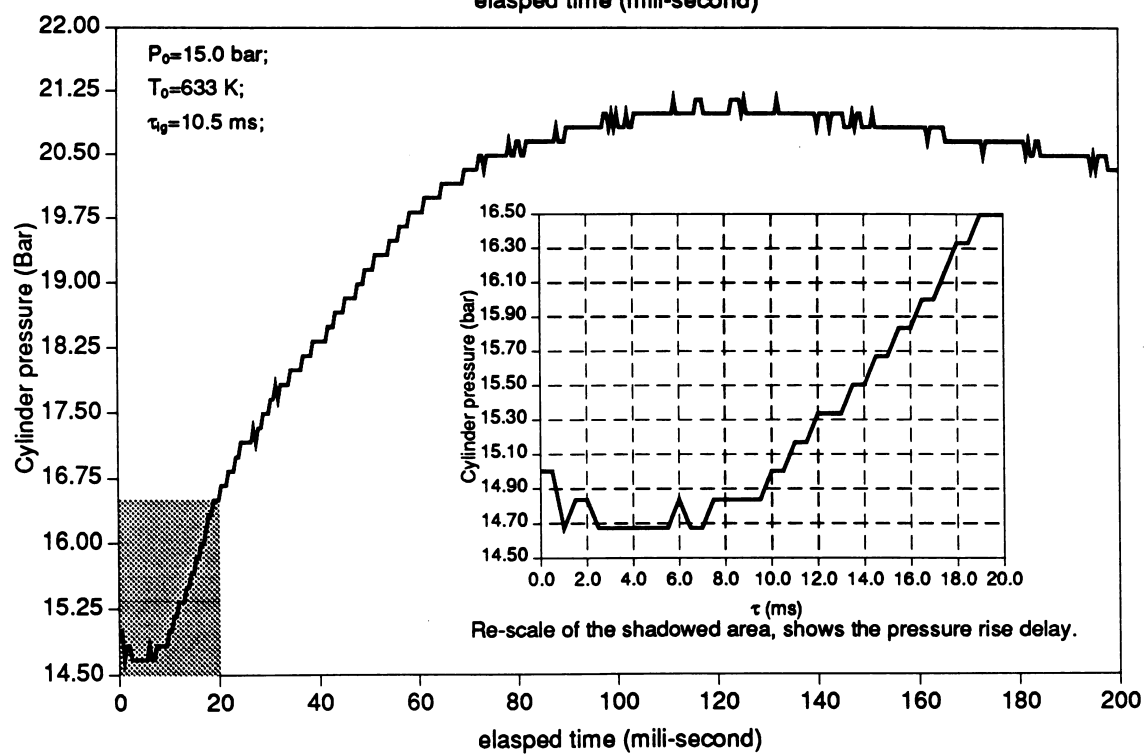
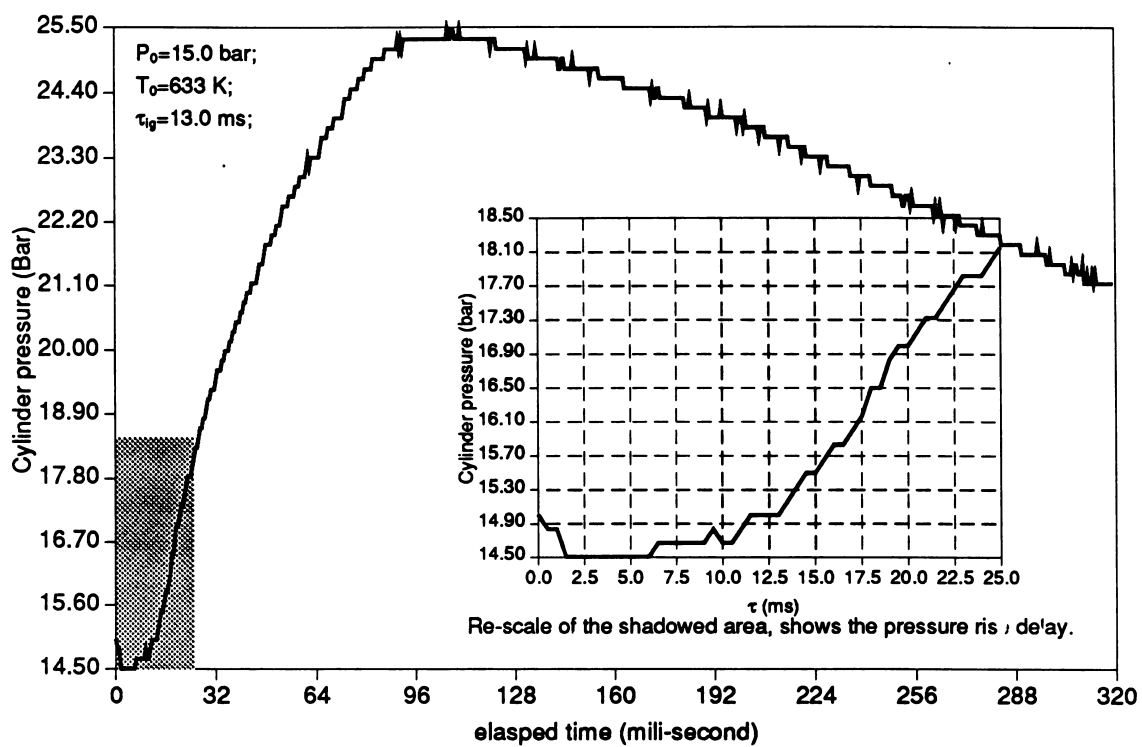


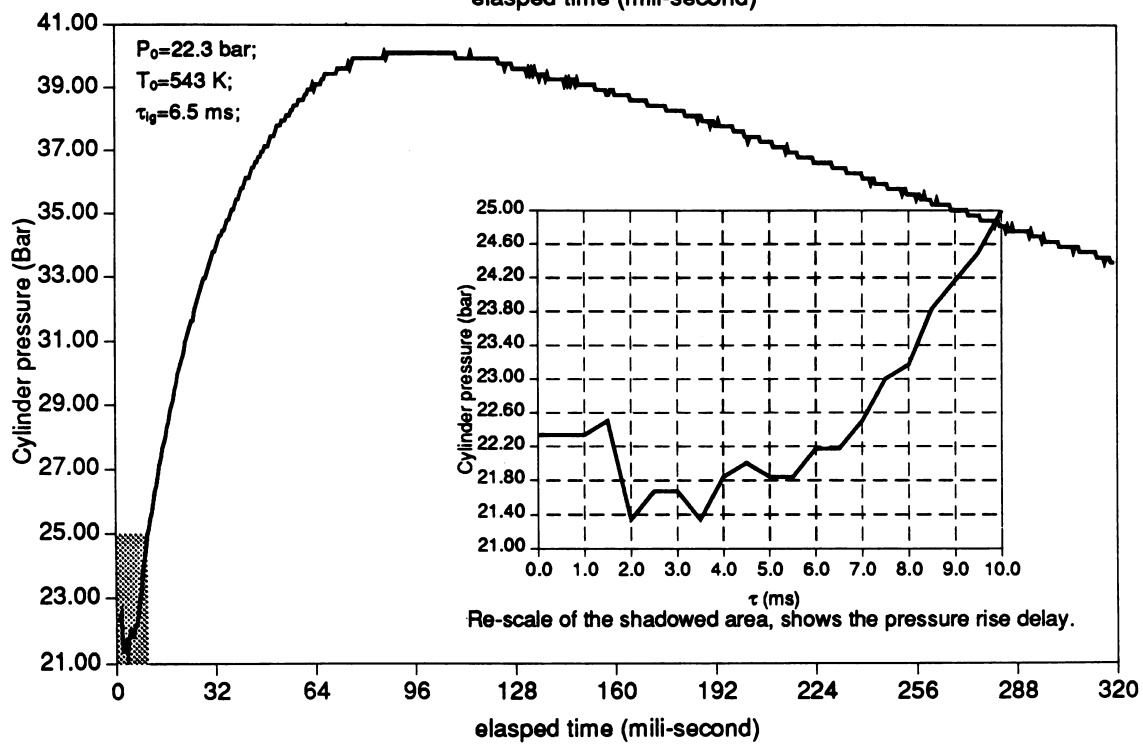
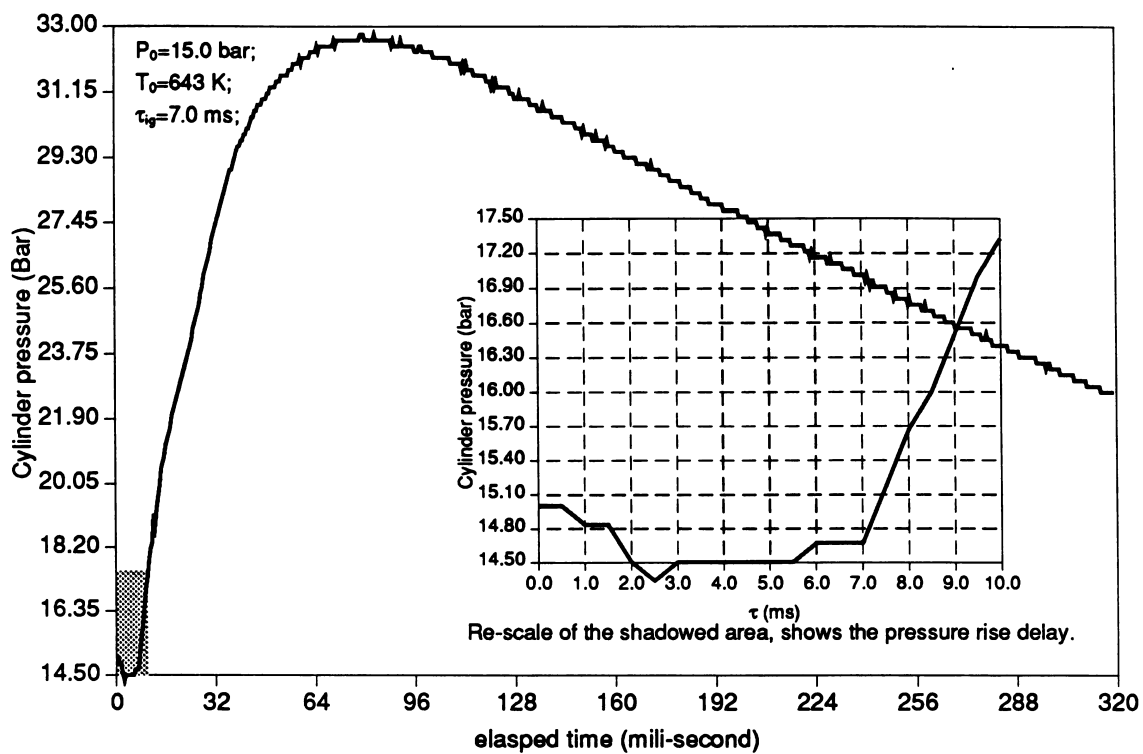


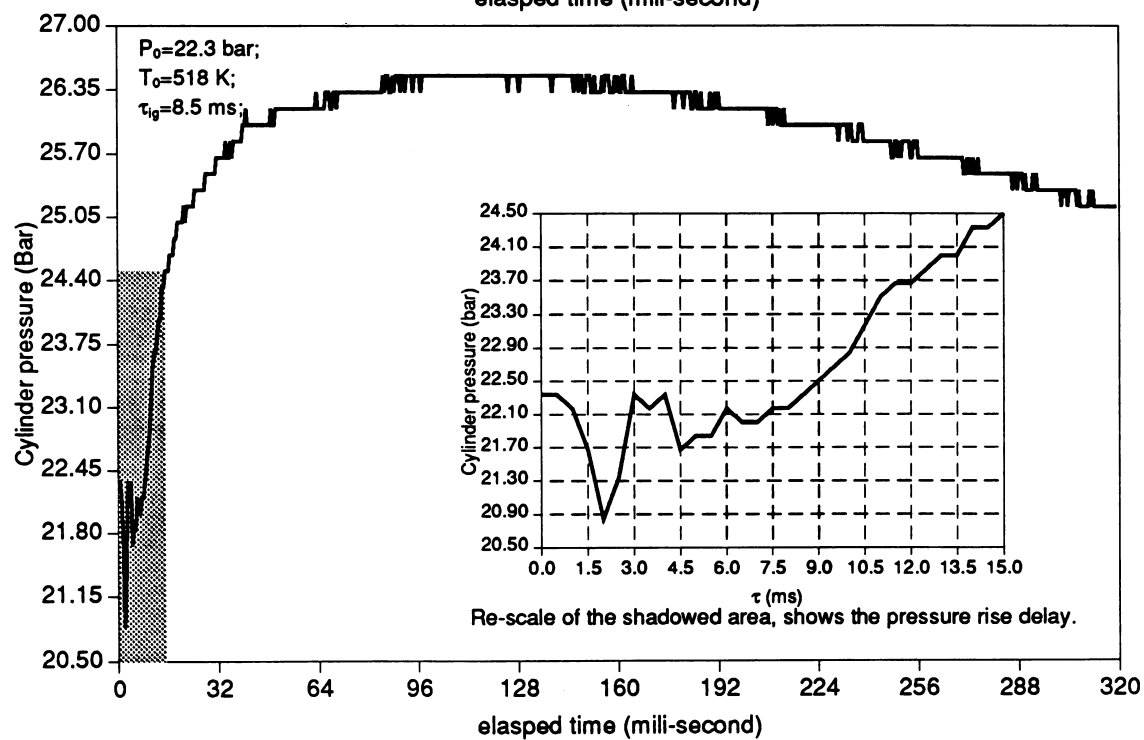
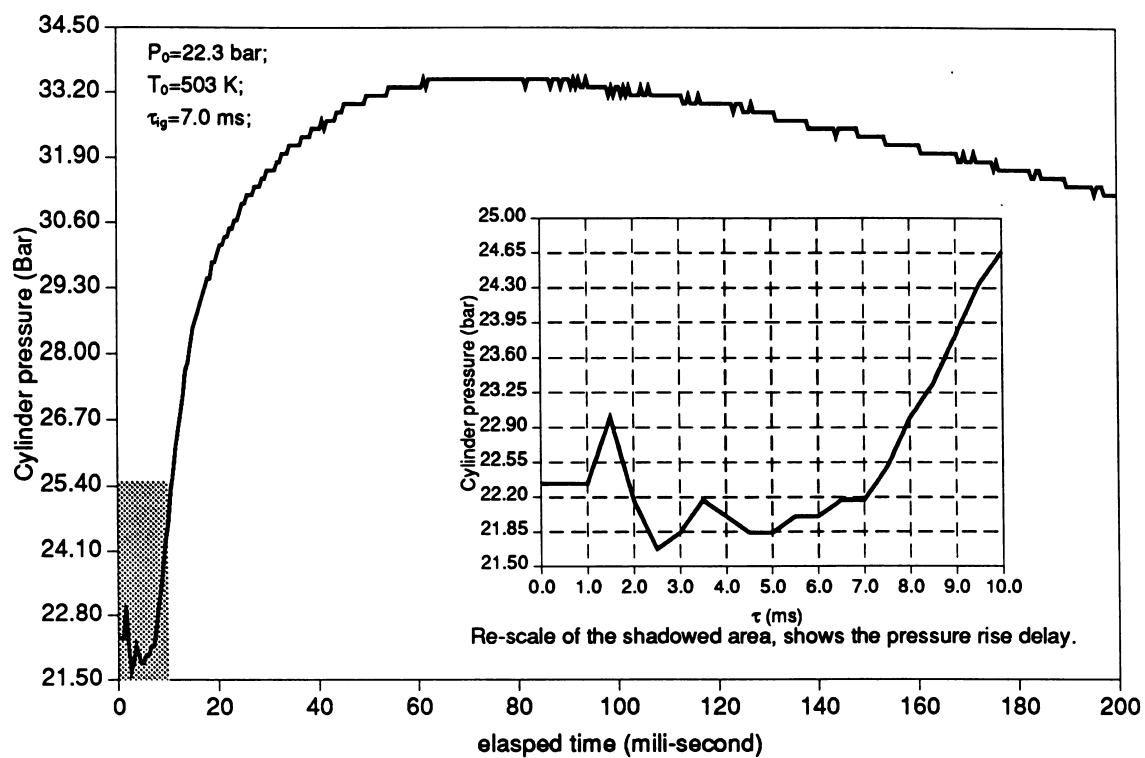


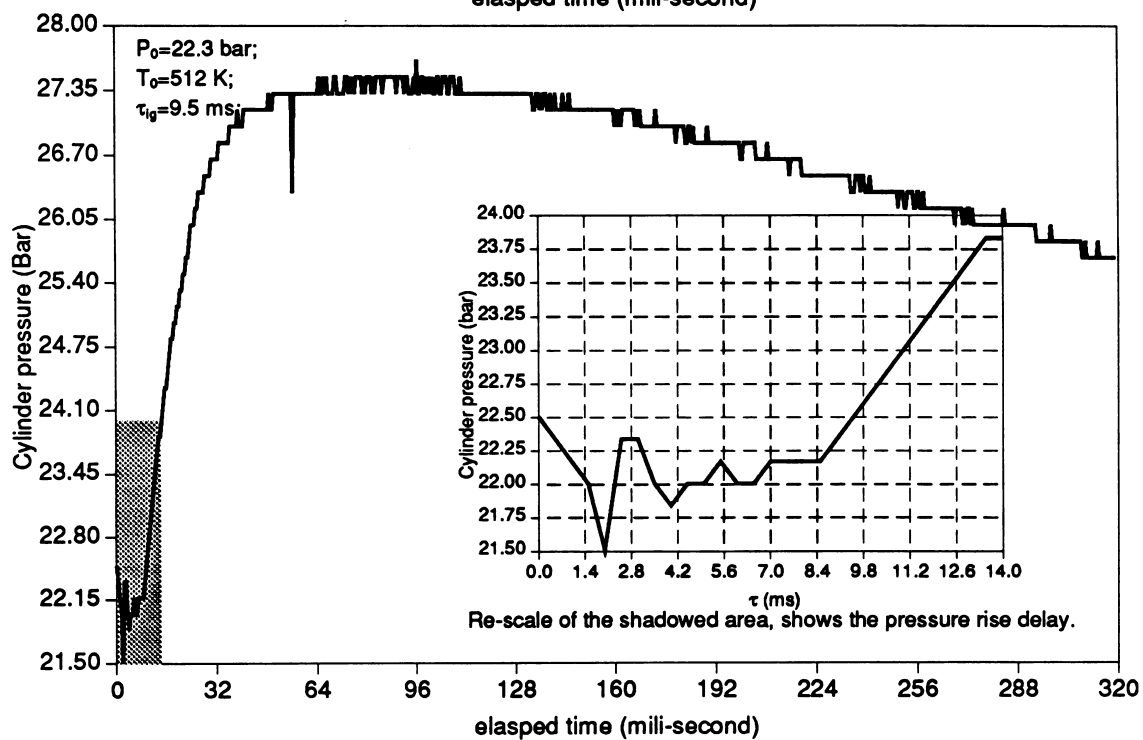
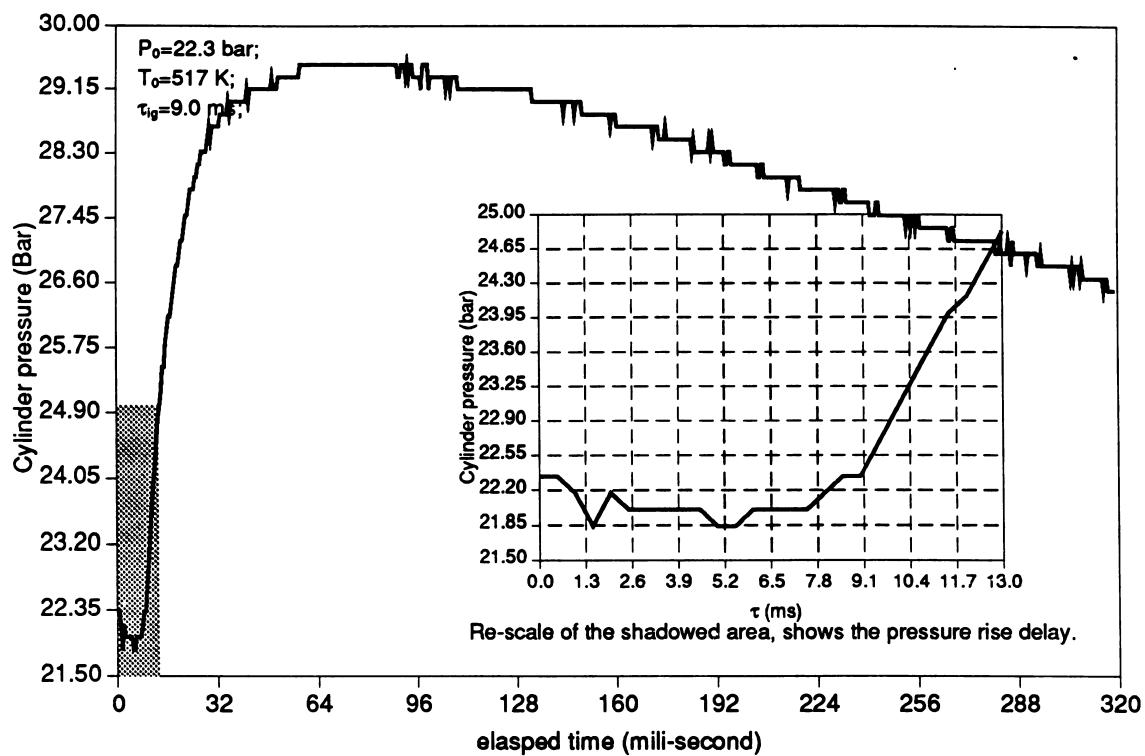


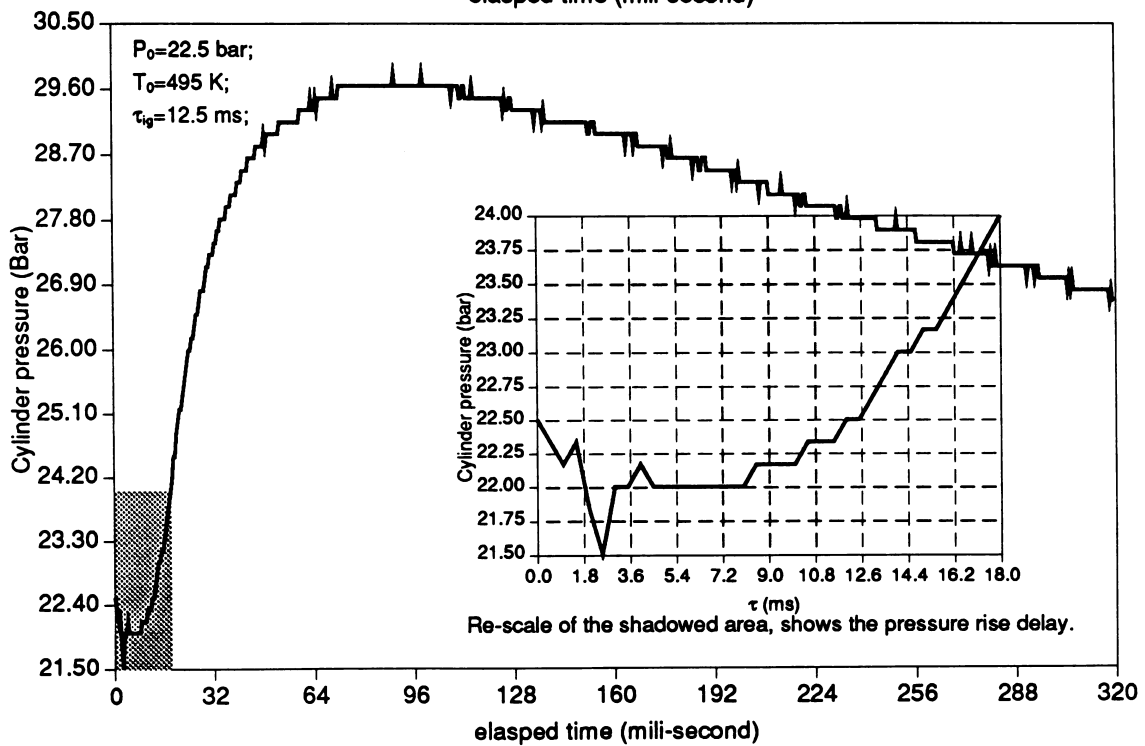
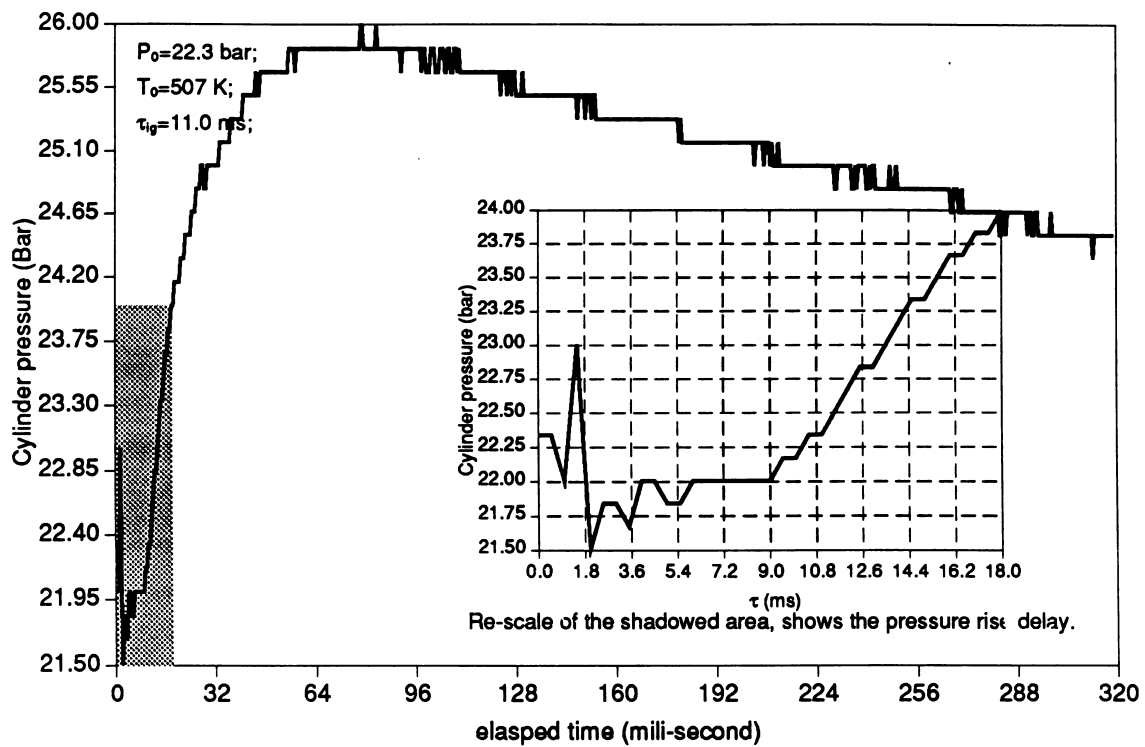


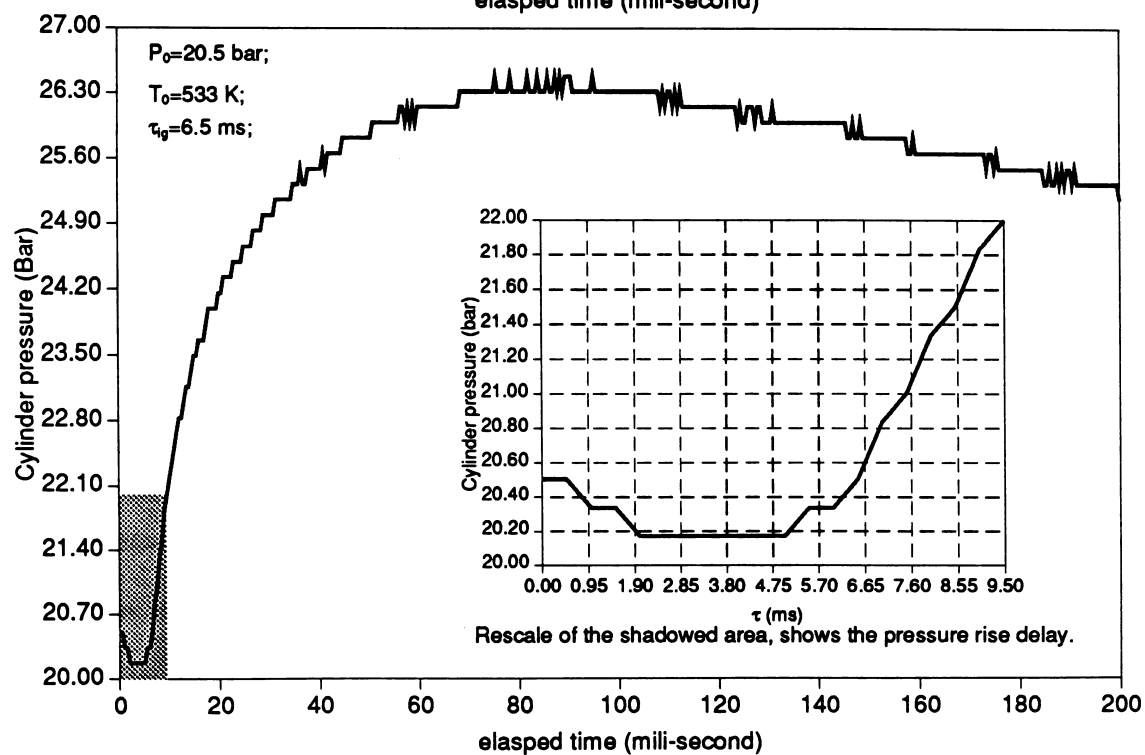
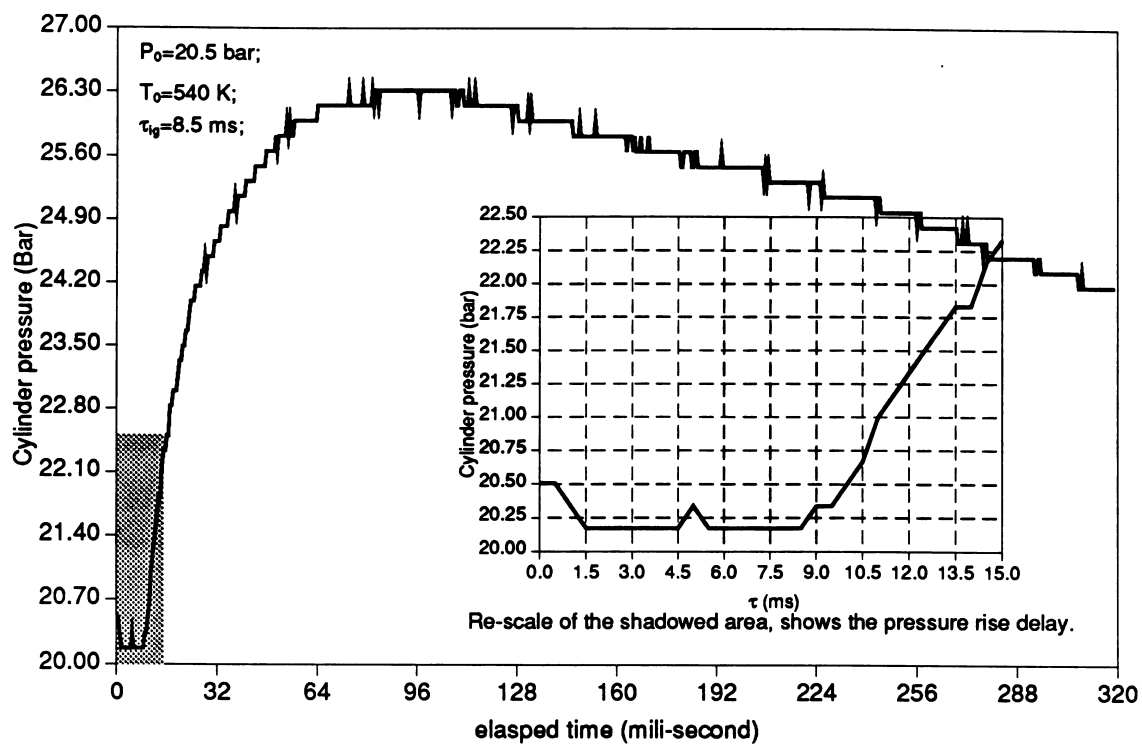












Appendix D

Experimental results of dynamic pressure trace of diesel-natural gas dual-fueled combustion in a constant volume bomb

